Table of contents

Abbreviations

α	alpha
Å	angstrom
β	beta
δ	chemical shift
J	coupling constant
θ	ellipticity
γ	gamma
μ	micro
ϕ	phi
Ψ	psi
AA	amino acid
AAMP	Anionic antimicrobial peptides
Abu	Aminobutyryic acid
AcOH	acetic acid
AMP	Antimicrobial peptide
AHL	acyl-homoserine lactone
AOP	azabenzotriazol-1-yl-oxy-tris-(dimethylamino) phosphonium hexafluorophosphate
APTES	3-aminopropyltrietoxysilane
Arg	arginine
Asp	aspartic acid
AU	arbitrary unit
Boc	*tert*-butyloxycarbonyl
BOP	benzotriazol-1-yl-oxytris(dimethylamino)phosphonium hexafluorophosphate
cAMP	Cationic antimicrobial peptide
CCR	2-chlorotrityl chloride resin
CD	Circular dichroism
CFU	colony forming unit
Dab	α,γ-diaminobutyric acid
DCC	dicyclohexylcarboiimide
DCM	dichloromethane

DCU	dicyclohexylurea
DIC	diisopropylcarbodiimide
DIPEA	*N*, *N*- diisopropylethylamine
$DiSC_35$	3,5-dipropylthiacarbocyanine
DMF	*N*,*N*-dimethylformamide
DMPC	dimiristoylphosphocholine
DVB	divinylbenzene
Ea	*Erwinia amylovora*
EDC	*N*-ethyl-*N'*-(3-dimethylaminopropyl) carbodiimide
EDT	1,2-ethanedithiol
EPS	Exopolysaccharide
ESI-MS	Electrospray ionisation mass spectrometry
eV	Electron volt
FDA	US Food and Drug Administration
Fmoc	9-fluorenylmethyloxycarbonyl
Glu	glutamic acid
HATU	*O*-(7-azabenzotriazol-1-yl)-*N,N,N',N* tetramethyluronium hexafluorophosphate
HBTU	*O*-(benzotriazol-1-yl)-*N,N,N',N* tetramethyluronium hexafluorophosphate
HCTU	*O*-(6-chlorobenzotriazol-1-yl)-*N,N,N',N* tetramethyluronium hexafluorophosphate
HF	hydrogen fluoride
HMPA	hexamethylphosphoramide
HOAt	1-hydroxy-7-azabenzotriazole
HOBt	1-hydroxybenzotriazole
HRMS	High resolution mass spectrometry
IM	Inner membrane
LCMS	Liquid chromatography mass spectrometry
LD_{50}	median lethal dose
Leu	leucine
LPS	lipopolysaccharide
Lys	lysine
M	Molar
m	multiplet

MAL	maleimide
MALDI	Matrix-assisted laser desorption/ionisation
MDR	multi-drug resistant
MIC	minimum inhibitory concentration
MRSA	methicillin-resistant *Staphylococcus aureus*
MRSE	methicillin-resistant *Staphylococcus epidermidis*
MS	Mass spectrometry
Mtt	4-methyltrityl
m/z	mass to charge ratio
NAG	N-acetylglucosamine
NAM	N-acetylmuramic acid
NHS	*N*-hydroxysuccinimide
NMR	Nuclear magnetic resonance
NOE	nuclear Overhauser effect
NPN	*N*-phenyl-naphthylamine
NRP	non-ribosomal peptide synthetase
OD	optical density
OM	outer membrane
Orn	ornithine
Pbf	2,2,4,6,7-pentamethyl-dihydrobenzofuran-5-sulfonyl
PBS	phosphate buffered saline
PDA	polydiacetylene
PDB	Protein Data Bank
PEG	polyethylene glycol
PGs	protecting group
Phe	Phenylalanine
PI	propidium iodide
PIA	polysaccharide intercellular adhesion
PMB	polymyxin B
PMBN	polymyxin B nonapeptide
Pmc	2,2,5,7,8-pentamethyl-chroman-6-sulfonyl
ppb	parts per billion
ppm	parts per million

PRSP	penicillin-resistant *Streptococcus pneumoniae*
PS	polystyrene
Psa	*Pseudomonas syringae pv. actinidiae*
PS-DVB	Polystyrene cross linked to divinylbenzene
PyAOP	7-aza-benzotriazol-1-yloxy-tris-[pyrrolidino] phosphonium hexafluorophosphate
PyBOP	benzotriazol-1-yloxytri[pyrrolidino]-phosphonium hexafluorophosphate
QS	quorum sensing
RBC	red blood cells
ROESY	Rotating Frame Overhauser Effect Spectroscopy
RP-HPLC	Reversed phase high performance liquid chromatography
s	singlet
SAR	Structure-activity relationship
SDS	sodium dodecyl sulfate
SEM	Scanning electron microscopy
SMH	Shai-Matsuzaki-Huang model
SPPS	Solid-phase peptide synthesis
t	triplet
TBTU	*N,N,N',N'*- tetramethyluronium tetrafluoroborate
*t*Bu	*tert*-butyl
TFA	trifluoroacetic acid
TFE	2,2,2 trifluroethanol
Thr	threonine
TOCSY	Total Correlation Spectroscopy
TOF	time of flight
TRCDA	10,12-tricosadiynoic acid
Trt	trityl
VRE	vancomycin-resistant enterococci
v/v	volume per volume
WHO	World Health Organisation
XPS	X-Ray photoelectron spectroscopy

Co-authorship form

THE UNIVERSITY OF AUCKLAND
SCHOOL OF GRADUATE STUDIES

Co-Authorship Form

Graduate Centre
ClockTower – East Wing
22 Princes Street, Auckland
Phone: +64 9 373 7599 ext 81321
Fax: +64 9 373 7610
Email: postgraduate@auckland.ac.nz
www.postgrad.auckland.ac.nz

This form is to accompany the submission of any PhD that contains research reported in published or unpublished co-authored work. **Please include one copy of this form for each co-authored work**. Completed forms should be included in all copies of your thesis submitted for examination and library deposit (including digital deposit), following your thesis Acknowledgements.

Please indicate the chapter/section/pages of this thesis that are extracted from a co-authored work and give the title and publication details or details of submission of the co-authored work. Chapter 3 and 4 Antimicrobial peptides with potential for biofilm eradication: synthesis and structure activity relationship studies of Battacin Peptides De Zoysa, G.H.; Cameron, A.J.; Hedge, V.; Raghothama, S.; Sarojini, V, *J. Med. Chem*, **2015**, 58, 625-639.	
Nature of contribution by PhD candidate	Synthesis, biological evaluation and write-up
Extent of contribution by PhD candidate (%)	80%

CO-AUTHORS

Name	Nature of Contribution
Alan Cameron	SEM imaging
Veena V. Hedge	NMR analysis
Srinivasarao Raghothama	NMR experiment design, data analysis and editing the NMR section
Viji Sarojini	Supervised the research design, reviewed the write-up and edited the draft version of the paper

Certification by Co-Authors

The undersigned hereby certify that:

- the above statement correctly reflects the nature and extent of the PhD candidate's contribution to this work, and the nature of the contribution of each of the co-authors; and
- in cases where the PhD candidate was the lead author of the work that the candidate wrote the text.

Name	Signature	Date
Alan Cameron	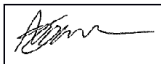	28/08/2015
S. Raghothama	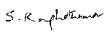	28/08/2015
Veena V Hegde	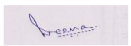	28/08/2015
Viji Sarojini		28/08/2015

Last updated: 25 March 2013

Chapter 1

Introduction

This page has been intentionally left blank

Chapter 1: Introduction

This chapter summarises the urgent need to develop alternative therapeutics to conventional antibiotics that fail against multi-drug resistant pathogens. Some of these multi-drug resistant (MDR) pathogens are capable of forming biofilms, further reducing the efficacy of antibiotics. The concept of antimicrobial peptides will be introduced with details including their classification based on the origin of isolation and structure, and their use as a better alternative to conventional antibiotics will be discussed. This will be followed by a discussion on the mechanisms of action of AMPs, which are known to have preferential selectivity towards bacterial membranes over eukaryotic cells. The limitations of AMPs as commercially viable drugs, and potential ways to overcome these, will be discussed, thereafter. Finally, a discussion on the clinically used cyclic lipopeptides daptomycin and polymyxin will be included followed by the potential of similar novel molecules such as battacin as future antibiotics.

1.1 Antibiotics

Antibiotics are organic compounds produced by numerous microorganisms, as part of their defence arsenal, to either inhibit (bactericidal) or slow down (bacteriostatic) the growth of other microorganisms. Some antibiotics (sulphonamides, quinolones and oxazolidinones), however, are of synthetic origin. Since the serendipitous discovery of penicillin by Alexander Fleming in 1928, several other classes of antibiotics, with diverse mechanisms of action to combat pathogenic bacteria (Table 1.1), have been discovered.

Table 1.1 Important classes of antibiotics[1-3]

Class	Example	Target	Year resistance observed	Year of introduction to commercial market
Arsenical*	Salvarsan	DNA, RNA and protein synthesis	1940	1908
Sulfonamide*	Prontosil	Folate pathway	1942	1936
β-lactams	Penicillin G, Carbapenem	Cell wall synthesis	1945	1938
Aminoglycoside	Streptomycin	Protein synthesis (binds to 30 S ribosomal subunit)	1946	1946
Tetracycline	Chlortetracycline	Binds to 30 S ribosomal subunit	1950	1952
Chloramphenicol	Phenylpropanoid	Binds to 50 S ribosomal subunit	1950	1948
Macrolides	Erythromycins	Binds to 50 S ribosomal subunit	1955	1951
Glycopeptides	Vancomycin	Cell wall synthesis	1960	1958
Ansamacyins	Rifamycin	RNA synthesis	1969	1957
Quinolones*	Ciprofloxacin	DNA synthesis	1968	1968
Streptogramin	Streptogramin B	binds to 50 S ribosomal subunit	1964	1998
Oxazolidinones*	Linezolid	50 S ribosomal subunit	2001	2000
Lipopeptide	Daptomycin	Cell membrane	1987	2003

* indicates synthetic origin

Antibiotics are heavily used in humans through proper prescriptions, and, unfortunately though, without these. Boeckel *et al.* estimated 36% increase in global consumption of antibiotic drugs from 54 billion standard units (defined as number of doses in the form of pill, capsule or ampoule sold) in 2000 to 74 billion standard units in 2010.[4] Additionally, in some countries the use of antibiotics is permitted in veterinary science and agriculture. It is estimated that of the 25022 tons of antibiotics prescribed annually in United States, 50% are used for human consumption and the remaining for agricultural and veterinary use.[5] This excessive use and misuse of antibiotics has led to antibiotic resistance which is classified as a major public health problem by the World Health Organisation.[6]

During the two decades spanning the 1940s to the 1960s, a large influx of novel antibiotic moieties were isolated from various microorganisms, and it was dubbed "the antibiotic era".[3] However, from the 1960s to the 1990s no novel antibiotics were discovered creating a huge void in antibiotic discovery, which also contributed to the current global health issue of antibiotic resistance. The late 1990s and early 2000s saw the introduction of streptogramin, oxazolidinones and daptomycin to the commercial market.[1-3]

A major factor that led to this discovery void is the lack of interest from global pharmaceutical giants due to want of financial gains. During this period research and development of novel antibiotics was primarily carried out by small biotech companies. Several such small scale operations had to be terminated because of financial pressures for these smaller players in the market.[7]

As evident from Table 1.1, resistance has been developed against all major classes of antibiotics. Additionally, some pathogenic bacteria, such as methicillin-resistant *Staphylococcus aureus* (MRSA), penicillin-resistant *Streptococcus pneumoniae* (PRSP), and vancomycin-resistant enterococci (VRE), are becoming resistant to multiple

antibiotic classes.[1] Bacteria acquire resistance to antibiotics through multiple means such as by modifying their cell walls, expressing drug efflux pumps and producing drug inactivating enzymes (β-lactamases).[8] The need to modify existing antibiotic classes and create newer generations of antibiotics that can evade the common mechanisms of resistance used by bacterial pathogens was evident since the 1960s.[1-2] Unfortunately, though, resistance development rapidly occurred against majority of the second-generation antibiotics in the market.[9]

An indirect effect of antibiotic resistance is the greater financial burden on patients, due to prolonged hospitalisation periods and the necessity to rely on more expensive antibiotics treatments. According to a recent survey, the total cost of dealing with infectious diseases in the USA is estimated to be approximately $5 billion per annum.[2]

Making things worse, several multi-drug resistant pathogens have the ability to aggregate and colonise onto numerous surfaces, to form bacterial biofilms.

1.2 Biofilms: formation, pathogenicity and health consequences

Biofilm formation is an ancient evolutionary process, evident from fossil records where filamentous biofilms were identified from 3.2 billion year old deep-sea hydrothermal rocks at Pilbara Craton, in Australia.[10] Bacterial biofilms were first noticed in the 17th century, by Antonie van Leeuwenhoek, who is known as the father of microbiology, while examining plaque on his own teeth under the microscope. He observed that the plaque was surrounded by single-celled organisms, which he originally referred to as "animalcules".

Biofilm development can be summarised in the following key steps (Figure 1.1). The first step begins with free-flowing or planktonic bacteria reversibly attaching to the surface,

through weak van der Waals interactions. This is followed by irreversible surface attachment facilitated by the secretion of a protective layer of exopolysaccharide (EPS) (Step 3). EPS is crucial for biofilm maturation (Step 4), as it provides the mechanical strength needed for bacterial growth.[11-12] During biofilm formation, bacteria communicate with each other by releasing chemical compounds, or autoinducers, in a process known as quorum sensing (QS). Gram-negative and positive bacteria release autoinducers, known as acyl-homoserine lactone (AHL), and oligopeptides, respectively. QS helps the bacteria to coordinate responses, such as generation of virulence factors and biofilm formation, in response to surrounding environmental stimuli.[13] Therefore, bacterial cells within the matured biofilms exhibit distinct phenotypes (Step 5) to planktonic cells. The final step involves the dispersion of bacteria from within the mature biofilm to the surrounding environments (Step 6). This allows better access to nutrients and at the same time helps to further progress the biofilm growth. [11-12]

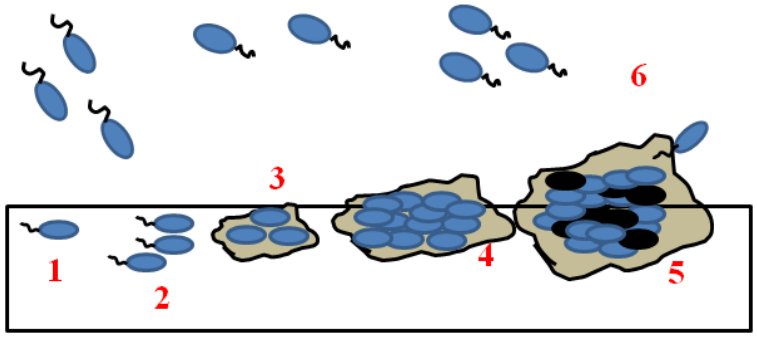

Figure 1.1 Stages of biofilm formation. **(1)** Reversible attachment of bacteria onto the surface. **(2)** Irreversible attachment. **(3)** Secretion of exopolysaccharide and formation of biofilm. **(4)** Biofilm maturation. **(5)** Biofilm differentiation. **(6)** Detachment of mature bacterial cells to colonise onto new site.

It is estimated that biofilm-related infections account for 60% of all bacterial infections.[14] These infections can be categorised as non-implant related chronic diseases or implant-related infections. Common, non-implant related infections include periodontitis, urinary tract infections, acute septic arthritis and cystic fibrosis pneumonia.[15] During these infections, bacteria within the biofilm release antigens to stimulate an antibody response. However, the antibodies produced are ineffective against bacterial biofilms, and usually end up damaging the surrounding cells.[15] This is because of the inability of the phagocytes to engulf bacterial biofilm, leading to the release of toxic agents (also known as frustrated phagocytes) capable of causing host damage to surrounding cells.[15]

Additionally, biofilms are capable of colonising dead tissue, as well as medical devices, such as prosthetic heart valves, central venous catheters, joint replacements and contact lenses.[16-17] Approximately 4.3% of medical implants become colonised by bacterial biofilms annually, according to a US health statistic.[18] The surface materials used in prosthetic implants are capable of supporting a conditional layer of proteins, such as fibronectin, fibrinogen, albumin and immunoglobulin, consequently facilitating the initial attachment of pathogens to the implant's surface.[19-20]

Current viable treatments against infected implants involve surgical removal of the infected device, followed by vigorous antimicrobial therapy to prevent any recurring infections. However, these treatments often lead to prolonged hospitalisation of and increased mortality in patients. It is also estimated to cost up to 5-7 times more than the cost of the original implantation, to remove the implant ($15,000-50,000) from the infected site.[21-22]

1.2.1 Biofilm resistance mechanisms

Current evidence shows that biofilm-forming bacteria are up to 1000 times more resistant to antibiotic treatments than their planktonic counterparts.[23] Bacterial biofilms can withstand several cycles of antibiotic treatments, and upon termination of the antibiotic treatment, the bacteria within the biofilm can colonise new surfaces, leading to an exacerbation of symptoms. Three main features of the biofilm structure can be accountable for the high antibiotic resistance: the EPS, heterogenic architecture of the biofilm and the presence of persisters.[14,23-25]

The bacterial EPS accounts for 50-90% of the biomass in biofilms, and can act as a physical barrier against hostile environmental conditions such as UV exposure, acid stress, metal toxicity and antibiotics.[24] The bacterial EPS is slimy, due to the nature of its hydrated matrix, and can dilute antibiotics to sub-lethal concentrations, slowing down its diffusion into the bacterial cell. In addition, the bacterial EPS can localise enzymes that are capable of either deactivating (β-lactamase) or modifying (aminoglycoside-modifying enzymes and chloramphenicol acetyltransferase) antibiotics.[25-26]

Biofilm architecture is heterogeneous since some of the bacteria within the biofilm have limited access to key nutrients and are exposed to increased osmotic pressure and pH variations. These bacterial cells have adapted to diminished conditions by down regulating several cellular processes such as DNA, protein and cell wall biosynthesis resulting in a dormant or metabolically inactive state. Generally, most of the antibiotics act by targeting the cellular activity of bacteria; hence, dormant cells within biofilms are immune to antibiotic treatment.[14,25]

Persisters are bacterial cells with multi-drug resistant traits acquired via biological programming rather than environmental cues.[15,25] These cells are highly concentrated

within the biofilm and are extremely resistant to antibiotics, due to their dormant metabolic state.[25] Persisters are created when most of the bacterial cells within a biofilm are killed rapidly by antibiotics, but a small fraction of the cells remains unaffected, despite prolonged treatment. These persisters then have the capability to reconstruct the bacterial biofilm.[16] Some biofilm-forming bacteria, such as *E. coli*, can encode genes (*hip*) for a high level of persister cell production. *Hip* mutant *E. coli* cells can generate persisters up to 1000 times more frequently than their wild type counterparts.[14]

There is a desperate need for novel antibiotics to tackle MDR, biofilm-forming pathogens. The dependence on "last-resort" antibiotics, such as vancomycin, linezolid and carbapenem, as the first line of defence against these pathogens, is growing. Boeckel *et al*. have reported 45% increase in the consumption of carbapenem from 2000 to 2010.[4] Increasing emphasis is being put on antimicrobial peptides (AMP), as possible alternatives to antibiotics, due to their unique mechanism of action that reduces chances of resistance and their ability to inhibit multi-drug resistant pathogens and bacterial biofilms.

1.3 Antimicrobial Peptides (AMP)

Antimicrobial peptides are produced by numerous organisms, ranging from microorganisms to vertebrates, as part of their innate and adaptive immune system.[27-30] These peptides are usually 15-50 amino acids in length, cationic, due to the presence of multiple Lys and Arg residues and amphiphilic, due to the presence of hydrophobic and hydrophilic amino acids. This amphiphilicity is crucial for bacterial selectivity, where positively charged amino acids form an electrostatic interaction with the negatively charged head groups of the bacterial membrane. The hydrophobic core of the AMP

interacts with the phospholipid tail of the bacterial membrane leading to membrane disruption and cell death.[27-30]

1.3.1 Classification of antimicrobial peptides

More than 5000 AMPs, with diverse structural characteristics, have been identified from numerous organisms.[31] These AMPs can be classified into two broad categories: non-ribosomally synthesised and ribosomally synthesised peptides (Figure 1.2).

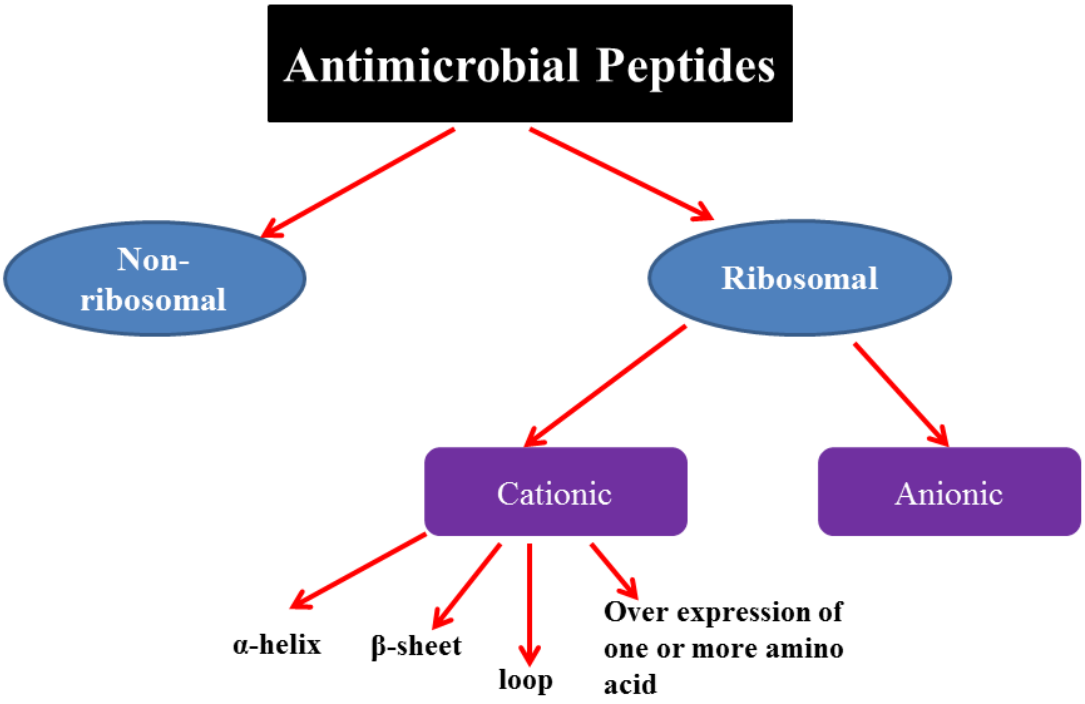

Figure 1.2 Classification of antimicrobial peptides based on the origin of their isolation.

Non-ribosomally synthesised peptides are only produced by prokaryotes, as part of their defence arsenal to inhibit the growth of other pathogens. These peptides display structural characteristics and activities that are similar to conventional antibiotics.[28,32] AMPs in this class are characterised by the presence of one or more modified amino acids, produced by a large, complex multi-domain enzyme, known as non-ribosomal peptide-synthetases (NRP).[33-35] NRP can modify amino acids or the peptide backbone either by changing the

stereochemistry of the L amino acid, the *N*-methylation of α-amino group, ring formation, C-terminal amidation or glycosylation.[28,34-35] Such extensive modification of amino acids has led to the production of numerous non-ribosomal AMPs, with diverse, complex structures that are stable against enzymatic degradation. An important class of non-ribosomal AMPs are lipopeptides, which will be discussed in detail in section 1.6.

Ribosomally synthesised peptides are produced by both prokaryotic and eukaryotic organisms, as part of their innate immune systems, where they act as host defence during the early stages of pathogenic infection.[27,30,36] These AMPs can adopt diverse secondary structures, mainly to expose the segregated hydrophilic and hydrophobic moieties of the sequence that are crucial for the selective bacterial interactions (Figure 1.3).[29-30] Most of the ribosomally synthesised AMPs are cationic in nature and can be sub-classified, based on their secondary structure and amino acid sequences, as α-helical linear peptides, extended linear peptides with over-expression of one or more amino acids, peptides containing a looped structure and β-sheet peptides consisted of multiple disulphide bridges.[29-30]

Anionic AMPs (AAMPs) have been isolated from various organisms, as part of their innate immune system, although not as commonly as cationic AMPs. Common features of AAMPs include the presence of several anionic amino acids such as Glu and Asp and an overall net anionic charge between -1 to -7.[30] AAMPs secreted by humans generally adopt helical conformations, while AAMPs isolated from plants show β-sheet secondary structures.[37] Most AAMPs exhibit a non-membrane lytic mechanism of action against bacteria, by affecting intracellular targets rather than the bacterial membrane.[30]

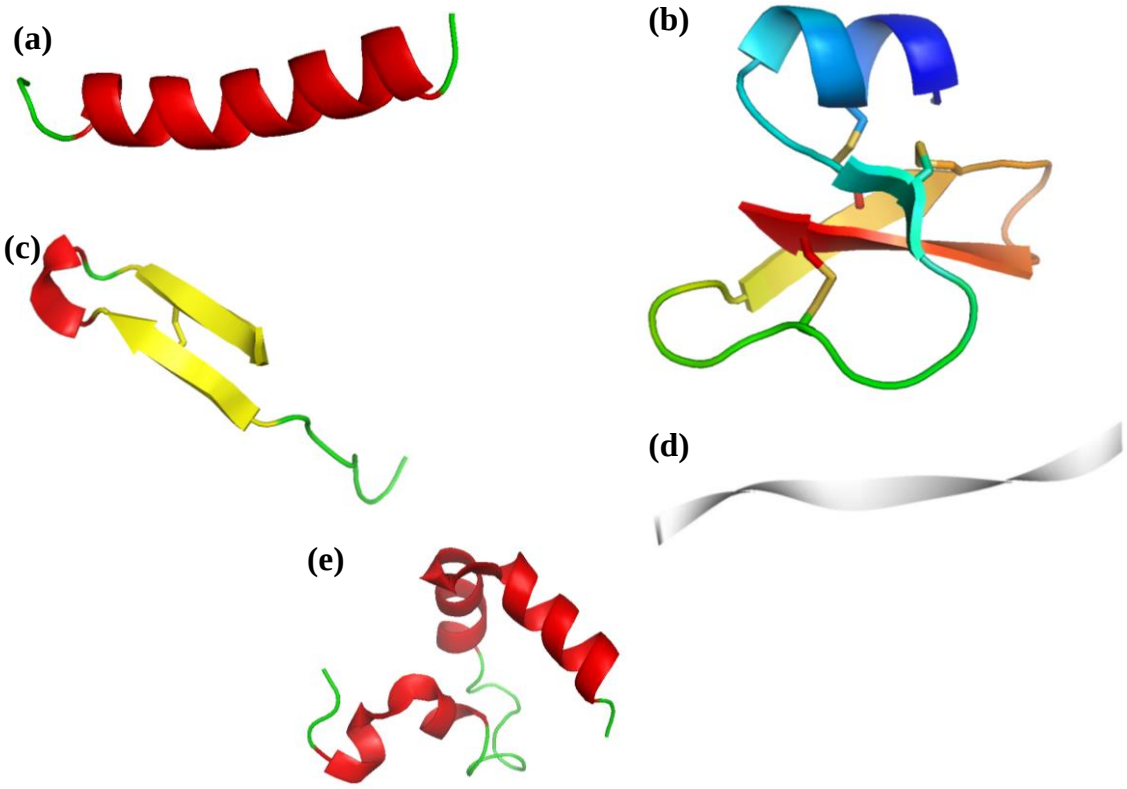

Figure 1.3 Different structural classes of ribosomally synthesised peptides. (**a**) α-helical magainin 2 (Protein Data Bank (PBD) code: 2MAG).[38] (**b**) β-sheet rich β-defensin 1 (PDB code: 1LJU).[39] (**c**) Loop structure of thanatin (PDB code: 8TFV).[40] (**d**) Proline rich bovine Bac7 (PDB code: 4JWC).[41] (**e**) Anionic Asp rich dermcidin-1L (PDB code: 2KSG).[42]

Table 1.2 Examples of antimicrobial peptides belonging to each class.

Class	Peptide	Species/source	Special characteristics	Ref
α-helical	Cecropin	Insects, haemocytes	Contains two well-defined helices, separated by a hinge region.	43
	Magainin	Frog, haemocytes	Broad-spectrum pathogenic activity as well as anti-cancer. activity. Adopts a right-handed α-helical structure.	44
	Melittin	Bee, venom	High haemolysis at 1 mg/mL.	45
over expression of amino acids	Histatin 5	Human, saliva	His rich, antifungal against *C. albicans*, adopts β-turn poly-proline type II turn.	46
	Indolicidin	Bovine, neutrophil	Trp rich.	47
	Bac5, Bac7	Bovine, neutrophil	Pro rich, adopts proline type II turn.	48
Loop structure	Brevinin 1 , brevinin 1E	Frog, skin	Forms a loop via disulphide bridge, haemolytic.	49
	Thanatin	Insect, haemolymph	Potent Gram-positive, negative and anti-fungal activity.	50
β-Sheet	Defensin	Vertebrates, epithelia, haemocytes	Triple stranded β-sheet via 3 disulphide bridges, immunogenic.	51
	Protegrin	Pig, intestine	Antiparallel β-sheet formed with 2 disulphide bridges.	52
	Tachyplesin	Horseshoe, haemocytes	Antiparallel β-sheet formed with 2 disulphide bridges.	53

Anionic	Daptomycin	Bacteria (*Streptomyces roseosporus*)	Cyclic depsi-lipopeptide. Used clinically against MDR Gram-positive pathogens. Multiple aspartic residues (-3 net charge). Can also be classified as non-ribosomally synthesised AMP.	54
	Enkelytin	Vertebrates/Invertebrates, secretory granules	Glu acid rich, neuro-immunogenic peptide.	55
	Dermcidin	Human, sweat glands	Aspartic acid rich.	56
Non-ribosomally synthesised	Polymyxin	Bacteria (*Paenibacillus (Bacillus) polymyxa*)	Cyclic lipopeptide, clinically active against multi-drug resistant Gram-negative pathogens, high abundance of unnatural α,γ-diaminobutyric acid (Dab) amino acid.	57-58
	Nisin	Bacteria (*Lactococcus lactis sub sp*)	Cationic lantibiotic consist of unnatural amino acids such as lanthionine and methyllanthionine. Nanomolar activity against Gram-positive pathogens, used commercially as a food preservative.	59
	Gramicidin	Bacteria (*Bacillus brevis*)	Alternating L- and D-amino acids and non-proteogenic amino acid ethanolamine at the C-terminus. Clinically used as a topical application against Gram-positive and negative bacteria.	60-61

1.3.2 Mode of action of AMPs

1.3.2.1 Bacterial cell wall architecture

Although the exact mechanism of action is currently unknown, cationic AMPs are known to interact with the bacterial membrane.[27,30] Bacteria can be broadly categorised into Gram-positive and Gram-negative bacteria, based on their ability to retain crystal violet stain (Gram-positive bacteria retain crystal violet stain and Gram-negative bacteria cannot, due to their thicker peptidoglycan layer). Gram-positive and negative cell wall architecture will be briefly discussed below in order to understand the interaction of AMPs with bacterial membrane (Figure 1.4).

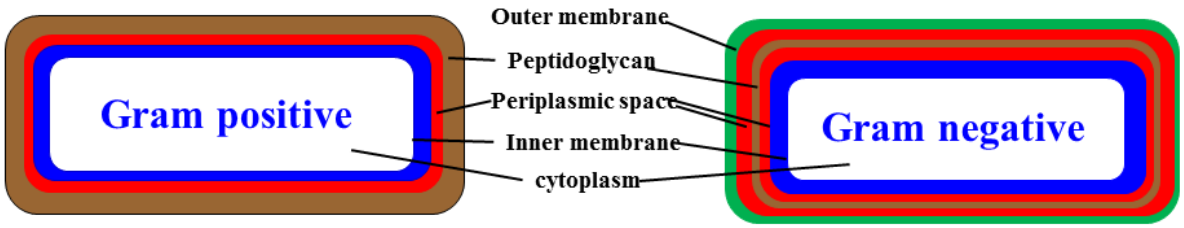

Figure 1.4 Schematic representation of Gram-positive and negative bacteria.

Both Gram-positive and negative bacteria have a periplasmic space and a cytoplasmic membrane. The periplasmic space mainly consists of water and proteins, and has numerous functions such as the transport of small molecules (amino acids and sugar residues) to the cytoplasm, and the degradation of larger molecules (nucleic acids and proteins) to smaller molecules, using proteases to ease the transportation into the cytoplasm. Bacterial cytoplasm is a gel-like matrix, mainly containing water and enzymes, surrounding vital elements such as the DNA, mRNA, chromosomes and plasmids, required for cell survival.

1.3.2.1.1 Gram-positive cell wall

Both Gram-positive and negative bacteria are surrounded by a cell wall, mainly composed of a thick layer of peptidoglycan which accounts for 40-90% of cell materials.[62] These peptidoglycans consist of alternating units of N-acetylglucosamine (NAG) and N-acetylmuramic acid (NAM), linked via a β 1-4 linkage.[63-64] The carboxylic acids of some NAM molecules are linked to tetrapeptide chains, consisting of D- and L- amino acids, such as D-alanine and L-glutamic acids. These tetrapeptides act as a bridge linking adjacent NAM-NAG sugar chains to form a complex mesh-like structure. The peptidoglycans are responsible for the strength, rigidity and shape of the bacterial cells, as well as protection against external pressures such as UV exposure, acid stress, metal toxicity and antimicrobial agents.[63-64]

In addition to the peptidoglycan layer, Gram-positive bacterial cell walls also consist of teichoic acid, which stabilises and strengthens the cell wall. Teichoic acids are water-soluble polymers of glycerol or ribitol phosphate, with D-alanine attached via ester linkages.[65-66] The presence of the multiple phosphate groups contributes to the overall negative charge of the Gram-positive cell wall.

The two major classes of teichoic acids, embedded, within the peptidoglycan layer, to different extents, are lipoteichoic and wall teichoic acids. Lipoteichoic acids are embedded deeply within the peptidoglycan layer, stimulate autolysin and act as a scaffold for cell binding proteins.[67] Wall teichoic acids protrude onto the surrounding environment and can bind monovalent and divalent cations to minimise their repulsive interactions with anionic phosphate molecules.[68] Due to their overall negative charge, wall teichoic acids provide a cationic reservoir that is crucial for enzymatic activity and for maintaining osmotic balance in bacteria.[68]

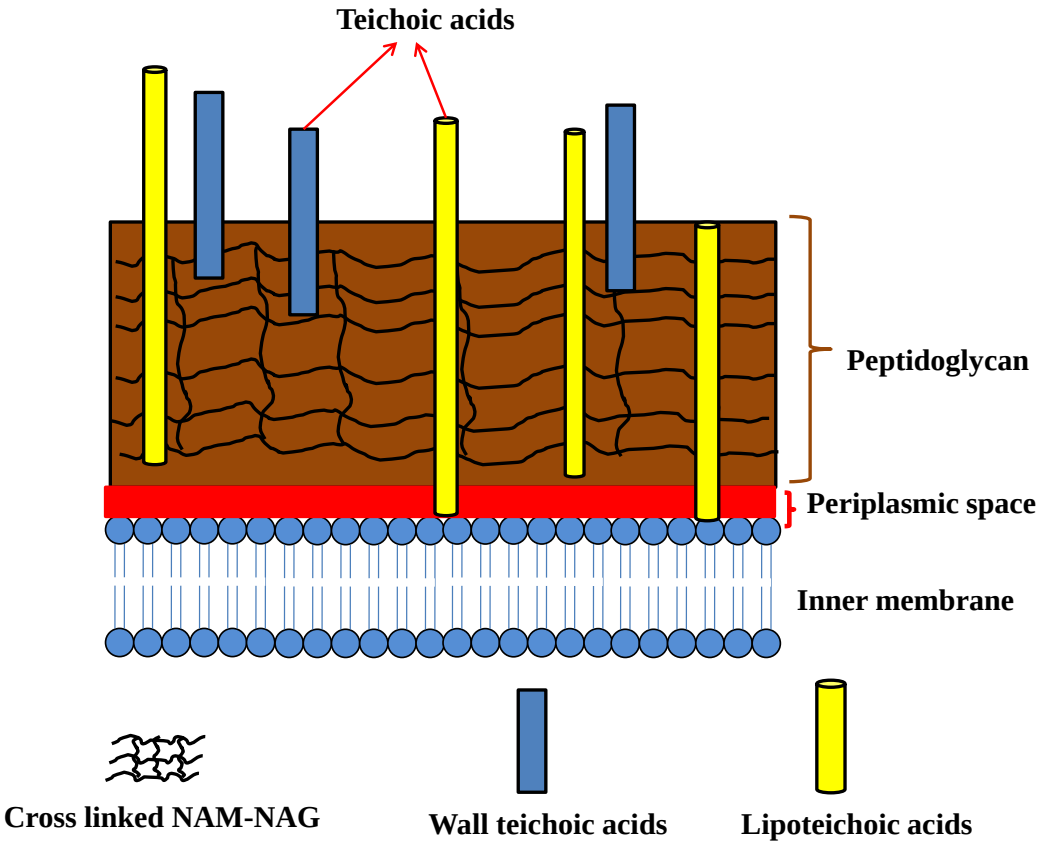

Figure 1.5 Schematic representation of Gram-positive cell wall.

1.3.2.1.2 Gram-negative cell wall

Gram-negative bacteria have more complex cell-wall architecture. They contain a thinner layer of peptidoglycan, accounting for 10% of the total cell materials, and are not heavily cross-linked as in Gram-positive bacteria.[62] The thin peptidoglycan layer is surrounded by an outer membrane of anionic lipoproteins, lipopolysaccharide (LPS) and phospholipids (Figure 1.6). Porins are the most abundant lipoprotein present in the outer membrane, which form channels that allow small hydrophilic substances to cross through the membrane while blocking bulky hydrophobic molecules.[69]

LPS are high molecular weight, negatively charged molecules that can be sub-divided into three portions: lipid A, the core oligosaccharide and the O-antigen. Lipid A also known, as the endotoxin portion of the LPS, mainly consists of the β-1,6 linked disaccharide,

glucosamine, containing 6 fatty acid chains of various carbon chain lengths, attached to the non-reducing sugar ends of glucosamine.[69-70] The disaccharides of lipid A are phosphorylated at positions 1 and 4 of each end of the glucosamine moiety and is embedded into the outer leaflet of the outer membrane.[70]

Lipid A is then attached to a core oligosaccharide domain consisting of 8-12 variable sugar molecules and 3-8 phosphate residues. Some of these sugar molecules contain the negatively charged octasaccharide, 2-keto-3-deoxyoctanate (Kdo-C and Kdo-D).[70] The variable O-antigen, covalently attached to the core oligosaccharide domain, protrudes out of the outer membrane. The variable O-antigen domain consists of multiple 3-5 polysaccharide repeats. [70]

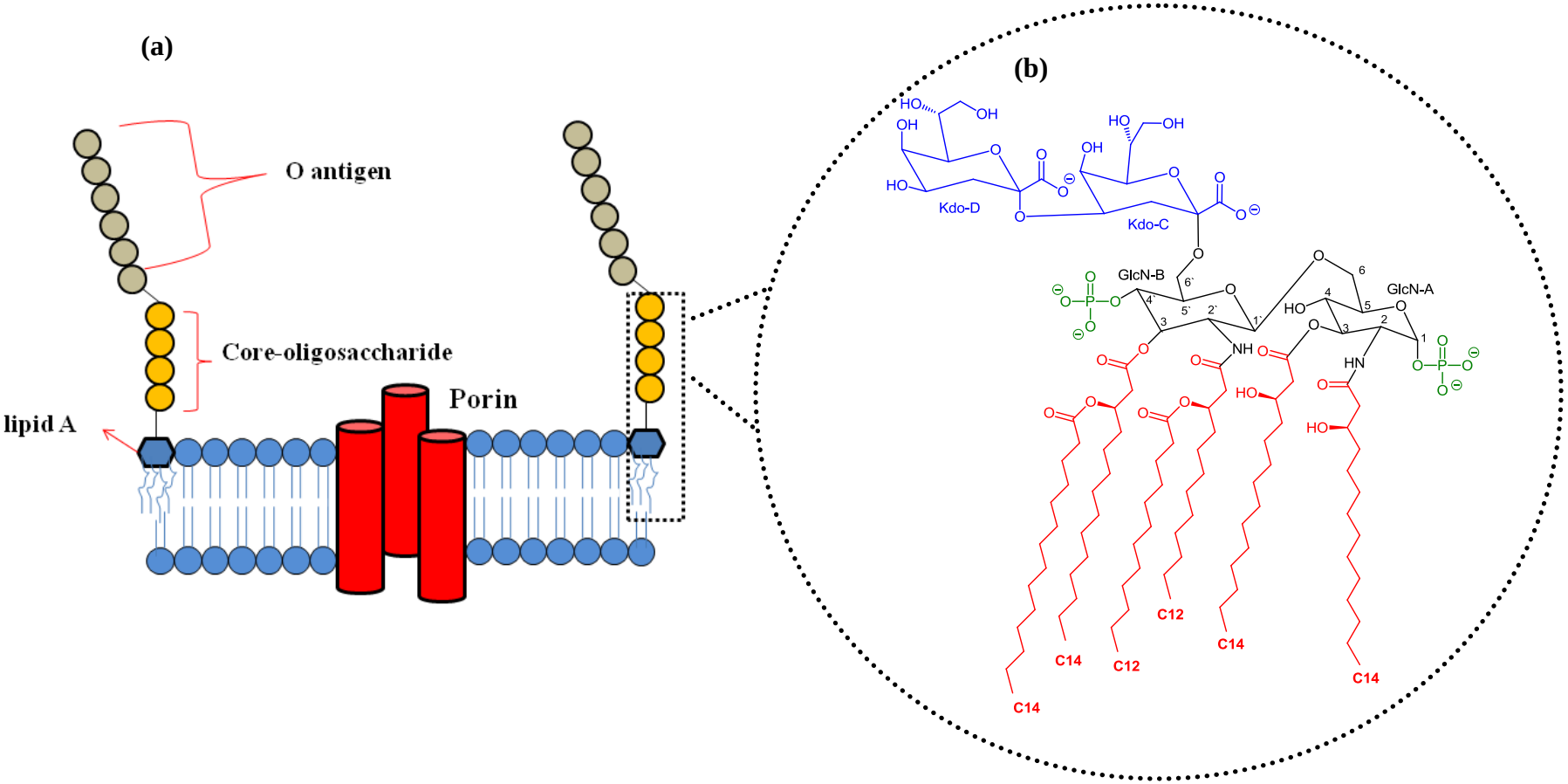

Figure 1.6 (a) Schematic representation of the outer membrane structure of Gram-negative bacteria. **(b)** Chemical structure of lipid A and core oligosaccharide domain of *E. coli*. The disaccharide glucosamine, fatty acid chains and phosphate groups of lipid A are highlighted in black, red and green respectively. The Kdo domains of the core oligosaccharide are highlighted in blue.[70]

1.3.2.2 Selectivity of AMPs to bacterial cells

While cationic AMPs (cAMPs) selectively interact with the anionic teichoic acids of Gram-positive bacteria, they form selective electrostatic interactions with the anionic phospholipids and the LPS of Gram-negative bacteria.[27,30] Upon this interaction, the peptide undergoes a "self-uptake", via the peptidoglycan layers in both bacterial membranes, towards the cytoplasmic membrane.[71]

In both cases, a high density of anionic phospholipids, such as phosphatidylglycerol (PG) and cardiolipin, is present in the outermost leaflet of the bacterial membrane (Figure 1.7). Eukaryotic membranes, conversely, contain zwitterionic phospholipids, such as phosphorylethanolamine, phosphatidylcholine and sphingomyelin allowing selective binding of cAMPs onto the bacterial membrane. Eukaryotic membranes also contain rigid cholesterol moieties, which are known to increase the cohesion and mechanical stiffness of the membrane, causing membrane fluidity, and further preventing interaction with AMP.[27,72]

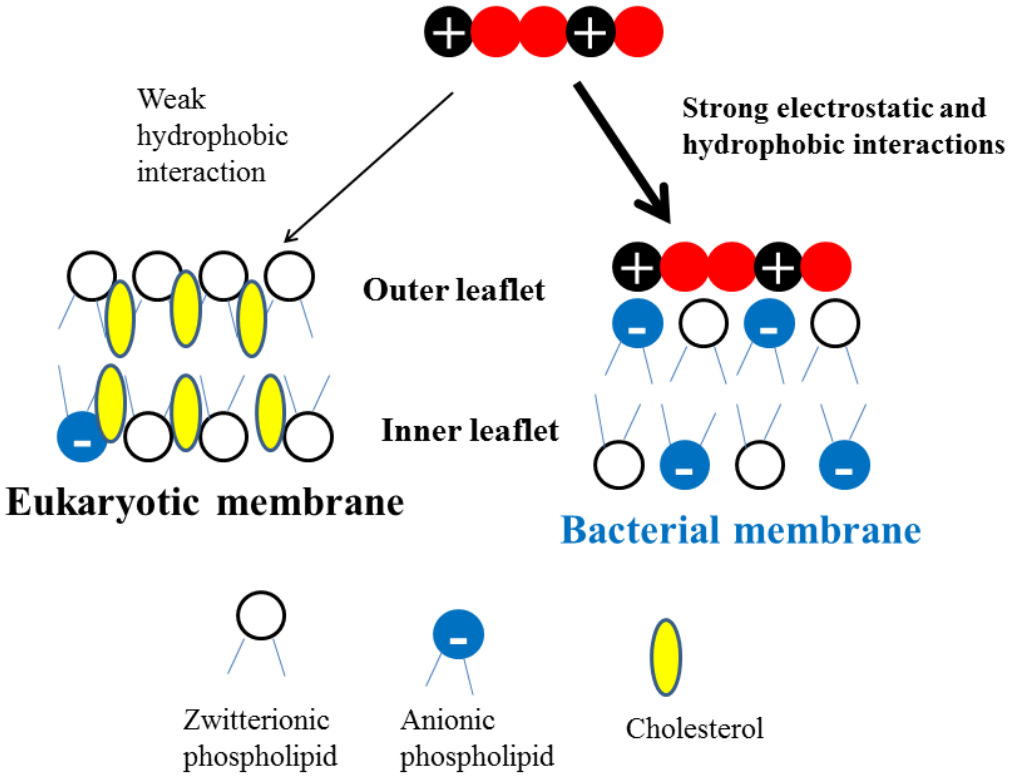

Figure 1.7 Selective interaction of AMPs with bacterial membranes.[73]

Several models have been proposed in the literature regarding the orientation of cAMPs during membrane interaction and subsequent membrane lysis. These models include the barrel stave, toroidal pores, carpet model and Shai-Matsuzaki-Huang (SMH) models.[27,30,74] The SMH model attempts to combine the different models proposed into a single, universal model, to describe how most cAMPs initiate antibacterial activity.[27,74-75]

1.3.2.3 Shai-Matsuzaki-Huang (SMH) model

According to the SMH model, antibacterial activity can be initiated at low micromolar concentrations of AMPs. The initial interaction with the membrane occurs in a manner similar to the carpet model.[27,75] The peptides bind to the bacterial surface at multiple locations, and cover the surface, like a carpet, parallel to the bacterial membrane.[30] This, in

turn, leads to the thinning of the outer membrane, resulting in a strain within the bilayer. The strain causes the membrane to fold inwards, leading to the formation of wormholes, or transient pores, which facilitate the translocation of the cAMP into the inner membrane, resulting in its fragmentation and disruption. In some cases, the cAMPs can also diffuse, through an intracellular target, to the inner leaflet.[27,76]

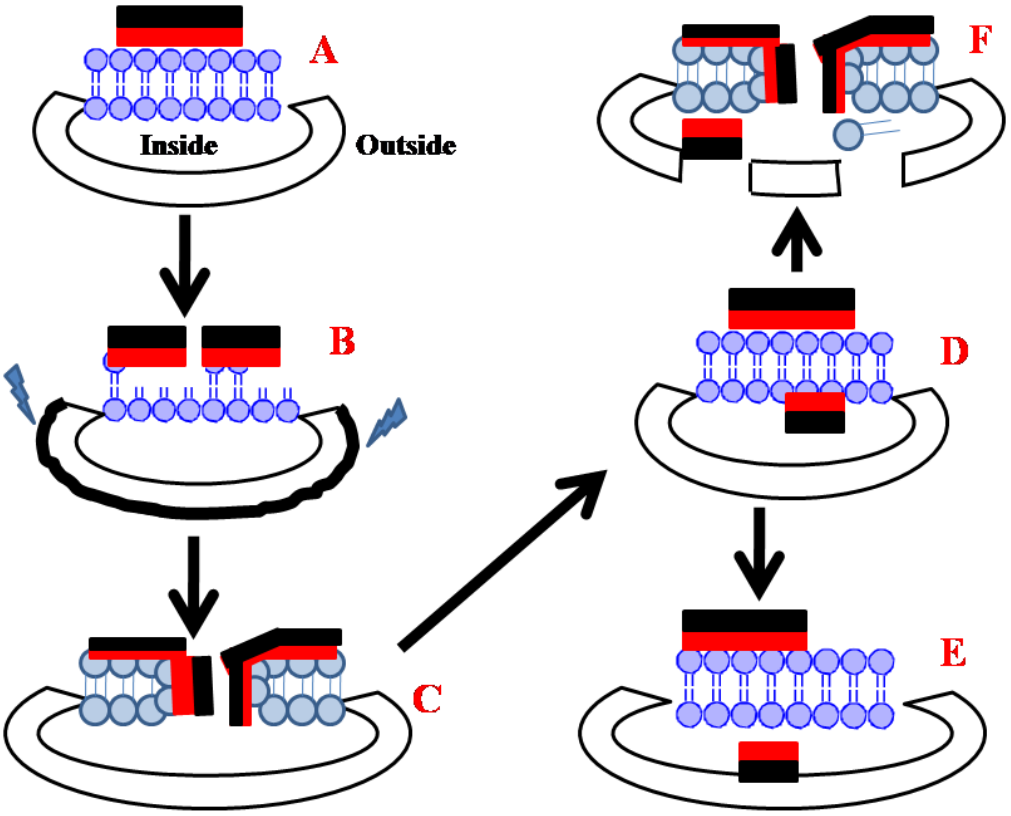

Figure 1.8 Shai-Matsuzaki-Huang model. (**a**) AMPs bind to the membrane in a parallel orientation similar to carpet model. (**b**) Membrane thinning in presence of the bound peptide. (**c**) Formation of transient or wormhole pores. (**d**) Translocation of AMP into the inner leaflet. (**e**) In some cases, translocation to inner leaflet occur in a non-membrane lytic fashion. (**f**) Membrane disruption and cell lysis.[27]

1.3.2.4 Inhibitory activity of AMPs against biofilms

Table 1.3 provides a comprehensive summary of AMPs that have been successfully used to inhibit bacterial biofilms, by targeting different stages of biofilm formation. Most AMPs are membrane-lytic and, unlike antibiotics, can inhibit slow-growing and dormant cells within biofilms. Generally, AMPs exhibit faster kinetics and diffuse more efficiently than antibiotics. Therefore, AMPs have the ability to prevent the initial attachment of planktonic bacteria to surfaces, and to eradicate pre-formed biofilms, by penetrating through the EPS matrix. In addition, AMPs can be used synergistically, with antibiotics, to inhibit bacterial biofilms.[77] The generation of antibacterial surfaces using AMPs as surface coatings is another application of AMPs that has tremendous potential in medical industry and will be discussed in Chapter 5.

Table 1.3 Selected examples of AMPs active against bacterial biofilms.

Peptide	Class	Anti-biofilm activity	Ref
LL-37	α-helical, cationic	Preventing initial attachment of biofilms of *P. aeruginosa*, *E. coli*, *S. Epidermidis* and *S. aureus.*	78-80
		Inhibition of pre formed biofilms of *P. aeruginosa.*	78
		Inhibition of biofilm formation of *P. aeruginosa* by QS down regulation.	78
		Eradicate biofilms of *P. aeruginosa* in sinus mucosa of rabbits.	81
Indolicidin	High Trp content	Prevention of biofilm formation of *P. aeruginosa* and MRSA.	78,82
		Prevention of MRSA biofilm formation in conjugation with antibiotics (daptomycin, linezolid, ciprofloxacin and azithromycin).	82
Human β defensins	β- Sheet	Prevent biofilm formation and dispersion of mature biofilms of MRSA and MRSE.	83
		Reduce the metabolic activity of fungal *C. neoformans* biofilms.	84
		Human β defensins have been combined with ultra-targeted microbubbles as delivery vectors to inhibit biofilms of *S. aureus* and *S. epidermidis.*	85
Tachyplesin III	β- Sheet	Prevent biofilm formation of *P. aeruginosa.*	86
		Used in conjugation with piperacillin-tazobactam to prevent biofilms of *P. aeruginosa.*	86
		Inhibit *P.aeruginosa* biofilms infecting urethral stent of rats.	86
Nisin	Lantibiotic	Prevent biofilm attachment of MRSA.	82
		Prevention of MRSA biofilm formation in conjugation with antibiotics (daptomycin, linezolid, ciprofloxacin and azithromycin).	82

1.4 Therapeutic limitations of AMPs

Despite showing potent antibacterial activity against MDR pathogens, only a few AMPs have gone into clinical trials, as highlighted in Table 1.4. Apart from the non-ribosomally derived AMPs, none of the AMPs isolated from eukaryotes have reached the commercial market yet.[87] Commercially available AMPs and AMPs in clinical trials are commonly used as a last resort treatment option against MDR pathogens where conventional antibiotics have failed.

Table 1.4 Peptide based antimicrobials approved for clinical use or at different stages of clinical trials.[27,87-88]

Name	Type	Application	Stage of Development	Ref
Gramicidin S	Cyclic peptide	Used topically against Gram-positive and negative pathogens.	Clinically used	89
Oritavancin	Glycopeptide	Used topically against Gram-positive pathogens.	Recently approved	90
Dalbavancin	Lipoglycopeptide	Used intravenously against Gram-positive skin infections.	Recently approved	91
Vancomycin	Glycopeptide	Used intravenously against Gram-positive pathogens.	Clinically used	92
Daptomycin	Cyclic lipopeptide	Used intravenously against Gram-positive pathogens.	Clinically used	54
Polymyxin B	Cyclic lipopeptide	Used against Gram-negative pathogens.	Clinically used	57-58
Colistin	Cyclic lipopeptide	Used against Gram-negative pathogens.	Clinically used	93
Nisin	Lantibiotic	Used as a food preservative.	Clinically used	94
MBI-594	Cationic peptide	Used topically against acne.	Phase III	95

	(indolicidin analogue)			
MBI-226	Cationic peptide (indolicidin analogue)	Catheter-related infections.	Phase III	[96]
P-113	Cationic peptide (histatin derivative)	Mouthwash against candidiasis.	Completed phase II	[97]
IB-367	Cationic peptide (protegrin analogue)	Use as aerosol by cystic fibrosis patients with chronic respiratory infections.	Phase II	[98]

Synthetic AMPs are at least 20 times more expensive than conventional antibiotics due to the excessive use of starting materials required for successful chemical synthesis.[29,36] AMP treatment against bacterial infections could cost between $USD 50-400 per gram, whereas the same treatment with aminoglycoside would cost $USD 0.8 per gram.[99] AMPs have low bioavailability due to their increased hydrophobicity. The flexibility of the peptide bond can result in the AMP interacting with various receptors, leading to poor selectivity and side effects from the activation of several targets in the body.[100]

One of the biggest challenges in AMP research is finding a good balance between *in vitro* and *in vivo* activity. Most AMPs have been reported to show excellent *in vitro* activity but very poor *in vivo* stability, because they are highly susceptible to degradation by proteases.[101]

Proteases can be generalised into two broad categories: exopeptidases and endopeptidases. Exopeptidases hydrolyse the terminal ends of peptides and can be further categorised as aminopeptidases and carboxypeptidases, which cleave the N-terminus and C-terminus of the peptide, respectively.[29,100-102]

Endopeptidases are capable of cleaving internal peptide, and can be divided into five subclasses based on their catalytic mechanism: aspartic, cysteine, threonine, serine and

metallo proteinases.[100-102] Most cAMPs are highly susceptible to trypsin (serine protease), which is capable of cleaving peptide bonds containing Arg-X and Lys-X (X being any of the 20 naturally occurring amino acids).[103] Because of this, AMPs have a short half-life and they are removed from circulation before they can reach their site of action.[29] The rapid clearance of AMPs can also prevent any immunogenic responses by the body.[29]

Several bacterial pathogens such as *P. aeruginosa* (elastase), *P. mirabilis* (proteinase), *E. faecalis* (gelatinase), *S. pyrogenes* (cysteine proteinase) and *S. aureus* (aureolysin and V8 protease) are known to secrete various proteases, as indicated in parentheses. This requires an increase in the concentration of the peptide to mediate the killing, to compensate for the partial or incomplete degradation by these proteases.[104]

1.5 Improving AMP stability through peptide modification

In order to evade peptide proteolysis, the amino acids in the sequence of AMPs can be chemically manipulated. N and C- terminal modification, the incorporation of unnatural amino acids into the sequence, and peptide cyclisation are potential methodologies to improve peptide stability.

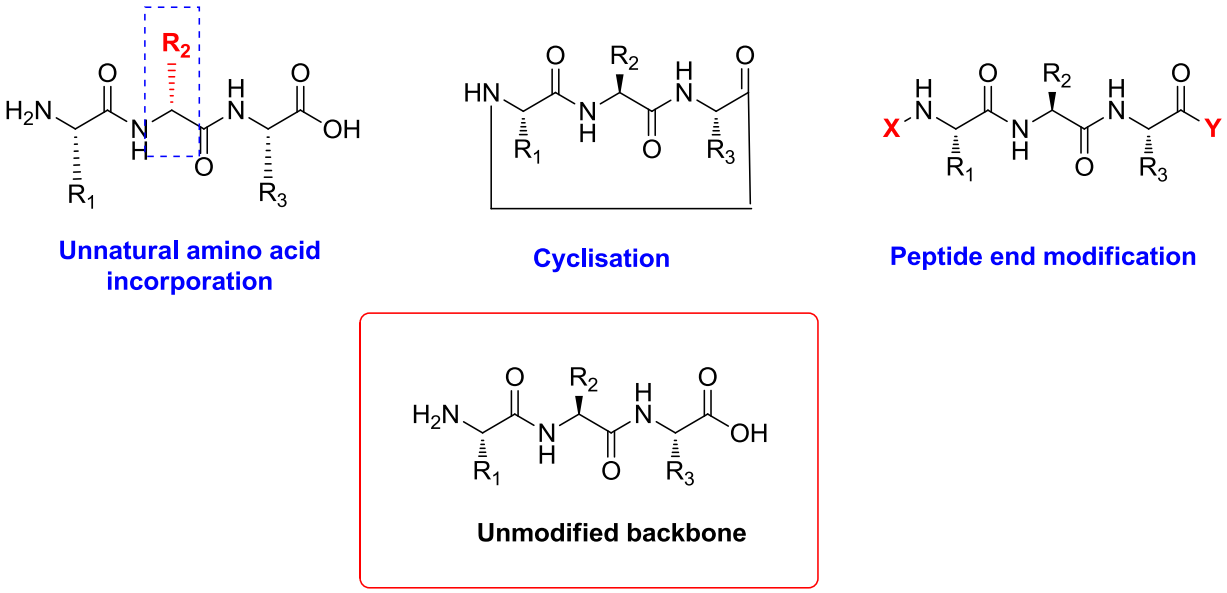

Figure 1.9 Schematic representation of peptide sequence modification to improve stability.

1.5.1 Unnatural amino acid incorporation

This strategy involves the modification of the side chains of the amino acids involved in protease recognition, by replacing them with natural or unnatural amino acids, bearing chemically similar side chains. The modified amino acids should evade the recognition site of the enzyme, to prevent cleavage, while preserving the original activity of the peptide. The introduction of unnatural amino acids can also modify the secondary and tertiary structures, which can lead to enhanced stability and activity of the sequence.[105]

Replacement of L amino acids with their D counterparts not only enhances the *in vivo* stability, but D-amino acids are also less immunogenic as compared to their L amino acid counterparts. Shai *et al.* previously replaced the L amino acids proline[7] and leucine[17],[18]of the haemolytic peptide paraxin, with D-amino acids, to improve the cytotoxicity with negligible change to the antibacterial activity.[106] Similar results were observed with melittin and gramicidin analogues, where the selective replacement of L amino acids with D amino acids

led to reduced cytotoxicity with no significant changes in the observed antibacterial activity.[107-108]

Substitution with D-amino acids can break the secondary structure of AMPs, reducing the hydrophobic interaction with mammalian cells. Hong *et al.* reported that complete D-amino acid substitution of the AMP, KSLK, led to an increased half-life (more than 400 minutes), with negligible changes in the antibacterial activity, in comparison to the natural sequence (6 minutes) in the presence of serum proteases.[109] However, partial D-amino acid substitutions in the middle of the sequence of KSLK led to loss of antibacterial activity against the tested pathogens (>100 μg/ mL), due to the disruption of the helix structure.[109] These similar studies in the litreature emphasised that systematic chirality changes with D-amino acids is necessary to maintain both stability and the antibacterial activity of the peptide.

1.5.2 Cyclisation

Cyclisation of the linear chain is a widely used strategy to improve peptide stability. Cyclisation improves peptide stability by inducing structural constraints, which can reduce the conformational flexibility and provides reduced access to the catalytic domains of proteases.[105,110]

Cyclisation has led to enhanced potency, selectivity, and bioavailability as well as increased membrane barrier permeability in AMPs.[105] This is due to the increased amphiphilicity, creating more defined hydrophobic and hydrophilic domains, due to the constraints imposed by the cyclisation. In addition, the loop formed by the cyclic peptide can mimic the secondary structure of proteins, which can also increase the binding potency and selectivity.[105]

Cyclic peptides are categorised as homodetic when cyclisation occurs via a peptide bond or heterodectic when cyclisation occurs via non-amide bond linkage such as disulfide, ester (lactone), ether or thioether bridges; carbon-carbon bonds using ring closing metathesis or

triazoles or tetrazoles, using click chemistry.[110] However, disulfide-bridged and lactone-cyclised peptides may be unstable against proteases, since these modifications occur naturally in AMPs, which are still susceptible to degradation.[110] This can be mitigated by cyclisation via carbon-carbon bonds, either by ring closing metathesis or click reactions.

Peptide bond cyclisation can occur between two terminal ends (head-to-tail cyclisation), N-terminal and side chain carboxylic acid (head-to-side chain), side chain amino group and C-terminal end (side chain-to-tail) or between two side chains (side chain-to-side chain), as illustrated in Figure 1.10. Head-to-tail cyclisation exhibits the greatest constraints, due to the intrinsic rigidity imposed by the presence of multiple consecutive amide bonds, while cyclisation involving side chain forms flexible rings.[111]

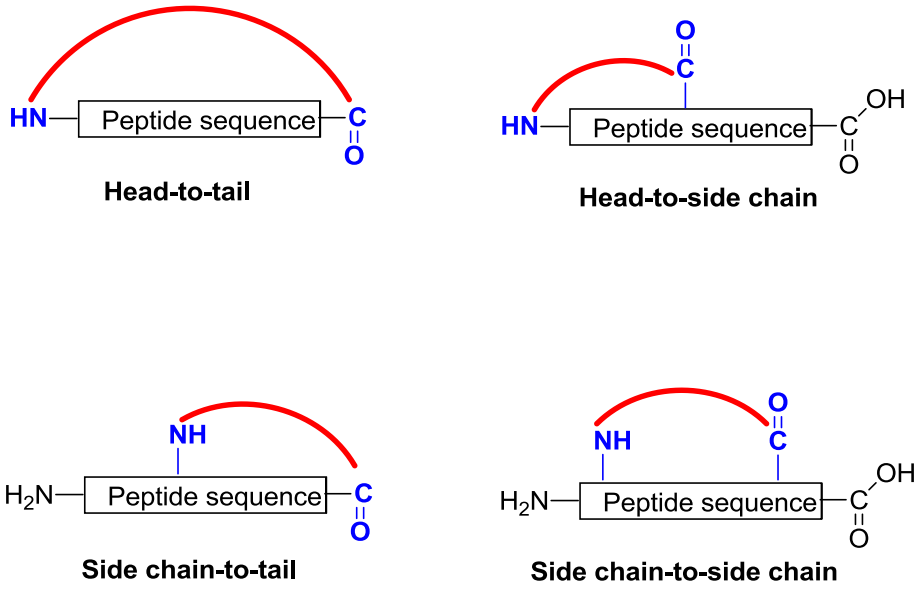

Figure 1.10 Types of homodetic cyclisation.

1.5.3 N- and C-terminal modification

N- and C-terminal modification is commonly used to improve peptide stability against exopeptidases.[105,112] C-terminal modification by amidation and N-terminal modification by acetylation can increase the stability against exopeptidases.[103,105]

Several naturally occurring AMPs such as melittin, cecropin, PR39 and polyphemusin are amidated.[43-44,113] However, no clear correlation exists between C-terminal modification and antibacterial activity.[114-116]

Gallis *et al.* reported that the N-terminal acetylation and C-terminal amidation of the AMP bactenecin did not improve its antibacterial activity.[114] However, Nakajima *et al.* reported reduced antibacterial activity of sarcotoxin 1A against *E. coli,* when the amidated C-terminus of the natural peptide was replaced with a carboxylic acid group.[115] According to Nakajima, the reduced antibacterial activity of the sarcotoxin analogues is because of the decrease in net positive charge that causes reduced membrane interaction with the negatively charged phospholipids.[115] Mor *et al.* synthesised ten truncated analogues of dermaseptin.[116] The truncated, C-terminally amidated analogue showed a to two-fold increase in antibacterial activity, compared to the C-terminal acid analogues and the natural peptide, against several bacteria (*P. aeruginosa*, *E. coli* and *E. faecalis*) and fungi (*A. niger*, *C. albicans*).

In addition to C- terminal amidation, the conjugation of bulky, hydrophobic amino acids, such as Trp, Phe and β-naphthylalanine, at the C-terminus has been shown to increase the antibiotic potency of short Trp rich AMP S1 and AMP derived from kininogen (KNK10) as well as serum stability against human elastase, autolysin and V8 proteinase, in *Staphylococcus.*[117-118]

Conjugation of long aliphatic chains to the N-terminus of the peptides to generate lipopeptides is another important modification used to enhance the therapeutic potential of

AMPs, which will be reviewed in the next section. Several lipopeptides are of natural origin and are currently being used as "last resort" therapy against MDR pathogens.

1.6 Improving AMP stability using lipidation

Lipidation is another common strategy, used by peptide chemists, to improve *in vivo* stability and to decrease peptide clearance.[119] Conjugation of longer fatty acids (> 8 carbons) can have a strong influence on secondary structure formation, due to the stronger hydrophobic interaction of the fatty acid with the peptide backbone or the side chains.[119] Laverty *et al.* have successfully demonstrated that the conjugation of long chain fatty acids (>12 carbons) to ornithine (Orn) and Trp repeated tetrapeptide led to at least a 10 fold increase in antimicrobial activity.[120] The increased antibacterial activity can be attributed to superior binding interactions of the lipidated peptide with the membrane.

Lipopeptides are also synthesised by the NRP of some bacterial species (*Bacillus, Paenibacillus, Pseudomonas* and *Streptomyces*) and fungi (*Aspergillus*).[121] Like many of the non-ribosomally produced AMPs, lipopeptides are structurally diverse due to variations in the fatty acid sequence, amino acid composition and the type of structure (linear, lactam or lactone). Therefore, these diverse lipopeptides target a wide range of pathogens with different mechanisms of action.

Synthetic or naturally derived lipopeptides offer several advantages that can be developed into potential therapeutics. In addition to the N-terminal acetylation by various fatty acid moieties, lipopeptides contain non-proteogenic amino acids as well as a cyclic ring structure via peptide or an ester bond, which make them generally more stable against proteases than ribosomally synthesised AMPs.[119,122]

Most clinically approved peptide antibiotics are of lipopeptide origin (Table 1.4). Several cationic lipopeptides display the ability to neutralise endotoxins, produced by Gram-negative pathogens, by binding to the LPS and can therefore, suppress septic shock syndrome.[122]

Lipopeptides such as surfactin are used in dermatological cosmetic applications due to their strong surfactant property, high biocompatibility and low cytotoxicity against mammalian cells. [123-124] Surfactin and rhamnolipids are also used in the food industry to maintain stability, texture, and as an emulsifier.[124]

1.6.1 Classes of lipopeptides

Naturally occurring lipopeptides can be categorised into three different classes (Table 1.5).

Table 1.5 Naturally occurring lipopeptides based on their structure.[88]

Type	Source	Susceptible strains	Ref
Lactam			
Polymyxin	*Paenibacillus polymyxa*	Gram-negative *(P. aeruginosa, A. baunmannii*, and *K. pneumoniae*).	57-58
Octapeptin	*Bacillus* and *Paenibacillus* sp	Various Gram-negative (*P. aeruginosa, A. baunmannii* and *K. pneumoniae*), positive (*S. aureus*) and fungi (*C. albicans*).	125
Polypeptin	*Paenibacillus* sp	Various Gram-negative (*P. aeruginosa*), positive (MRSA) and fungi (*F. graminearum*).	126
Friulimicins	*Actinoplanes friuliensis*	Gram-positive (MRSA and VRE).	127
Marihysin A	*Bacillus marinus B*	Low broad spectrum activity against	128

		plant pathogens.	
Laspartomycin	*Streptomyces viridochromogenes*	Gram-positive (MRSA and VRE).	[129]
Echinocandins	*Aspergillus nidulans var*	Potent antifungal (*C. albicans* and *Aspergillus* sp).	[130]
Iturins	*Bacillus subtilis* and *Bacillus amyloliquefaciens*	Antifungal (*Aspergillus* sp, *Penicillium* and *Pyricularia* sp).	[131]
Bacillomycin	*B. subtilis*	Antifungal (*Aspergillus* sp, *C. albicans*).	[132]
Lactone			
Daptomycin	*Streptomyces roseosporus*	Gram-positive (MRSA and VRE).	[54]
Surfactin	*B. subtilis*	Gram-positive (*E. faecalis*) and Gram-negative (*E. coli*).	[133]
Fengycin	*B. subtilis*	Antifungal (*Pyricularia oryzae* and *Curvularia lunata*).	[134]
Empedopeptin	*Empedobacter haloabium*	Gram-positive (MRSA and PRSP).	[135]
Tripropeptin	*Lysobacter* sp	Gram-positive (MRSA, PRSP and VRE).	[136]
Calcium dependent antibiotics (CDAs)	*S. coelicolor* A3	Gram-positive in presence of calcium (*S. aureus*).	[137]
Brevistin	*B. brevis*	Gram-positive (*S. aureus* and *S. pneumoniae*).	[138]

Fusaricidins	*Paenibacillus polymyxa*	Antifungal (*Fusarium* and *Aspergillus*) and Gram-positive (*S. aureus*).	[139]
Linear			
Cerexin	*Bacillus cereus*	*S. aureus* and *S. Pneumoniae.*	[140]
Tridecaptin	*Paenibacillus polymyxa*	*K. pneumoniae* and *E. Cloacae.*	[141]
Tauramadine	*Brevibacillus laterosporus*	*Enterococcus* sp.	[142]
Dragomide	*Lyngbya majuscula*	*Plasmodium falciparum, Leishmania. donovani* and *Trypanosoma cruzi.*	[143]

Lipopeptides can exist as either lactams, where the cyclic peptide is formed via peptide bond, as lactones (depsipeptide), where cyclisation occurs via an ester bond or in the linear form. As is evident from Table 1.5, most of the isolated lipopeptides have a cyclic structure.

Daptomycin (see section 1.6.1.1) and polymyxins (see section 1.6.1.2) are two important cyclic lipopeptides with lactone and lactam rings respectively. These cyclic lipopeptides are used clinically against multi drug-resistant Gram-positive (daptomycin) and negative (polymyxin) pathogens. Both daptomycin and polymyxin are extensively studied in the literature to understand their mode of action against pathogens, as well as to identify chemical moieties important for their potent antibacterial activity, thus will be summarised in the following sections.

In 2011, the US Food and Drug Administration (FDA) approved polymyxin B for parenteral administration against *P. aeruginosa, H. influenzae, E. coli, A. aerogenes* and *K. pneumoniae*.[144] This recent approval is an encouraging sign and testimony to the potential

lipopeptides as emerging antibiotics, to treat life threatening infections caused by MDR pathogens. Recently octapeptins (1.6.1.3) have been evaluated as new source of antibiotics against both Gram-positive and negative bacteria.

1.6.1.1 Daptomycin

Daptomycin is a cyclic depsipeptide, isolated as the minor component of a complex lipopolysaccharide mixture (A21978C) in the 1980s, from the soil actinomycete *Streptomyces roseosporus*.[54,124] Daptomycin showed potent activity, with MIC less than 1 µg/mL, against several Gram-positive bacteria including MRSA, VRE, PRSP and methicillin-resistant *Staphylococcus epidermidis* (MRSE).[145]

Daptomycin was approved by the FDA in 2003, for treatment against complicated skin and skin-structure infections, right-sided endocarditis and serious bacterial infections caused by MRSA, VRSA and enterococci.[121] Daptomycin can target these pathogens during the logarithmic growth phase as well as the dormant stationary growth phase of the bacteria and is able to prevent bacterial adhesion to the surfaces of medical devices and the colonisation of pre-existing biofilms.[146-148]

It consists of a 10-membered, cyclic core structure with unnatural amino acids (ornithine, threo-3-methylglutamic acid and kynurenine) and D-amino acids (Asn, Ala and Ser) (Figure 1.11). The peptide core is cyclised by an ester bond between the terminal kynurenine and the hydroxyl group of Thr. Subsequently, the N-terminally linked decanoyl fatty acid is conjugated to a linear tripeptide sequence (Trp-Asn-Asp), which is further conjugated to the peptide ring via an amide bond.[54] Daptomycin is an anionic (-3 at neutral pH) lipopeptide, due to the presence of multiple Asp acids, with well-segregated hydrophobic and hydrophilic domains.

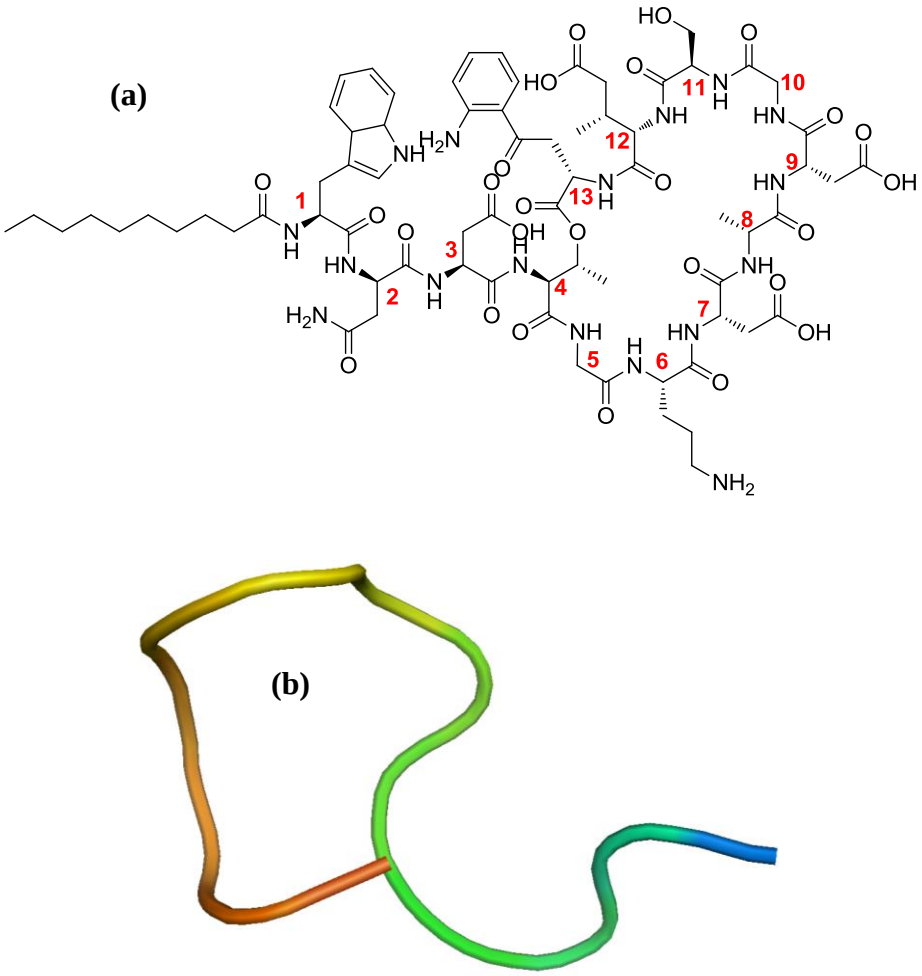

Figure 1.11 (a) Chemical structure of daptomycin and **(b)** 3D structure of daptomycin (PDB code: 1T5N).[149]

CB-183,315 is an orally available lipopeptide developed by Cubist Pharmaceuticals currently undergoing phase III trials for treatment against *Clostridium difficile* associated diarrhoea. This lipopeptide has similar peptide backbone structure and mechanism of action as daptomycin but a short, unsaturated fatty acid, (*E*)-3-(4-pentylphenyl) but-2-enoic acid is linked to the tripeptide sequence.[150]

1.6.1.1.1 Mode of action

Calcium, at 1.25 mM or 50 mg/L, is a pre-requisite for the observed antibacterial activity of daptomycin.[54,124] The importance of calcium ions was confirmed by the observed reduction in the antibacterial activity of daptomycin, against Gram-positive species such as *Staphylococcal*, *Enterococci* and *Pneumococcal* between 16 to 64 folds, in the absence of calcium ions at physiological concentration.[151-152]

Daptomycin aggregates into an oligomeric structure (14 to 16-mers), in the presence of Ca^{2+}, to initiate the antibacterial activity.[121] Daptomycin interacts with the negatively charged cytoplasmic membrane like a cationic AMP; by forming a pore like structure within the cytoplasmic bilayer, leading to membrane perturbation, leakage of intracellular ions and depolarisation followed by rapid cell death.[153]

However, the exact sequence of events leading to bacterial cell death caused by daptomycin is still unknown. Jung *et al*. suggested that membrane depolarisation is a consequence of cellular death.[149] They simultaneously studied the rate of antibacterial activity of and membrane depolarisation by daptomycin, at 10 µg/mL, against *S. aureus*, using a cyanine dye- 3, 5-dipropylthiacarbocyanine ($DiSC_35$) and observed that 99% of the bacterial cells were killed within 90 minutes of incubation, but only 36% membrane depolarisation was observed within the same time frame. In fact, membrane depolarisation was not evident within the first 20 minutes of the experiment; however, a majority of the bacterial cells were killed within the first 10 minutes due to the faster killing kinetics of this lipopeptide. This delay between the antibacterial activity and membrane depolarisation could suggest that depolarisation occurs as a consequence of bacterial cell death.

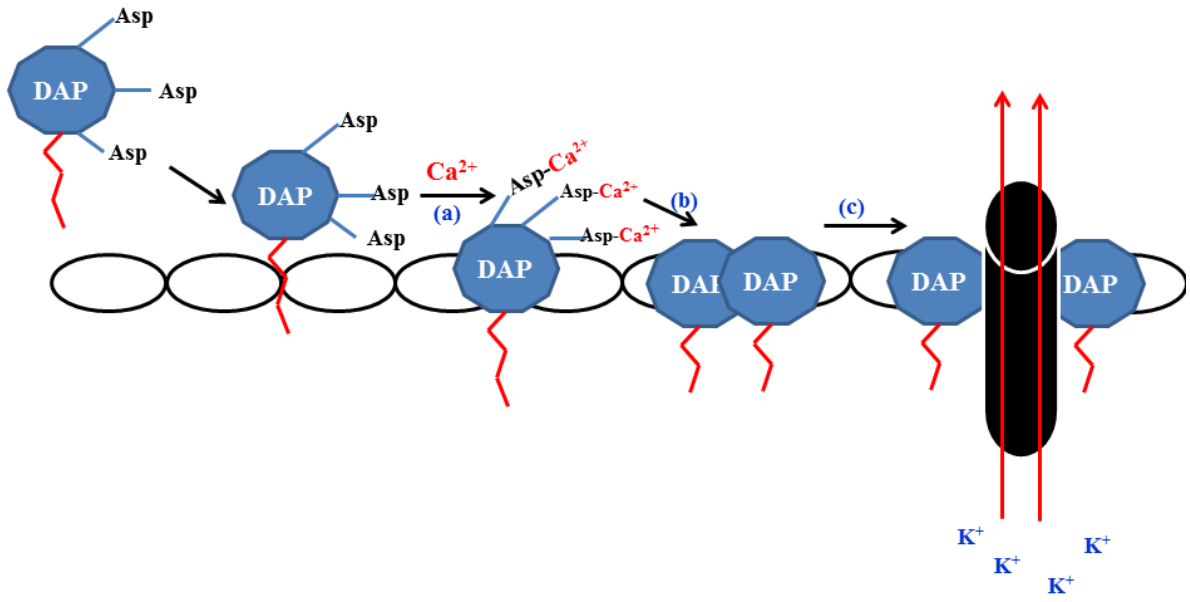

Figure 1.12 Mechanism of action of daptomycin. (**a**) Side chain of Asp interacts with Ca^{2+} facilitating interaction with bacterial membrane similar to cationic AMPs. (**b**) Once inserted into the membrane, daptomycin oligomerizes. (**c**) The aggregated daptomycin forms pore like structures, which leads to leakage of intracellular ions, such as potassium, leading to bacterial cell death.[154]

1.6.1.1.2 Structure-activity relationship (SAR) studies

Several structure-activity relationship (SAR) studies have been carried out on daptomycin to identify potent analogues.[155] Increasing the fatty acid chain length to 13 carbons resulted in improved *in vitro* and *in vivo* antibacterial activity against *S. aureus*.[155] However, the increased activity was compromised by an increase in acute toxicity with the modified analogues.

Removal of the fatty acyl chain from daptomycin resulted in a complete loss of antibacterial activity, highlighting the importance of hydrophobic interaction between the fatty acid chain and the bacterial membrane. The Orn was not crucial for the observed antibacterial activity; however, the free amine on one of the side chains of Orn was critical to maintain it.[155]

Replacement of the anionic Asp residues at positions 7 and 9 led to decreased antibacterial activity, whereas replacement of the Asp residues at position 3 and 12 did not affect it at all.

These observations suggest that the Asp at positions 7 and 9 are critical to Ca^{2+} binding activity.[155]

1.6.1.2 Polymyxin

Polymyxins are a closely related family of cyclic lipopeptides, isolated in the early 1940s from the soil bacterium *Paenibacillus* (*Bacillus) polymyxa*.[57-58] Polymyxins are active against MDR Gram-negative pathogens and have a high affinity toward the lipid A component of the lipopolysaccharides of outer bacterial membranes.

The lipid A of Gram-negative bacteria is known to cause septic shock, by inducing an uncontrollable immune response. Macrophages have Toll like receptors (TLR-4), which bind to the lipid A, to induce the release of cytokines such as interferon-γ, tumour necrosis factor (TNFα) and interleukin-1 and 6 (IL-1 and IL-6), involved in immune responses. However, during an uncontrollable bacterial invasion, these macrophages can also damage the surrounding endothelial cells such as blood vessels, resulting in a decrease in cardiac function and consequently leading to septic shock.[156] In addition to their potent activity, polymyxins are also capable of minimising this septic shock by binding to the LPS, neutralising their ability to cause any immune response.[157]

Polymyxin B (PMB) and polymyxin E (colistin) have had extensive use clinically.[158] Polymyxin B (B_1 and B_2) and colistin (A and B) are commercially available as a mixture of fatty acid analogues. Polymyxin B_1 and colistin A contain the N-terminally linked fatty acid, (*S*)-6-methyl-octanoic acid whereas polymyxin B_2 and colistin B are conjugated to a shorter fatty acid, (*S*)-6-methyl-heptanoic acid (Figure 1.13).[159-160]

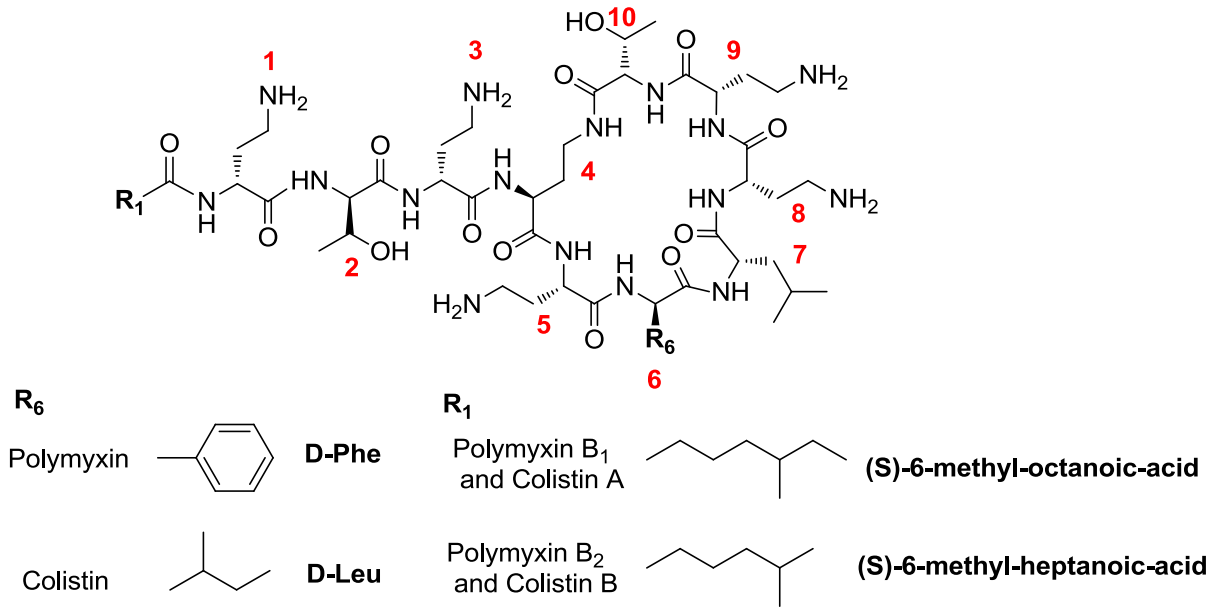

Figure 1.13 Structure of polymyxin B and colistin.

PMB is currently administered as a water-soluble sulphate salt, while colistin is formulated as a methane sulfonate sodium salt, which hydrolyses to form the active polymyxin E, as a prodrug to eliminate toxic side effects. Colistin is also administrated as a sulphate salt.[161] Colistin methanesulfonate is available as an aerosol formulation while colistin sulphate can be used as a topical application and orally.[160]

Both polymyxin B and colistin contain a high abundance of the unnatural amino acid α,γ-diaminobutyric acid (Dab) and one Thr. Polymyxin and colistin are both cyclised by a peptide bond between the side chain of Dab^4 and the carboxylic acid of Thr^{10}, to form a seven membered lactam ring. The acyl fatty acid chains of polymyxins are linked to the α-amino group of terminal Dab. Colistin contains D-Leu at position 6, whereas polymyxin B contains D-Phe in the same position of the peptide sequence.[159-160]

1.6.1.2.1 Anti-biofilm activity of polymyxins

Polymyxin and colistin have also shown anti-biofilm activity at higher concentrations.[162-164] Polymyxin, at ten times the MIC (20 mg/L), managed to inhibit the formation of *P. aeruginosa* biofilms by more than 1 log difference (>90% inhibition).[164] The anti-biofilm activity of polymyxin was further enhanced by a factor of 0.5 log (~ 45%) in the presence of electrical current.[164]

P. mirabilis is a Gram-negative opportunistic pathogen that resides in the urinary tract of humans, and is highly resistant to polymyxin B. Liu *et al.* demonstrated planktonic and biofilm cells of *P. mirabilis* becoming increasing susceptible to PMB treatment when it was accompanied by a concurrent treatment with heptadecadienylhydroquinone (HQ17-2), a hydroquinone derivative.[165]

Marumo *et al.* have reported that the minimum concentration of colistin, required to inhibit the biofilms of the multi-drug resistant *P. aeruginosa* strains MDRP-YMD and ATCC27853, was 42 μg/mL, which is ten times the MIC required to inhibit the planktonic cells.[162] Colistin has been successfully used in conjugation with tobramycin to effectively inhibit the biofilm formation of *P. aeruginosa, in vitro* as well as *in vivo*, in the lungs of rats infected with *P. aeruginosa* strain.[163] This combination therapy managed to inhibit static biofilms up to 3 logs killing difference (>99% killing) and demonstrated up to an 80% reduction in dynamic biofilm architecture. All of the infected rats survived up to seven days with the combination therapy, whereas 20% of the infected rats, treated with colistin, died.[163] These results emphasise the synergistic effect that lipopeptides have with conventional antibiotics, to effectively treat bacterial biofilms.

1.6.1.2.2 Mode of action

The mechanism of action of polymyxin antibiotics is highlighted in Figure 1.14. The initial step involves an electrostatic interaction of the cationic Dab molecules with the lipid A of LPS, by displacing divalent cations, such as Ca^{2+} and Mg^{2+}. These cations are known to stabilise lipid A by acting as a "bridge".[27] The initial electrostatic interaction facilitates the positioning of the hydrophobic portion (fatty acid and "D-Phe^{6}-L-Leu^{7}" dipeptide) of polymyxin closer to the outer membrane. The hydrophobic core of PMB interacts with the fatty acid chain of the outer membrane, thus weakening the lipid A and expanding the outer membrane.[160,166]

This hydrophobic interaction is crucial for the LPS neutralisation capability of PMB, since the fatty acid devoid polymyxin B analogue, polymyxin nonapeptide (PMBN), had similar affinity towards the LPS but did not show any anti-endotoxin activity.[167-168] This resulted in the leakage of intracellular ions and membrane lysis.

Subsequently, PMB interacts with the inner membrane via a "self-uptake" mechanism, causing membrane disruption, either by thinning or by the formation of pores, eventually leading to cellular death. [166,169]

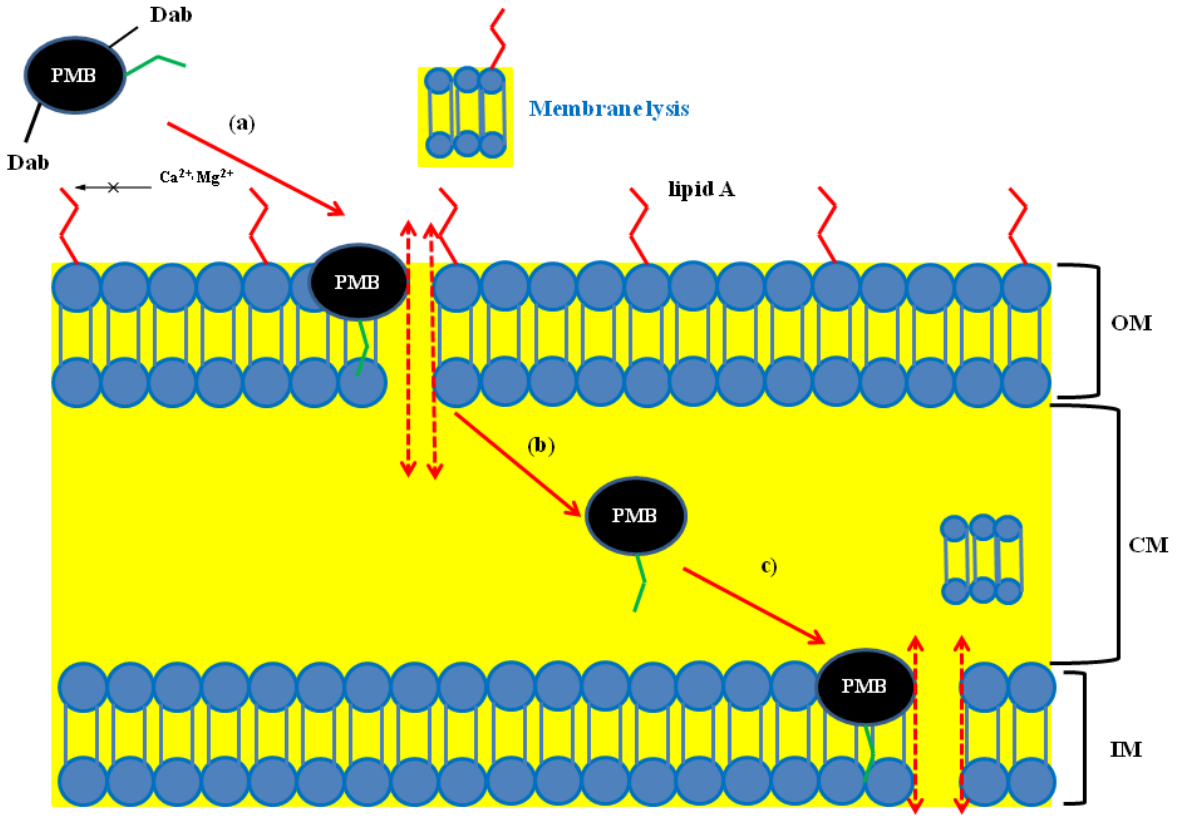

Figure 1.14 Mechanism of action of polymyxin antibiotics: (**a**) PMB interacts with the lipid A of the lipopolysaccharide by displacing divalent cations. The hydrophobic core of PMB interacts with the fatty acid tail of the outer membrane (OM), causing lysis and leakage of intracellular ions. (**b**) PMB translocates from cytoplasmic membrane (CM) using "self-uptake" mechanism to the inner membrane (IM). (**c**) PMB interacts with the inner membrane, leading to thinning of the membrane structure and further causing lysis of the inner membrane, ultimately leading to cellular death. Adapted from Velkov. [160]

1.6.1.2.3 Nephrotoxicity of polymyxin

Despite entering the clinic several decades ago, polymyxins were abandoned in the 1980s due to their nephrotoxicity. It is believed that the nephrotoxic effect of PMB is related to its cationicity and the N-terminal fatty acid.[170] The fatty acid-devoid PMB analogue PNB, showed reduced antibacterial activity but with minimum toxicity.[170] It is hypothesised that the nephrotoxicity of PMB is due to its interaction with the megalin receptor, which is abundant in the apical membrane of the proximal tubules of the kidneys.[171]

Recent studies have shown that the side effects of polymyxin can be controlled by using a lower dosage of polymyxin than used during early clinical settings with less toxicity than previously reported.[172] For instance, Azad *et al.* demonstrated that significantly high concentration of polymyxin B at 1000 x MIC (2 mM) was required to induce apoptosis (80% apoptosis after 24 hours).[173]

Northern Antibiotics Ltd. has developed two polymyxin analogues, NAB739 and NAB7061, to improve the toxicity profile of PMB. Both analogues contain the same lactam core ring as polymyxin, but the fatty acid portion and terminal Dab are replaced with an octanoyl fatty acid conjugated to a dipeptide sequence, Thr-D-Ser and Thr-Abu (aminobutyric acid) for NAB739 and NAB7061 respectively. These analogues have a lower charge (+3) than PMB (+5) and showed up to a 5-7 fold lower affinity than PMB to an isolated brush border membrane of rat kidney, indicating reduced nephrotoxicity.[174-175]

The improved nephrotoxicity of NAB7061 was compromised by reduced antibacterial activity, but was restored when administered along with a hydrophobic antibiotic, such as rifampin.[174-175] Although no synergistic effect was reported with NAB739, potent antibiotic activity was observed. Currently, these analogues are in phase I clinical trials.

1.6.1.3 Octapeptins

Octapeptins are isolated from *Bacillus* species and are a family of closely related cyclic lipopeptides. They contain a heptapeptide ring moiety, with Dab and Leu as the major components and Phe and Ser present to a lower extent. A dipeptide, consisting of N-terminally conjugated β-hydroxy fatty acid, is linked via a peptide bond to the heptapeptide ring moiety. As evident from Figure 1.15, octapeptins have a very similar structure to polymyxins. Both polymyxins and octapeptins have Dab at position 2, 3, 6 and 7 and hydrophobic amino acids at positions 4 and 5 of the cyclic ring. Position 8 has L-Leu and L-

Thr in octapeptins and polymyxins respectively. The fatty acids conjugated to octapeptins are β-hydroxy fatty acids, which are also present in polymyxin B_6. In fact octapeptins can be classified as "truncated" polymyxins.[144]

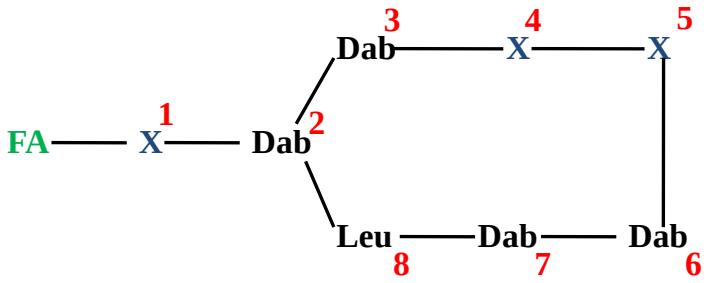

Octapeptin	X^1	X^4	X^5
A	D-Dab	D-Leu	L-Leu
B	D-Dab	D-Leu	L-Phe
C	D-Dab	D-Phe	L-Leu
D	D-Ser	D-Leu	L-Leu

Figure 1.15 General structure of octapeptins. FA denotes a fatty acid. Common amino acids within each of the octapeptin family are highlighted in black and dissimilar amino acids (X) between the octapeptin families are highlighted in blue.

Currently there are four sub-classes of octapeptins (octapeptin A-D), each with subtle structural variations. Octapeptin A has no Phe in the sequence, whereas octapeptins B and C contain one Phe in position 5 and 4 respectively. Octapeptin D has a Ser instead of a Dab at position 1. These sub classes of octapeptins can be further categorised based on the size of their fatty acid chains.[176]

In 2012, Qian *et al.* isolated a novel, cyclic lipopeptide from the Gram-negative pathogen *Paenibacillus tianmunesis*.[177] The newly isolated lipopeptide was named battacin, or octapeptin B5, and it is the first octapeptin to be isolated from the *Paenibacillus* species.

1.6.1.4 Battacin

The overall chemical structure of battacin was resolved using a combination of mass spectrometry (ESI and tandem MS/MS), ion exchange chromatography, liquid chromatography mass spectrometry (LCMS) and gas chromatography.[177] The following structure was proposed based on the spectral information (Figure 1.16).

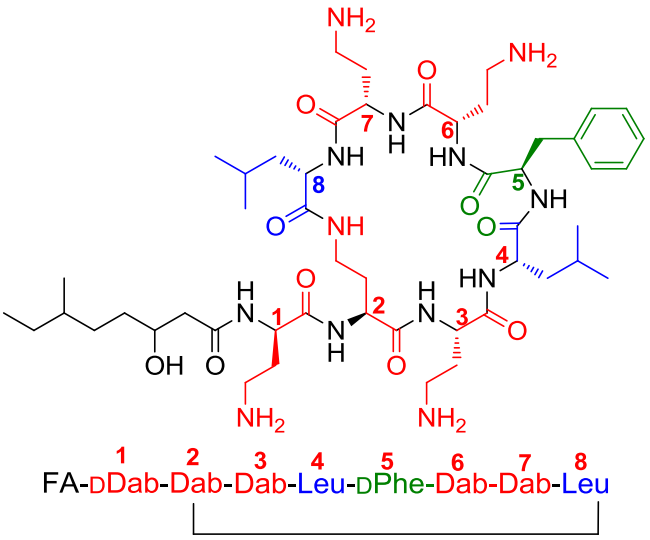

Figure 1.16 Proposed structure and sequence of battacin; FA denotes 3-hydroxy-6-methyl-octanoic acid.[177]

As evident from Figure 1.16, battacin has five Dab, two Leu and one Phe residues, with the side chain of Dab^2 forming a peptide bond with the carboxylic acid of Leu, to form a heptapeptide ring. A dipeptide, also consisting of N-terminally conjugated β-hydroxy fatty acid, 3-hydroxy-6-methyl-octaonic acid is linked via a peptide bond to the heptapeptide ring moiety. Battacin has been proposed to have L and D chiral amino acids at positions 4 (L-Leu) and 5 (D-Phe) of the peptide sequence, unlike other octapeptins and polymyxins which is known to have D and L conformations at position 4 and 5 respectively.[177] The difference in the sequence order at positions 4 and 5 for octapeptins and battacin could possibly be because these peptides have been isolated from different bacteria.

1.6.1.4.1 Therapeutic potential of battacin

The antibacterial activity of the isolated battacin was tested against MDR Gram-negative (*P. aeruginosa*, *E .coli*, *K. pneumonia* and *A. baumannii*) and Gram-positive (*S. aureus* and *E. faecalis*) pathogens.[177] Battacin was found to be highly active against Gram-negative bacteria, with an MIC between 2-16 µg/mL. It is highly potent against *P. aeruginosa* and *E. coli*, with MIC between 2-4 µg/mL. A time-kill assay of battacin revealed a dose-dependent bactericidal effect against both *P. aeruginosa* and *E. coli*, with no significant re-growth occurring after 24 hours of incubation. [177]

Battacin also showed membrane-lytic mechanism of action similar to polymyxins.[160,166] The membrane-lytic action of battacin was confirmed by outer and inner membrane penetration assays using the fluorescent dyes *N*-phenylnaphthylamine (NPN) and $DiSC_35$ respectively.[177] The fluorescence intensity of NPN and $DiSC_35$ increased as the concentration of battacin increased, indicating the ability of battacin to penetrate both the outer and inner bacterial membrane.

The cytotoxicity of battacin against mammalian cells was evaluated following haemolysis of human red blood cells, 3-(4,5-dimethylthiaol-2-yl)-2,5-dipheynyltetrazolium bromide assay of human embryonic kidney cell lines HEK 293. The *in vivo* acute toxicity of battacin in mice was evaluated following the median lethal dose (LD_{50}) assay.[177] The concentration of battacin required to cause complete lysis of human erythrocytes was found to be 375 x MIC (750 µg/mL). Also battacin tested at a range of concentrations (from 1 µg/mL to 128 µg/mL) did not show any cytotoxicity against the HEK 293 cell lines.

Comparison of the LD_{50} of battacin (15 mg/kg) and polymyxin (6 mg/kg) indicates that battacin is at least two times less toxic than polymyxin. Mice treated with a hospital strain *E.*

coli survived up to 6 days with 4 mg/kg of battacin, which indicates that battacin has significant *in vivo* activity.[177]

The observed *in vitro* and *in vivo* activity exhibited; in conjugation with its good safety profile, could imply that battacin could potentially be a safer and better alternative to old antibiotics such as polymyxin.

1.7 Overall Aim (s) of the project.

The overall aim of my project was to investigate the potential of battacin peptides as novel broad spectrum antibacterials. To this end, the following specific objectives were undertaken.

1. The first objective of my project was to chemically synthesise battacin as well as generate a short library of battacin peptides (a series of linear and cyclic analogues) for antibacterial screening. This was achieved using a combination of solid and solution phase peptide syntheses techniques as detailed in chapter 3.
2. The second objective of my research was to evaluate the antibacterial activity of the battacin library to identify potent analogues (see chapter 4). The battacin library was screened against several plant and human pathogenic bacteria, following a minimum inhibitory concentration (MIC) assay.
3. The antibacterial mechanism of action and the anti-biofilm potential of the most potent analogue from the MIC assay was assessed by evaluating its ability to inhibit the formation of biofilms, to disperse mature biofilms and cause bacterial membrane lysis. Alanine scanning and secondary structure determination of the lead peptide was conducted to identify residues crucial for the observed activity and correlate structure to activity.
4. The final objective of the project was to evaluate the most potent lipopeptide identified from this study to be used as a potential antibacterial coating in medical implants (see chapter 5). This was undertaken through the covalent immobilisation and structural functional characterisation of glass, silicon and titanium surfaces coated with a cysteinylated analogue of the potent lipopeptide.

Chapter 2

Methodology

This page has been intentionally left blank

Chapter 2: Methodology

This chapter provides background information about the individual experimental techniques reported in this thesis. Detailed experimental procedures utilising these techniques are mentioned in Chapter 3 to Chapter 5. The linear lipopeptides (GZ3.130, GZ3.27, GZ3.38, GZ3.26 and GZ3.37) described in Chapter 3 were synthesised using solid-phase peptide synthesis (SPPS) and the cyclic lipopeptides (GZ3.15, GZ3.21, GZ3.19, GZ3.40, GZ3.55) were synthesised using a combination of SPPS and solution-phase peptide synthesis. The synthesised peptides were characterised using mass spectrometry and purified using reverse-phase high performance liquid chromatography (RP-HPLC).

The antimicrobial activities of the synthetic peptides against bacterial pathogens were determined using a broth dilution minimum inhibitory concentration (MIC) assay. An *in vitro* colorimetric assay and scanning electron microscopy (SEM) was used to elucidate the mechanism of action of the antimicrobial peptides. Structure of the most active lipopeptide was thoroughly investigated using circular dichroism (CD) and nuclear magnetic resonance (NMR) spectroscopies.

The most active lipopeptide was conjugated onto solid surfaces and these surface conjugations were characterised using water contact angle measurements, ellipsometry and X-Ray photoelectron spectroscopy (XPS).

2.1 Solution-phase peptide synthesis

In solution-phase peptide synthesis, two protected peptide fragments, dissolved in an appropriate solvent, are condensed in the presence of coupling reagents, to form the desired amide bond and peptide sequences (Scheme 2.1).

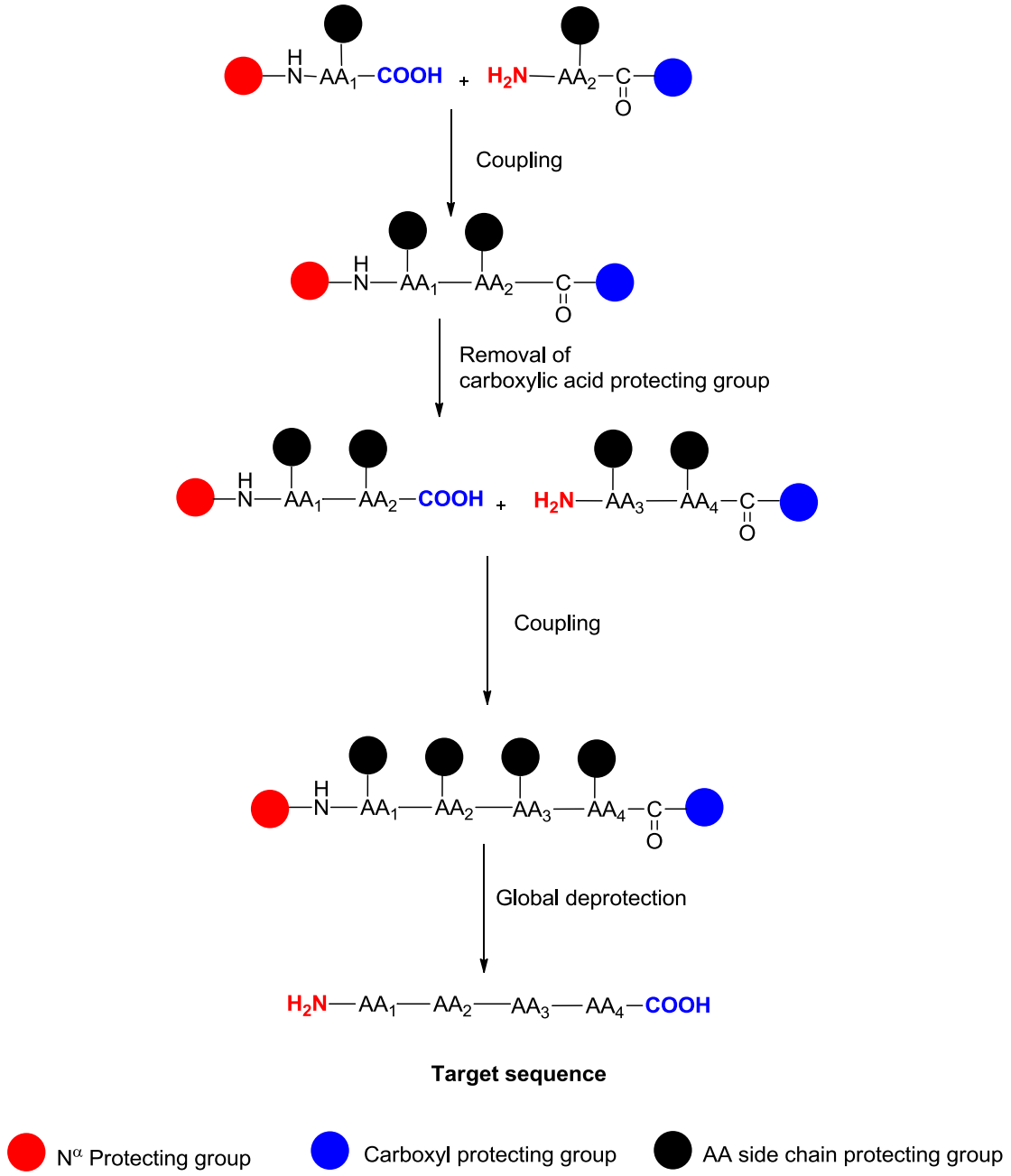

Scheme 2.1 General synthetic scheme for solution-phase peptide synthesis. AA denotes to amino acid.

Prior to the peptide bond formation, the reactive side-chains of the peptide and N- and C-terminal fragments are masked with protecting groups to prevent any undesired side reactions such as oligomerization. The newly formed peptide sequence can then be identified and purified by mass spectrometry and RP-HPLC respectively, before coupling it to another appropriately protected peptide fragment. Once the desired sequence has been synthesised, the remaining protecting groups are removed to produce the final deprotected peptide.

This technique has been successfully used, in the past, to synthesise complex peptides. For example, oxytocin is a naturally occurring cyclic hormonal peptide, used to induce labour in pregnant females. In 1953, Du Vigneaud *et al.* successfully synthesised the nine residue cyclic peptide oxytocin using solution-phase peptide synthesis, and in the subsequent year, was awarded the Nobel prize in Chemistry for the isolation, characterisation and total synthesis of this peptide.[178] Furthermore Yajima *et al.* successfully synthesised the challenging 124 residue peptide, namely ribonuclease A, using solution-phase synthesis.[179]

Due to several limitations, solution phase synthesis is currently employed less frequently to generate peptides. These limitations include prolonged reaction conditions, solubility issues of the peptide fragments, low peptide yields due to several purification cycles and the increased risk of side reactions, such as peptide racemisation.[180] Thus peptides are frequently synthesised by solid-phase peptide synthesis (SPPS) (see section 2.2). However, for the preparation of more complex peptides a combination of SPPS and solution-phase chemistry is frequently utilised.

2.2 Solid-phase peptide synthesis (SPPS)

In 1963, Bruce Merrifield reported the synthesis of a tetrapeptide on an insoluble solid support.[181] This ground breaking invention by Merrifield simplified the synthesis of long (<50 amino acids) and complex peptides, and Merrifield was awarded the Nobel prize in Chemistry, in 1984, for this discovery.[182]

During SPPS, the peptide chain is assembled from the C-terminus (carboxy terminus) to the N-terminus (amino terminus), on an insoluble solid support (resin). A linker is incorporated between the growing peptide chain and the resin to act as a spacer and to provide the required functionality to the C-terminal end of the peptide. The amino terminus of the growing peptide chain is protected with temporary protecting groups (PGs), while the reactive side-chains of the amino acids are protected with PGs that are stable during the removal of the N-terminal PG. The peptide chain is elongated by removing the N-terminal protecting group and forming a selective peptide bond with the free carboxyl end of the incoming amino acid. Any unreacted amino acids are simply filtered off and this process of chain elongation continued on the resin. Once the required sequence is assembled, the peptide is cleaved from the resin, with simultaneous removal of the side-chain protecting groups (Scheme 2.2). The crude peptide is then analysed and purified.

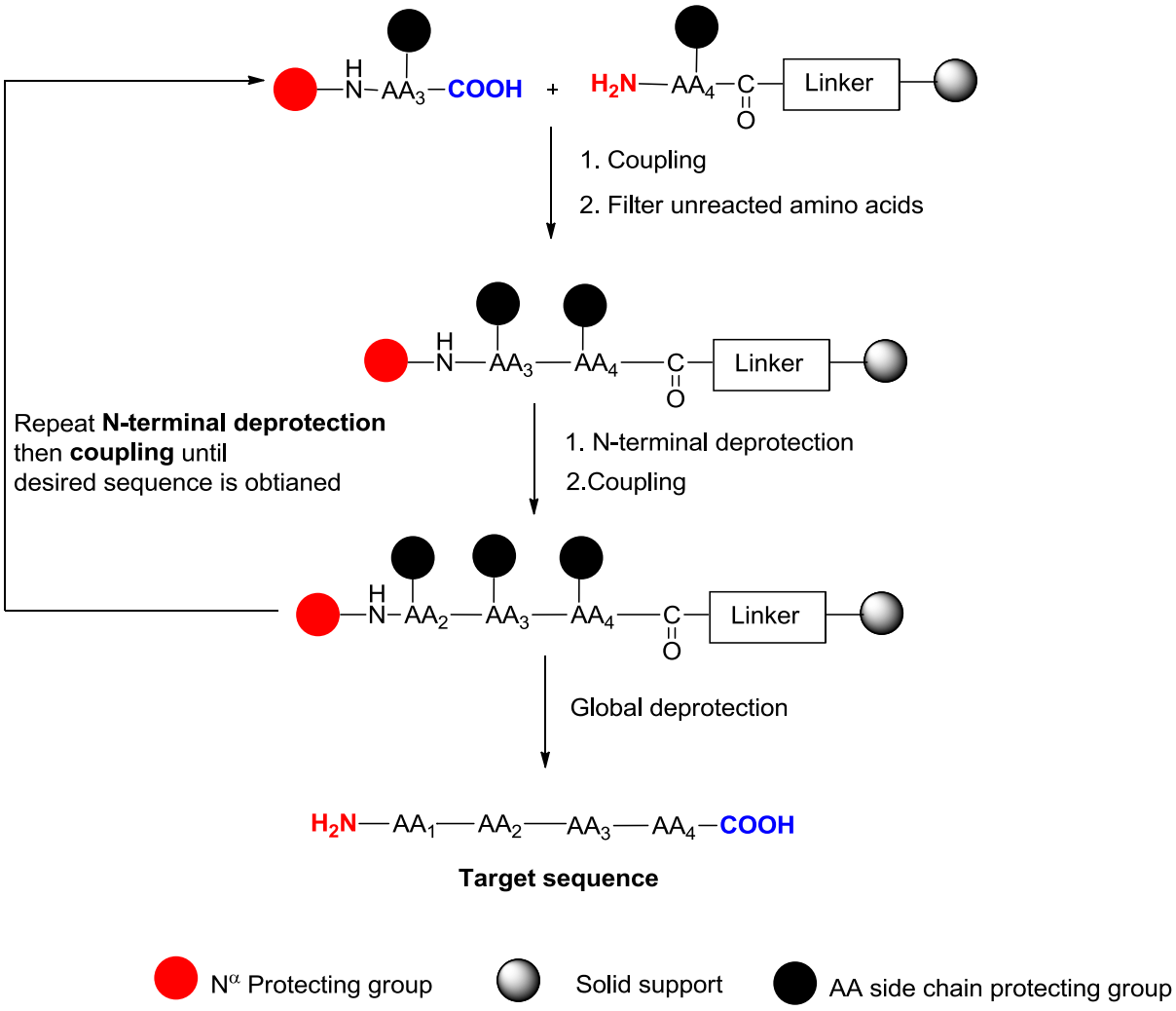

Scheme 2.2 General scheme illustrating the synthesis of a peptide using SPPS. AA denotes to amino acid.

SPPS has numerous advantages over solution-phase synthesis. Synthesis of peptides via SPPS is faster due to the use of excess starting materials that drive the reaction to completion, which can also minimise racemisation. Crude peptides can be isolated from the solid support in high purity, as any unreacted starting materials are simply filtered off from the resin. Currently, two dominant SPPS strategies employed in the literature are Boc-SPPS, discovered by Merrifield and Fmoc-SPPS reported by Sheppard. [181,183]

The Merrifield method, originally reported in 1963, involves the use of benzyl based side-chain protecting groups, with the N-terminus protected by the more acid-labile, *tert*-

butoxycarbonyl (Boc) group.[181] The temporary Boc group is removed under acidic conditions, e.g., using trifluoroacetic acid (TFA) whilst the side-chain benzyl groups and the chloromethyl resin (Merrifield resin) are resistant to TFA. The desired peptide is cleaved from the resin and the benzyl side-chain protecting groups removed under strong acidic conditions, such as using hydrogen fluoride (HF).[181]

The Sheppard method, or Fmoc SPPS, employs base-labile protecting groups, such as 9-fluorenylmethyloxycarbonyl (Fmoc), for the α -amine, while the side-chains are protected by acid-labile, *tert*-butyl (*t*Bu)-type protecting groups. The peptide chain is elongated by removing the Fmoc group under basic conditions, and is followed by selective peptide bond formation with the C-terminus of the subsequent amino acid. The desired peptide sequence, along with the acid-labile protecting groups, is removed from the resin by treating it with TFA. The Merrifield methodology relies on extremely toxic HF to release the resin-bound peptide; therefore, the Sheppard methodology is more frequently used by peptide chemists and reported in the literature. The lipopeptides reported in this thesis were synthesised via the Fmoc/tBu method.

2.2.1 General overview of Fmoc SPPS

Scheme 2.3 depicts a general synthetic scheme used in Fmoc-SPPS.

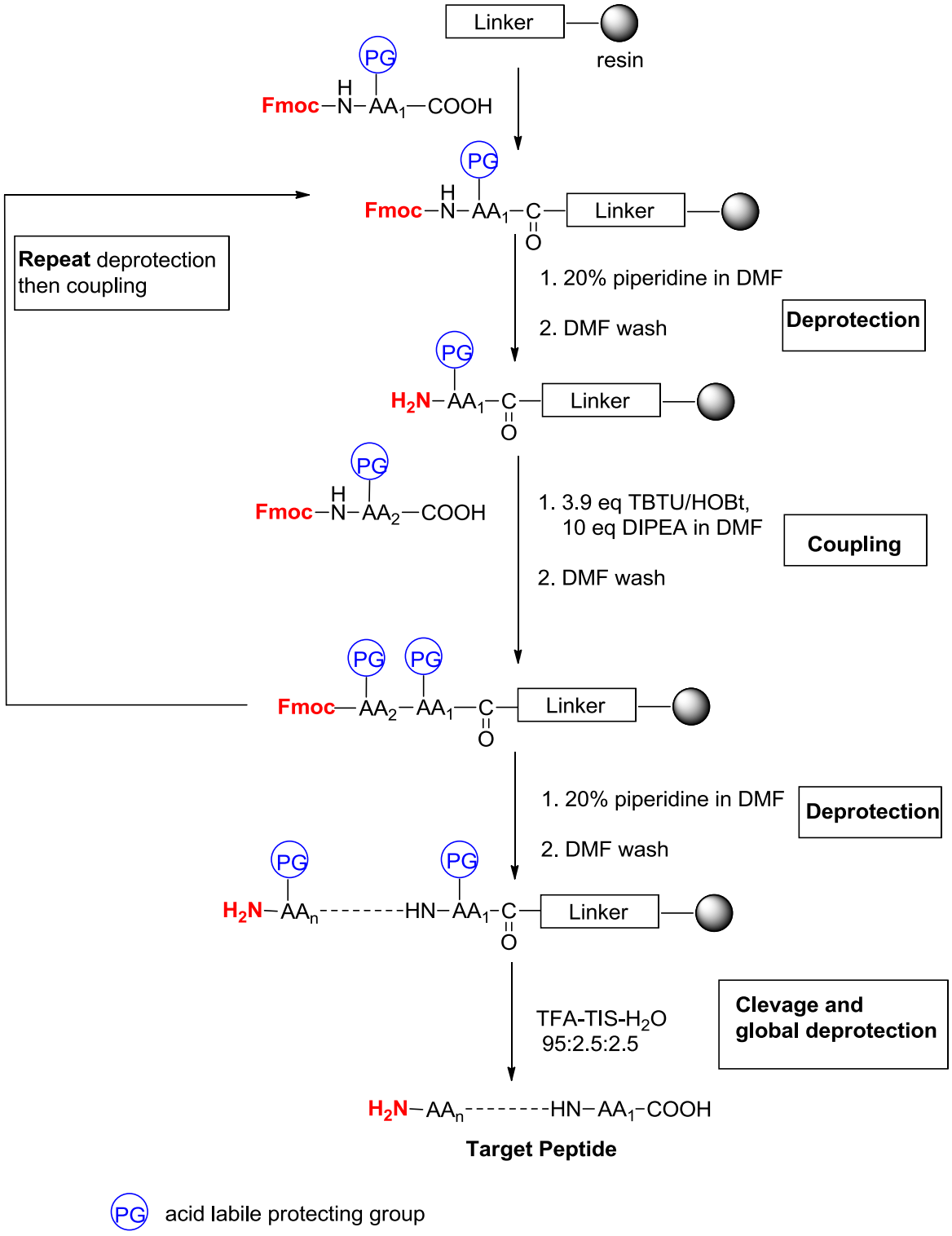

Scheme 2.3 General scheme used in Fmoc SPPS.

The first step involves the conjugation of the C-terminal amino acid (Fmoc-AA_1) onto the inert resin, via a linker (Scheme 2.3). The Fmoc group of the resin-bound AA_1 is deprotected using 20% piperidine in *N*,*N*-dimethylformamide (DMF).[183-184] The resin is thoroughly washed with DMF, to remove any excess piperidine. The N-protected subsequent amino acid (Fmoc-AA_2), at a concentration four times in excess to the resin, is then coupled to the unprotected N-terminus of the resin-bound AA_1. The peptide bond formation between AA_1 and AA_2 is facilitated by converting the C-terminal carboxylic acid moiety of AA_2 into a more reactive ester, using excess coupling reagents (3.9 eq. to the resin), in the presence of the tertiary amine base *N*,*N*-diisopropylethylamine (DIPEA). The Fmoc deprotection and coupling for each subsequent amino acid is repeated until the desired sequence is assembled on the resin. The peptide is then released from the resin, while simultaneously cleaving off the orthogonal protecting groups, under acidic conditions such as TFA.

2.2.1.1 Solid support

A solid support or resin provides the "micro-environment" required for peptide synthesis to occur. Several criteria need to be satisfied when choosing an appropriate resin for peptide synthesis. The resin must be chemically inert to all coupling reagents and insoluble in the solvents used in SPPS, so that any excess, unreacted materials can be simply filtered off. The resin must be physically stable during the peptide coupling and N-terminal deprotection steps, which require constant agitation of the amino acids in the resin mixture.[181] Finally, increased swelling of the resin is favourable for efficient peptide coupling and generating crude peptides in a higher yield. It can also enhance the exposure of reactive sites for first amino acid loading, and allows for better diffusion of reagents to these sites, for improved peptide coupling.[185]

Polystyrene (PS) based resins are extensively used in SPPS. PS resins can be modified, either by cross-linking with divinylbenzene (DVB) or polyethylene glycol (PEG) such as Tentagel, to improve the efficiency of on-resin reactions (Figure 2.1). Due to this favourable property, all of the peptides reported in this thesis were synthesised either on preloaded PS-DVB or on Tentagel resins.

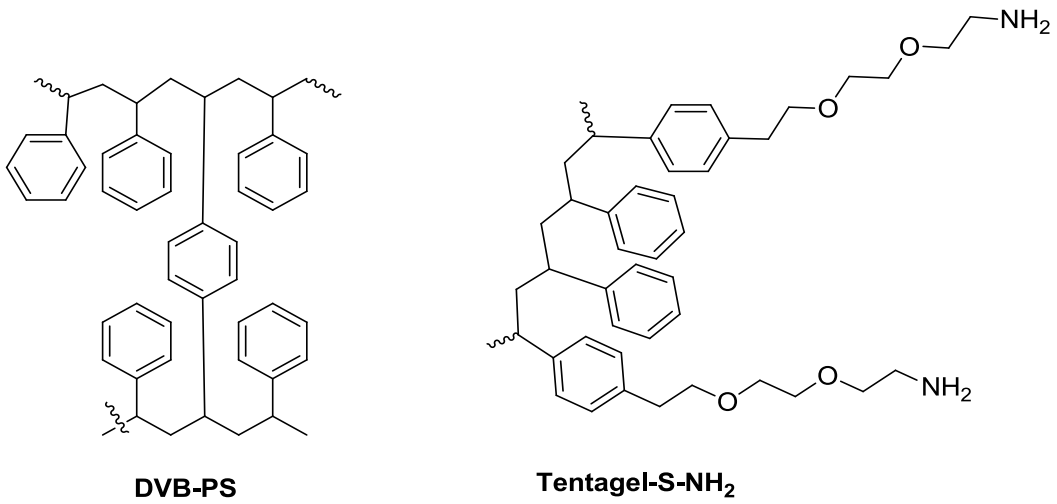

Figure 2.1 Structure of DVB-PS and Tentagel resins.

2.2.1.1.1 Divinylbenzene (DVB) cross-linked polystyrene resin (PS-DVB)

PS-DVB resin was first described by Merrifield in 1963, and was prepared by cross-linking PS resin with 2% DVB, via radical polymerisation.[181] The cross-linkage improves the solvation of the resin and prevents aggregation of the covalently attached peptide. However, the 2% DVB cross-linked resins swell poorly in dichloromethane (DCM). Improvements were made to the originally reported Merrifield resin, by cross-linking 1% DVB to PS, which thus increased the resin swelling in DCM by approximately five fold.[186-187] Although PS-DVB swells efficiently in most non-polar solvents, such as DCM, diminished swelling is observed in polar solvents such as DMF and 1-methyl-2-pyrrolidinone, which are routinely

used in SPPS. This has led to the development of other PS based resins with improved solvation.

2.2.1.1.2 PEG-PS (Tentagel-S-NH_2)

Tentagel-S-NH_2 resin was developed by the *in situ* polymerisation of the ethylene glycol moiety to cross-linked DVB-PS. The terminal end of ethylene glycol contains an amine functionality. The incorporation of the hydrophilic ethylene glycol moiety leads to enhanced solvation of the resin in polar solvents. However, Tentagel-S-NH_2 resins are up to 5 times more expensive than PS-DVB resins.[188]

2.2.1.2 Linkers

Linkers are used in SPPS to link the carboxy end of the C-terminal amino acid to the insoluble resin. As a result, the C-terminal end of the peptide is protected during peptide-chain elongation. The choice of the linker determines the C-terminal functionality of the peptide. Similar to the resin, the linker should be inert and stable during the amino acid deprotection and coupling conditions. In the literature, the term "resin" is sometimes also used to describe the linker-bound resin, leading to confusion. This is because most commercially available resins are pre-loaded with linkers. 2-Chlorotrityl chloride (CCR) and rink amide linkers were used for the synthesis of the lipopeptides reported in this thesis.[187]

2.2.1.2.1 2-Chlorotrityl chloride linker

2-Chlorotrityl chloride is extensively used to produce side-chain protected peptides that can subsequently be used to generate cyclic peptides. CCR is highly acid-sensitive and can be cleaved under mildly acidic conditions, such as 0.5% TFA in DCM or 20% TFE in DCM.[189-190] The side-chain protecting groups of the peptides are usually *t*Bu-type protecting groups, which require higher concentrations of the acid for deprotection. Due to the bulky aromatic

residues of CCR, this linker can minimise racemisation and diketopiperazine side-reactions, and can also be used to couple C-terminally problematic amino acids, such as cysteine, which is known to cause epimerisation.[189-190]

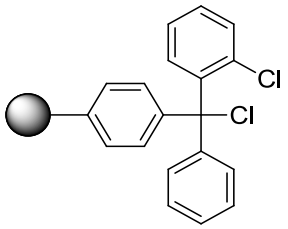

Figure 2.2 Structure of 2-chlorotrityl chloride resin.

2.2.1.2.2 Rink amide linker

The Rink amide linker is an acid-labile linker, extensively used for generating C-terminally amidated peptides. The C-terminally amidated peptides are produced by cleaving the peptides from the resin, either using 50% TFA in DCM or 90-95% TFA in presence of scavengers for 1-3 hours.[191]

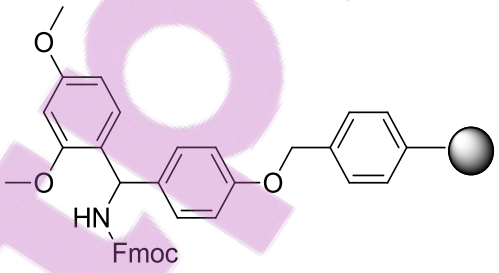

Figure 2.3 Structure of Rink amide linker.

2.2.1.3 Fmoc deprotection

For Fmoc-SPPS, the N-terminus of the amino acid is protected with the base-labile Fmoc protecting group. Protection of the N-terminus is necessary as this minimises any undesired

polymerisation during peptide bond formation. The Fmoc group can be removed under mildly basic conditions, such as 20% piperidine in DMF (Scheme 2.4).[184,187]

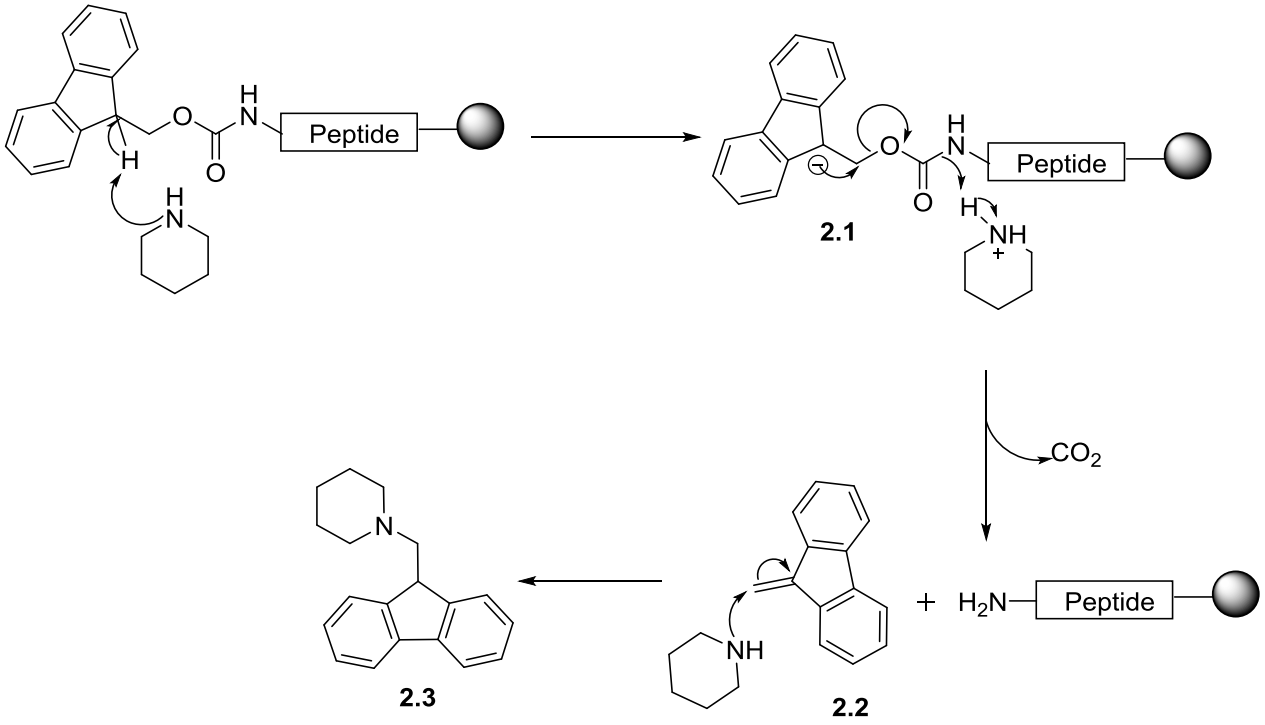

Scheme 2.4 Fmoc deprotection mechanism, using piperidine.

The initial reaction involves the deprotonation of the fluorene ring of the Fmoc group with piperidine, to yield an aromatic cyclopentadiene intermediate **2.1**. This intermediate rapidly eliminates the carbamate moiety, to form a dibenzofulvene adduct **2.2**. Excess piperidine acts as a scavenger to form a stable Fmoc-piperidine adduct **2.3**, which can be filtered off during the DMF washing. The elimination of dibenzofulvene exposes the unprotected α-amino terminus, for subsequent peptide elongation. [184,187]

Even though the Fmoc deprotection with piperidine is effective for most cases, longer peptide sequences can suffer from incomplete Fmoc deprotection, even with increasing the concentration of piperidine. Incomplete Fmoc deprotection can be minimised by increasing

the piperidine washing time or by using a stronger base such as 1,8-diazabicyclo[5.4.0]undec-7-ene.[184,187]

2.2.1.4 Coupling reagents

Peptide bond formation involves a reaction between the amine and the carboxylic acid moieties, resulting in the loss of a water molecule. However, amide bond formation in the absence of coupling reagents is favoured at high temperatures (>200 °C), which is detrimental for the amino acids in the sequence.[192] This is due to the poor reactivity of the hydroxyl group at the carboxylic acid terminus, which can be mitigated by converting the carboxylic acid into either reactive acyl halides, symmetrical or mixed anhydrides or reactive esters. Peptide chemists commonly use *in situ* generation of the reactive ester, via coupling reagents, to activate the carboxylic acid terminus. Three different types of coupling reagents, namely carbodiimides, phosphonium salts and uronium salts, are extensively used in the literature, and these will be described in the following sections.

2.2.1.4.1 Carbodiimides

Carbodiimides are the first-generation coupling reagents developed to facilitate peptide bond formation. Dicyclohexylcarbodiimide (DCC) is the earliest known of the carbodiimides and has been routinely used since 1955 for solution-phase peptide chemistry.[193] DCC facilitates peptide bond formation by converting the carboxylic acid into reactive *O*-acyl urea **2.4,** due to the reactive nitrogen groups in the DCC moiety.

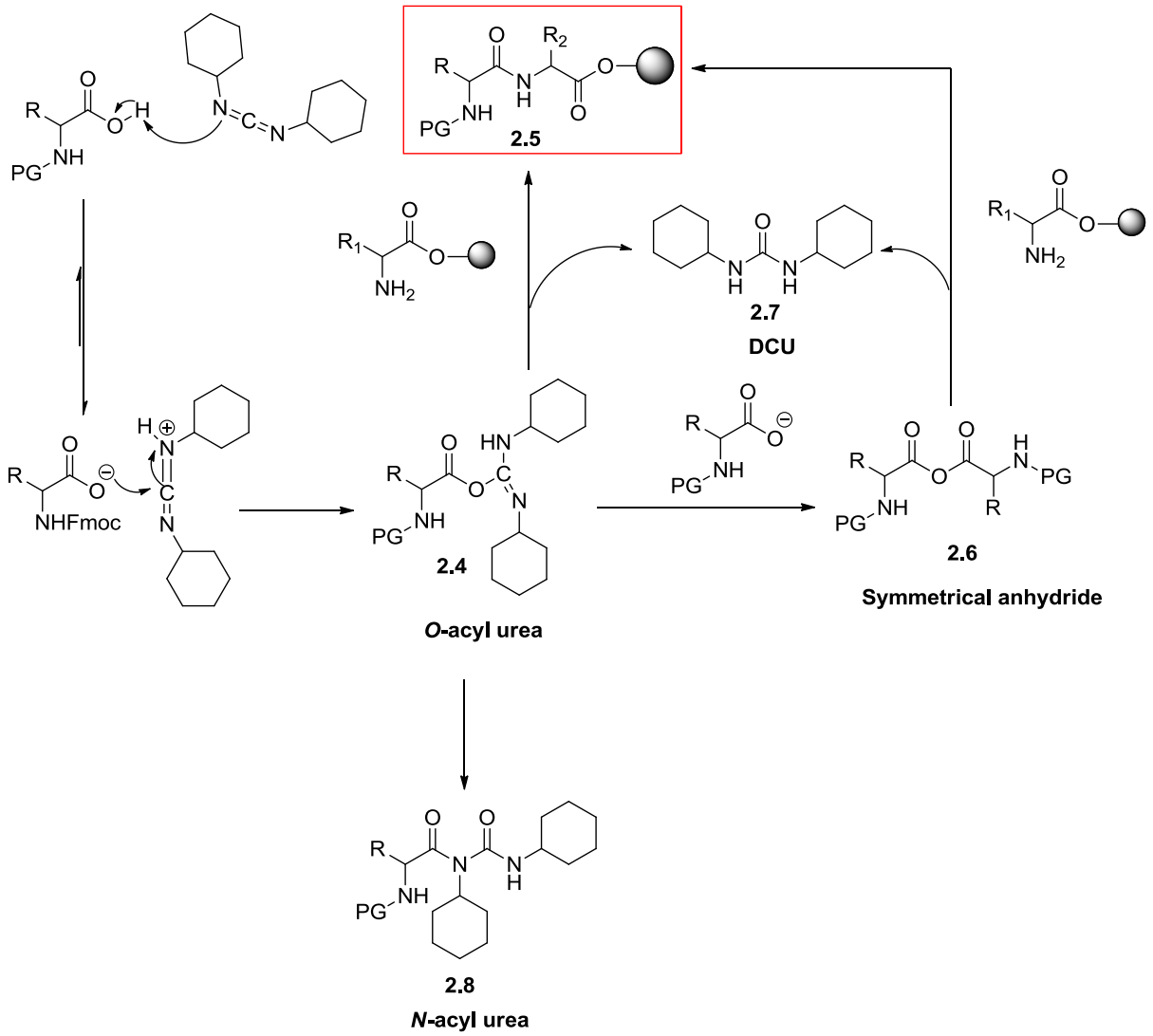

Scheme 2.5 Peptide bond formation using DCC as the coupling reagent.

The acyl urea can either react directly with the amine to yield the peptide bond **2.5**, or in the presence of excess carboxylic acid (2 equivalent of acid per 1 equivalent of DCC), yield a symmetrical anhydride **2.6**, which can react with the amine to produce the peptide bond.[194-195] One of the major by-products of DCC-mediated couplings is the insoluble dicyclohexylurea (DCU) **2.7,** which is only soluble in TFA. Therefore, DCC is only restricted to solution phase or Boc solid-phase peptide chemistry. The reactive *O*-acyl urea intermediate **2.4** can tautomerize to form a cyclic oxazolone. This cyclic oxazolone ring can also react slowly with

the upcoming amino acid, to form the peptide bond. However, it is extremely prone to epimerisation.

The epimerisation observed in the carbodiimide reagents can be minimised by the use of an additive or a suppressor, such as 1-hydroxybenzotriazole (HOBt) or the more reactive 1-hydroxy-7-azabenzotriazole (HOAt), in combination with the coupling reagents (Figure 2.4).[196-197]

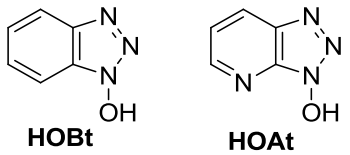

Figure 2.4 Chemical structures of additives commonly used in peptide synthesis.

These suppressors can prevent epimerisation as well as increase the overall yield of the crude peptide. They prevent the formation of *N*-acyl urea **2.8**, an irreversible by-product, which consumes the C-terminal amino acid without forming a peptide bond. The suppressor protonates the *O*-acyl urea **2.4**, leading to the formation of an active ester **2.9**, thus facilitating the peptide bond formation by stabilising the amines of the upcoming amino acid, by forming multiple hydrogen bonds. The superior yield and reactivity of HOAt can be attributed to the additional nitrogen on the benzotriazole ring, which acts as an additional electron withdrawing group and chelation effect with the incoming amino group leading to greater reactivity.[194,197]

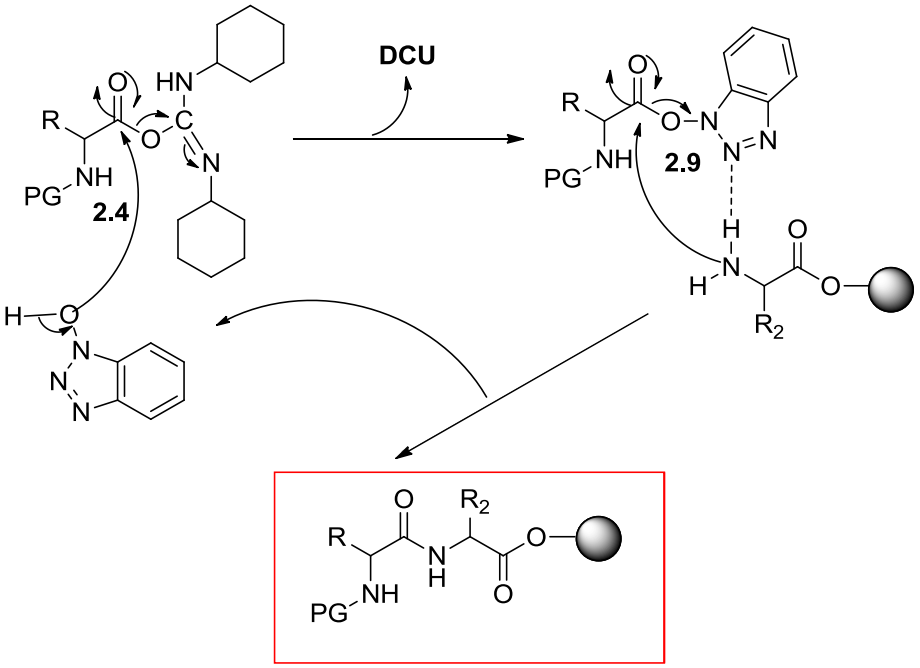

Scheme 2.6 Minimisation of epimerisation using HOBt by activating the *O*-acyl urea **2.4**.

DCC has been replaced by superior carbodiimides, such as diisopropylcarbodiimide (DIC) and *N*-ethyl-*N'*-(3-dimethylaminopropyl) carbodiimide (EDC), which are compatible with Fmoc-SPPS, since the urea by-product produced by these superior carbodiimide derivatives are soluble in DMF and can be simply filtered off.

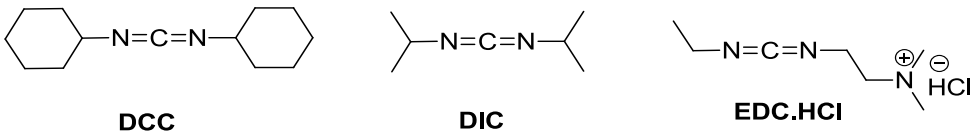

Figure 2.5 Chemical structures of commonly used carbodiimide type coupling reagents.

2.2.1.4.2 Phosphonium salts

Phosphonium-salt based coupling reagents were developed based on the HOBt and HOAt structures.[194-195,198] Benzotriazol-1-yl-oxytris(dimethylamino)phosphonium hexafluorophosphate (BOP) and azabenzotriazol-1-yl-oxy-tris-(dimethylamino)phosphonium

hexafluorophosphate (AOP) are the first-generation phosphonium salts designed from the HOBt and HOAt scaffolds respectively.[199-200] Even though BOP is a superior coupling reagent compared to the benzotriazole additives, the formation of a toxic by-product, hexamethylphosphoramide (HMPA), during its use led to the development of alternative phosphonium based coupling reagents.[201] Benzotriazol-1-yloxytri[pyrrolidino]-phosphonium hexafluorophosphate (PyBOP) and 7-aza-benzotriazol-1-yloxy-tris-[pyrrolidino] phosphonium hexafluorophosphate (PyAOP) are pyrrolidine derivatives of BOP and AOP respectively.[202-203] The phosphoramide by-products produced by these derivatives are less toxic than HMPA.

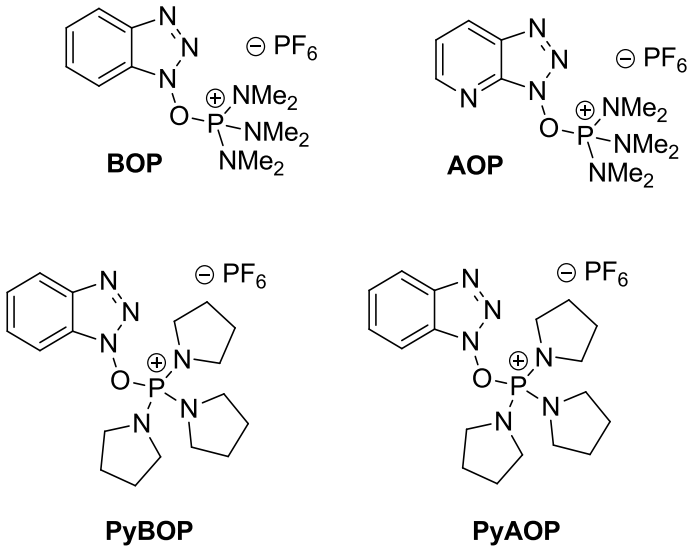

Figure 2.6 Chemical structures of the common phosphonium salt coupling reagents.

Phosphonium salts react with the reactive carboxylate anion, in the presence of excess base, such as DIPEA, to generate the reactive acyloxyphosphonium intermediate **2.10** and HOBt. The HOBt anion then reacts with this intermediate to produce the reactive ester **2.12** and HMPA **2.11** or the less toxic phosphoric amide by-product. Nucleophilic attack of the free amine at the electrophilic carbonyl group of the reactive ester **2.12** then produce the peptide bond as shown in Scheme 2.7.

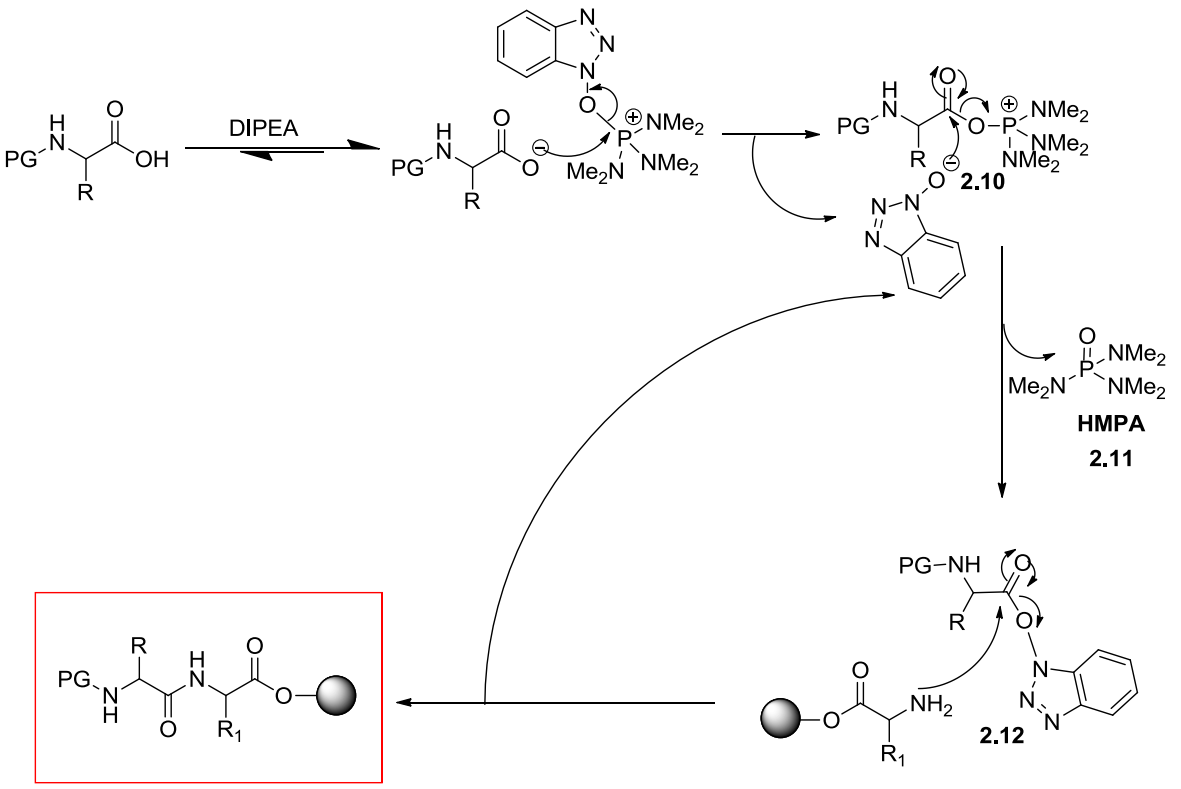

Scheme 2.7 Peptide bond formation using phosphonium based coupling reagents.

2.2.1.4.3 Aminium/Uronium salts

Aminium/Uronium based coupling reagents, such as *O*-(benzotriazol-1-yl)-*N,N,N',N* tetramethyluronium hexafluorophosphate (HBTU) and *N'N'N* tetramethyluronium tetrafluoroborate (TBTU), are most widely used for the *in situ* generation of active esters on-resin (Figure 2.7).[194-195,198]

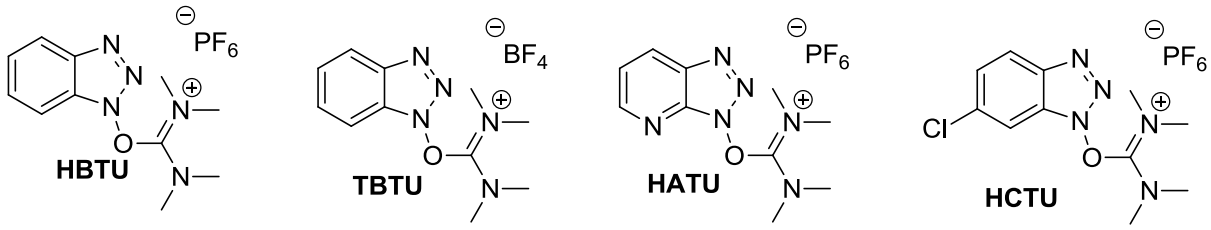

Figure 2.7 Chemical structures of frequently used uronium based coupling reagents.

The lipopeptides reported in this thesis were synthesised using aminium/uronium based coupling reagents. In a similar manner to the phosphonium salts, uronium based coupling reagents are also derived from the benzotriazole backbone, where the phosphonium portion is replaced by a tetramethyl uronium species. The main difference between HBTU and TBTU is the counter anion associated within the structure. HBTU and TBTU have hexafluorophosphate and tetrafluoroborate cations respectively; however, both HBTU and TBTU have exhibited similar reactivity. In solution these coupling reagents exist in equilibrium between the uronium **2.13** (*O*-form) and the aminium **2.14** (*N*-form) form (Figure 2.8). However, in the crystalline state, the aminium form is the dominant species.[204]

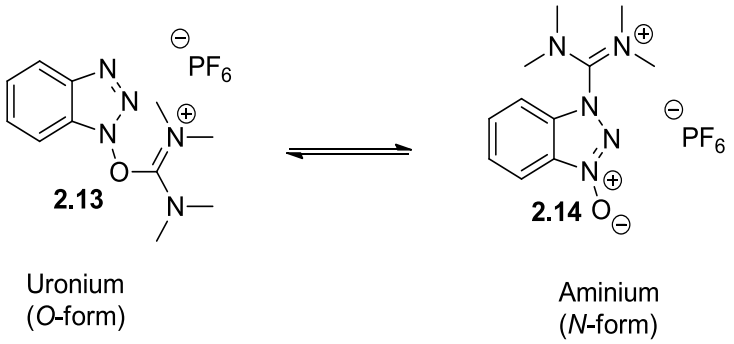

Figure 2.8 Tautomerization of HBTU in solution.

Uronium based coupling reagents have a similar mechanism of action as the phosphonium salts. The carboxylate anion, in the presence of excess DIPEA, reacts with the uronium moiety of HBTU to generate the acyl uronium intermediate **2.15** and HOBt. The HOBt anion reacts with the uronium intermediate to form the active ester moiety **2.17** and tetramethyl-urea **2.16** as the by-product. This is followed by peptide bond formation at the amino terminus to afford the desired dipeptide.

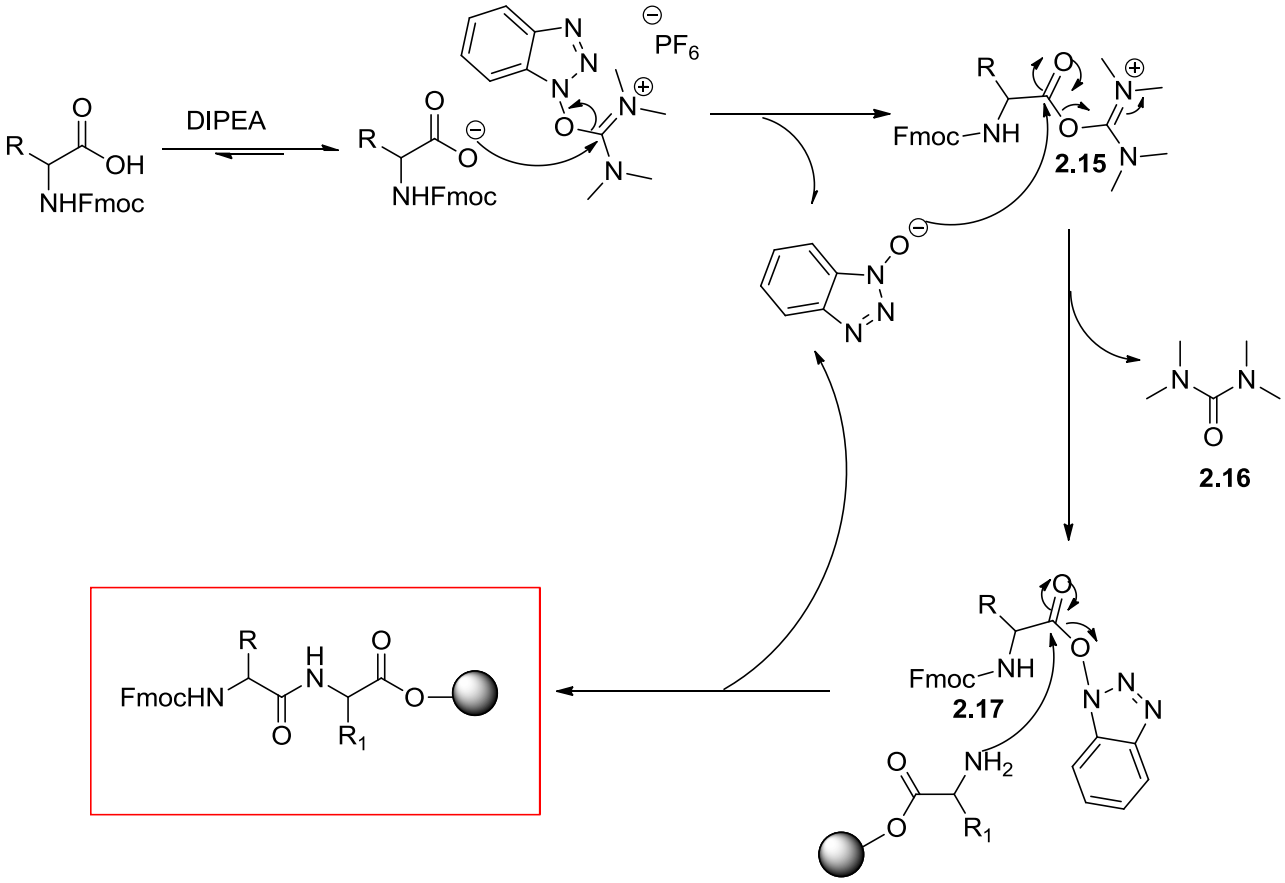

Scheme 2.8 Amide bond formation via uronium based coupling reagents.

HOAt-based uronium coupling reagents *O*-(7-azabenzotriazol-1-yl)-*N,N,N',N* tetramethyluronium hexafluorophosphate (HATU) and 6-chloro-HOBt derived *O*-(6-chlorobenzotriazol-1-yl)-*N,N,N',N* tetramethyluronium hexafluorophosphate (HCTU) are superior coupling reagents for the synthesis of difficult and long peptide sequences (Figure 2.7).[200,205] The superior reactivity of HATU can be attributed to the generation of the extremely reactive 7-azabenzotriazol-1-yl ester, formed due to the intramolecular base catalysis of the additional nitrogen in the benzotriazole ring. The superior reactivity of HCTU can be attributed to the electron-withdrawing effect of the chlorine in the sixth position of the benzotriazole ring. Both HCTU and HATU have exhibited similar coupling efficiencies in the literature, but HCTU is cheaper than HATU.[206]

A major limitation of uronium based coupling reagents is the formation of guanidine side products, which can lead to peptide chain termination (Scheme 2.9).[194-195,198] Guanidine formation was not observed with phosphonium or carbodiimide coupling reagents. A guanidine side product **2.18** is formed when the free amino terminal of the resin bound amino acid attacks the uronium moiety of the coupling reagent. This side reaction is observed during the slow pre-activation of the carboxylic acid moiety in hindered amino acids, during fragmentation of two protected sequences, and during the macrocyclisation and use of excess coupling reagents. The unwanted guanidinylated side product formation can be mitigated by using slightly less than molar quantities of coupling reagents per amino acid (0.95 eq. of coupling reagents per 1 eq. of amino acid) and by the use of HOBt/HOAt as suppressors.[194-195,198]

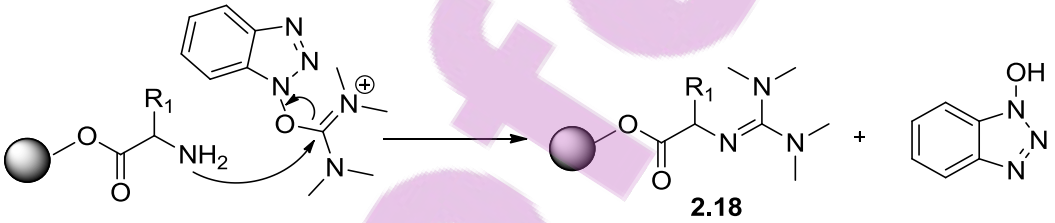

Scheme 2.9 Guanidine side product formation.

2.2.1.5 Release of the target peptide

For Fmoc-SPPS, the target peptide is released from the resin using a high concentration of TFA (~95 %) for 1-3 h. In the presence of a high concentration of TFA, the following acid-labile protecting groups can also be removed: *t*Bu (PGs for alcohols and carboxylic acids), Boc (PGs for side-chain amines), Pmc and Pbf (PGs for guanidine side-chain of Arg) and Trt (PGs for side-chain amides and thiols).[184,187] However, TFA-mediated cleavage can generate highly reactive protecting group cations and cleaved linkers, which can react and modify the

electron rich side-chains of Tyr, Trp, Met and Cys. As a result, peptide cleavage is carried out using a TFA cocktail solution, in presence of nucleophilic reagents known as scavengers, to quench the reactive species generated.[184]

Water was used as one of the earliest scavengers, to neutralise *t*-butyl cations, with moderate success. 1,2-ethanedithiol (EDT) is a better *t*-butyl cation quencher than water, and it can also neutralise Trt protecting groups and offer moderate protection to the unprotected amine in the indole ring of Trp. Reactive Trt cations can also be neutralised with EDT and thioanisole. Thioanisole is also effective against Pmc and Pbf protecting groups in Arg. Triisopropylsilane (TIS) is very effective against Boc, Trt, Pbf and rink amide linkers.

Based on these observations two universal cleavage cocktail solutions, Reagent K (TFA-thioanisole-water-phenol-EDT, 82.5:5:5:5:2.5, v/v) and Reagent R (TFA-thioanisole-anisole-EDT, 90:5:3:2,v/v) have been designed, to remove and quench almost all the protecting groups used in SPPS.[207] However, reagent K and R contain toxic and odorous reagents, such as thioanisole and anisole, which are unnecessary for standard cleavage conditions. Only Boc, Trt and Mtt were utilised as side-chain protecting groups for the peptide synthesis reported in this thesis. Therefore, two different cleavage conditions were used to release these peptides. A cocktail solution of TFA-TIS-water (95:2.5:2.5 v/v) was used to cleave peptide sequences without any cysteine and a TFA-TIS-water-EDT (94:1:2.5:2.5 v/v) cocktail solution was used for the release of cysteine containing peptides.

2.3 Mass spectrometry

Mass spectrometry (MS) is routinely used in peptide chemistry to confirm the identity of the synthetic peptides, by measuring their mass to charge ratio (m/z).[208] Peptides can be ionised under certain conditions to generate a charged species, whose m/z ratio can be detected using

a mass spectrometer. The molecular weight of the peptide can be determined since the ionised peptide is quite stable.[208]

Mass spectrometry is a highly sensitive analytical technique and only requires very low concentration of the peptide sample (10^{-6} to 10^{-15} M). Electrospray ionisation (ESI) and Matrix-assisted laser desorption/ionization (MALDI) are two ionisation methods routinely used in mass spectrometry, and both of these were used to validate the successful synthesis of the peptides in this thesis. The ionised peptides were separated by m/z ratio by using time of flight (TOF) methodology as the mass analyser. This involves the acceleration of the ions, by providing a short voltage gradient and measuring the time taken for the ionised samples to pass through the detectors.[209] The ionised peptides with a high mass to charge ratio will travel through the free flight tube slower, due to their slower velocity compared to those with a low mass-to-charge ratio. The separated ions pass through a detector and the results are displayed as a mass spectrum showing m/z ratio against relative intensity.

2.3.1 Electrospray ionisation (ESI)

The peptides are prepared for ESI by dissolving the solid in solvents such as water, acetonitrile or methanol, with a small percentage of formic acid (0.01%) and ammonium hydroxide (0.3%) to aid the ionisation in positive and negative ion modes, respectively. In ESI, the peptide solution is introduced as charged droplets through a needle held at high voltage, under atmospheric temperature conditions.[210] These droplets are evaporated by either nebulising with nitrogen gas or heating (100-300 °C), leading to a decrease in the radius of the charged droplets. As the droplet shrinks, the charged density of the surface of the droplet increases and at a critical size, the charge repulsion becomes too powerful and these charged ions are released into the gaseous phase. These ions are then separated by their m/z using TOF and the results are displayed as a mass spectrum.[211]

In the positive ion mode, the droplets can be charged by the addition of protons $(M+H)^+$ or by the addition of small molecular ions such as Na $(M+Na)^+$ or K $(M+K)^+$, presented in the solution at acidic pH, and the spray needle is kept at positive potential.[211] In the negative ion mode, protons (M-H) or small molecular ions (M-Na) or (M-K) are removed under basic conditions, and the needle is kept at a negative potential.

Electrospray ionisation mass spectrometry (ESI-MS) spectra often show multiple ions of a single species, due to the presence of several cationic and anionic side-chain amino acids, with characteristic isotopic patterns.[208] Therefore, multiple molecular weight calculations can be generated from a single spectrum, allowing for accurate validation of the molecular weight of the peptide. Generally, ESI-MS provides better resolution and accuracy than MALDI, mainly due to the averaging of individual measurements in the spectrum, and the technique is also compatible with liquid chromatography.[208] However, ESI-MS is less sensitive (~ 1 picomole) compared to MALDI-MS (< 1 picomole).

2.3.2 Matrix-assisted laser desorption/ionization (MALDI)

The peptides are prepared for MALDI by dissolving the sample in a mixture of water-acetonitrile (50:50), with a small volume of TFA (0.1%) to aid the ionisation.[212] The dissolved peptide solution is spread onto a matrix, which is made up of co-crystallised small organic acids capable of absorbing the energy of the laser. The matrix also aids in the ionisation of the sample, mainly due to its acidic nature. [212]

Generally, α-cyano-4-hydroxycinnamic acid is used as a matrix for analysing peptides, usually at a concentration 100 fold in excess to the peptide, to maximise the surface area required for laser absorption. The peptide-matrix mixture is dried before firing the laser. MALDI uses UV lasers such as a nitrogen laser (emits at 337 nm) or frequency-tripled nd:YAG laser (emits at 355 nm) to excite the peptide-matrix by discharging the laser in short

pulses (10-15 ns), to prevent thermal decomposition.[213-214] The matrix absorbs the energy of the laser and undergoes a phase transition from solid to gas, leading to the desorption of the matrix-peptide crystals into the gas phase.[212,215] These ionised vapours are then passed through the mass analyser (TOF) and the separated ions are displayed as a mass spectrum.

Like ESI, MALDI can produce multiply charged ions of the molecule, but usually in MALDI, a singular charged ion is observed, since multiple charges are less likely to desorb from the surface because of the increased electrostatic interaction, and because multiple charges are less stable in the gas phase, which makes it easier to identify individual molecules.[216] MALDI allows for rapid sample analysis since multiple samples can be placed on a single matrix plate, and a very low sample concentration (femtomole) is required for MALDI analysis.

2.4 Reversed-phase high performance liquid chromatography (RP-HPLC)

After successfully validating the synthesis of the peptide by mass spectrometry, reversed-phase high performance liquid chromatography (RP-HPLC) was used for peptide purification. HPLC techniques have a stationary and a mobile phase to aid in the purification process.

The stationary phase consists of tightly packed silica beads (particle size 3-10 μm, and 100-300 Å pore size), with *n*-butyl (C_4), *n*-octyl (C_8) or *n*-octadecyl (C_{18}) ligands. The mobile phase consists of a hydrophilic solvent A (water and 0.1% TFA v/v) and miscible organic solvent B (acetonitrile and 0.1% TFA v/v).[184,217] Acetonitrile is a popular organic solvent used in RP-HPLC, due to its low absorbance at 214 nm, low viscosity that allows for a high flow rate with low back pressure, and high volatility that allows the solvent to be removed under low vacuum. A low concentration of TFA is incorporated into the mobile phase, to

facilitate crude peptide solubility and to increase the spectral resolution by increasing the sharpness and symmetry of the peaks.[218]

Peptide interaction with the stationary phase is governed by hydrophobic forces. As the hydrophobicity of the mobile phase is gradually increased, the peptide partitions into the mobile phase from the stationary phase, due to the decrease in the surface tension. The elution of the peptide from the column is monitored using UV light with detection at two wavelengths, 214 nm and 280 nm.[184,217] Peptide bonds strongly absorb in the 190-215 nm range, while the aromatic rings in the sequence strongly absorb in the 250-280 nm regions. The purified peptides are then lyophilised to afford a fluffy solid and their identity is once again confirmed by mass spectrometry. The purity of the lyophilised peptides is checked using analytical RP-HPLC.

2.5 Broth dilution minimum inhibitory concentration (MIC) assay

The potency of the purified lipopeptides against bacterial pathogens were analysed using a minimum inhibitory concentration (MIC) assay. MIC is the lowest concentration of a compound required to inhibit the growth of the bacteria visually, under standard conditions. Two common methodologies utilised to determine the MIC are agar diffusion and broth dilution.

Agar diffusion assays involve the inoculation of diluted bacteria (1×10^5 CFU/mL) onto a nutrient-rich agar plate incorporated with antibacterial compounds at different concentrations. The antibacterial activity can be assessed by counting the number of colonies that grow in the presence of the antibacterial compound.

In the broth dilution method, a diluted bacterial culture is inoculated onto a liquid growth medium, consisting of nutrients and the antibacterial compound at specific concentrations.

The potencies of the compounds are analysed by comparing the turbidity of the solutions in the presence and absence of the bacteria, either visually or by measuring the optical density (OD) at 600 nm.

The potencies of the lipopeptides reported in this thesis were tested using the broth dilution method, since the agar dilution assay depends on the diffusivity of the test compounds. Hydrophobic compounds, such as some peptides, diffuse slowly into the solid agar medium and hence the inhibitory activity, even if present, may be undetected in this method.[219]

2.6 Scanning electron microscopy (SEM)

SEM can be used to visualise bacterial cell morphology, in the presence and absence of the synthesised lipopeptides. SEM can provide information about the surface topology of the top 1 μm layer of a surface; hence any morphological changes induced by the lipopeptides to the bacterial membrane can be detected. This could provide vital information about the possible mechanisms of action.

One of the main advantages of SEM is the convenience in sample preparations, since samples only require mounting onto a solid stub for analysis. Sample size is also not an issue in SEM, in the case of bacterial samples. However, the samples must be stable under vacuum and should be able to withstand constant electron bombardment. Before analysis, the peptide samples are sputter coated with a thin layer of platinum (2-20 nm) to make them electrically conductive and to increase production of secondary electrons leading to increase signal to noise ratio.[220-222]

SEM produces high-resolution images by emitting a narrow beam of high-energy electrons (2-40 keV) onto the sample. The electrons travel to the sample, via a tube, under vacuum (< $1x\ 10^{-4}$ Torr), to prevent any scattering of electrons. The beam scans the samples in a

rectangular orientation. The interaction of the electron beam with the sample produces "secondary electrons" with weaker energies (5-10 eV), which are picked up by detectors in the instrument that convert them into a pixel image, with a resolutions of up to 1 nm.[220-222]

2.7 Circular dichroism (CD)

Circular dichroism is a common characterisation technique used to estimate the relative quantities of secondary and tertiary structures of peptides and proteins, under varying conditions of temperature and concentration of ions and biomolecules, such as lipids.

Plane-polarised light is made up of two components of equal magnitude, polarised light rotating counter clockwise (left) and clockwise (right). CD measures the difference in the absorbance of polarised light as it passes through a chiral sample, such as a peptide, and this difference, known as the ellipticity, θ, is measured in millidegrees. CD only requires low sample concentration (1-10 mg/mL) and structural information using CD can be generated much faster compared to other characterisation techniques.[223-224]

2.7.1 Characteristics of CD spectra

The far UV region (190-250 nm) provides valuable information about the secondary structure of peptides, due to the specific interactions associated with the peptide bond in this region. In this region, the peptide bond shows two key absorptions which are weak but broad absorption around 220 nm due to n→π transitions, and a more intense absorption around 190 nm due to π→π* transitions. However, the intensities of these two transitions vary between different peptide secondary structures and give rise to characteristic shapes in the far UV region of the CD spectrum as shown in Figure 2.9.[223-224]

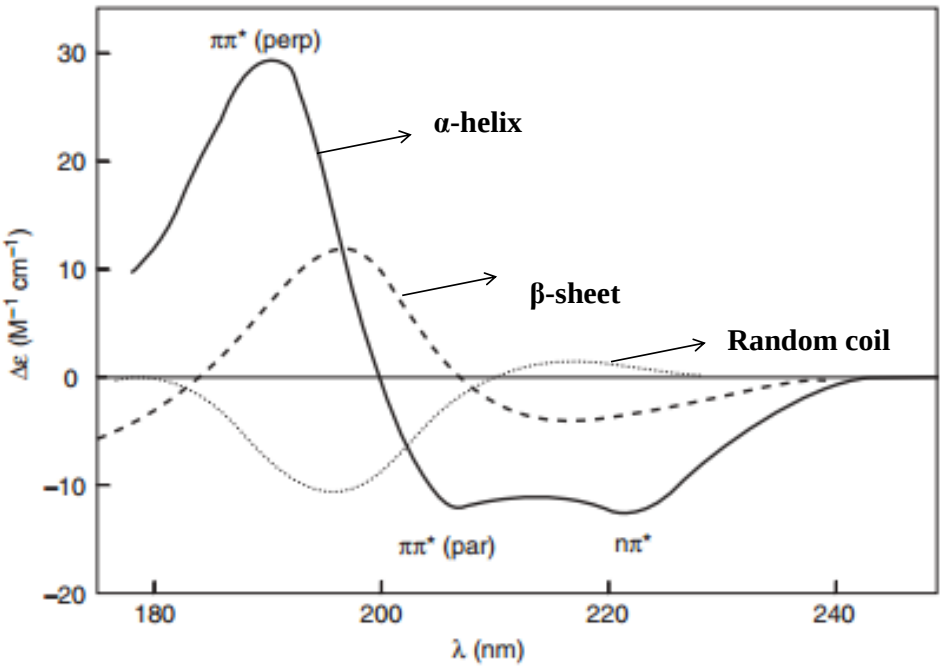

Figure 2.9 Characteristic peptide secondary structures in the far UV regions of the spectra.[225-226]

The n→π transition gives rise to a negative peak at 222 nm and between 216-218 nm, corresponding to α-helical and β-sheet structures respectively. The π→π* transition gives rise to a positive peak at 190 nm and a negative peak at 208 nm corresponding to the α-helical structure while a positive peak at 198 nm is characteristic of β-sheet conformation. Random coil or unstructured peptides give rise to a negative band at ~195 nm and a positive band at ~217 nm.[223-224]

2.8 Nuclear magnetic resonance spectroscopy (NMR)

Nuclear magnetic resonance spectroscopy (NMR) is used for a more detailed structural analysis of peptides. The detailed structure of the most active lipopeptide was resolved by using two-dimensional proton NMR and NMR parameters, which include chemical shifts, coupling constant ($^3J_{NH,C\alpha H}$) and temperature dependence of NH chemical shifts. Each of these parameters is described, in further detail, below.

2.8.1 Chemical shifts

The atomic nuclei of molecules have a small magnetic field (**B**) due to the electrons circulating around the nucleus. When a large external magnetic field ($\mathbf{B_0}$) is applied to the nuclei, the magnetic field of the nuclei opposes the external magnetic field. Therefore, in the presence of this external magnetic field, there is a change in the resonance frequency. The magnitude of the change in resonance frequency is known as a chemical shift, δ, which depends on the type of chemical nuclei, as well as the influence of the surrounding nuclei of the molecule. Chemical shifts are measured in parts per million (ppm) by relative to a standard reference molecule, tetramethylsilane or 4,4-dimethyl-4-silapentane-1-sulfonic acid.

For peptides, ^{1}H NMR is extensively used for structural analysis, due to the low sample concentration required to generate a proton spectrum. Characteristic proton chemical shifts can be obtained for different chemical environments present in the peptide sequence. For example, amide protons are clustered around 6-10 ppm, whereas C^{α} protons are located around 3.5 to 5 ppm and C_{β}, C_{γ} and C_{δ} are clustered around 0.5 to 3.5 ppm in the proton spectrum.[227-228] Peptide secondary structures can induce a small change in the chemical shift values in comparison to an unstructured conformation. Generally, the amide and C^{α} protons are shifted upfield by ~0.4 ppm with respect to random coil conformation for α-helical peptide and are shifted downfield by ~0.4 ppm for β-sheet conformations.[229] The chemical shift changes with respect to peptide secondary structures can be influenced by chain flexibility, hydrogen bond length and the dihedral angle.

2.8.2 Coupling constant: ($^3J_{NHC\alpha H}$)

A coupling constant (J) refers to the through bond-interaction that exists between nuclei linked via covalent bonds. The three bond, or vicinal coupling, between the amide bond and the C^{α} proton ($^3J_{NH,C\alpha H}$) can provide information about the magnitude of the dihedral torsion angle, ϕ.[228,230] The relationship between the torsion angle and $J_{NHC\alpha H}$ can be expressed using the Karplus equation (2.1) as shown below:[231]

$$^3J_{NHC\alpha H} = A \cos^2 \theta - B \cos \theta + C \qquad (2.1)$$

where $\theta = (\phi - 60°)$ and $^3J_{NHC\alpha H}$ is given in hertz. The coefficients A, B and C have estimated values of 6.4, -1.4 and 1.9 respectively for peptides and proteins, based on the experimentally derived coefficients from globular proteins, basic pancreatic trypsin inhibitor globular protein.[232] Characteristic $^3J_{NHC\alpha H}$ and torsion angle values for different peptide secondary structures are highlighted in Table 2.1.

Table 2.1 Characteristic $^3J_{NHC\alpha H}$ coupling constant and torsion angle values for different types of secondary structure.

Secondary Structure	**$^3J_{NHC\alpha H}$ (Hz)**	**ϕ (°)**
Random coil	7	-155
α-helix	3.9	-57
3_{10}-helix	4.2	-60
Antiparallel β-sheet	8.9	-139
Parallel β-Sheet	9.7	-119

2.8.3 Temperature dependence of NH chemical shifts

Temperature dependence of NH chemical shifts in hydrogen bonding solvents, such as methanol, can be used to identify the amide protons that are exposed to the solvent. These exposed amide protons can form hydrogen bonds with the solvent. Upon heating, the hydrogen bonding between the amide protons and the solvent weakens, causing an upfield shift of the amide protons.[233-235]

The temperature and the amide proton chemical shift have a linear relationship and the slope of the linear plot gives the temperature coefficient values ($d\delta/dT$). The temperature coefficient can then be used to deduce the extent of hydrogen bonding by the amide protons. Generally, the intramolecular hydrogen bonds in amides are shielded by the solvent and have a higher temperature requirement to break these interactions. Therefore, a low temperature coefficient (< 3 ppb/K) indicates strong intramolecular hydrogen bonding between the amide bonds and the solvent, and a high temperature coefficient (> 5ppb/K) indicates solvent exposed amide protons to the solvent environment.[233-235]

2.8.4 Two dimensional ^{1}H NMR (2D-NMR)

2D-NMR facilitates a more complex, structural analysis of proteins and peptides. Two types of 2D proton NMR experiments were used in this thesis for the structural analysis of the most active lipopeptide.[227] Both of these are listed below and described in further detail in the following sections (2.8.4.1 and 2.8.4.2)

1. 2D proton NMR for analysing **through bond**, scalar spin-spin connectivities, using Total Correlation Spectroscopy (TOCSY).
2. 2D proton NMR for analysing **through space**, dipolar spin-spin connectivities, using Rotating Frame Overhauser Effect Spectroscopy (ROESY).

2.8.4.1 Total Correlation Spectroscopy (TOCSY)

TOCSY spectroscopy produces cross peaks as contours arising from the scalar coupling of all the spin systems, for each of the amino acids in the peptide sequence. Generally, each of the 20 natural amino acids has a characteristic TOCSY fingerprint region, that gives rise to a unique pattern which this enables individual amino acids to be identified in a given peptide.[236]

2.8.4.2 Rotating Frame Overhauser Effect Spectroscopy (ROESY)

Nuclear Overhauser Enhancement Spectroscopy (NOESY) and ROESY are two commonly used 2D NMR experiments to provide information about the spatial proximity of protons, also indicated as off-diagonal contours, by transferring the nuclear spin polarization from one nuclear spin population to another, via cross-relaxation. In NOESY and ROESY, these transfers of nuclear spin are known as nuclear Overhauser effects (NOEs) and rotational Overhauser effects (ROE). However, ROESY spectroscopy is more ideal for studying smaller peptides with molecular weights between 1-2 kDa, since little or no NOEs are observed at that range in the NOESY spectrum.[227]

The intensity of the NOE or ROE depends on the distance between the two protons, and is usually observed when protons are less than 5 Å apart. The NOE intensity is governed by the following equation:

$$\text{NOE} \propto (1/r^6) \times f(\tau_c) \qquad (2.2)$$

Where, r is the distance between the nuclei and f (τ_c) is the function of rotation correlation time of the molecule. According to the above equation, the intensity of NOE increases as the distance between the cross peaks decreases. The intensity of the NOE cross peak can be characterised as intense NOE for short distances (< 2.5 Å), medium cross peak for medium

range distances (2.5-3.5 Å) and weak NOE is observed for distances greater than > 3.5 Å.[237] For most polypeptide secondary structures, in addition to sequential NOEs distances, a variety of medium range and long range ^{1}H-^{1}H distances are also observed as shown in Table 2.2.

Table 2.2 NOE observable distances (Å) for peptide secondary structures.[227-228]

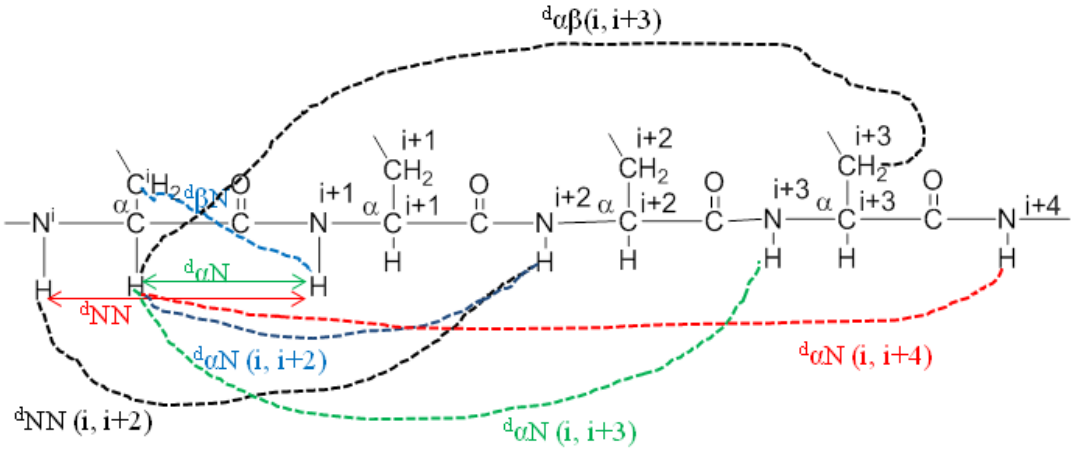

Distance	α-Helix	3_{10}-Helix	β (antiparallel)	β (parallel)	turn I	turn II
$d_{\alpha N}$	3.5	3.4	2.2	2.2	3.4	2.2
$d_{\alpha N}$(i, i+2)	4.4	3.8			3.6	3.3
$d_{\alpha N}$(i, i+3)	3.4	3.3			3.1-4.2	3.8-4.7
$d_{\alpha N}$(i, i+4)	4.2					
d_{NN}	2.8	2.6	4.3	4.2	2.6	4.5
d_{NN}(i, i+2)	4.2	4.1			3.8	4.3
$d_{\beta N}$	2.5-4.1	2.9-4.4	3.2-4.5	3.7-4.7	2.9-4.4	3.6-4.6
$d_{\alpha\beta}$(i, i+3)	2.5-4.4	3.1-5.1				

2.9 Contact angle

The surface-tethered peptide, GZ3.163, was characterised using water-contact angle measurements, ellipsometry and X-Ray photoelectron spectrometry. Water contact angle (θ_c) measures the angle between the solid-liquid (SL) interface between the water droplet and the solid surface, and the liquid-gas (LG) interface between the water droplet and its vapour, using a high resolution infrared camera based on Young's equation as shown in Figure 2.10a.[238-239]

The contact angle measurements provide information about the surface wettability, which refers to the interaction of the liquid droplet with the solid surface. Perfect wettability refers to a strong affinity of the water droplet to the surface, indicating a hydrophilic surface, and poor wettability indicates a hydrophobic surface, due to weak interaction between the liquid and the surface. Hydrophobic surfaces are characterised by high water contact angles as depicted in Figure 2.10b whereas hydrophilic surface have low water contact angles as shown in Figure 2.10c. Therefore, changes in the water contact angle during each of the immobilisation steps can indirectly indicate successful surface functionalisation.[238-239]

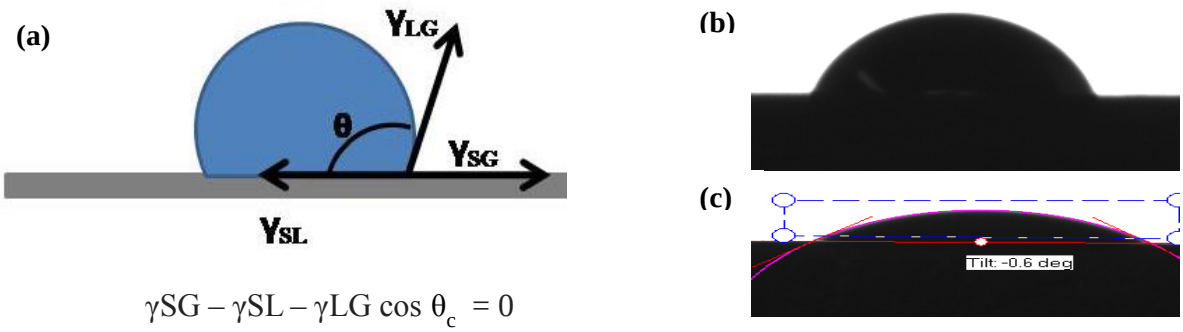

$$\gamma SG - \gamma SL - \gamma LG \cos \theta_c = 0$$

Figure 2.10 (a) Measurement of water-contact angle using Young's equation where γ is the surface tension of the interface and SG is the surface tension of the solid and vapour interface. Water droplet morphology on **(b)** hydrophobic and **(c)** hydrophilic surfaces.

2.10 Ellipsometry

Ellipsometry is a non-destructive and convenient tool used accurately to measure the thicknesses of thin films, such as tethered peptides on surfaces, in real time. Ellipsometry measures the change in amplitude (Ψ) and the phase difference (Δ) of polarised light (p and s polarised light), when reflected from a surface by using the following equation.[240-241]

$$\rho = \frac{R_P}{R_s} = Tan\,(\Psi)e^{i\Delta} \qquad (2.3)$$

where: ρ is the reflection of coefficient polarised light parallel (R_p) and perpendicular (R_s) to the plane of incidence.

Ellipsometry does not measure the thickness of the surface directly. The amplitude and phase difference measured from the ellipsometry is modelled using Thin Film Companion and the data is fitted using the Levenberg-Marquardt algorithm to minimise Chi-squared. The ellipsometry measurements reported in this thesis was carried out on silicon wafers. This is because silicon wafers are not transparent and can form uniform and highly reflective substrates which are mandatory requirements to generate accurate thickness of the surface.[240-241]

2.11 X-Ray photoelectron spectroscopy (XPS)

X-Ray photoelectron spectroscopy (XPS) is a non-destructive surface-sensitive technique, capable of providing semi-quantitative determination of the elemental composition and information about the chemical state of elements present in the first 10 layers of atoms at the surface of the sample. It is a common technique, which has been widely used to characterise peptide-immobilised surfaces.

XPS operates by irradiating the surface of a sample with a beam of soft X-rays causing electrons to be emitted. The number of emitted electrons and their kinetic energy is measured and gives rise to XPS spectra.[242-244]

The kinetic energy (KE) of the emitted electrons is measured using the following equation (2.4):

$$KE = h\nu - BE - \phi_s \qquad (2.4)$$

where hν is the energy of the photon, BE is the binding energy of electron that can be defined as the amount of energy required to release the electron from its molecular orbital and ϕ_s is the spectrometer work function. Since the energy (hv) of the X-ray and ϕ_s is already known, the binding energy (BE) of each of the electron can be experimentally determined, which can then be used to determine the kinetic energy of the emitted electron.[242-244]

The XPS spectrum represents the number of electrons emitted (per unit time) against the binding energy. Each element has characteristic binding energies for each electronic level, thus allowing for the identification of different elements present in the sample. In addition, the intensity of spectral peaks can be used to estimate the relative quantity of elements present in the sample. The shape of the XPS spectra can provide information about the chemical state, as well as the different chemical environments present in the samples.[242-244]

Chapter 3

Synthesis of battacin and its analogues

This page has been intentionally left blank

Chapter 3: Synthesis of battacin and its analogues

This chapter describes the synthesis of the lipopeptide battacin following convergent peptide synthesis strategy. This methodology involved the initial synthesis of the linear protected peptide sequence **3.11** on acid-sensitive 2-chlorotrityl chloride resin (CCR), where the side chain amine in Dab^2 was protected with highly acid sensitive protecting group Mtt and the remaining reactive side chains functionalities were protected with Boc groups that require stronger acidic conditions for their removal. The linear protected peptide **3.12** was then subjected to side-chain-to-tail cyclisation using solution-phase peptide chemistry under high dilution followed by removal of the remaining protecting groups resulting in battacin **3.14**. A series of cyclic (GZ3.21, GZ3.15, GZ3.19, GZ3.40 and GZ3.55) and linear analogues (GZ3.130, GZ3.27, GZ3.38, GZ3.26 and GZ3.37) were also designed, part of the structure-activity relationship (SAR) study.

3.1 Synthetic strategy of battacin 3.14

Battacin **3.14** has the same seven membered lactam ring as the polymyxin B (PMB), in which the cyclic ring occurs as a selective side-chain-to-tail cyclisation between the side chain amine of Dab^2 and the C-terminal carboxylic acid of Leu^8 (Figure 3.1).[177] Detailed studies of the structure of polymyxin, as well as the synthesis of its analogues, have been conducted and reported in literature because of their clinical relevance.[175,245-250] Therefore, the synthetic strategy of battacin was based on the information gathered from the polymyxin studies.

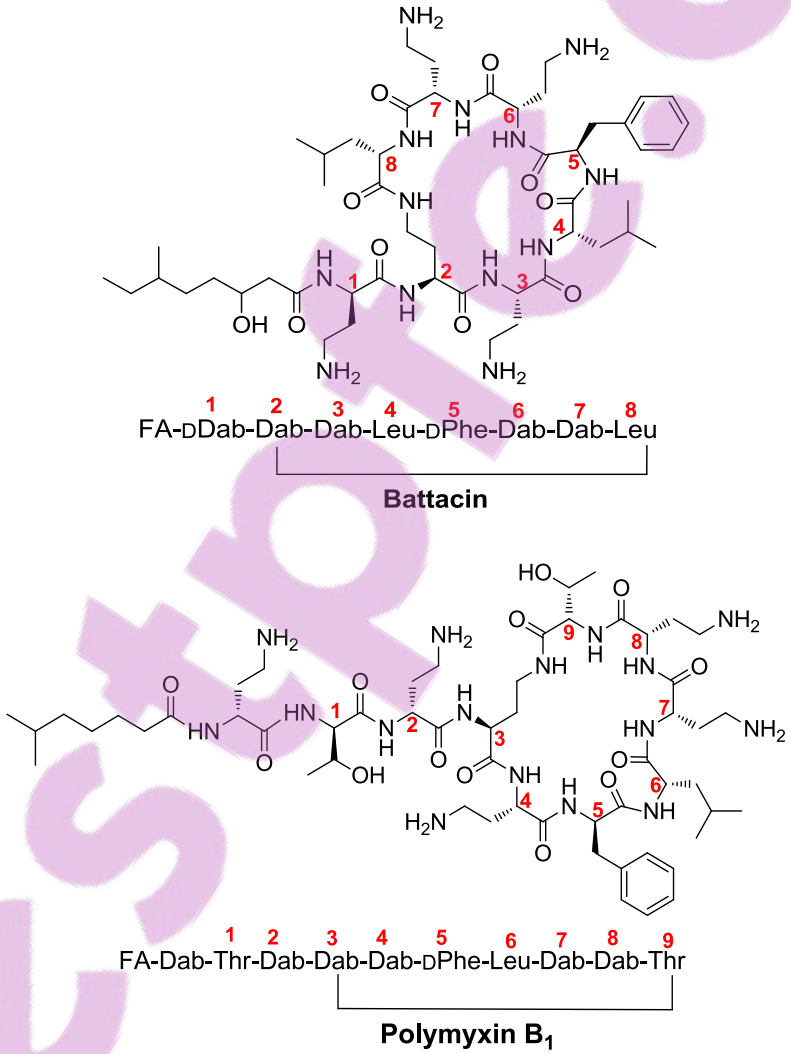

Figure 3.1 Chemical structure and amino acid sequence of battacin **3.14** and polymyxin B_1. FA denotes to fatty acid.

The synthesis of battacin was based on the methodology described by Tsubery *et al.* using acid sensitive 2-chlorotriyl chloride resin (CCR) to generate the PMBN **3.4** (Scheme 3.1).[248] According to this methodology, the protected linear PMBN sequence **3.1** was assembled on CCR.[189] The side chains of Dab and Thr in linear sequence **3.1** were protected with a *t*Bu protecting group, whereas the side chain in Dab^4 was protected with an acid-sensitive 4-methyltrityl (Mtt) group.[251] The protected linear PMBN peptide **3.2** was cleaved from the resin with simultaneous removal of the Dab^4 Mtt group, using a mixture of acetic acid (AcOH) and 2,2,2-trifluoroethanol (TFE) in DCM. Tsubery *et al*. then investigated the selective cyclisation of the protected peptide **3.2**, in solution, using four different coupling agents: PyBOP, HATU, HBTU, and DCC/HOBt, with the PyBOP showing optimum results in terms of yield and purity to generate the cyclic protected PMBN **3.3**.[248] Global deprotection of the cyclic **3.3** with TFA yielded polymyxin nonapeptide **3.4** with a 40% crude yield.[248]

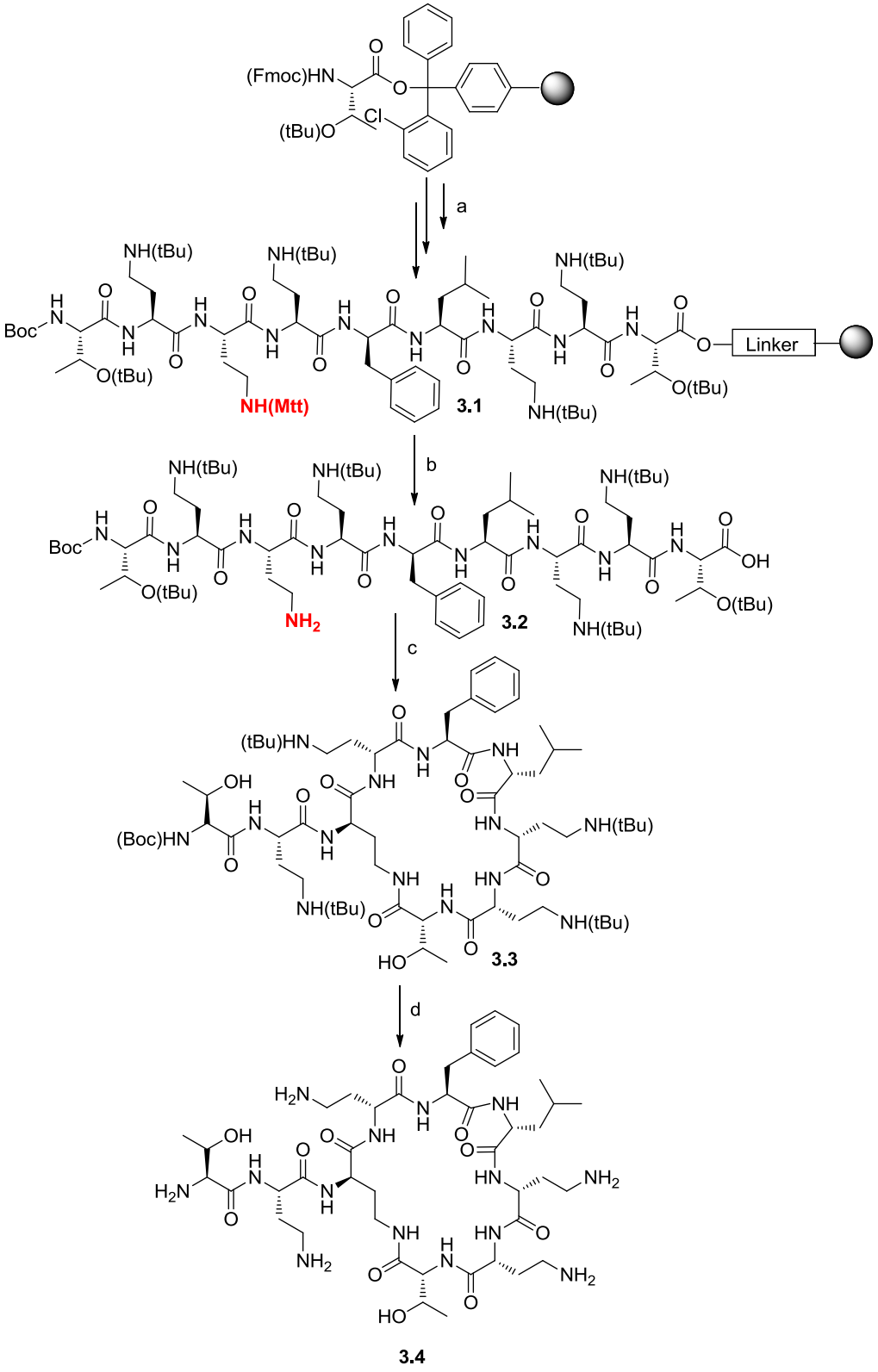

Scheme 3.1 Synthesis of PMBN **3.4** on acid sensitive 2-chlorotrityl chloride resin described by Tsubery *et al*.: **(a)** (i) Deprotection: 20% piperidine in DMF, 20 min; (ii) coupling Fmoc amino acid (4 eq), PyBOP (4 eq), 4-methylmorpholine (8 eq); **(b)** AcOH-TFE-DCM (1:1:8 v/v); **(c)** PyBOP (4 eq), HOBt (4 eq), 4-methylmorpholine (8 eq) in DMF, 2 h; (d) TFA-triethylsilane-H_2O (95:2.5:2.5 v/v),1 h, 40%.[248]

The synthesis of battacin involved two crucial steps: synthesis of the fatty acid segment and selective side-chain-to-tail cyclisation. This required initial synthesis of the fatty acid separately, followed by conjugation to the lipopeptide using SPPS. Subsequently, selective side-chain-to-tail cyclisation was attempted in solution to provide the desired peptide.

3.1.1 Synthesis of the fatty acid segment 3.10

The fatty acid segment of battacin, namely 3-hydroxy-6-methyl-octanoic acid **3.10** was synthesised following the protocol reported by Sakura *et al*.[249] As evident from Scheme 3.2, commercially available 4-methyl-hexanoic acid **3.5** was converted to the desired fatty acid **3.10** in five steps.

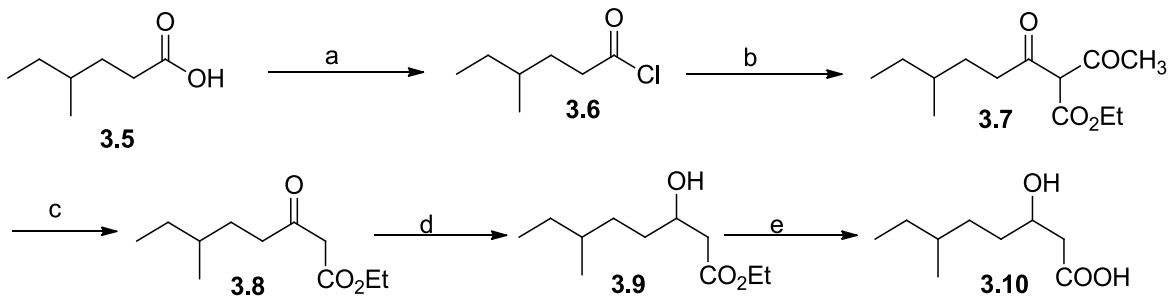

Scheme 3.2 Synthesis of 3-hydroxy-6-methyl-octanoic acid **3.10**. Reagents and conditions: **(a)** $SOCl_2$, reflux, 5 h, 95%; **(b)** ethyl acetoacetate, Na, dry Et_2O, N_2, 24 h, into which **3.6**, reflux, 24 h, 52%; **(c)** NaOH, 100 °C, 45 min, 54%; **(d)** $NaBH_4$, EtOH, 2h, 50%; **(e)** KOH, EtOH, reflux 90 min, 64%.

4-Methyl-hexanoic acid was first converted to the reactive acyl chloride **3.6** using thionyl chloride in 95% yield. This was followed by the addition of the ethyl acetoacetate to produce compound **3.7** in 52% yield. The methyl ketone moiety in **3.7** was removed under basic conditions, followed by reduction of the carbonyl group in **3.8** using the mild reducing agent sodium borohydride, to afford the hydroxylated ester **3.9** in 50% yield. The desired fatty acid, 3-hydroxy-6-methyl-octanoic acid **3.10** was produced by ester hydrolysis of the hydroxylated ester **3.9** under basic conditions in 64% yield. The hydroxyl group in the fatty

acid was left unprotected, as Sakura *et al.* successfully conjugated the same unprotected fatty acid to polymyxin. The desired fatty acid was synthesised as a racemic mixture because Qian *et al.* did not report the stereochemistry of the fatty acid of battacin.[177] However, most of the β-hydroxyl fatty acid conjugated lipopeptides have *R* configuration at the hydroxyl group.[252]

3.1.2 Synthesis of battacin 3.14

The linear version of battacin in the protected form, **3.14** was first assembled on the acid-sensitive 2-chlorotrityl chloride resin (Scheme 3.4). The C-terminal Leu^8 of battacin was attached to the CCR via esterification using DIPEA as the base. The trityl chloride moiety reacts extremely fast with the base, leading to the formation of a stable trityl cation, followed by a slow reaction between the cation and the nucleophile as shown in Scheme 3.3.[190] Following esterification, the resin was neutralised with methanol to convert the remaining active reactive chloride site to its corresponding ether, which was simply filtered off from the resin. The Fmoc group of the first amino acid was immediately cleaved with 20% piperidine, to prevent any premature amino acid cleavage that may arise from the resin, due to the instability of the Fmoc-ester bond.[184]

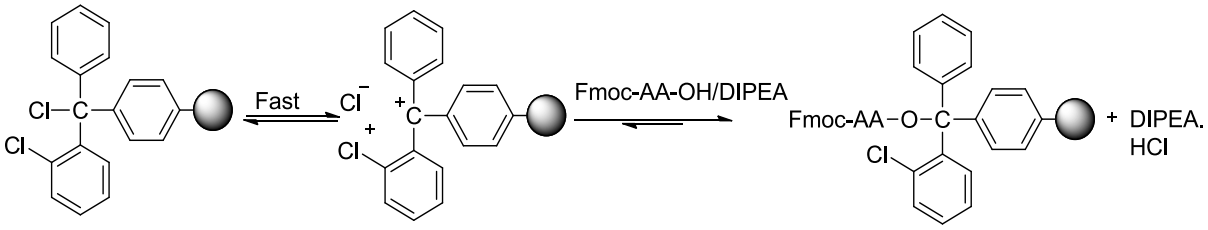

Scheme 3.3 Mechanism of action of first amino acid attachment to 2-CCR.

The remaining amino acids and the fatty acid were coupled to the resin bound Leu using 3.9 equivalents of TBTU/HOBt as the coupling reagent and suppressor respectively (Scheme 3.4). In naturally occurring battacin, the side chain of Dab^2 forms a selective peptide bond

with the COOH group of C-terminal Leu, resulting in a cyclic structure. Therefore, the side chain amine of Dab^2 was protected with an acid-sensitive Mtt protecting group, while the remaining Dab side chains were protected with Boc groups.[251,253] The linear version of battacin **3.12** with all side chains protected (except for Dab^2), was generated by the selective removal of Mtt and simultaneous cleavage of the protected peptide **3.11**, using 20% TFE in DCM for 1 h.

Selective side chain (side chain amine of Dab^2) to tail (carboxylic acid of Leu^8) cyclisation was then carried out using a mixture of 3 equivalents of TBTU/HOBt and 1% v/v DIPEA in DMF, for 3h to afford the cyclic peptide **3.13** under high peptide dilution (1.5 mM) to prevent dimerisation.[254-255] The remaining protecting groups of the cyclic peptide were removed, using a TFA-TIS-H_2O (95:2.5:2.5v/v), to produce battacin **3.14**, in an overall crude yield of 33%, as a mixture of isomers, as is the case for the isolated natural product (Scheme 3.4).

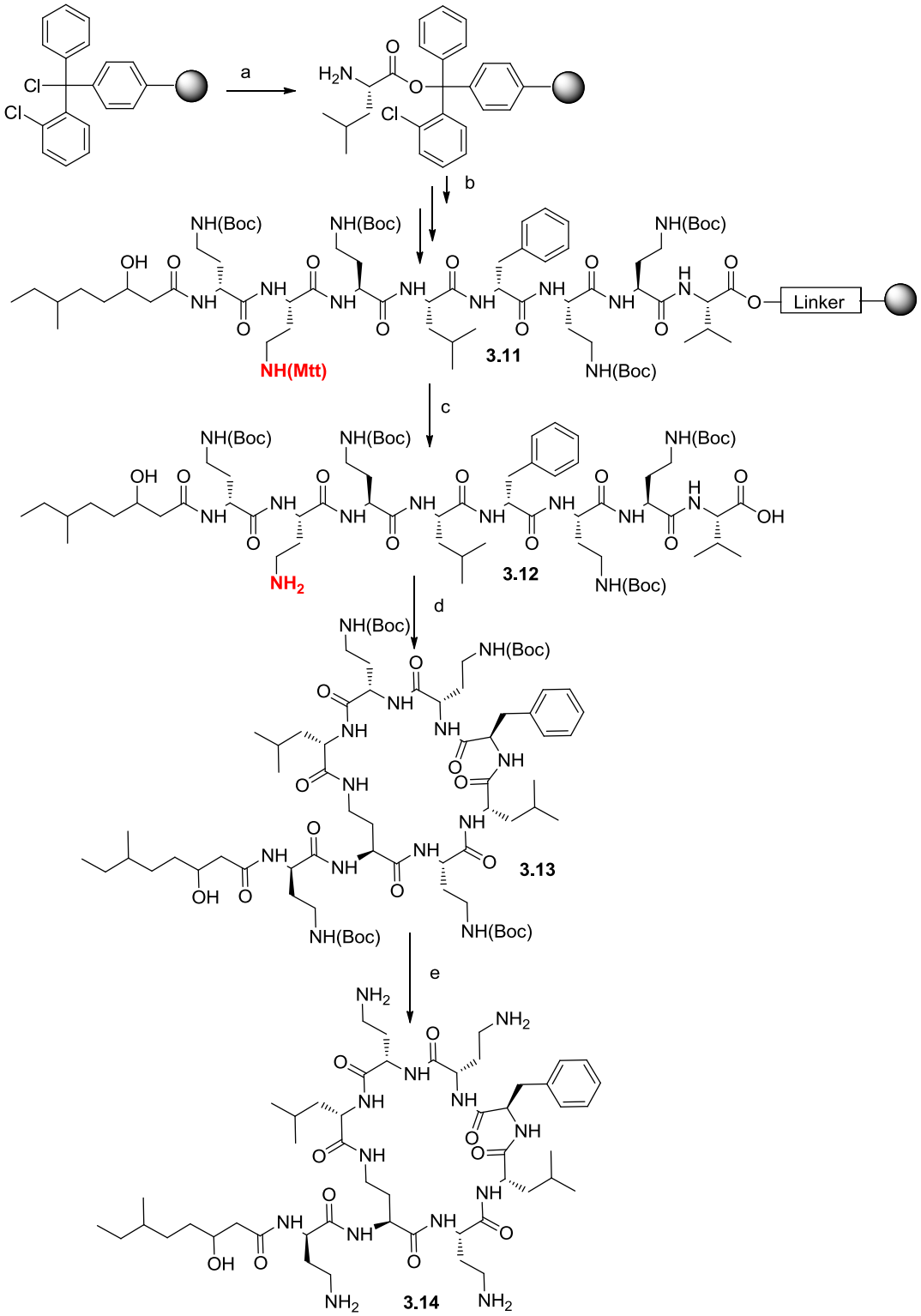

Scheme 3.4 Synthesis of battacin **3.14** on acid sensitive 2-chlorotrityl chloride resin. Reagents and conditions: **(a)** Fmoc-Leu-OH (4 eq), DIPEA (5 eq) in DCM for 1 h; Deprotection: 20% piperidine in DMF, 20 min; **(b)** (i) Coupling: Fmoc amino acid (4 eq), TBTU (3.9 eq), HOBt (3.9 eq), DIPEA (10 eq) in DMF, 45 min; (ii) Deprotection: 20% piperidine in DMF 20 min; **(c)** 20% TFE in DCM, 1h; **(d)** TBTU (3 eq), HOBt (3 eq), DIPEA (1% v/v in DMF), 3 h; **(e)** TFA-TIS-H_2O (95:2.5:2.5v/v), 3 h, 33%.

3.2 Synthesis of battacin analogues

3.2.1 Rationale behind the design of battacin analogues

A series of linear and cyclic analogues of battacin were designed to gain insight into the structure-activity relationship (SAR) of battacin (Figures 3.2 and 3.3). The cyclic analogues in Figure 3.2 were synthesised using the same protocol used for the synthesis of battacin (See Appendix A and B).

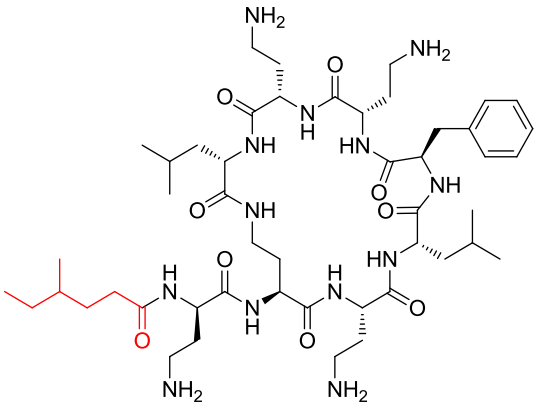

GZ3.15

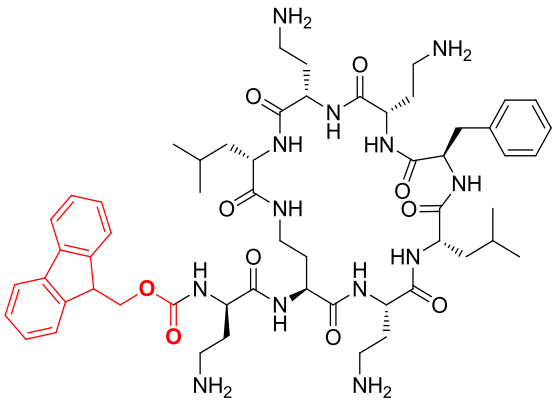

GZ3.21

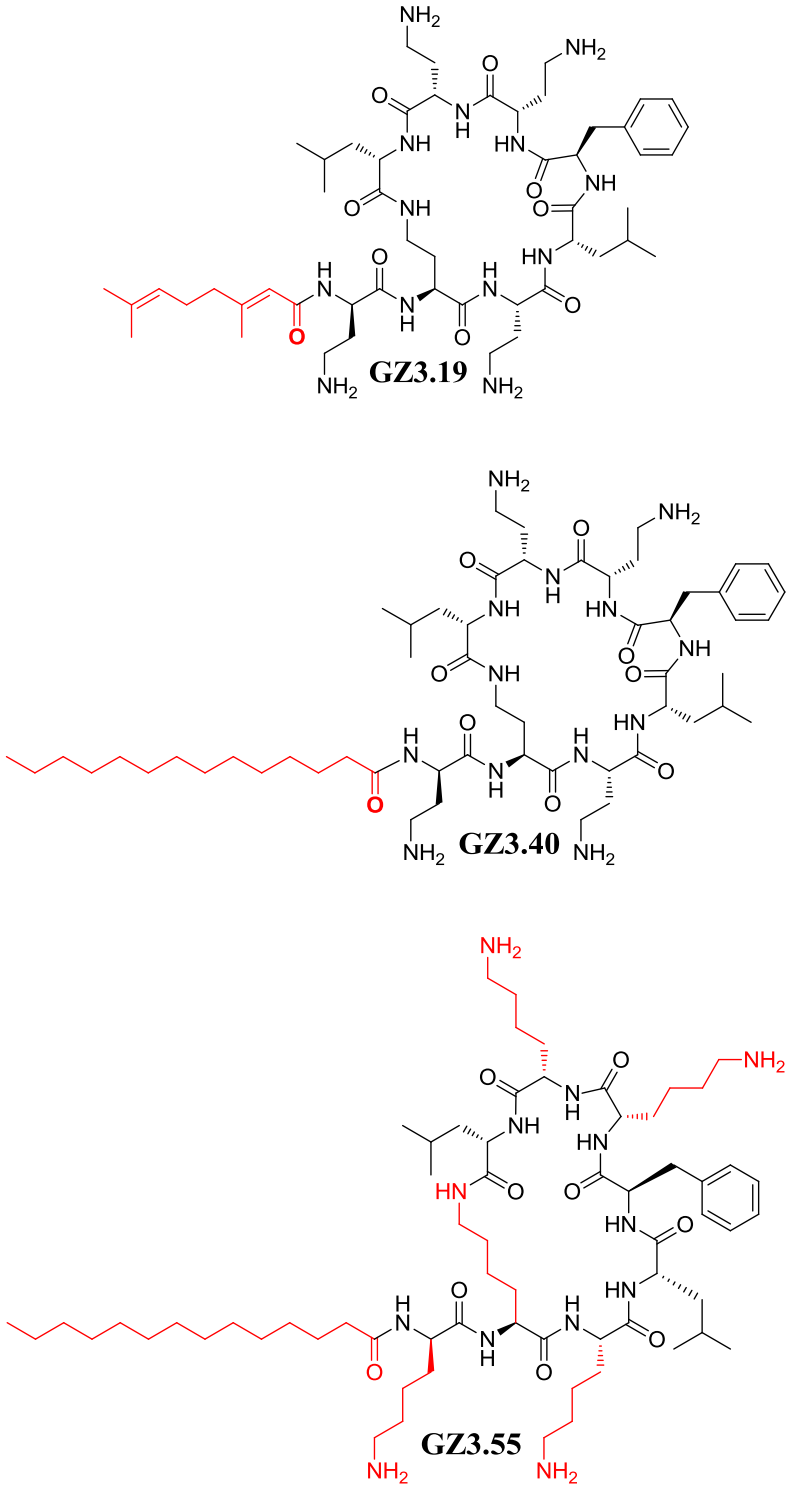

Figure 3.2 Structures of cyclic battacin analogues with the structural modifications highlighted in red.

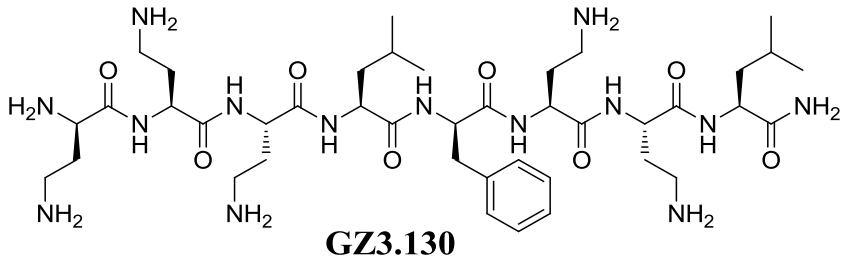

GZ3.130

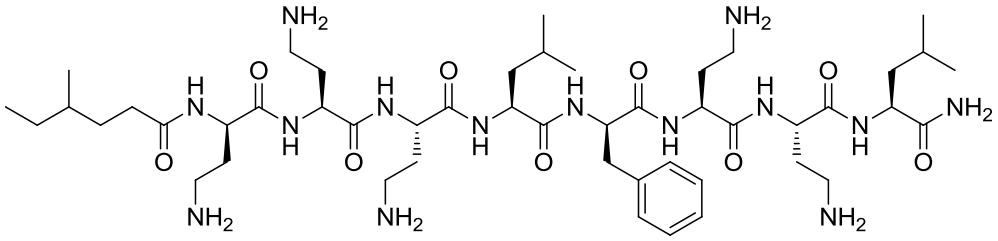

GZ3.27

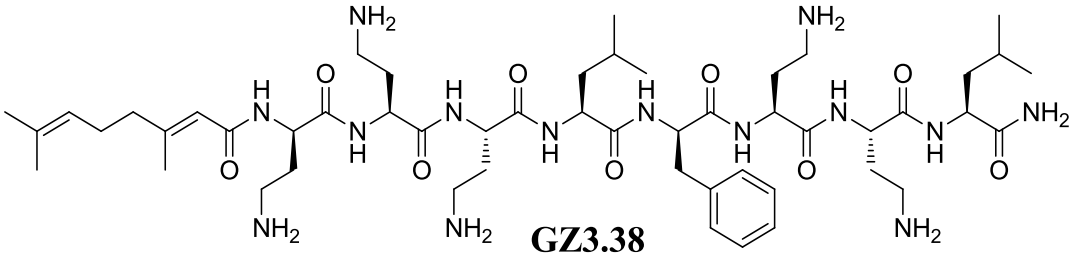

GZ3.38

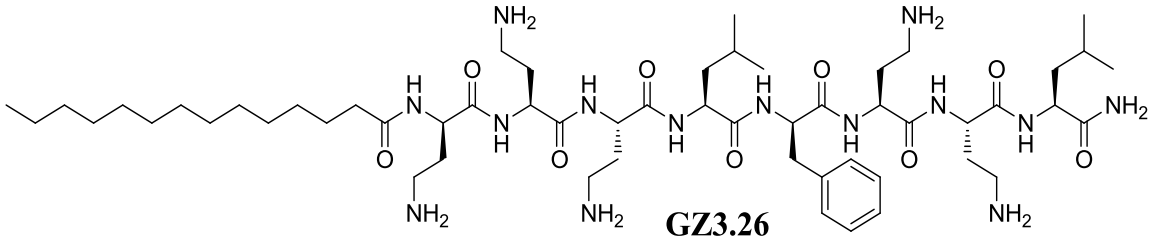

GZ3.26

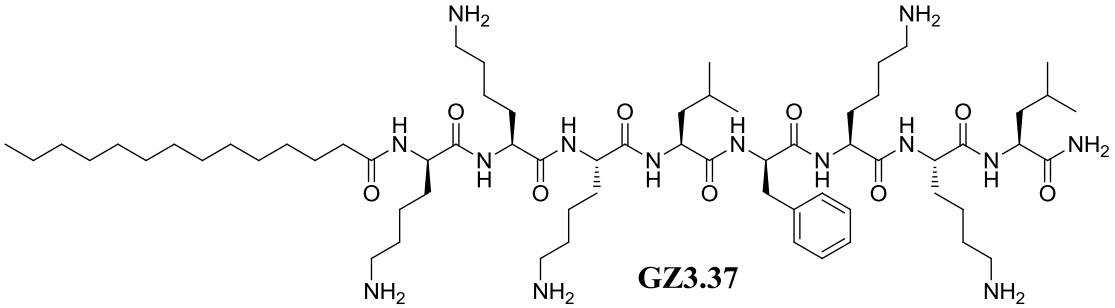

GZ3.37

Figure 3.3 Structures of linear battacin analogues.

All of the battacin analogues shared the same hydrophobic dipeptide sequence "L-Leu^5-D-Phe^6" as the natural product. As mentioned in section 1.6.1.2.2, the dipeptide sequence "D-Phe^6-L-Leu^7" of polymyxin is known to interact with the lipid A of the outer membrane of Gram-negative bacteria, and was found to be crucial for outer membrane penetration and antibacterial activity, some of which are discussed below.[248,250,256]

de Visser *et al.* synthesised a series of polymyxin analogues by substituting the hydrophobic dipeptide motif with dipeptide mimics that were capable of either inducing β-turns ((*S*)-3-amino-1-carboxymethyl-caprolactame **3.15**), favouring extended conformation (4-phenyl-4-carboxymethylpiperidine **3.16**), increasing the rigidity (*N*-carboxymethylpiperazine **3.17** and *m*-aminomethylbenzoic **3.18** acid) or increasing the flexibility (δ-aminovaleric acid **3.19**). These polymyxin analogues were highly inactive against *E. coli* ATCC 1175.[250]

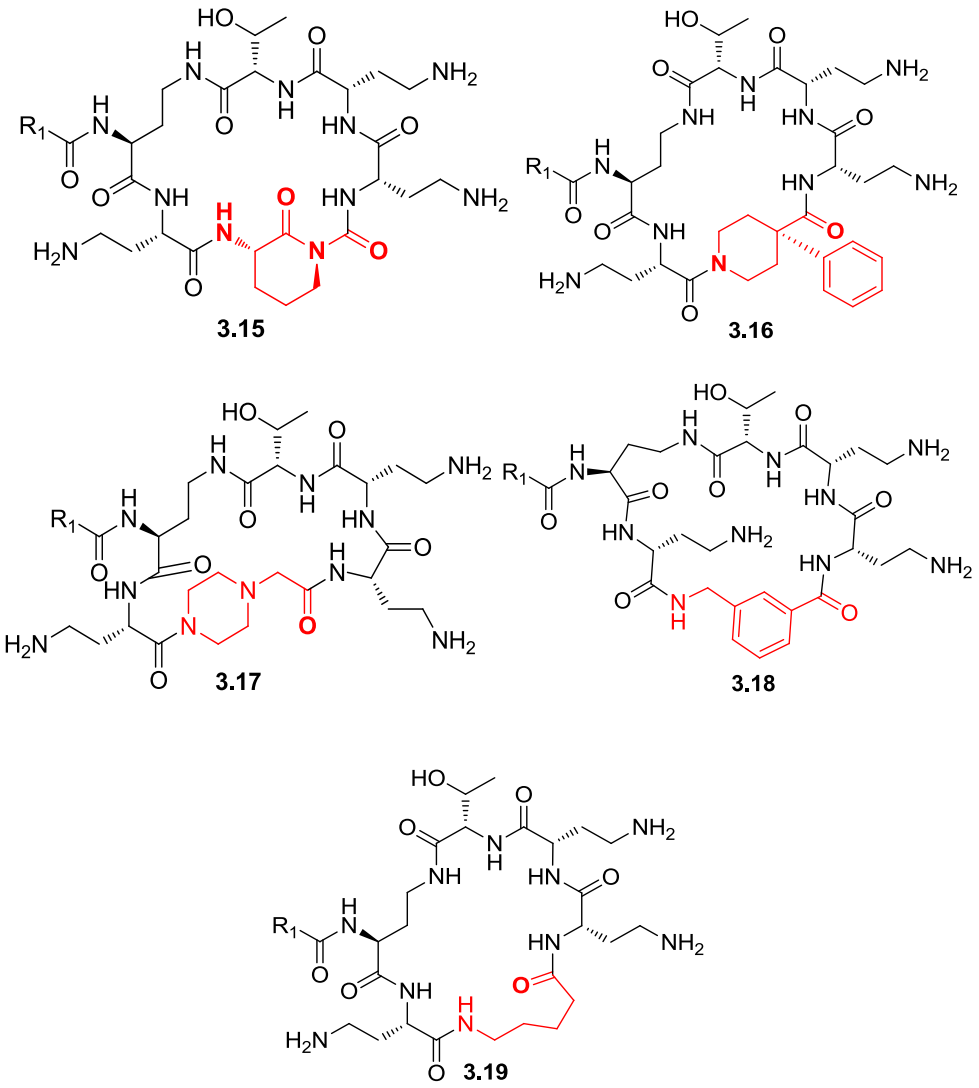

Figure 3.4 Structures of the polymyxin analogues with the structural modifications highlighted in red based on the study by Visser *et al.*[250] R_1 denotes to fatty acid conjugated to the Dab-Thr-Dab tripeptide sequence.

Tsubery *et al.* reported reduced outer membrane permeabilisation activity of PMBN analogues against the lipid A of *E. coli* when the D-Phe[6] of PMBN was substituted either with D-Trp **3.20**, D-Tyr **3.21** or L-Phe **3.22**, and when the L-Leu[7] of PMBN was substituted with L-Phe **3.23** or L-Ala **3.24**.[248,256]

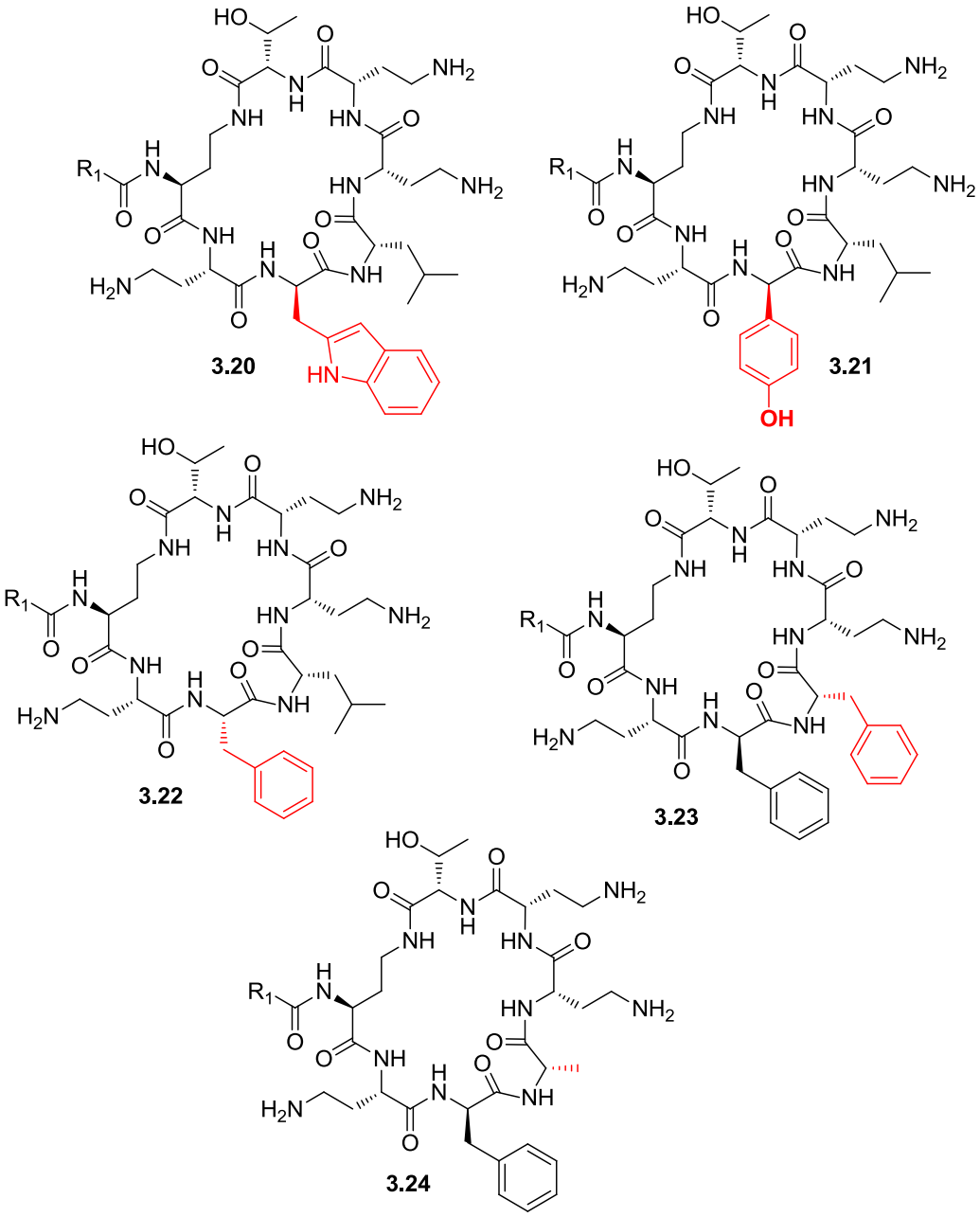

Figure 3.5 Structures of PMBN analogues described by Tsubery *et al.*[248,256] Structural modifications are highlighted in red. (R_1 denotes to Thr-Dab dipeptide sequence).

As stated above, the fatty acid moiety of PMB has also been found to be important for the observed antibacterial activity. Although the fatty acid moiety of polymyxin is crucial for its antibacterial activity, the nephrotoxicity associated with polymyxin is also attributed to this functionality.[170] Various examples of fatty acid modifications of polymyxin have been reported in a bid to identify potent analogues with a safe toxicity profile.

Several authors have reported contradictory information regarding the effect of fatty acid chain length on the antibacterial activity of polymyxin B (Figure 3.6). The Sakura,[249] Okimura[257] and O'Dowd[258] research groups have independently reported increased antibacterial activity with long chain myristoyl **3.25** and octanoyl **3.26** conjugated PMB analogues. However, Chihara *et al.* reported that the same fatty acid conjugated lipopeptides exhibited weaker antibacterial activity (20 x MIC) compared to polymyxin.[259] deVisser *et.al* reported that the replacement of (*S*)-6-methyl-octanoic acid fatty acid of PMB with the shorter hexanoic acid **3.27** led to potent antibacterial activity, although slightly less than the original PMB.[250] However, the same study reported a 10 to 20 fold reduction in antibacterial activity compared to PMB, upon conjugation of pentanoyl **3.28** and butanoyl **3.29** fatty acids to polymyxin.

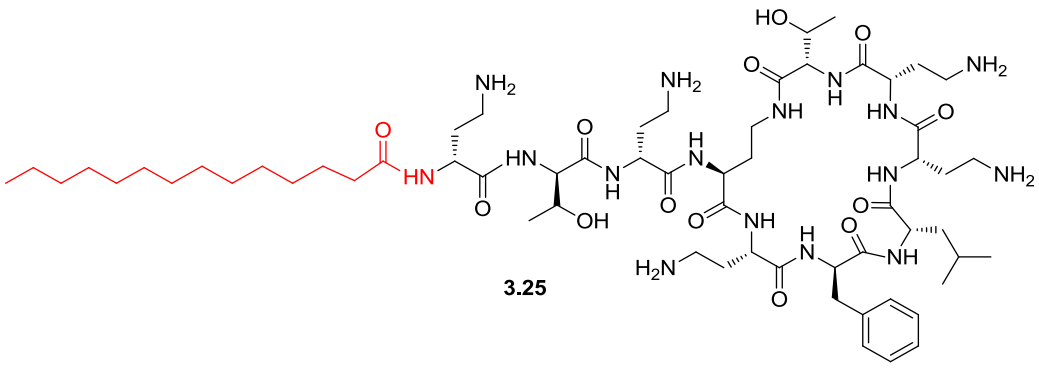

3.25

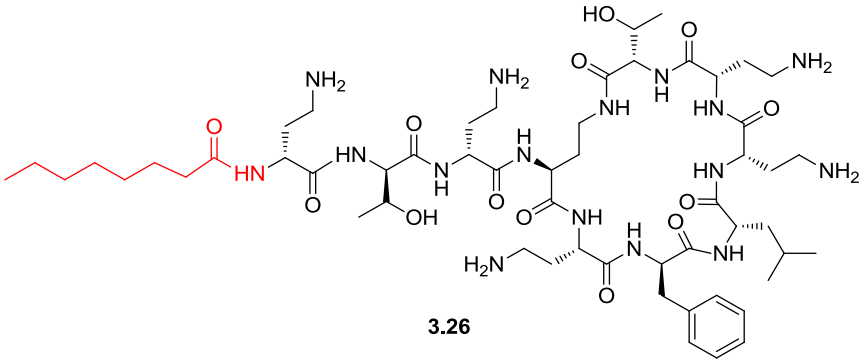

3.26

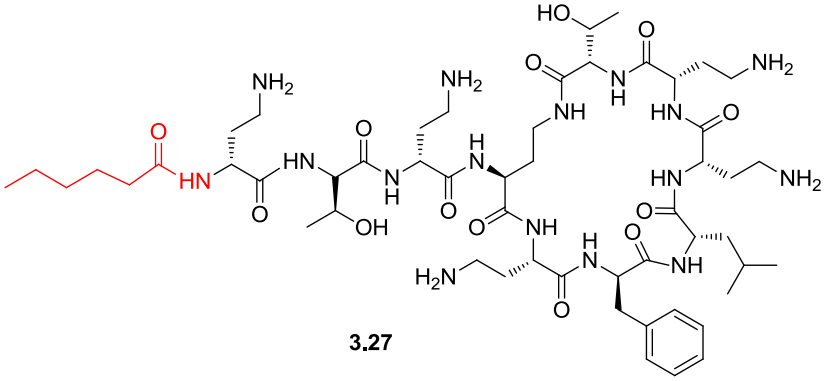

3.27

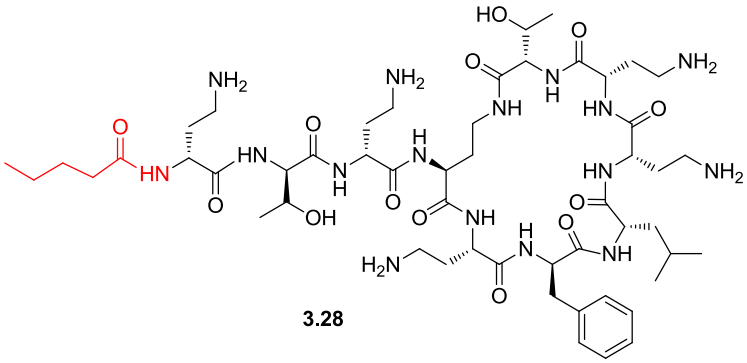

3.28

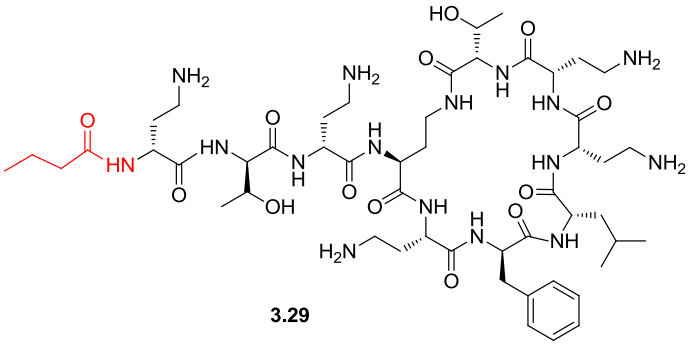

3.29

Figure 3.6 Structures of PMB analogues described by Sakura,[249] Okimura,[257] O'Dowd[258] and deVisser[250] with different chain length fatty acids (shown in red) conjugated to the N-terminus.

Tsubery *et al.* have reported that the conjugation of aromatic hydrophobic molecules, such as Fmoc to the PMBN **3.30**, led to a 60 fold, 8 fold and 2 fold reduction in the MIC against *E. coli*, *K. pneumoniae* and *P. aeruginosa* respectively.[260] The Fmoc conjugated PMBN **3.30** also showed low acute *in vivo* toxicity using mouse models compared to PMBN.

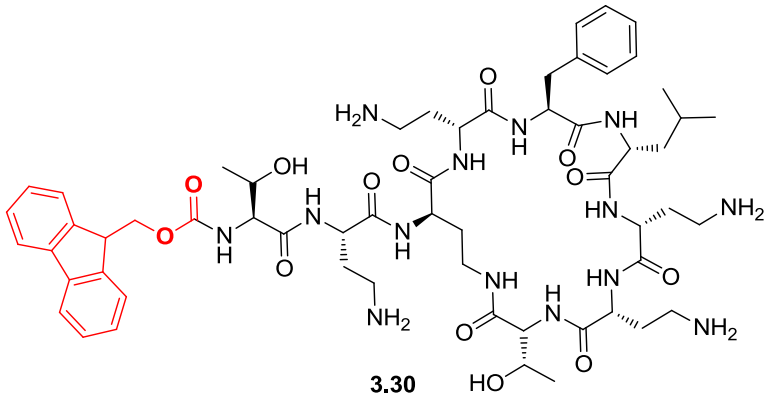

Figure 3.7 Structure of the Fmoc-conjugated PMBN analogue described by Tsubery *et al.*[260]

Based on these observations, four different cyclic battacin analogues, GZ3.21, GZ3.15, GZ3.19 and GZ3.40, were synthesised by conjugating Fmoc, 4-methyl-hexanoyl, geranyl and myristoyl groups respectively (see Figure 3.2), to evaluate the influence of fatty acid chain length, as well as the importance of the aromatic hydrophobic moiety, on the antibacterial activity.

Geranic acid **3.31**, which has a doubly branched carbon chain with two C-C double bonds, is the acid analogue of geraniol **3.32**. In previous literature, geraniol has shown antibacterial activity against the plant pathogens *Pseudomonas syringae pv. actinidiae* (Psa) and *Erwinia amylovora* (Ea).[261-262] Thus, a geranic acid-conjugated cyclic lipopeptide was designed to evaluate the antibacterial activity against these plant pathogens.

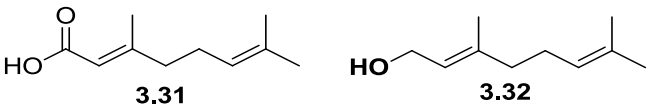

Figure 3.8 Structures of geranic acid and geraniol.

The cyclic heptapeptide moiety (23 atom-long lactam ring) of polymyxin is also crucial for the antibacterial activity.[245,248] The importance of the heptapeptide ring moiety was first reported by Vogler *et al.* in 1966. Vogler reported that the incorporation of one extra Dab **3.33** residue into the cyclic heptapeptide moiety led to significant reduction in antibacterial activity against *E. coli*.[245] Tsubery *et al.* reported that an increase in the ring size of the heptapeptide moiety from 23 atoms to 26 atoms, by replacing the Dab[4] of PMBN with Lys **3.34**, led to reduced LPS binding and outer membrane permeabilisation.[248,263] It is believed that the conserved 23 atom-long heptapeptide moiety acts as a scaffold for the electrostatic and hydrophobic LPS contact points. Thus it was decided to retain the cyclic heptapeptide moiety in cyclic battacin analogues included in this thesis.

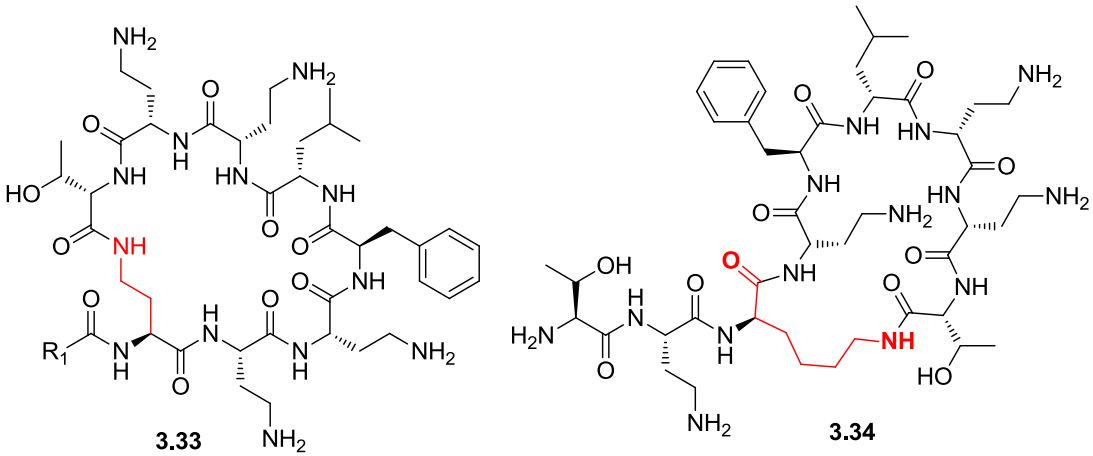

Figure 3.9 Structures of PMB (**3.33**) described by Vogler *et al.*[245] and PMBN analogue (**3.34**) described by Tsubery *et al.*[248,263] with increased ring size. R_1 of **3.33** denotes to fatty acid conjugated to the Dab-Thr-Dab tripeptide sequence.

For comparative purposes, five linear lipopeptides were also designed. These are linear lipopeptides without either the N-terminal fatty acid (GZ3.130), the 4-methyl-hexanoyl

(GZ3.27), the geranyl (GZ3.38) or the two myristoyl (GZ3.26 and GZ3.55) groups conjugated to it (see Figure 3.3).

Literature reports indicate that linearisation of polymyxin analogues as well as substitution of the Dab amino acids in the linear sequences have led to reduced activity.[264-265] Vaara *et al.* reported that the linear PMBN analogues, where all the Dab in the linear sequence were substituted with either Arg **3.35** or Lys **3.36**, led to a 100 fold reduction in outer membrane permeabilisation against *E. coli*.[264] Kurihara *et al.* reported a 100 fold decrease in antibacterial activity against *E. coli* with linear colistin analogue **3.37** where the all the Dab in the sequence were replaced with Lys.[265]

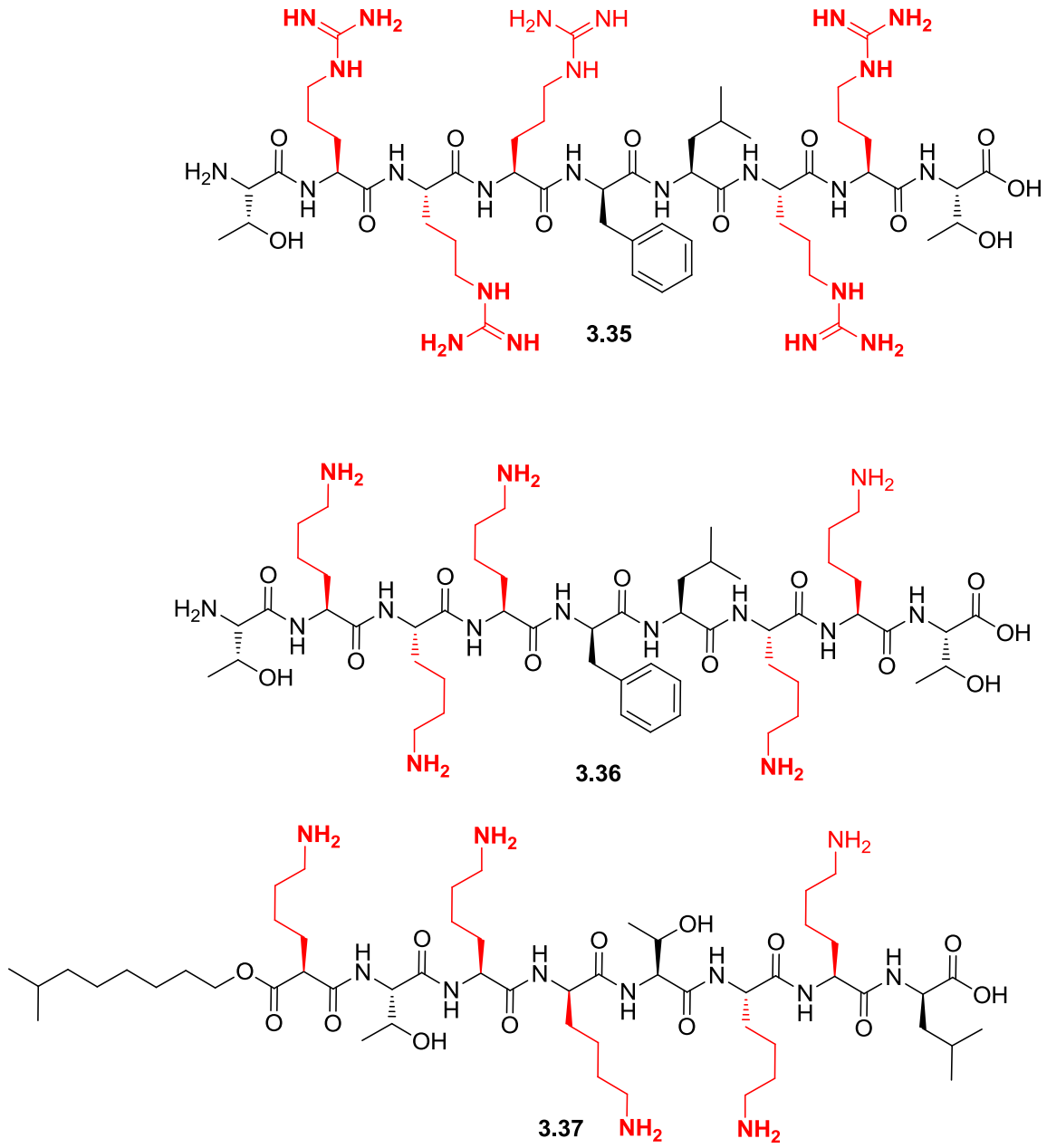

Figure 3.10 Structures of the linear PMBN (**3.35** and **3.36**) described by Vaara *et al.*[264] and colistin (**3.37**) analogues described by Kurihara *et al.*[265]

Numerous studies have shown that masking some or the all of the positive charges of the Dab amino acids in the peptide sequence in the cyclic PMBs, either by sulfomethylation **3.38**,[161] acetylation **3.39**,[266] deamination **3.40**,[267] or formylation **3.41**,[267] led to decreased antibacterial activity (Figure 3.11). Therefore, the five Dab residues in the natural product battacin were

retained in all the battacin analogues studied as part of this thesis and have an overall positive charge of five, equivalent to the isolated battacin.

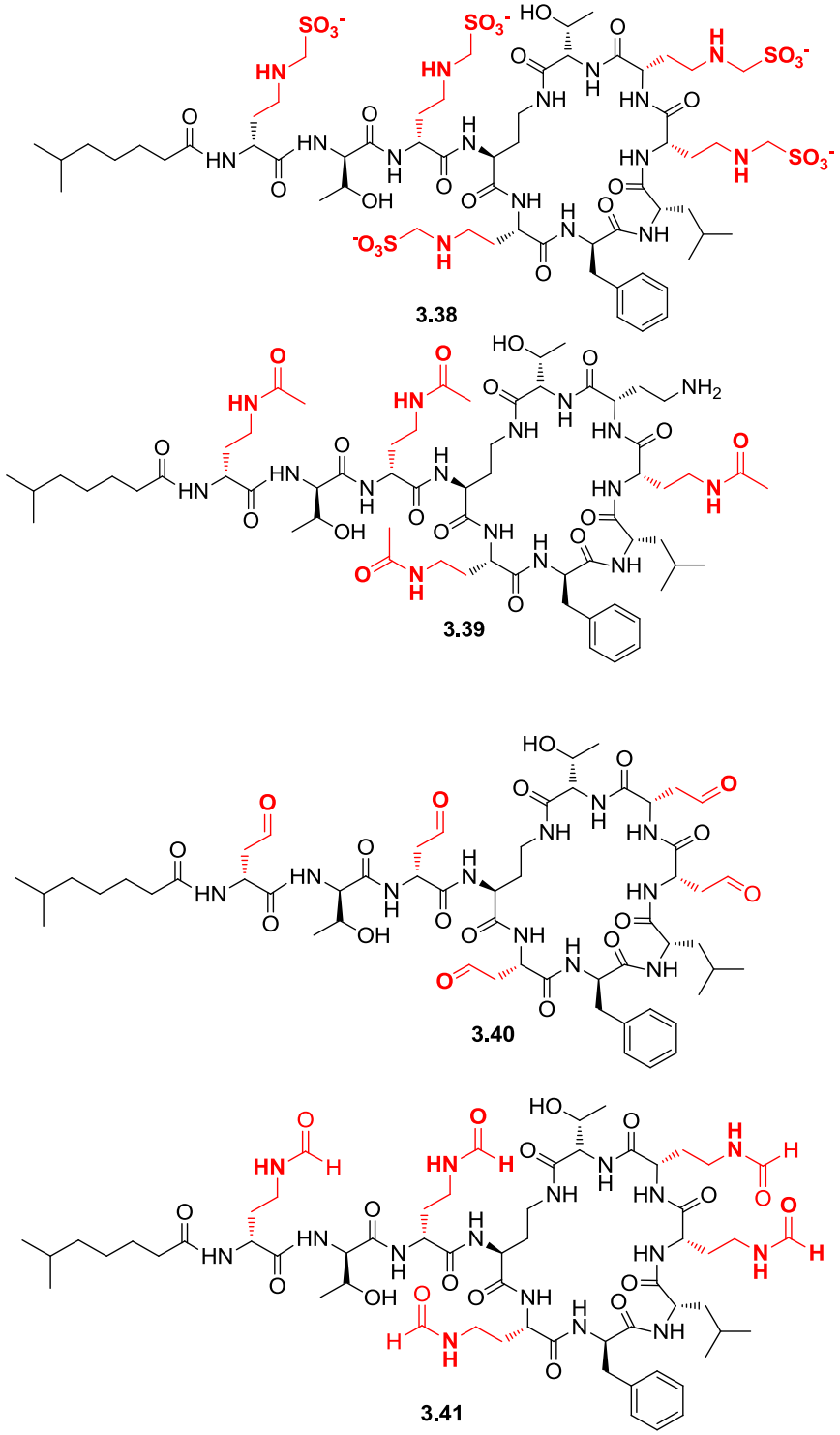

Figure 3.11 Structures of PMB analogues (**3.38-3.41**) in which some, or all, of the cationic Dab residue in the sequences were masked.[161,266-267]

In addition, Kurihara *et al.* reported that the substitution of all the Dab amino acids in colistin with Lys **3.42** led to the retention of the same level of antibacterial activity as colistin (0.2 μg/mL), against *E. coli*.[265] In a similar manner, Porro *et al.* synthesised a series of polymyxin analogues where all the Dab amino acids in the sequence were replaced with cationic amino acids such as Lys, Arg and His.[268] These polymyxin analogues exhibited a higher affinity than polymyxin for the binding pocket of lipid A, to neutralise endotoxins, and was subsequently filed as a patent in the USA, as a potential treatment against septic shock.[268] Based on the studies by Kurihara and Porro, Lys substituted cyclic (GZ3.55) and linear (GZ3.37) versions of the 14-carbon myristic analogues were designed.

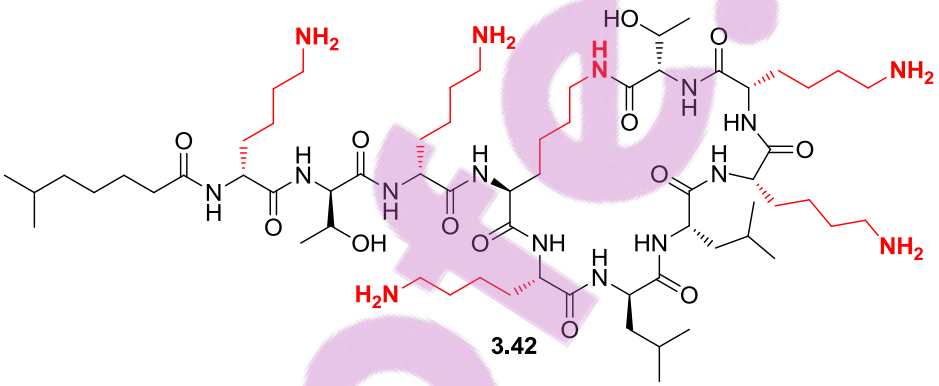

Figure 3.12 Structure of the Lys substituted colistin analogue described by Kurihara *et al.*[265]

3.2.1.2 Synthesis of linear battacin analogues

Linear battacin analogues (GZ3.130, GZ3.27, GZ3.38, GZ3.26 and GZ3.37) were synthesised as amidated peptides to maintain similar peptide stability as the cyclic lipopeptide analogues. All of the linear peptides were synthesised according to the same protocol, and this methodology is shown in Scheme 3.5, using the synthesis of GZ3.27 as an example. The rink amide linker was manually coupled to Tentagel-S-NH_2 resin under standard coupling conditions of 3.9 equivalents of TBTU and 10 equivalents of DIPEA in DMF (Scheme 3.5). Following the removal of the Fmoc group, the subsequent amino acid building blocks and the

commercially available fatty acids were assembled onto the resin, using TBTU/HOBt as the coupling reagent. The linear lipopeptide **3.45** was then cleaved from the resin, using a mixture of TFA-TIS-H_2O (95:2.5:2.5) and crude peptides purified using RP-HPLC. The purity of the linear and cyclic lipopeptides was verified using analytical HPLC and their identities confirmed using mass spectrometry (See Appendix A and B).

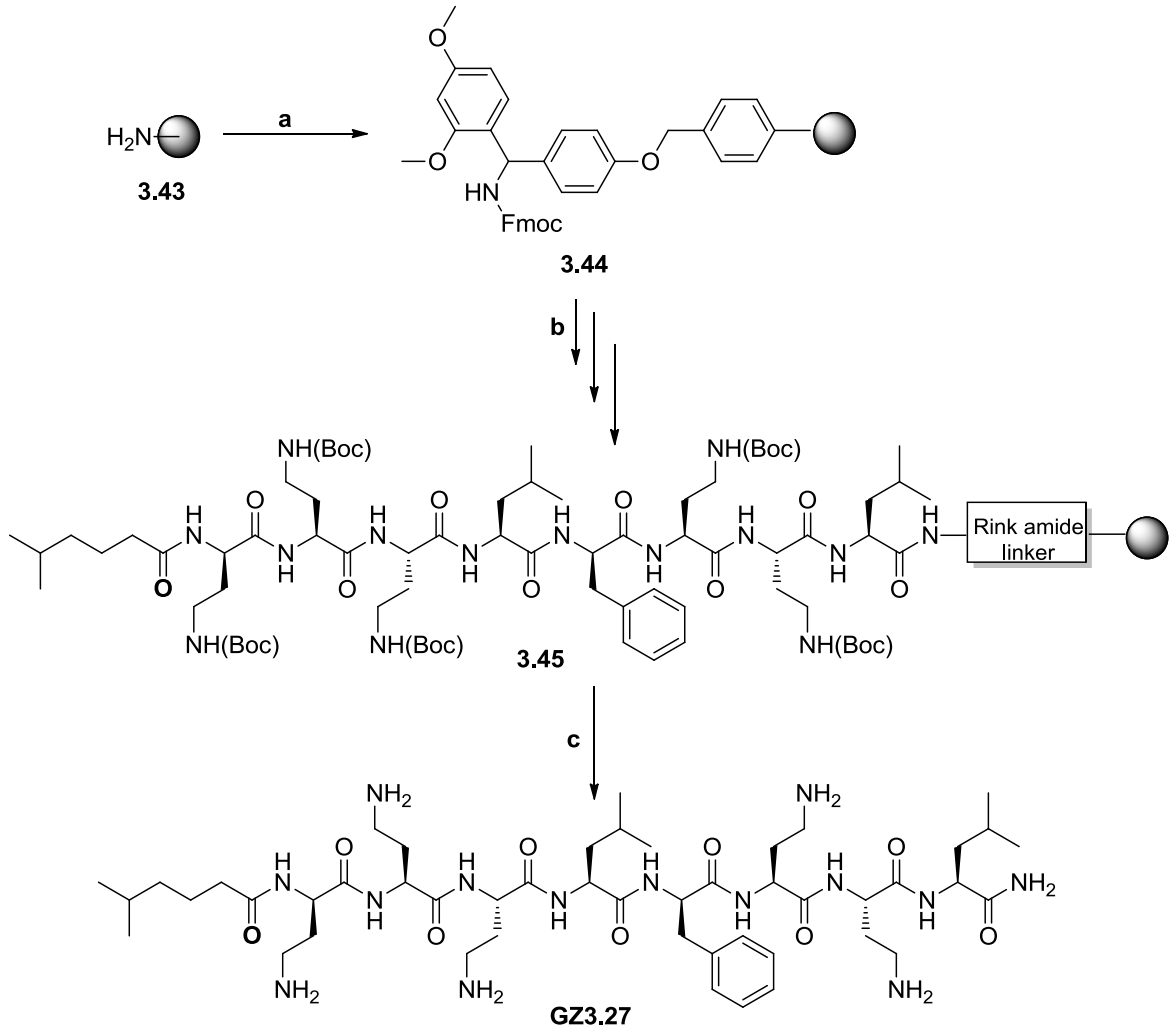

Scheme 3.5 Synthesis of linear battacin analogue GZ3.27. Reagents and conditions: **(a)** Rink amide linker (4 eq), TBTU (3.9 eq), HOBt (3.9 eq), DIPEA (10 eq) in DMF for 1 h; **(b)** (i) Deprotection: 20% piperidine in DMF, 20 min; (ii) coupling: Fmoc amino acid (4 eq), TBTU (3.9 eq), HOBt (3.9 eq), DIPEA (10 eq) in DMF, 45 min; **(c)** TFA-TIS-H_2O (95:2.5:2.5 (v/v), 3 h.

3.3 Summary

In summary, battacin **3.14** was successfully synthesised with a crude yield of 33%, using convergent peptide synthesis, where the protected linear lipopeptide **3.12** was synthesised on the acid-sensitive CCR. The selective side-chain-to-tail cyclisation of the protected peptide **3.13** was carried out under high peptide dilution in solution phase and was followed by global deprotection, to afford battacin. Following the successful synthesis of the battacin, five cyclic and linear battacin analogues were designed, based on the SAR information reported for polymyxin. The five cyclic lipopeptides were also successfully synthesised using the convergent peptide synthesis strategy and the linear lipopeptides as amidated peptides using a rink amide linker. These battacin analogues, along with the synthetic version of the natural product, were evaluated for potent antibacterial activity, and the screening results will be discussed in Chapter 4.

3.4 Experimental

3.4.1 General details

All chemicals were of reagent-grade quality and were used without further purification. Flash column chromatography was carried out using Silica flash P60 silica gel (Merck) with the indicated solvents. Fmoc protected Leu, D-Phe, 2-chlorotrityl chloride resin and Fmoc-rink amide linker were purchased from GL Biochem (Shanghai, China). Fmoc-Dab (Boc)-OH and Fmoc-Dab(Mtt)-OH amino acids were purchased from Alabiochem Tech Co. Ltd. (China). 4-methyl-hexanoic acid, trifluoroacetic acid, piperidine and myristic acid were obtained from Sigma Aldrich. Tentagel-S-NH_2 resin was obtained from Peptide International (Louisville, USA). 2, 2, 2-trifluroethanol and geranic acid were purchased from Alfa Aesar (Heysham, England). Solid phase peptide synthesis was carried out on a custom–made, glass reaction vessel fitted with a fritted filter.

NMR spectra were recorded on either Bruker AVANCE 400 (^{1}H, 400 MHz), Bruker AVANCE 500 (^{1}H, 500 MHz) or Bruker AVANCE 600 (^{1}H, 600 MHz) instruments at the School of Chemical Sciences, University of Auckland. The NMR spectrum of GZ3.26 was recorded on Bruker 800 MHz spectrometer at the NMR research centre, Indian Institute of Science. For ^{1}H NMR data, chemical shifts are described in parts per million (ppm) relative to tetramethylsilane (δ = 0.00 ppm) for organic solvents either using the residual water signal (δ = 4.87 ppm) or using trimethylsilyl propanoic acid (δ = 0.00 ppm) for aqueous solutions. ^{1}H NMR parameters are reported as chemical shift δ_H, relative integral, multiplicity (s = singlet; t = triplet; m = multiplet), coupling constant (*J* in Hz) and assignment. The NMR spectra were recorded either at 278 K or 300 K.

Accurate mass spectra were recorded using a Bruker microQTOF ESI- mass spectrometer at the School of Chemical Sciences, University of Auckland, and a Voyager-DE Pro MALDI-

TOF mass spectrometer at the Faculty of Medical and Health Sciences, University of Auckland.

The crude peptides were purified to homogeneity, using reversed-phase high performance liquid chromatography (RP-HPLC), on a GE Pharmacia ÄKTA purifier 10 system with a Phenomenex Luna 5 micron C_{18} 100Å (250 x 10 mm) column. 0.1% TFA in Milli-Q water was used as solvent A and 0.1% TFA-and 1% Milli-Q water, in 99% acetonitrile, as solvent B, at a flow rate of 4 mL per minute. The peptides were eluted using a linear gradient (see Appendix A) with UV detection at 214 nm. The purity and identity of the peptides were established by analytical RP-HPLC, using a Phenomenex Luna 5 micron C_{18} 100Å (250 x 4.6 mm) column, using the same solvent system as above, at a flow rate of 1 mL per minute.

3.4.2 Fatty acid synthesis

3.4.2.1 4-methyl-hexanoyl chloride 3.6[249]

A solution of 4-methyl hexanoic acid **3.5** (0.9 g, 0.007 mol) and thionyl chloride (2.27 eq, 1.4 mL) was refluxed for 5 hours. The thionyl chloride was distilled out to give **3.6**, as oil (1 g, 95%). δ_H (**400 MHz, $CDCl_3$**) 0.78-0.98 (6H, m, $C\underline{H}_3$) 1.1-1.8 (5H, m, $CH_3C\underline{H}_2(CH_3)C\underline{H}C\underline{H}_2$) 2.88 (2H, m, $C\underline{H}_2CO$).

3.4.2.2 Ethyl-2-acetyl-6-methyl-3-oxooctanoate 3.7[249]

Clean sodium (0.15 g, 0.007 mol) was added to a flame-dried flask, under N_2. Dry diethyl ether (50 mL) was added dropwise, to produce a cloudy solution. Ethyl acetoacetate (2 eq, 1.7 mL, 0.013 mol) was carefully added to the cloudy solution and stirred, at room temperature, overnight. The fatty acid **3.6** (1 g, 0.007 mol) was then added to the solution and it was refluxed for 24 hours, to produce a brown-coloured solution. Water was added to the reaction mixture, and it was extracted with diethyl ether. The organic layer was washed with

brine, and concentrated to produce a brown oil, **3.7** (1.8 g, 52%). **HRMS (EI): m/z** $[M+H]^+$ calculated for $C_{13}H_{22}NaO_4$ 265.1410; observed 265.1382. δ_H (**400 MHz, $CDCl_3$**) 0.78-0.98 (6H, m, $C\underline{H}_3$) 1.1-1.8 (5H, m, $CH_3C\underline{H}_2(CH_3)C\underline{H}C\underline{H}_2$) 1.28 (3H, t, *J* 7.4, $C\underline{H}_3CH_2$) 2.33 (3H, s, $COC\underline{H}_3$), 2.6 (2H, m, $C\underline{H}_2CO$), 4.05 (1H, s, $Ac(CO)C\underline{H}CO_2Et$), 4.22 (2H, m, $CH_3C\underline{H}_2$).

3.4.2.3 Ethyl-6-methyl-3-oxooctanoate 3.8[249]

The fatty acid **3.7** (4.8 g, 0.02 mol) was dissolved in water, and sodium hydroxide (0.8 g, 0.02 mol) was added to the solution. The solution was heated at 100 °C for 45 minutes, and then cooled in an ice bath. The fatty acid solution was extracted with diethyl ether and concentrated under reduced pressure to yield **3.8** (2.18 g, 54%). **HRMS (EI): m/z** $[M + Na]^+$ calculated for $C_{11}H_{20}NaO_3$ 223.1305; observed 223.1311.

3.4.2.4 Ethyl-3-hydroxy-6-methyl-octanoate 3.9[249]

Compound **3.8** (1.1 g, 0.005 mol) was dissolved in a minimum volume of ethanol (25 mL). Water (0.5 mL) and sodium tetrahydroborate (0.5 eq, 0.1 g, 0.03 mol) were added to this solution and it was stirred for 2 hours, at room temperature. The solvent was removed under pressure, and extracted with diethyl ether. The organic layer was washed with brine, dried and concentrated under reduced pressure to produce oil **3.9** (0.5 g, 50%). **HRMS (EI): m/z** $[M + Na]^+$ calculated for $C_{11}H_{22}NaO_3$ 225.1461; observed 225.1465.

3.4.2.5 3-Hydroxy-6-methyl-octanoic acid 3.10[249]

The fatty acid **3.9** (0.5 g, 0.002 mol) was dissolved in a solution of ethanol (6 mL) and water (3 mL). Potassium hydroxide (0.2 g, 0.004 mol) was added to the solution and it was refluxed for 90 minutes. The ethanol was removed via distillation, and followed by the addition of water (3 mL) and neutralisation with 2N hydrochloric acid. The product was extracted with DCM and washed with brine. The organic layer was then concentrated under reduced

pressure, to get the desired fatty acid as an oil **3.10,** which was further purified by flash column chromatography using DCM as the eluent.(0.3 g, 64%). **HRMS (EI): m/z** $[M- H]^-$ calculated for $C_9H_{17}O_3$ 173.1178; observed 173.1189.

3.4.3 Syntheses of cyclic lipopeptides

The peptides were assembled on the acid sensitive 2-chlorotrityl chloride resin (CCR) with a substitution level of 0.8-1.5 mmol/g at a 0.1 mmol scale. The C-terminal amino acid (4 eq) was dissolved in DCM. DIPEA (4 eq) was added to the solution, and reacted with CCR for 5 minutes. Excess DIPEA (6 eq) was added again to the agitated reaction mixture, and was reacted for a further 45 minutes. Excess trityl chloride groups in CCR were neutralised with a mixture of DCM-MeOH-DIPEA (85:15:5; 10 mL), for 10 minutes. The Fmoc group of C-terminally coupled amino acid was immediately removed with 20% piperidine in DMF (1 x 3 min, 1 x 20 min), to produce a yellow resin.[184]

The remaining amino acid couplings were mediated in a DMF solution, using TBTU (3.9 eq) as the coupling reagent, HOBt (3.9 eq) as the additive and DIPEA (10 eq) as the base. The side chain of Dab at position two was protected with Mtt, while the remaining side chain amines of Dabs were protected with Boc protecting groups.[269] On completion of chain assembly, the side-chain protected (except for Dab^2) linear lipopeptides were cleaved from the resin, under mild acidic conditions using 20% 2,2,2-trifluroethanol in DCM, for 1 hour.[270-271] The cleavage mixture was evaporated under a stream of nitrogen. The protected linear peptide was dissolved in acetonitrile and lyophilised to yield the peptides as white fluffy solids.

Peptide cyclisation was carried out in DMF at 1.5 mM concentration, with a 3 fold excess of TBTU, HOBt and 1% DIPEA (v/v), for 3 hours.[272] The reaction mixture was concentrated under reduced pressure, dissolved in water and lyophilised to yield the protected cyclic

lipopeptides as white fluffy solids. Global deprotection was carried out using TFA-TIS-H_2O (95:2.5:2.5; 10 mL) for 3 hours. The cleavage mixture was evaporated under reduced pressure, dissolved in water and lyophilised to obtain the crude cyclic lipopeptides, which were purified using RP-HPLC.

3.4.4 Syntheses of linear lipopeptides

All peptides were synthesized by manual solid phase peptide synthesis, using standard Fmoc protocols. The peptides were assembled on Tentagel-S-NH_2 resin (substitution level of 0.29 mmol/g) as C-terminal amides, using rink amide linker, on a 0.1 mmol scale. Boc protecting groups were used as the side-chain protecting group of Dabs. Amino acid (4 eq) couplings were mediated in DMF, using TBTU (3.9 eq) as the coupling reagent, HOBt (3.9 eq) as the additive and DIPEA (10 eq) as the base. The same coupling procedure was used for coupling the fatty acids to the N-termini of the peptides. The final lipopeptides were cleaved from the resin using a TFA cocktail mixture (TFA-TIS-H_2O - 95:2.5:2.5; 10 mL) for 3 hours. The cleavage mixture was evaporated under reduced pressure, and the crude peptides precipitated using a large excess of cold diethyl ether. The white solid was re-suspended in cold diethyl ether, centrifuged thrice to produce a white pellet, which was dissolved in water and lyophilised to recover the crude peptides as white fluffy solids. The crude peptides were purified to homogeneity using RP-HPLC.

Chapter 4

Antibacterial activity of battacin and its analogues

This page has been intentionally left blank

Chapter 4: Antibacterial activity of battacin and its analogues

This chapter describes the antibacterial studies of synthetic battacin and its analogues. The analysis of the antibacterial activity of the battacin library was undertaken against two horticultural pathogens relevant to New Zealand, and some common human pathogens, in order to identify potent analogues. The most potent lipopeptide was then evaluated for anti-biofilm activity by studying its capability to both inhibit the initial formation of biofilms and to disperse mature biofilms.

The ability of the lipopeptides to lyse bacterial membranes was initially assessed with colorimetric assays composed of dimiristoylphosphocholine (DMPC) and polydiacetylene polymers such as 10, 12-tricosadiynoic acid (TRCDA), to mimic the anionic bacterial membrane. The most potent analogue was studied in depth. Detailed evaluation of their antibacterial mechanism carried out using standard outer and inner membrane permeability assays, while scanning electron microscopy (SEM) revealed morphological changes to peptide-treated bacteria. The secondary structure of this lipopeptide was determined using NMR and CD spectroscopies, and correlated to the observed antibacterial activity.

4.1 Rationale behind the selection of the pathogens

As mentioned previously, battacin is highly potent against nosocomial *P. aeruginosa* and *E. coli* strains; hence, the antibacterial activity of the battacin analogues was evaluated against *P. aeruginosa* and *E. coli*. Even though battacin and the closely related polymyxin, showed only weak antibacterial activity (>50 μM) against *S. aureus*, the analogue series was evaluated against the Gram-positive bacterium *S. aureus* to probe if the structural modifications could improve the activity against Gram-positive strains as well. The antibacterial activity of the battacin analogues were also investigated against two plant pathogens that are of significance to New Zealand's horticultural industry.

4.1.1 Human pathogenic bacteria

4.1.1.1 *Pseudomonas aeruginosa*

Pseudomonas aeruginosa is a Gram-negative, rod-shaped, ubiquitous, opportunistic human pathogen. *P. aeruginosa* is known to grow in soil, moist environments, and plant and animal tissues.[273-274] In humans, *P. aeruginosa* can colonise the ear, nasal mucosa, throat, lungs and stools.[274] Generally, *P. aeruginosa* does not cause any infections in healthy individuals but immunocompromised patients are highly susceptible to this pathogen, and it can therefore be classified as a nosocomial pathogen.[274-275] Nosocomial infections caused by *P. aeruginosa* include pneumonia, urinary tract infections, septicaemia, surgical site infections and skin infections resulting from burn wounds.[274-275] *P. aeruginosa* is the most common bacterial pathogen isolated from the lungs of cystic fibrosis patients, and accounts for the majority of the causes of mortality. According to the USA Cystic Fibrosis Foundation Patient Registry, more than 57% of patient respiratory cultures contain *P. aeruginosa*.[276] *P. aeruginosa*, isolated from lungs of cystic fibrosis patients are either non-mucoid or have the ability to over-express the

exopolysaccharide, alginate (mucoid). Mucoid *P. aeruginosa* is mainly associated with chronic cystic fibrosis patients.[277-278]

Unfortunately, there is a steady increase in the number of MDR *P. aeruginosa* isolated from hospital environments.[279] For instance, a 9-year surveillance study of MDR pathogens isolated from a single US hospital, between 1994-2002, reported an increase from 1% to 16% in the number of isolated *P. aeruginosa* pathogens resistant to one or more antibiotics.[279] Several resistant strains can over-express drug efflux pumps such as MexA-MexB-OprM, MexC-MexD-OprJ, MexE-MexF-OprN and MexX-MexY-OprM three component systems to exclude antibiotic classes such as quinolones, aminoglycosides and β-lactams.[280] Intrinsic resistance of *P. aeruginosa* to most of the β-lactams is due to over expression of drug inactivating, β-lactamase enzymes such as Amp*C* β-lactamase, that are capable of hydrolysing the β-lactam ring in the antibiotics.[281] Many of the aminoglycoside antibiotics are ineffective against MDR *P. aeruginosa* strains that are capable of over-expressing enzymes such as aminoglycoside phosphoryltransferase, aminoglycoside acetyltransferase and aminoglycoside nucleotidyltransferase, that are capable of modifying the aminoglycoside structure, by either phosphorylation, acetylation or adenylation respectively, to render its activity ineffective.[282]

4.1.1.2 *S. aureus*

S. aureus is a Gram-positive, spherical opportunistic pathogen mainly found in respiratory system and on skin.[283-284] Generally, more than 30% of healthy human individuals are colonised by *S. aureus* mainly concentrated in the anterior nares and vagina. In healthy individuals, *S. aureus* can cause infections such as skin infections (pimples, boils), cellulitis, food poisoning and abscesses.[283-284] However, *S. aureus* is one

of the most frequently isolated pathogens in the hospital environment and can also cause life threatening infections, such as hospital-acquired pneumonia, toxic shock syndrome, sepsis and acute or right sided endocarditis.[283-284] *S. aureus* frequently colonises medical implants such as heart valves, central venous catheters and intrauterine devices.[23]

Several pathogenic strains of *S. aureus* are developing resistance to one or more classes of antibiotics at an alarming rate, by either horizontal gene transfer from a resistant organism, chromosomal mutation in the genes or selection pressure from the antibiotics.[284] Ever since the first reported outbreak of MRSA in 1960, this multi-drug resistant pathogen is now the most commonly recognised antibiotic-resistant pathogen affecting many parts of the world including Europe, Americas, North Africa, the Middle East and East Asia.[285] In the 1990s community-associated MRSA was isolated from healthy individuals.[286] Even though community-associated MRSA is more susceptible to antibiotics than the nosocomial MRSA, the former is still capable of causing serious skin illness such as necrotising fasciitis and necrotising pneumonia.[283]

4.1.1.3 *E. coli*

E. coli is a Gram-negative, rod-shaped bacterium that mainly colonises the gastrointestinal tract of warm-blooded organisms, and is often non-pathogenic. However, some strains of *E. coli* can cause serious illness such as urinary tract infections, sepsis and diarrhea. Rare Shiga toxin producing *E. coli* strains O157:H7 and O10:H4, often found in tainted food, are highly virulent pathogens capable of causing life threatening hemolytic-uremic syndrome.[287] Ever since the first reported outbreak of hemolytic-uremic syndrome caused by this pathogen in 1982 in USA, several other countries and regions such as the UK, Canada, Belgium, Africa and New Zealand have reported similar outbreaks.[288] In 2011, a severe outbreak of diarrhea and hemolytic uremic syndrome, caused by the *E. coli*

O10:H4, was reported in Germany. This virulent pathogen caused diarrhea in 3167 people with 16 fatalities, while further 908 people were diagnosed with uremic-syndrome diarrhea leading to 34 deaths.[289]

4.1.2 Plant pathogens

4.1.2.1 *Erwinia amylovora*

Erwinia amylovora (Ea) is a Gram-negative, rod-shaped plant pathogen that causes the fire blight disease in rosaceous species such as apple and pears. Currently, fire blight is known to affect over 40 countries, and causing havoc in the New Zealand apple and pear industry.[290] A severe fire blight outbreak has the potential to wipe out entire orchards in a single season. In fact, in 1998, an outbreak of fire blight in the Hawkes's Bay region of New Zealand, cost over $10 million in damages.[291] Due to the severity of the fire blight disease in New Zealand, Australia has restricted the export of New Zealand apples, causing a revenue loss of over $20 million.[290]

Successful management of the fire blight requires a combination of better horticultural practice to minimise the spread of disease and the use of chemical sprays such as copper compounds and streptomycin to protect the plants against *E. amylovora*.[290-291] However, most of the existing chemical options to control fire blight disease have the drawbacks of resistance development and phytotoxicity.[291] In fact many of the affected regions in Europe have either restricted or banned the use of streptomycin in agriculture to prevent other pathogenic microorganisms living in close proximity from acquiring resistance to it.[290]

4.1.2.2 *Pseudomonas syringae pv. actinidiae*

Pseudomonas syringae pv. actinidiae (Psa) is also a Gram-negative plant pathogen, affecting both green (*Actinidia deliciosa*) and yellow (*Actinidia chinensis*) fleshed kiwifruits.[292] This highly virulent pathogen is causing havoc in the kiwifruit industry in Japan, Korea, Spain and New Zealand. Kiwifruit export in New Zealand generates around $1 billion per annum, making it the second most economically valuable crop to be exported from New Zealand.[292] A severe Psa outbreak in New Zealand was first observed in the kiwifruit orchards in the Bay of Plenty, in November, 2010, and it has since spread, infecting 57% of the total orchards throughout the country.[292] The economic consequences of this outbreak is expected to cost between $410 million to $885 million in the long term.[293] Currently, no effective treatment against Psa is available other than to minimise the spread of the disease using a combination of good horticultural practices such as pruning and removal of the infected plants, as well as use of copper compounds and streptomycin as biocides against this pathogen. However, these chemical compounds are also toxic to the kiwifruit plant and are ineffective against resistant Psa strains.[294-295]

Previously, our laboratory successfully designed series of AMPs against both *E. amylovora* and Psa pathogens.[296] These analogues were designed from the cecropin-melittin hybrid peptide, BP76, a 12-amino acid long, C-terminally amidated peptide, reported by Ferre *et al.* as showing antibacterial activity against the plant pathogens *E. amylovora*, *Pseudomonas syringae* and *Xanthomonas vesicatoria*.[297] A lipopeptide analogue, myristoyl conjugated dodecapeptide (AC160) showed low micromolar potency (5.6-8.4 μM) activity against *E. amylovora* and Psa pathogen and has encouraged the investigation of the potency of the battacin analogues against these two plant pathogens.[296]

4.2 *In vitro* antibacterial activity of battacin peptides

The antibacterial potency of the battacin library was evaluated using the broth dilution MIC assay, the results of which are summarised in Table 4.1

Table 4.1 Antibacterial activity of synthetic analogues of battacin*

Peptide		Modification(s)	MIC (μM) Ea1501	Str4Ea	*E. coli*	Psa16027	*P. aeruginosa*	*S. aureus*
Cyclic	Battacin	-	24-49	24-49	10-15	5-10	5-10	>50
	GZ3.21	Fmoc	19-32	32-65	19-32	19-32	2-5	2-5
	GZ3.15	4-methyl-hexanoyl	15-25	25-50	15-25	5-10	2.5-5	101-507
	GZ3.19	geranyl	98-488	488-976	98-488	49-98	10-15	98-488
	GZ3.40	myristoyl	92-461	23-46	92-461	46-92	92-461	92-461
	GZ3.55	myristoyl and Lys	81-409	20-41	81-409	12-20	409-817	81-409
Linear	GZ3.130	No fatty acid	112-560	560-1120	500-1000	5-10	2-5	>1000
	GZ3.27	4-methyl -hexanoyl	2.5-5	5-10	2.5-5	1-2.5	1-2.5	1-2.5
	GZ3.38	geranyl	24-48	48-96	24-48	14-24	48-96	48-96
	GZ3.26	myristoyl	9-14	14-23	5-9	14-23	14-23	5-9
	GZ3.37	myristoyl and Lys	12-21	12-20	12-20	12-20	12-20	1-2.5
	Streptomycin	-	1-2.5	500-1000	1-2.5	1-2.5	N	N
	Gentamicin	-	N	N	N	N	<1	2.5-5

*Average of three independent experiments performed in triplicate. N: not tested

The cyclic lipopeptides showed weaker antibacterial activity than their corresponding linear counterparts did. For instance, the myristoyl-conjugated cyclic lipopeptide GZ3.55 showed weaker antibacterial activity against *P. aeruginosa* (409-817 μM) and *S. aureus* (81-409 μM), whereas the linear version of the same lipopeptide GZ3.37 was more potent antibacterial activity against *P. aeruginosa* (12-20 μM) and *S. aureus* (1-2.5 μM).

In both the linear and cyclic series, the shortest fatty acid (4-methyl-hexanoyl) conjugates (GZ3.15 and GZ3.27) were significantly more potent against the Gram-negative pathogens tested, than their longer fatty acid geranyl (GZ3.19 and GZ3.38) and myristoyl (GZ3.40, GZ3.55, GZ3.26 and GZ3.37), counterparts. For instance, the linear 4-methyl-hexanoyl conjugated lipopeptide (GZ3.27) showed low micromolar activity (1-2.5 μM) against *P. aeruginosa* and *S. aureus*, whereas the longer fatty acid geranyl conjugated linear lipopeptide GZ3.38 showed a higher MIC (48-96 μM) against *P. aeruginosa* and *S. aureus*.

This is in agreement with the trend reported by Storm *et al.* for a range of fatty acid derivatives of octapeptin B, where shorter fatty acid derivatives showed greater potency against *E. coli* and *B. subtilis*.[298] deVisser *et al.* also reported similar results with the hexanoyl-conjugated polymyxin B analogues (see structure **3.27** in Figure 3.6) showing potent activity (0.7 μg/mL) against *E. coli* ATCC 11775.[250] More recently, the dependence of fatty acid chain length on antimicrobial activity has been reported for synthetic analogues of tridecaptin A1, where peptides carrying shorter than C_6 or longer than C_{12} fatty acids had significantly less activity.[299]

The potency of Fmoc conjugated battacin (GZ3.15) against *P. aeruginosa* is similar to the MIC of Fmoc conjugated PMBN (see structure **3.30** in Figure 3.7) (4 μg/mL) analogue reported by Tsubery *et al.*[260]

The cyclic lysine analogue of the myristic acid conjugate (GZ3.55) was approximately four times more active against Psa, and marginally more active against Ea1501, Str4Ea, *E. coli*, and *S. aureus*, while showing marginally lower activity against *P. aeruginosa*, as compared to its Dab counterpart (GZ3.40).

The linear lysine analogue of the myristic acid conjugate (GZ3.37) was the most potent against *S. aureus* and exhibited approximately four times increased activity than its Dab counterpart (GZ3.26) against this pathogen. Otherwise, it demonstrated comparable activity against all other pathogens except for being approximately two-fold less active against *E. coli*. The activity of GZ3.37 was either the same as (Str4Ea, Psa, *P. aeruginosa*) or marginally lower (Ea1501 and *E. coli*) than the Dab counterpart (GZ3.26).

Three of the linear lipopeptides (GZ3.26, GZ3.27 and GZ3.37) and battacin in its Fmoc protected form (GZ3.21) showed low micromolar (< 10 μM) activity against the Gram-positive pathogen *S. aureus*. The 4-methyl-hexanoyl linear lipopeptide, GZ3.27 had the lowest MIC (1-10 μM) against all tested pathogens.

Analogous to the natural product, synthetic battacin did not show significant activity (> 50 μM) against the Gram-positive pathogen *S. aureus*, and its activity against the tested Gram-negative strains ranged between 5 and 49 μM.[177]

The linear peptide without the N- terminal fatty acid, GZ3.130, showed weak or no antibacterial activity against the fire blight pathogen, *E. coli* and *S. aureus*. However, both strains of *Pseudomonas* were highly susceptible to the linear peptide GZ3.130. Since

most of the *Pseudomonas* strains are pathogenic, the ability of GZ3.130 to target *Pseudomonas* species selectively, over other bacteria, may indicate the ability of this lipopeptide to act as a "target-specific" antimicrobial therapy.

The battacin library is effective against the kiwifruit pathogen, with all of the tested analogues showing MICs between 1-98 µM. Other than the myristic-acid conjugated cyclic lipopeptides (GZ3.40 and GZ3.55) which showed high MIC (92-817 µM), the battacin analogues were potent (1-100 µM) against *P. aeruginosa*. The Fmoc conjugated battacin (2.5-5 µM) was the only cyclic lipopeptide effective against *S. aureus*. GZ3.27, which emerged as the most potent in this study, was selected as the lead candidate for further analysis. It is to be noted that the MICs of GZ3.27, against the pathogens studied, are in the low micromolar range, similar to the antibiotic controls streptomycin and gentamicin.

The fatty acid moiety is clearly important for the antibacterial activity, as the linear peptide without any conjugated fatty acid, GZ3.130, showed significant loss of activity against most of the tested pathogens. As discussed previously, studies by other groups reported in the literature, have revealed that the fatty acid moiety of polymyxin interacts with the hydrophobic lipid A of the lipopolysaccharide (LPS), leading to a weaker packing of the outer membrane and eventually membrane lysis.[298] Although polymyxin B nonapeptide (PMBN) showed weak or no activity against most of the Gram-negative pathogens, *P. aeruginosa* was susceptible to PMBN.[248,300]

The greater susceptibility of *Pseudomonas* species to battacin analogues could be attributed to the varying fatty acid chain compositions of the lipid A in the outer membrane of Gram-negative bacteria.[160,301-302] The lipid A in *E. coli* and *E. amylovora* consists of four C_{14} and two C_{12} fatty acid chains.[301] The lipid A in *P. aeruginosa* and Psa

consists of four C_{12} and two C_{10} fatty acid chains.[302-303] Therefore, the outer membranes of *Pseudomonas* species are less tightly packed than *E. coli* and *E. amylovora*.[302] It is possible, therefore, that weaker hydrophobic interactions would be sufficient to disrupt the outer membranes of the *Pseudomonas* species.[302] In addition, Moore *et al.* have identified that polymyxin is capable of binding to multiple binding sites of the *P. aeruginosa* LPS, as a result of the higher number of negative charges on the outer membrane of this pathogen.[300] Therefore, the battacin analogues probably have greater electrostatic interaction with the LPS of the *P. aeruginosa*, contributing to the observed antibacterial activity.

In accordance with the literature, the results of the MIC assay on the battacin library demonstrated the importance of the fatty acid chain length, with the shorter and branched 4-methyl-hexanoyl being the most potent. Although the fatty acid chain can increase the hydrophobic interaction with the bacterial membrane, the more hydrophobic, longer fatty acid conjugated lipopeptides (myristoyl), or the extensively branched (geranyl) ones, may self-associate, or sterically hinder the insertion of the fatty acid into the outer membrane. The lipid packing of the outer membrane may not be sufficiently disrupted by these peptides to induce the potent antibacterial activity.[160,299] In fact, Nikaido *et al.* have suggested that the bacterial outer membrane is generally impermeable to hydrophobic molecules, therefore it is possible that the increasingly hydrophobic lipopeptides may find it difficult to penetrate the outer membrane of the Gram-negative bacteria.[304]

The short 4-methyl-hexanoic acid seems to provide the optimal hydrophobic interaction in the current series of peptides, without actually hindering the effective membrane disruption.

Finally, the potency of the antibacterial activity of Fmoc conjugated battacin (GZ3.21) can possibly be attributed to the planar fluorene ring of the Fmoc moiety, which can intercalate with the bacterial outer membrane leading to a disruption of the lipid packing in LPS and eventual cell death.

Probably the most interesting result of the SAR study was that, contrary to the findings in the vast majority of modern literature, the linearisation of both the natural product and analogues not only provided greatly enhanced potency against Gram-negative bacterial strains, but also resulted in low micromolar activity against the Gram-positive pathogen *S. aureus*.

Generally, it is considered that macrocyclisation of peptides offers numerous advantages. Eliminating the charged N- and C-termini increases hydrophobicity, and can hence improve passage through or integration into hydrophobic membranes.[105] A large reduction in flexibility can help to create bias towards or populate a more well-defined structure, that is appropriate for membrane or even receptor binding.[305] Additionally, improved activity may result from increased resistance to enzymatic degradation derived from the inherent reduction in flexibility.[105]

However, for the battacin analogues it appears that the improved flexibility provided by linearisation actually promotes effective membrane interaction and hence, disruption. It is possible that the cyclic peptides may still bind to the membrane with similar effectiveness (see colorimetric assay, section 4.7.1) but instead their mode of membrane interaction does not invoke a significantly detrimental disruption to the membrane structure. For *S. aureus* in particular, this discrepancy was exaggerated, an effect that may be related to the change of target. For Gram-negative bacteria, AMPs can target the outermost layer of the cell, the outer membrane, while for Gram-positive bacteria such as *S. aureus*; AMPs must

target the cell membrane, and hence must cross the cell wall, before inducing any antimicrobial effects. Seemingly, enhanced flexibility may improve access through the cell wall resulting in greater peptide concentration at the site of action. In addition, despite linearisation, GZ3.27 also possesses a lipopeptide moiety and an abundance of non-protein amino acid D-Dab, which could potentially offer enhanced proteolytic resistance even in the linear form.[105,119]

4.3 Time-kill assay of GZ3.27

The kinetic assay involves incubating diluted bacterial cultures with antibacterial compounds at different concentrations and plating onto nutrient rich agar plate at different time intervals. After overnight incubation, the surviving colonies are counted to determine the colony-forming unit (CFU). The assay can be used to determine the kinetics of bacterial growth inhibition. The time kill assay of GZ3.27 was performed against *S. aureus*, *P. aeruginosa*, *E. coli*, Ea1501 and Psa16027, as summarised in Figure 4.1.

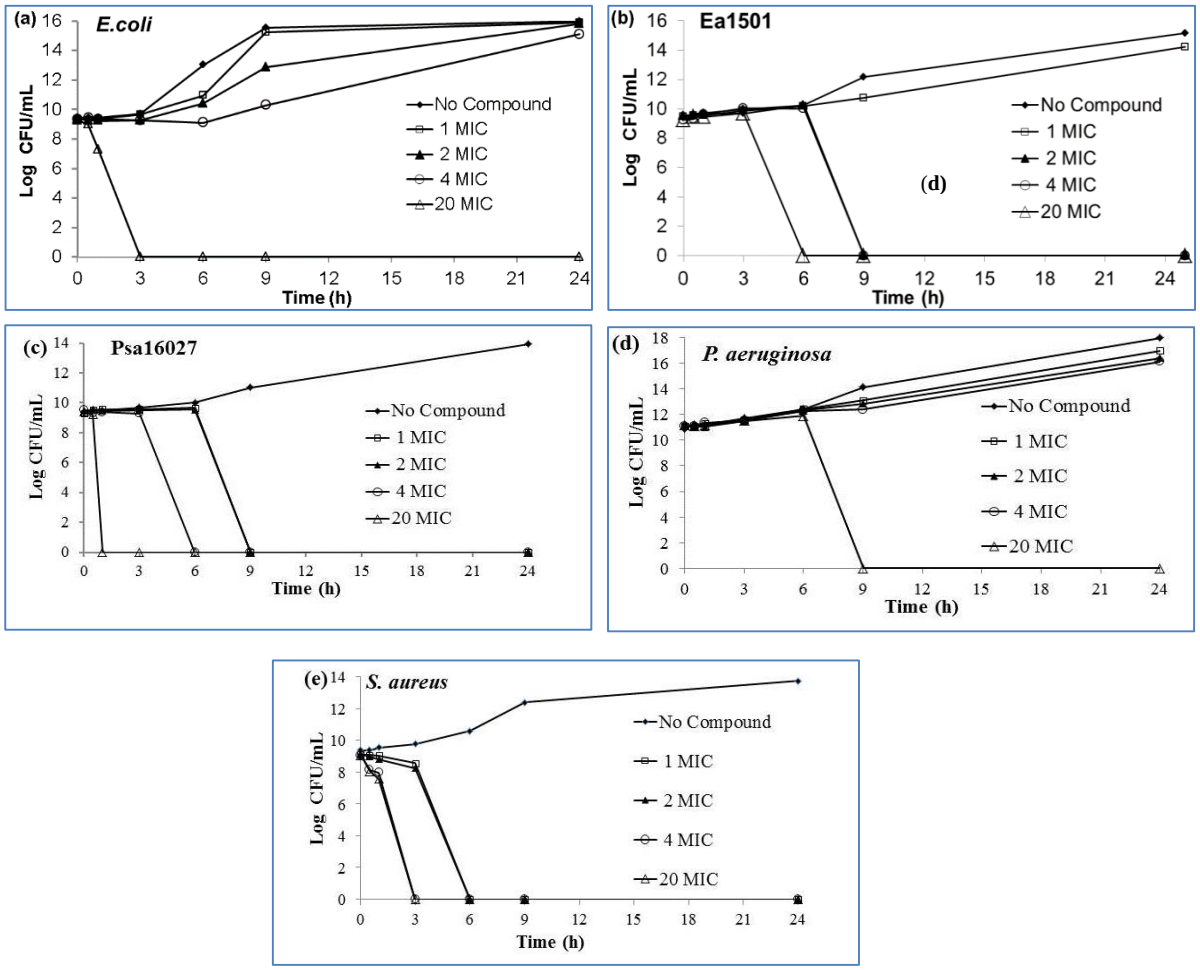

Figure 4.1 Time-kill assay of GZ3.27 against **(a)** *E. coli*, **(b)** Ea1501 **(c)** Psa16027, **(d)** *P. aeruginosa*, **(e)** *S. aureus.* Mean values of the CFU/mL obtained from duplicate measurements have been plotted.

The peptide showed a dose-dependent bactericidal effect against all of the tested pathogens. The kinetics varied between different bacterial species. *E. coli* was completely killed by GZ3.27 at 20 x the MIC (50 μM), within 3 hours of incubation in comparison to the control bacterial culture (no peptide). Complete inhibition of bacterial growth is defined as more than 3-log reduction (more than 99.9% inhibition) in CFU compared to the control culture. At 2 x and 4 x MICs, more than 3-log difference in bacterial growth was observed up to 9 hours, confirming the bactericidal nature of of the peptide, at these concentrations.[306] However, at 24 hours, significant re-growth was observed at 2 x and 4 x MICs, indicating that the peptide is bacteriostatic at these concentrations.

In comparison, slower kinetics were observed against Ea1501, which could be due to the slow growing nature of this bacterium rather than the nature of the peptide. Ea1501 did not grow during the initial 6 hours of incubation, in either the sample or the control cultures. At 1 x MIC, the bacteria regrew after 9 hours of incubation. Complete killing of Ea1501 was observed after 9 hours of incubation with the peptide at 2, 4 and 20 x MIC, indicating that the peptide is bactericidal against Ea1501 at these concentrations.

The peptide showed rapid action against the kiwifruit pathogen, Psa16027. Complete killing of Psa was observed within 1 hour of incubation at 20 x MIC (20 μM). At 4 x MIC, complete killing was observed after 6 hours of incubation. Despite lowering concentrations further (1 x MIC and 2 x MIC), complete killing of Psa was observed after 9 hours of incubation with the peptide. No significant regrowth was observed even after 24 hours, confirming the sustained bactericidal effect of the peptide, against Psa16027.

The peptide also showed bactericidal activity against the human pathogen, *P. aeruginosa*. Despite having the same potency (MIC: 1-2.5 μM) against Psa and *P. aeruginosa,* the rate of killing of *P. aeruginosa* was slower than that of Psa possibly due to the rapid growth of *P. aeruginosa*. At 2 x and 4 x MIC, *P. aeruginosa* showed more than 2 log difference (>99%) in growth, after 24 hours of incubation with the peptide. At 20 x MIC, complete killing was observed after 9 hours of incubation, with no significant regrowth occurring even after 24 hours confirming bactericidal activity even at these lower concentration.

The peptide also showed low micromolar activity (MIC: 1-2.5 μM) and rapid killing of the Gram-positive pathogen, *S. aureus*. The peptide completely killed *S. aureus* cells after 3 hours of incubation at 4 x and 20 x MICs, with no significant re-growth observed after 24 hours. At the lower concentrations (1 x and 2 x MICs) complete killing of *S. aureus* was observed after 6 hours of incubation and the effect was sustained after 24 hours.

Qian *et al.* reported no significant re-growth of *E. coli* ATCC 35318, *E. coli* 5539, *P. aeruginosa* 5215 or *P. aeruginosa* ACC 27853, after incubating in the presence of battacin at different concentrations, for 24 hours.[177] The authors also noted that polymyxin B showed more rapid initial kinetics than battacin, leading to complete inhibition of *E. coli* 5539 growth within 60 minutes at 8 x MIC (4 µg/mL). However, regrowth started to occur 3 hours after incubation and substantial regrowth occurred 24 hours later at the same concentration. In fact, significant regrowth of *E. coli* 5539 was observed after 24 hours of incubation even at higher polymyxin concentration (16 µg/mL).

Tam *et al.* reported similar results where polymyxin B induced rapid killing kinetics of *P. aeruginosa* within the first hour of incubation but substantial re-growth of the bacteria started to occur after 4 hours of incubation and maintained for 24 hours, even at high concentration (16 µg/mL).[307]

Even though GZ3.27 showed slower kinetics than battacin and polymyxin B against *E. coli* and *P. aeruginosa*, it can sustain the bactericidal effect for a longer period at higher concentration (20 x MIC), with none of the tested bacterial pathogens showing regrowth even after 24 hours of incubation.

4.4 Inhibition and eradication of biofilms using GZ3.27

4.4.1 Eradication of Psa biofilms

In 2012, two independent researchers reported that Psa forms biofilms both on the inside and outside of affected kiwifruit plants.[308-309] Currently, treatment against Psa biofilm is yet to be reported and inhibition of Psa biofilm could stop the maturation and colonisation of this pathogen. The ability of GZ3.27 to prevent the formation and eradicate any pre-

formed biofilms of Psa was investigated, using a crystal violet staining experiment. Crystal violet is a dye that binds to the exopolysaccharide (EPS) matrix allowing visualization of the biofilm architecture.[310] The crystal violet stained Psa biofilm, grown for 48 hours in the presence and absence of GZ3.27, is shown in Figure 4.2.

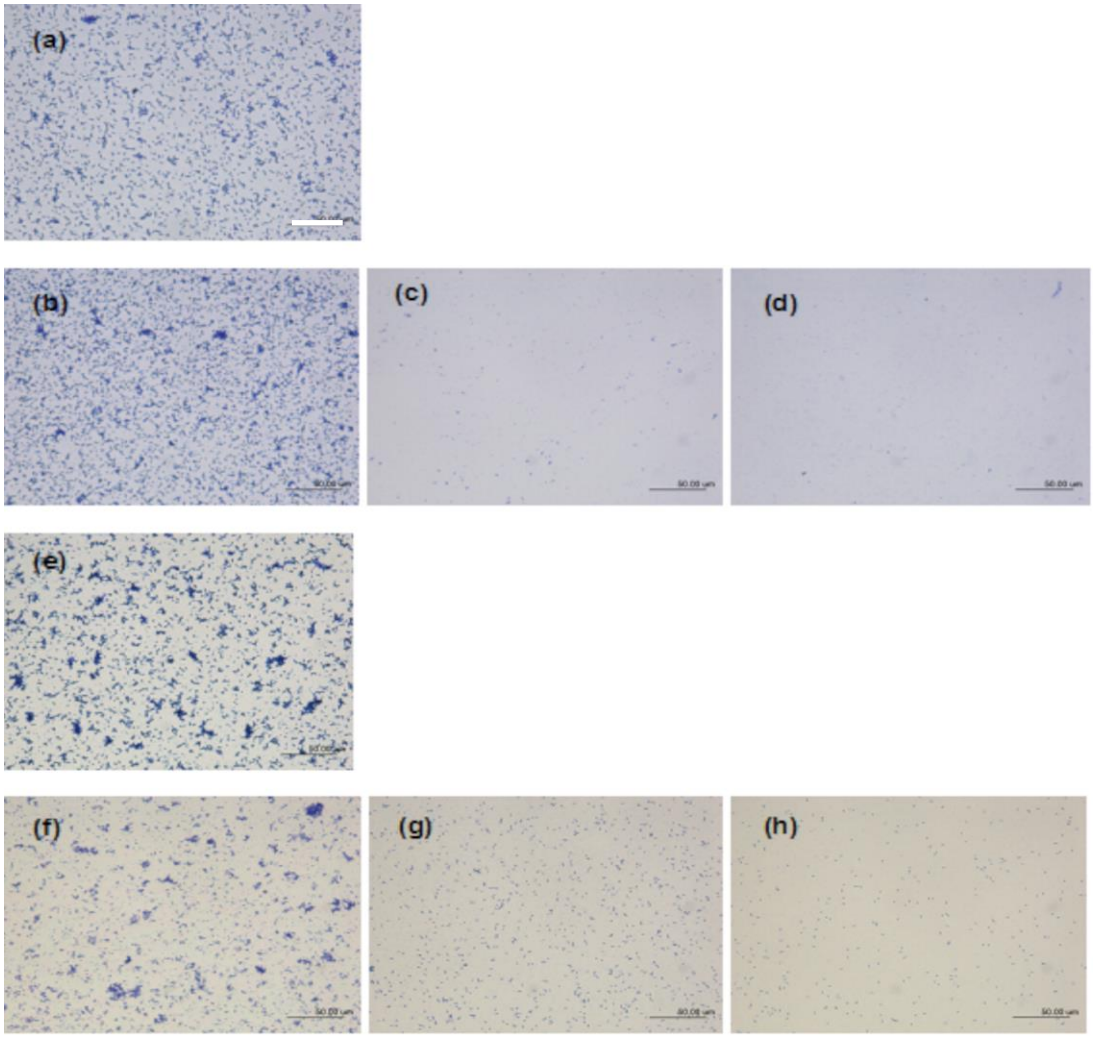

Figure 4.2 Representative crystal violet stained images of Psa16027 biofilms incubated for 48 hours in the **(a)** absence of and presence of the lipopeptide at **(b)** 1 μM; **(c)** 5 μM and **(d)** 50 μM respectively. **(e)** Untreated pre-formed biofilms of Psa16027 for 48 hours and the effect of treatment with lipopeptide at **(f)** 1 μM; **(g)** 5 μM and **(h)** 50 μM for additional 24 hours respectively. Scale bar = 50 μm.

As is evident from Figures 4.2a and 4.2e, the Psa pathogen formed mature biofilms at 48 hours, present as aggregated cell clusters evident in these images. The lipopeptide at 1 μM (Figure 4.2b and 4.2f) did not prevent the initial attachment or disperse the mature

biofilm. However, at higher concentrations (5 and 50 μM), the lipopeptide managed to both prevent the initial attachment and inhibit mature biofilm, as indicated by the fewer numbers of bacterial cells in the images.

The crystal violet stained biofilms were then solubilised with ethanol to release the stain, and the optical density (OD) of the solubilised stain at 560 nm was used for a semi-quantitative estimate of the attached biofilm biomass (Figure 4.3).[311] Results indicate that the lipopeptide GZ3.27 prevents the initial attachment of Psa biofilms, at concentrations as low as 5 μM (2x MIC) (Figure 4.3a). Additionally, a 24-hour treatment with the peptide resulted in significant reduction of the pre-formed biofilms of Psa (formed for 48 hours), at peptide concentration above 5 μM (Figure 4.3b). The MIC and biofilm analysis demonstrates the ability of GZ3.27 to inhibit planktonic cells as well as disperse mature biofilms of Psa.

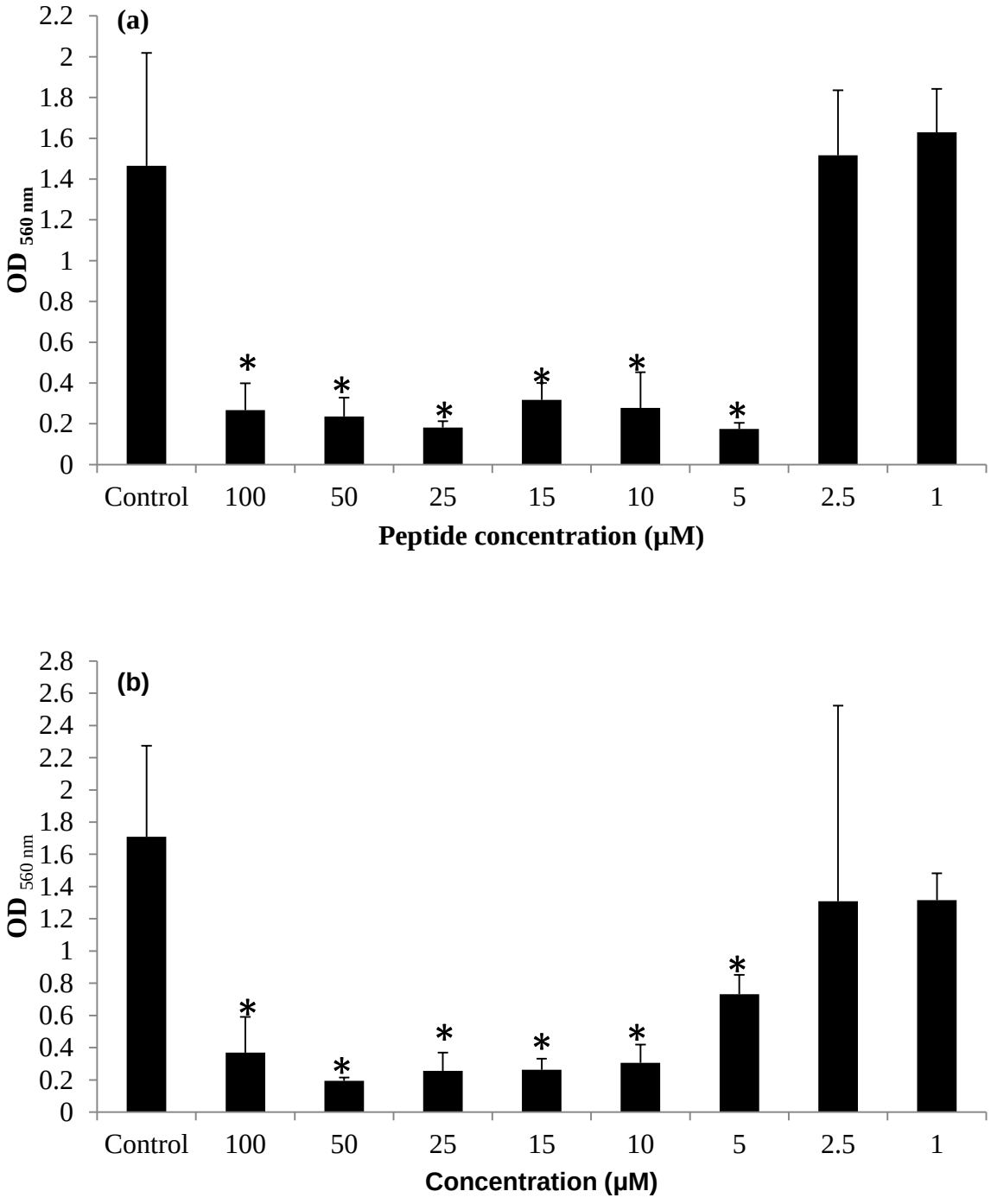

Figure 4.3 (a) Psa16027 biofilms formed during incubation with various concentrations of GZ3.27 for 48 hours and **(b)** effect of treating Psa16027 pre-formed biofilms (48 hours) with various concentrations of GZ3.27 for an additional 24 hours. * Indicates $p < 0.05$.

4.4.2 Eradication of *P. aeruginosa* biofilms

Biofilm formation of *P. aeruginosa* and *S. aureus*, both in the presence and absence of GZ3.27, was visualised using the LIVE/DEAD staining assay. The crystal violet stain cannot distinguish between metabolically active and inactive cells, since the dye can penetrate the polysaccharide of both intact and compromised cells.[312] The LIVE/DEAD staining assay, which is used for detailed studies, can distinguish between both metabolically active and inactive cells.

This assay makes use of two fluorescent dyes-a green fluorescent SYTO 9 nucleic acid and red fluorescent propidium iodide. These two dyes have different spectral characteristics, with excitation and emission at 480/500 nm for SYTO 9 and at 490/635 nm for propidium iodide. SYTO 9 stains both healthy and compromised bacteria, whereas propidium iodide only stains compromised cells. When the two dyes are used in conjugation with each other, at appropriate ratios, a reduction in SYTO 9 fluorescence intensity is observed, and bacterial cells with intact and compromised membrane are visualised as green and red fluorescent respectively. Metabolically inactive cells fluoresce orange.[312] The results of biofilm inhibition and pre-formed biofilm dispersion assay of *P. aeruginosa* are shown in Figure 4.4.

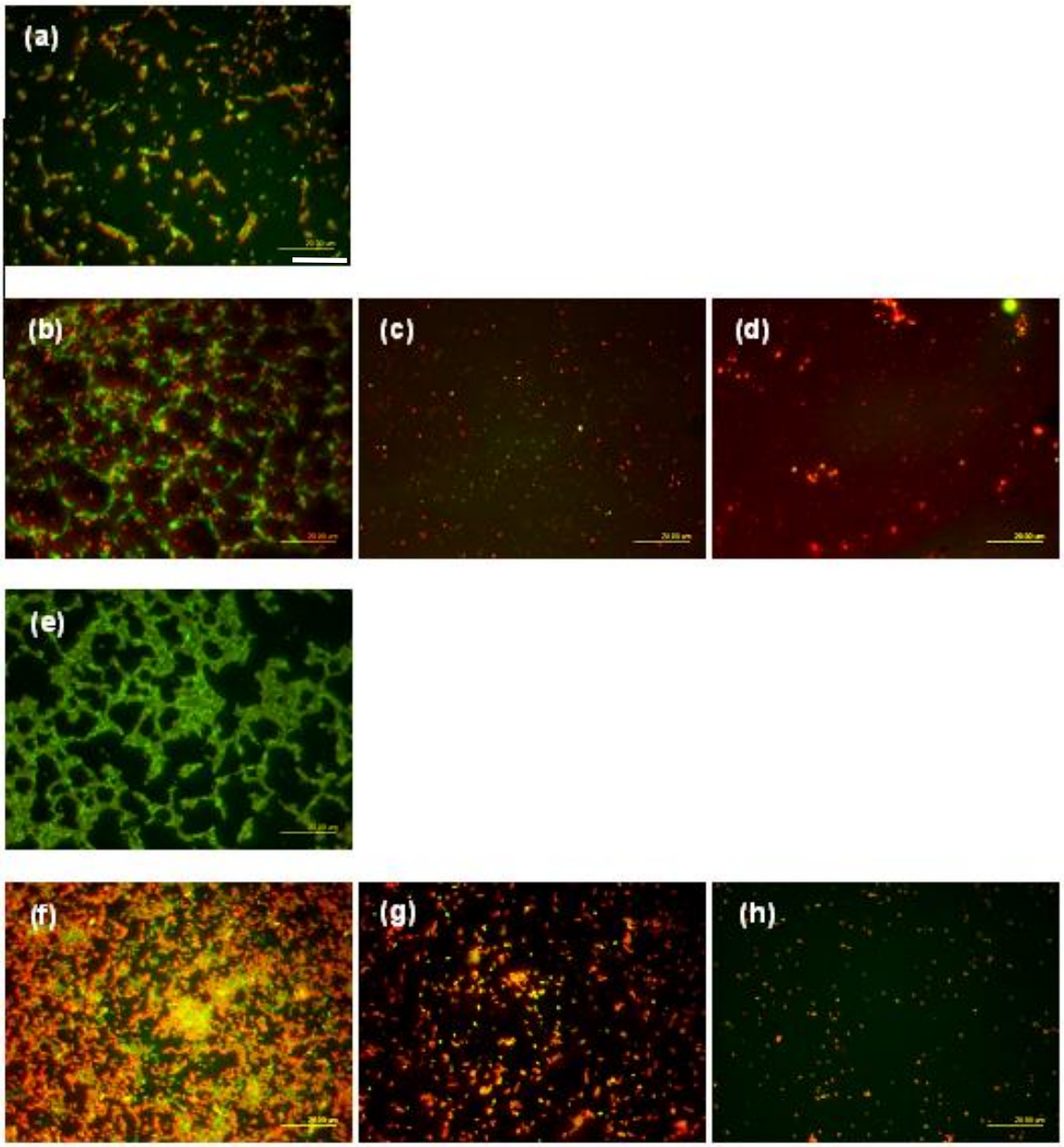

Figure 4.4 Representative Live/Dead stained images of *P. aeruginosa* biofilms incubated for 48 hours in the **(a)** absence of and presence of the lipopeptide at **(b)** 10 μM; **(c)** 50 μM and **(d)** 100 μM respectively. **(e)** Untreated pre-formed biofilms of *P. aeruginosa* for 48 hours and the effect of lipopeptide treatment for further 24 hours at **(f)** 10 μM; **(g)** 50 μM and **(h)** 100 μM respectively. Scale bar = 20 μm.

In the absence of the lipopeptide (4.4a and 4.4e) and at 10 μM of GZ3.27 (4.5b and 4.5f), mature biofilms of *P. aeruginosa* are evident. The Live/Dead staining assay revealed *P. aeruginosa* biofilms consist of both metabolically active (green fluorescent) and metabolically inactive (orange) bacterial cells validating the heterogeneous architecture.

The dark circular patches surrounding the EPS (Figure 4.4e) are known as matrix voids. These are water channels which allow the diffusion of nutrients and for oxygen to be transported throughout the biofilm architecture.[77,313]

The lipopeptide at 10-50 μM concentration managed to inhibit the initial attachment, and to disperse the mature biofilm structure as indicated by a reduction in the number of bacterial cells seen in the peptide treated images (Figure 4.4b-d and 4.4f-h). These results indicate the peptide's ability to target both metabolically active and inactive cells within the bacterial biofilm. However, a higher peptide concentration (10-50 μM) is required to inhibit the biofilm formation of *P. aeruginosa* whereas only low peptide concentration (1-2.5 μM) is required to inhibit *P. aeruginosa* in the planktonic state.

A possible explanation for the need for higher peptide concentrations to prevent biofilms of *P. aeruginosa* could be the production of alginate polysaccharide by the pathogen. Alginate is an anionic polysaccharide composed of D-mannosyluronic acid covalently linked via β 1 → 4 glycosidic linkage and is produced by brown sea weed and two families of bacteria, *Pseudomonadaceae* and *Azobacteriaceae*.[314] Alginate produced by bacteria is often *O*-acetylated at carbons 2 or 3.[314] Due to the anionic characteristics of this polysaccharide, cationic AMPs will be trapped in alginate, due to the selective electrostatic interaction before reaching the cells within the biofilm.[315] As a result higher peptide concentration may be required to overcome this barrier to target the biofilm cell.

4.4.3 Eradication of *S. aureus* biofilms

Biofilm formation of *S. aureus* was also analysed using LIVE/DEAD staining assay and the results are shown in Figure 4.5.

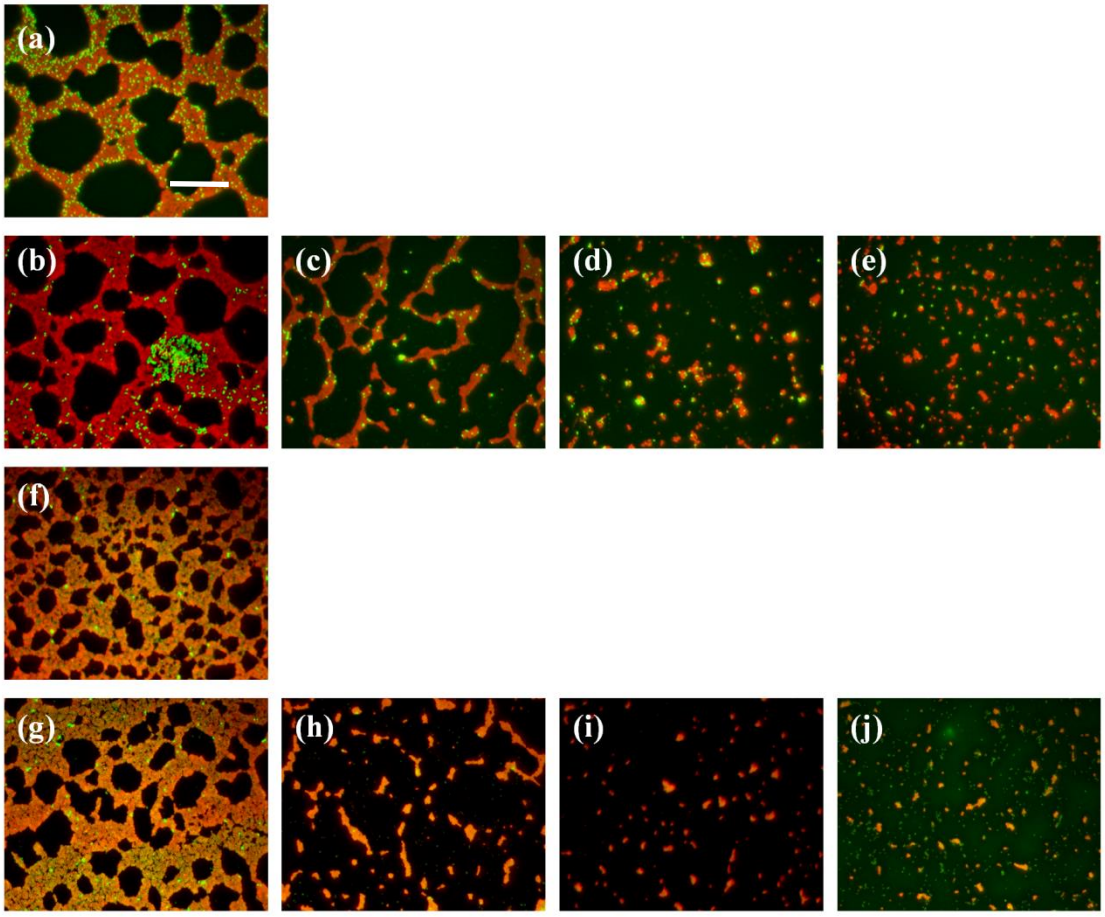

Figure 4.5 Representative Live/Dead stained images of *S. aureus* biofilms incubated for 48 hours in the **(a)** absence and presence of the lipopeptide; **(b)** 10 μM; **(c)** 25 μM; **(d)** 50 μM; **(e)** 100 μM and respectively. **(f)** Untreated pre-formed biofilms of *S. aureus* for 48 hours and the effect of lipopeptide treatment for further 24 hours at **(g)** 10 μM; **(h)** 25 μM; **(i)** 50 μM; **(j)** 100 μM and respectively. Scale bar = 20 μm.

In the absence of the lipopeptide (4.5a and 4.5f), *S. aureus* also formed an elaborate biofilm structure with matrix voids. Like *P. aeruginosa*, the biofilm architecture of *S. aureus* is dynamic, with random associations of metabolically active and dormant bacterial cells spread within the biofilm. The lipopeptide also showed a dose-dependent

inhibition of initial biofilm attachment to the surface as well as dispersion of pre-formed biofilms where the minimum concentration was found to be within 10-25 μM.

The EPS of both *S. aureus* and *S. epidermidis* mainly consists of positively charged polysaccharide intercellular adhesion (PIA).[316] PIA are polymers of β-1,6-linked N-acetyl-glucosamine with partially N-deacetylated amine groups. Vuong *et al.* reported that a higher, LD_{50} (dose required to kill 50 % of the bacterial pathogen) of the cationic AMPs cathelicidin (LL-37) (14.2 μg/mL) and human β-defensin (hBD3) (5 μg/mL) and the anionic AMP dermcidin (22 μg/mL) were required to inhibit wild type *S. epidermidis*, which contains the *Isa* gene responsible for PIA production.[317] However, a lower LD_{50} of LL-37 (9.1 μg/mL), hBD3 (3 μg/mL) and dermcidin (7 μg/mL) were required to inhibit mutant Isa^- strain which lacks the ability to produce PIA.[317]

Vuong *et al*. suggested that cationic AMPs have diminished activity in the presence of PIA, mainly due to increased electrostatic repulsion between it and the cationic amino acids in these AMPs, while PIA can also act as an auxiliary membrane by trapping negatively charged AMPs such as dermcidin before it can reach its target.[317] Based on these observations, higher peptide concentration may be required to overcome the electrostatic repulsion between GZ3.27 and PIA of *S. aureus* to target the bacterial cells within the biofilm.

Initial results showed that GZ3.27 inhibited the initial attachment of and dispersed mature biofilms in Psa, *P. aeruginosa* and *S. aureus*. However, a higher concentration of GZ3.27 was required to inhibit the biofilm cells of the human pathogens, *S. aureus* and *P. aeruginosa*, highlighting the complex nature of biofilms. If the initial attachment of bacterial cells to the surface is prevented, it can restrict access to nutrients needed for their survival. The ability to disperse the pre-formed biofilms of the tested pathogens may

be an indicator of the capability of this lipopeptide to penetrate through dense EPS matrices.

4.5 Structure-activity relationship (SAR) studies

Structure-activity relationship (SAR) studies of GZ3.27 were carried out to identify importance of the sequence and chain length for the observed antimicrobial activity. This can be achieved by synthesising several peptide analogues where one or more amino acids in the original sequence are replaced by either similar or chemically distinct amino acids to verify the importance of that amino acid(s) to the sequence as well as the length of the sequence (oligomers).

4.5.1 Oligomeric analogues of GZ3.27

Firstly, the effect of peptide chain length on the antibacterial activity was determined by synthesising a peptide dimer (GZ3.148) and trimer (GZ3.149) of GZ3.27 as amidated peptides using the rink amide linker (Figure 4.6).

GZ3.27 FA-D-Dab-Dab-Dab-Leu-D-Phe-Dab-Dab-Leu-NH_2

GZ3.148 FA-D-Dab-Dab-Dab-Leu-D-Phe-Dab-Dab-Leu-D-Dab-Dab-Dab-Leu-D-Phe-Dab-Dab-Leu-NH_2

GZ3.149 FA-D-Dab-Dab-Dab-Leu-D-Phe-Dab-Dab-Leu-D-Dab-Dab-Dab-Leu-D-Phe-Dab-Dab-Leu- D-Dab-Dab-Dab-Leu-D-Phe-Dab-Dab-Leu-NH_2

Figure 4.6 Amino acid sequences of the dimer (GZ3.148) and trimer (GZ3.149) lipopeptides. FA denotes the fatty acid, 4-methyl-hexanoyl.

The dimeric and trimeric lipopeptides were tested for the antibacterial activity against *P. aeruginosa, S. aureus, E. coli* and Psa16027 (Table 4.2).

Table 4.2 MIC (μM) of GZ3.27, dimer (GZ3.148) and trimer (GZ3.149)*

Peptide	**MIC (μM)**			
	P. aeruginosa	***S. aureus***	***E. coli***	**Psa16027**
GZ3.27	1-2.5	1-2.5	2.5-5	1-2.5
GZ3.148	10-15	25-50	15-25	15-25
GZ3.149	10-15	25-50	25-50	5-10

*Average of three independent experiments performed in triplicate.

As is evident from the table, the dimer and trimer were equally active against *P. aeruginosa* and *S. aureus* at 10-15 μM and 25-50 μM respectively. The trimer was slightly less active (25-50 μM) than the dimer (15-50 μM) against *E. coli* but more active (5-10 μM) than the dimer (15-25 μM) against the Psa pathogen. Overall, both the trimer and dimer of GZ3.27 have similar antibacterial activity against the tested pathogens.

However, the dimeric and trimeric versions were moderately less active than GZ3.27. The MIC values of GZ3.27 against all of the tested pathogens are about 2-20 times lower than the dimer and the trimer. Increase in chain length of the lipopeptide may have caused peptide aggregation possibly leading to reduced interaction with the bacterial membrane and causing a moderate reduction in the observed antibacterial activity.

4.5.2 Alanine scanning study of GZ3.27

The importance of each of the amino acid residue in GZ3.27 to the observed antibacterial activity was probed using an alanine scanning study where eight peptide sequences were synthesised by substituting one amino acid at a time with alanine. Table 4.3 lists the sequences of the alanine-scanned library.

Table 4.3 Sequences of alanine-scanned peptides of GZ3.27. FA denotes the fatty acid, 4-methyl-hexanoyl.

Code	Sequence
GZ3.27	FA-D-Dab-Dab-Dab-Leu-D-Phe-Dab-Dab-Leu-NH_2
Ala^8	FA-D-Dab-Dab-Dab-Leu-D-Phe-Dab-Dab-**Ala**-OH
Ala^7	FA-D-Dab-Dab-Dab-Leu-D-Phe-Dab-**Ala**-Leu-OH
Ala^6	FA-D-Dab-Dab-Dab-Leu-D-Phe-**Ala**-Dab-Leu-OH
Ala^5	FA-D-Dab-Dab-Dab-Leu-**Ala**-Dab-Dab-Leu-OH
Ala^4	FA-D-Dab-Dab-Dab-**Ala**-D-Phe-Dab-Dab-Leu-OH
Ala^3	FA-D-Dab-Dab-**Ala**-Leu-D-Phe-Dab-Dab-Leu-OH
Ala^2	FA-D-Dab-**Ala**-Dab-Leu-D-Phe-Dab-Dab-Leu-OH
Ala^1	FA-**Ala**-Dab-Dab-Leu-D-Phe-Dab-Dab-Leu-OH

Alanine scanning is routinely used to rapidly identify residues which are important for antibacterial activity, as alanine is a small and chemically inert amino acid that usually does not contribute to biological activity.[318] Kanazawa *et al.* carried out an alanine scanning study of polymyxin B_3 to determine the contribution of each of the amino acids to the antibacterial activity and LPS binding by synthesising nine sequential alanine substituted analogues.[319]

The Ala analogues of polymyxin B_3 were tested against *E. coli*, *S. typhimurium* and *P. aeruginosa*. An LPS binding assay was carried out by measuring the ability of the

synthesised analogues to displace and quench a Dab(dansyl-Gly^{1})-polymyxin B_3 fluorescent probe bound to the LPS of *E. coli* by increasing the concentration of these analogues in a concentration-dependent manner.[319] Results from their investigations indicated that the side chain amine of Dab^{5} is crucial for antibacterial activity as replacement of Dab^{5} with Ala led to 4-16 fold reduction in antibacterial activity against all of the tested pathogens.[319] The study also reported that Ala substitution of Dab amino acids in the heptapeptide ring lead to marginal loss of antibacterial activity whereas Ala substitution of Dab amino acids outside of the heptapeptide ring retained the same activity as polymyxin B_3. Surprisingly, Ala substitution of the dipeptide hydrophobic core (D-Phe^{6}-L-Leu^{7}) retained the same activity as the parent peptide.[319] LPS binding assay studies have shown that replacement of all the Dab amino acids in the sequence with Ala led to significant reduction in the LPS binding possibly due to reduced electrostatic interaction between LPS of *E. coli*.[319]

4.5.2.1 Combinatorial synthesis of Ala scanned battacin peptides using SynPhase lanterns

Alanine-scanned analogues were generated using combinatorial synthesis using SynPhase lanterns.[320-321] Combinatorial synthesis of peptides involves rapid generation of several peptides in a single process. SynPhase lanterns are modular solid rigid supports, coated with unreactive polymers such as polystyrene or polyamide allowing solvation in most of the protic and aprotic solvents used in standard SPPS.[320-321] The lanterns can be functionalised with a variety of linkers, allowing for the generation of peptides with different C-terminal functionalities. Therefore, these lanterns are similar to commonly used resins in SPPS. However, the modular design of SynPhase lanterns can favour increased surface area and allow increased access to free flowing solvents, leading to the generation of peptides with increased yield and purity.[320-321]

SynPhase lanterns offer desirable characteristics suitable for combinatorial synthesis. These lanterns can be easily picked up and transferred into different reaction vessels ("sort and combine" methodology) allowing parallel synthesis and multiple cleavages in a single process. In addition, the lanterns can be easily colour coded by attaching either spindles or cogs or both to allow easy identification of each peptide during the combinatorial synthesis (Figure 4.7).[320-321]

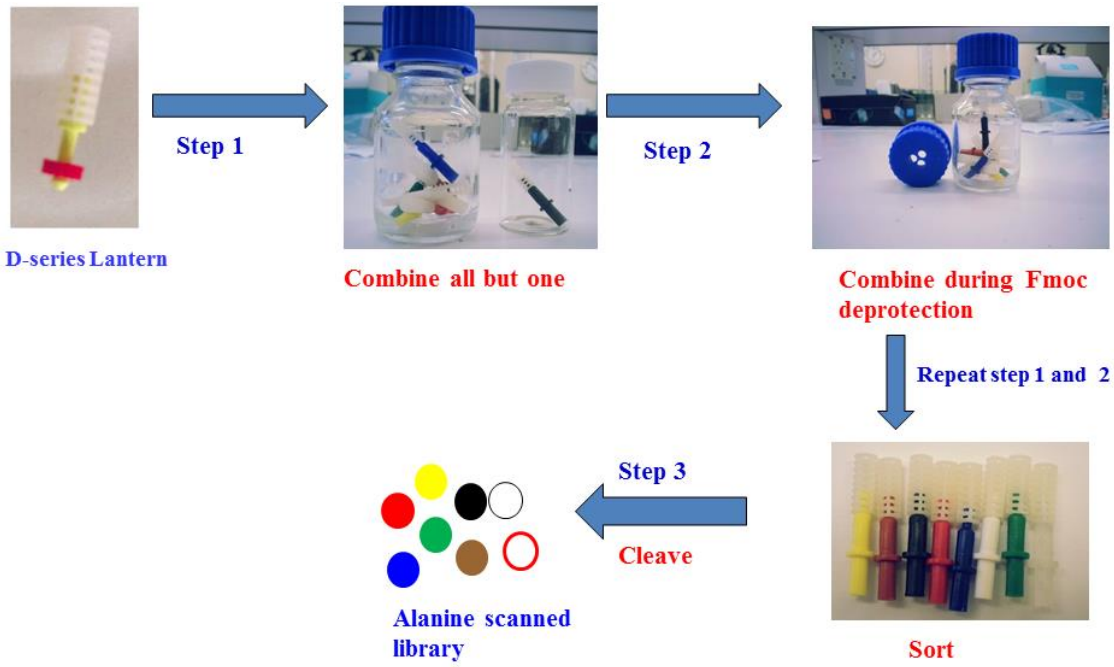

Figure 4.7 Schematic illustration of alanine-scanned library using D-series lanterns.

The alanine-scanned library was synthesised using "sort and combine" methodology with D-series SynPhase lanterns preloaded with a trityl alcohol linker (Scheme 4.1).

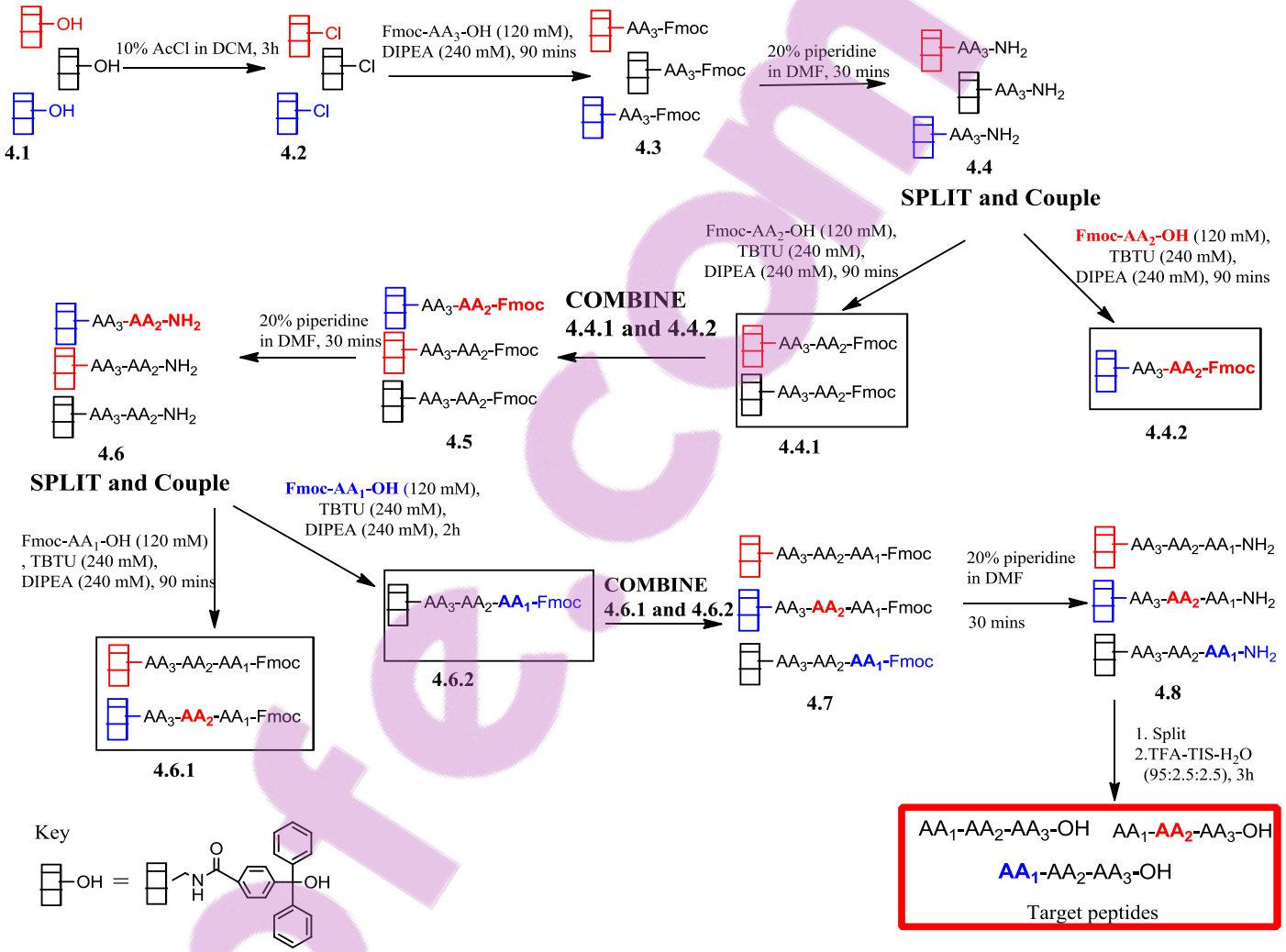

Scheme 4.1 Synthesis of a general tripeptide combinatorial library using the SynPhase lantern-trityl alcohol. Different colours indicate different AAs used at the respective positions.

The first step involves the conversion of the trityl alcohol linker **4.1** in the lanterns to the reactive trityl chloride moiety **4.2** using acetyl chloride (10% AcCl in DCM).[322] The excess reagent is drained and the subsequent C-terminal amino acid (Fmoc-AA_3) at 120 mM, is immediately coupled to the lantern to produce lantern, in the presence of DIPEA (240 mM), to produce the lantern-Fmoc bound amino acid **4.3**.[320] The Fmoc group of the lantern bound AA_3 **4.3** is deprotected with 20% piperidine, to generate a lantern-bound, free amine **4.4**. Lanterns sharing common amino acids **4.4.1** at the same position are kept in the same reaction vessel, whereas the lanterns in which amino acids at specific positions are replaced with alanine **4.4.2** (indicated by coloured amino acids) are suspended in separate reaction vessels. The lanterns are combined into one reaction vessel during the Fmoc removal step **4.5**. Then the lanterns are sorted for the subsequent coupling and combined for the Fmoc deprotection step. The sort and combine procedure is repeated until the desired sequences are obtained **4.8**. The lanterns are then separated into different reaction vessels and the peptide sequences are released from the lanterns under acidic conditions (TFA-TIS-H_2O, 95:2.5:2.5 v/v), to generate the alanine-scanned library.

Following Scheme 4.1 and as described above, the Ala scanned library of battacin was successfully synthesised (See Appendix A and B). Apart from Ala^5, most of the Ala scanned peptides have crude purity more than 80%, which is in agreement with that reported for these lanterns in the literature (See Appendix A).[323-324] Bioassay results are summarised in Table 4.4.

Table 4.4 MIC (µM) of GZ3.27, alanine-scanned analogues and the pentapeptide*

Peptide	MIC (µM)			
	P. aeruginosa	***S. aureus***	***E. coli***	**Psa16027**
GZ3.27	1-2.5	1-2.5	2.5-5	1-2.5
Ala^{8}	5-10	5-10	15-25	10-15
Ala^{7}	5-10	5-10	5-10	2.5-5
Ala^{6}	50-100	500-1000	100-500	100-500
Ala^{5}	>1000	25-50	25-50	>1000
Ala^{4}	>1000	>1000	500-1000	>1000
Ala^{3}	10-15	25-50	25-50	25-50
Ala^{2}	2.5-5	2.5-5	25-50	2.5-5
Ala^{1}	25-50	>1000	500-1000	100-500
GZ3.159	1-2.5	2.5-5	10-15	1-2.5

*Average of three independent experiments performed in triplicate

Results from the antibacterial studies on the alanine-scanned peptides indicated that Leu^{8}, Dab^{7} and Dab^{2} were not critical for the observed antimicrobial activity of GZ3.27, as the replacement of these amino acids with alanine did not lead to significant changes in MIC values against the tested pathogens. Dab^{3} was reasonably tolerant to alanine substitution, with moderate activity (10-50 µM) retained in Ala^{3} against all tested pathogens. However, the substitution of Leu^{4} with Ala led to complete loss of antimicrobial activity (500-1000 µM) against all the tested pathogens. D-Phe^{5} to Ala substitution abolished the activity against the *Pseudomonas* strains, while moderate antibacterial activity (25-50µM) was retained against *S. aureus* and *E. coli*. D-Dab^{1} and Dab^{6} substitutions abolished the antimicrobial activity against *S. aureus*, *E. coli* and Psa, while moderate activity was maintained against *P. aeruginosa* (25-100 µM).

Even though the alanine-scanning assay of GZ3.27 showed different results to those reported by Kanazawa *et al.*, the structure-activity profile of GZ3.27 generated from the

above study still can be correlated to the overall polymyxins SAR reported in the literature.[161,248,250,256] Alanine-scanning assay and the observed activity of GZ3.130, referred to earlier, have further validated the significance of the hydrophobic domain in battacin lipopeptides. In addition to selective electrostatic interactions between the cationic Dabs and the bacterial membrane, Dab^1, Dab^3 and Dab^6 can act as spacers between the two hydrophobic domains, which may be crucial to maintaining the observed antibacterial activity.

Even though the effect of sequential alanine replacements in GZ3.27 on antibacterial activity was not uniform across the strains studied, the data was used to arrive at a truncated pentapeptide version (GZ3.159) (Figure 4.8). This truncated peptide contains the 4-methyl-hexanoyl fatty acid, conjugated to a pentapeptide sequence consisting of the central hydrophobic dipeptide unit (Leu-D-Phe) with the flanking Dab residues, and the D-Dab at position 1 crucial for the observed antibacterial activity against the tested pathogens. This core pentapeptide (GZ3.159) sequence was equipotent as GZ3.27 against *P. aeruginosa*, *S. aureus* and Psa but was slightly less active (10-15 μM) against *E. coli*, probably due to reduced electrostatic interactions between the side chain amines of Dabs and the outer-membrane of *E. coli*.

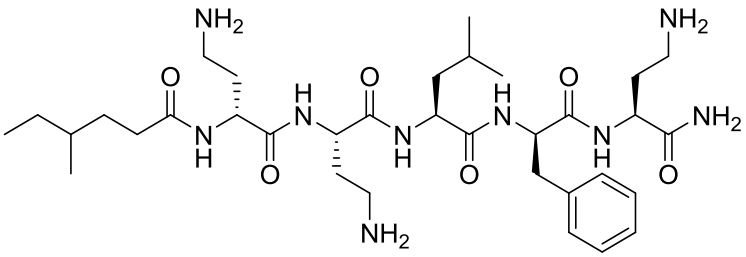

FA-(D)Dab-Dab-Leu-(D)Phe-Dab-NH_2

Figure 4.8 Structure of the active pentapeptide moiety (GZ3.159). FA denotes the fatty acid, 4-methyl-hexanoyl.

The alanine-scanned peptides were all generated as C-terminal acids, whereas the parent peptide was a C-terminal amide. The chemistry of the lanterns used for generating the alanine-scanned library generated the peptides as C-terminal acids, whereas the parent peptide was generated on rink amide linker, which resulted in C-terminal amidated peptides. It can be argued that the net cationic charge of the alanine-scanned peptides (C-terminal OH), which is one less than the parent peptide (C-terminal amide), could have also contributed to the observed MICs in Table 4.4. However, significant differences in the MICs between the different alanine replacements (all C-terminal acids in Table 4.3) confirm the importance, or lack thereof, of the respective amino acids, and their position within the sequence, to antimicrobial activity. Therefore, it is fair to conclude that screening amidated versions of the alanine-scanned peptides would not have led to a different outcome, in terms of the importance of the amino acid residues, to the antimicrobial activity observed in the current study. As stated above, the overall outcome of the current SAR study agrees with the SAR reported for polymyxin B and, as described below, has led to a truncated peptide GZ3.159 (Figure 4.8) with the same level of antimicrobial potency as GZ3.27.

4.6 Haemolysis of mouse blood cells by selected battacin analogues

Some cationic AMPs have a high haemolytic activity associated with their potent antibacterial activity. In order for peptides to be viable drug candidates, they must show potent *in vitro* and *in vivo* activity, while showing very low toxicity to host tissues. The haemolytic activity of the most potent lipopeptides from this study, GZ3.21, GZ3.15, GZ3.27, GZ3.26 and GZ3.159 was assessed using mouse blood cells, to gain further insight into their therapeutic potential. The inactive lipopeptide, GZ3.130 was also

assayed to evaluate the influence of the fatty acid on haemolytic activity. Figure 4.9 shows representative haemolytic assay plate.

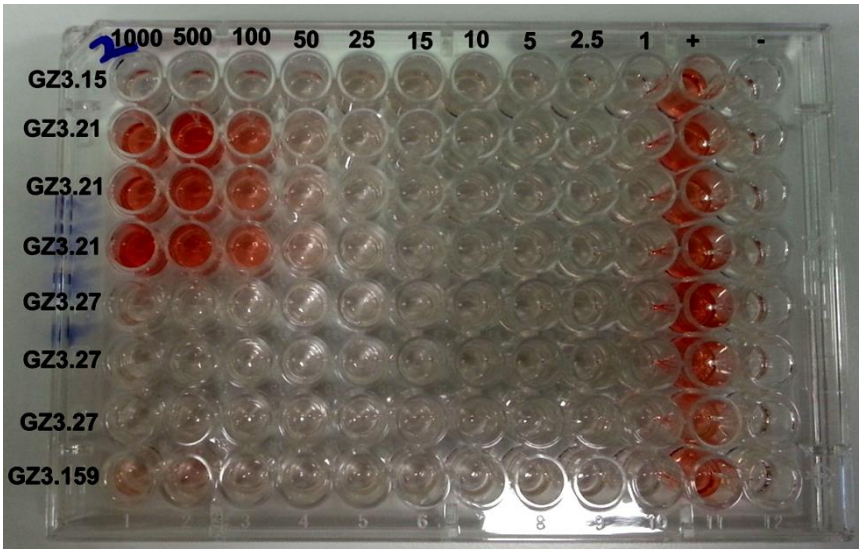

Figure 4.9 Haemolytic assay plate layout. The battacin analogues were tested between 1-1000 µM against fresh mouse blood cells (2% v/v). Triton X-100 (0.1%) and tris buffer were used as positive (+) and negative (-) controls respectively.

As is evident from Figure 4.9, lysis of mouse RBCs is indicated by the change from a colourless to red solution. Highly haemolytic compounds, such as GZ3.21, are identified as causing membrane lysis of red blood cells (RBC) up to 100 µM. The overall results of the haemolytic assay is summarised in Figure 4.10.

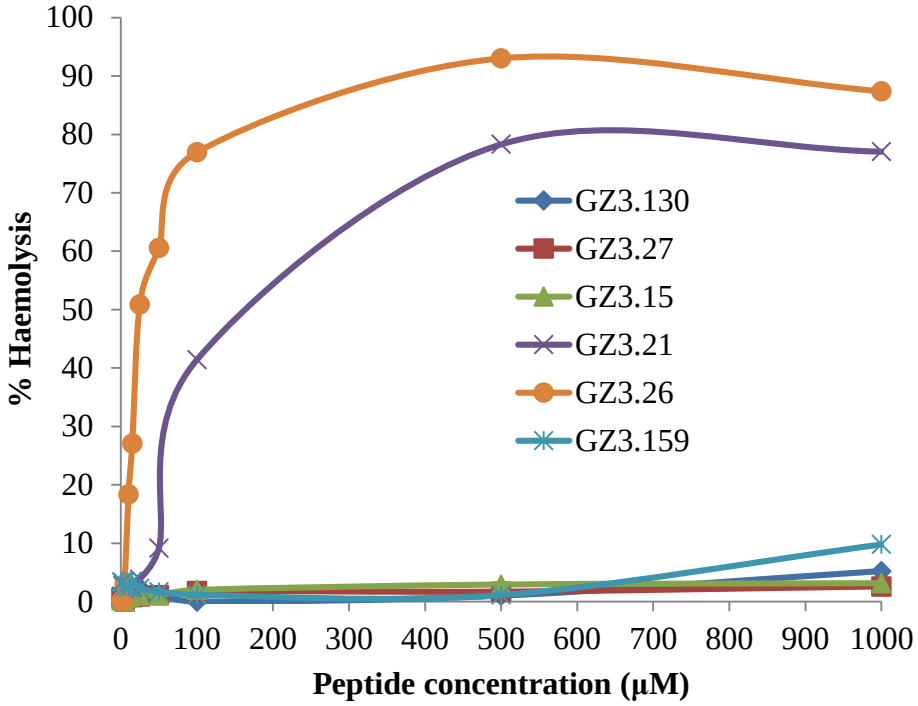

Figure 4.10 Percentage of haemolysis of mouse-blood cells at various peptide concentrations. The experiment was performed in triplicate and results averaged out.

The percentage of haemolysis at 100 µM was negligible for GZ3.130 (0.01%), GZ3.159 (1.14%), GZ3.27 (1.79%) and the cyclic shorter fatty acid lipopeptide, GZ3.15 (2.02%). However, the Fmoc conjugated cyclic lipopeptide GZ3.21 showed 41% haemolysis at 100 µM. This observation is analogous to the study by Cochrane *et al.* on tridecaptin A1 where the Fmoc-conjugated version, exhibited increased antimicrobial activity as well as severe haemolysis.[299] The lipopeptide GZ3.26, with the longest fatty acid used (myristic acid) at 100 µM, showed the greatest haemolysis (76.9%) of RBCs.

Two key parameters- hydrophobicity and cationicity- determine the haemolytic activity of the peptides.[325] Although red blood cells contain zwitterionic phospholipids, such as phosphatidylcholine and sphingomyelin, an increase in the hydrophobicity and cationic characteristics of the peptide can increase their affinity towards the RBCs.[325] The active pentapeptide, has an overall charge of +3, whereas the overall charge of GZ3.27, and all

other peptides studied, is +5. Vaara *et al.* reported reduced nephrotoxicity of the polymyxin analogue, NAB7061, where the overall charge was reduced from +5 in polymyxin to +3.[175] However the reduction in nephrotoxicity was compromised by a reduction in the antibacterial activity, unlike the case of GZ3.159.[175] The absence of haemolysis with the pentapeptide can be attributed to its reduced cationicity.

Lack of haemolysis with GZ3.130 can be attributed to the overall reduction in the hydrophobicity of the compound, due to the absence of the fatty acid chain, as has been observed with PMBN.[170]

The myristic acid-conjugated and Fmoc-conjugated battacin analogues were highly haemolytic, probably due to their increased hydrophobicity. The results, taken together, indicate that conjugation of the shorter fatty acid (4-methyl-hexanoyl) gives the best therapeutic index (defined as low micromolar antibacterial activity and RBC haemolysis at high peptide micromolar concentration) for the battacin family of peptides studied here.

4.7 Mechanistic studies of GZ3.27

The structural similarities in the peptide sequences of polymyxin (PMB), a membrane-lytic lipopeptide, and GZ3.27, suggest that they would have similar mechanisms of action. The mechanism of action of GZ3.27 was investigated using a combination of colorimetric assay using vesicles composed of dimiristoylphosphocholine:10,12-tricosadiynoic acid, scanning electron microscopy of bacterial cells in the presence and absence of the lipopeptide, and outer and inner-membrane permeabilisation assay using the fluorescent dyes *N*-phenyl-naphthylamine (NPN) and propidium iodide (PI).

4.7.1 Colorimetric assay of battacin library

Kolusheva *et al.* reported a colorimetric assay to rapidly identify membrane-lytic AMPs.[326] In this assay a mixture of the phospholipid, dimiristoylphosphocholine (DMPC) and polydiacetylene (PDA) polymer such as 10, 12-tricosadiynoic acid (TRCDA) at a molar ratio of 4:6 (DMPC-TRCDA) is irradiated at 254 nm.[326-328] UV irradiation produces intense blue coloured vesicles, with absorption maxima at 630 nm, due to the conjugated structure of the TRCDA backbone (Figure 4.11). Although, DMPC phospholipids are zwitterionic, the DMPC-TRCDA system is anionic, as TRCDA is an acidic molecule. Hence, DPMC-TRCDA artificial membranes are excellent model systems representing anionic bacterial membranes.

In the presence of membrane-lytic AMPs, the DPMC-TRCDA vesicles undergo an immediate colour transition from blue to red, due to the disruption of the organised vesicles caused by the interaction of the peptide with the lipids.[326] Upon interaction, the membrane-lytic peptide will cause a strain on the PDA backbone, which causes re-arrangement of the pendant side chains of the PDA vesicles.[329] This results in a "gauche-trans" configuration of the PDA backbone, leading to a shortening of the backbone and absorption in the shorter wavelength (490 nm), leading to red coloured vesicles.[328]

The overall membrane interaction of AMP with the colorimetric vesicles is highlighted in Figure 4.11.

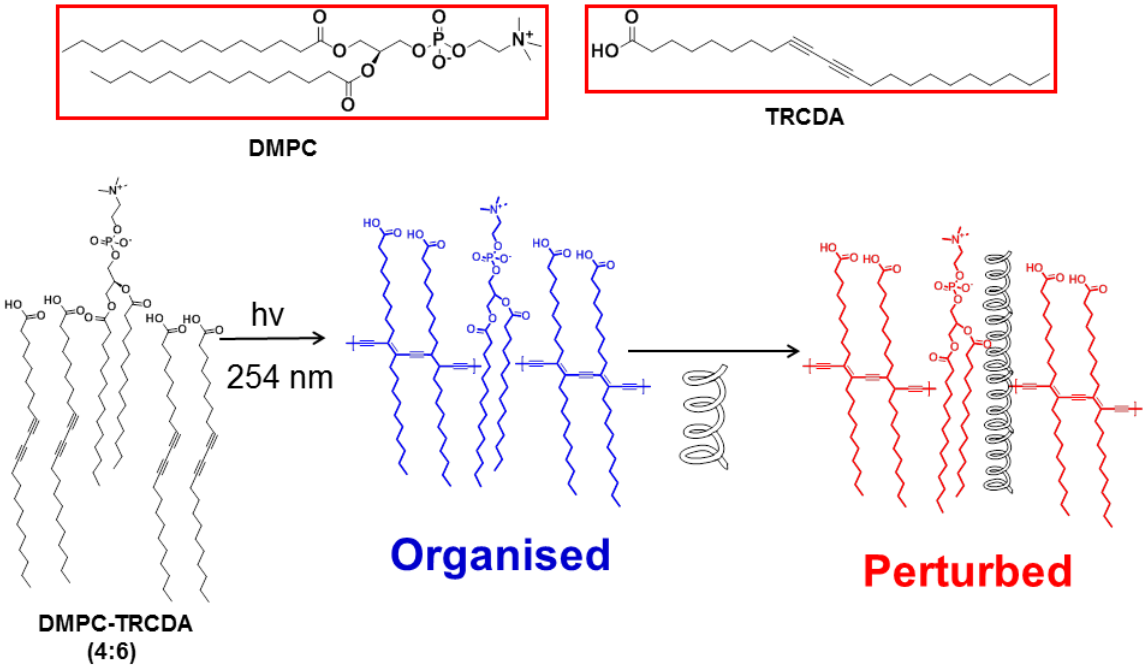

Figure 4.11 Schematic representation of the interaction of a membrane-lytic peptide interaction with DMPC-TRCDA vesicles.

The results from the colorimetric assay using the battacin library are summarised in Figure 4.12.

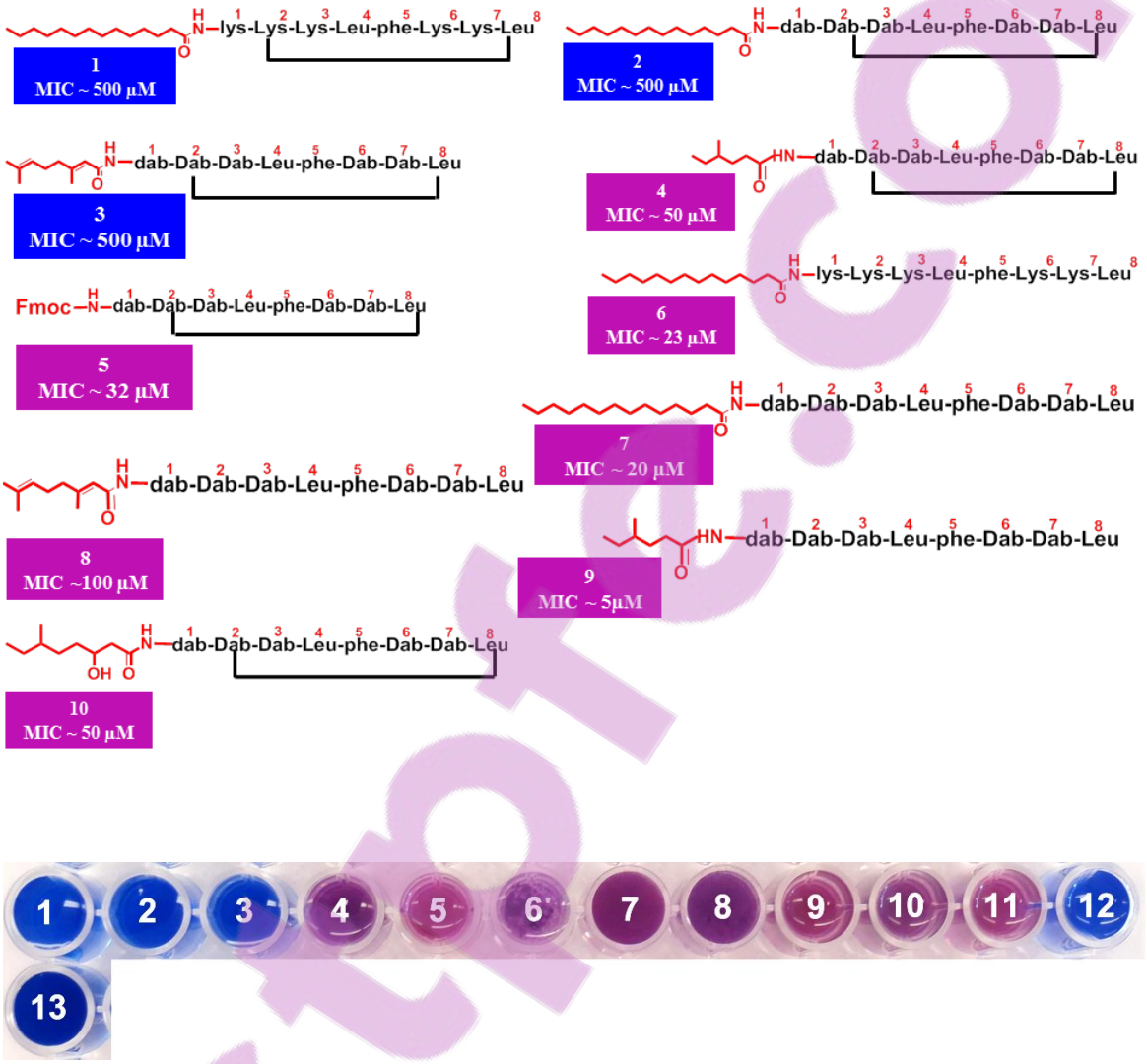

Figure 4.12 DMPC-TRCDA solutions at room temperature after immediate addition of the following compounds: **(1)** GZ3.55; **(2)** GZ3.40; **(3)** GZ3.19; **(4)** GZ3.15; **(5)** GZ3.21; **(6)** GZ3.37; **(7)** GZ3.26; **(8)** GZ3.38; **(9)** GZ3.27; **(10)** battacin; **(11)** pexiganan; **(12)** streptomycin; **(13)** no peptide. Each well contains 200 µL of 1 mM DMPC- TRCDA (4:6) vesicle and 200 µL of 0.1 mM peptide dissolved in 2 mM tris buffer at pH 8.5.

As expected, pexiganan, a well-known membrane-lytic peptide, used as the positive control (well 11), showed an intense colorimetric response from blue to red immediately on addition to the vesicles.[330] Streptomycin (well 12) did not show any color change,

which is in accordance with its known mechanism of action which does not involve membrane perturbation.[331]

The average MICs of the tested analogues are shown in coloured boxes next to the respective structures. The blue coloured boxes represent unperturbed DMPC-TRCDA vesicles in presence of the analogues, whereas red boxes represent perturbed membranes in the presence of the peptides. The observed colorimetric responses of the lipopeptides tested here correlate with their observed antimicrobial potencies (MIC). For instance, the cyclic peptides with myristic acid on the N-terminus (GZ3.55 and GZ3.40) and the geranic acid conjugated cyclic peptide (GZ3.19) showed high MICs (~500 μM) against the tested pathogens. These peptides did not perturb the vesicles as can be seen in Figure 4.12.

Thus, the poor antibacterial activity of these cyclic peptides could be due to lack of membrane interactions with the lipid vesicles possibly caused by the steric interference from the longer fatty acid.

Battacin (well 10), 4-methyl-hexanoic conjugated cyclic lipopeptide (well 4), Fmoc cyclic battacin (well 5) and all the linear lipopeptide analogues (wells 6 to 9) showed significant colorimetric responses immediately on addition to the vesicles, indicating that these peptides cause structural perturbations in the vesicles. These lipopeptides have low to moderate MICs (5-50 μM) against all of the tested pathogens. The results of the colorimetric assay, taken together with their MICs, indicate that lipopeptides with low to moderate MICs (5-50 μM) possibly exhibit their antibacterial activity through membrane interaction.

4.7.2 Scanning electron microscopy (SEM)

The results from the colorimetric assay were validated by studying the morphological changes due to peptide treatment in both Gram-negative and positive bacterial membranes, using scanning electron microscopy. *E. coli*, *P. aeruginosa*, *S. aureus* and Psa, were incubated with GZ3.27 at two times the MIC for 20 minutes. Representative SEM images of the control pathogens and the pathogens treated with the lipopeptide GZ3.27 are shown in Figure 4.13.

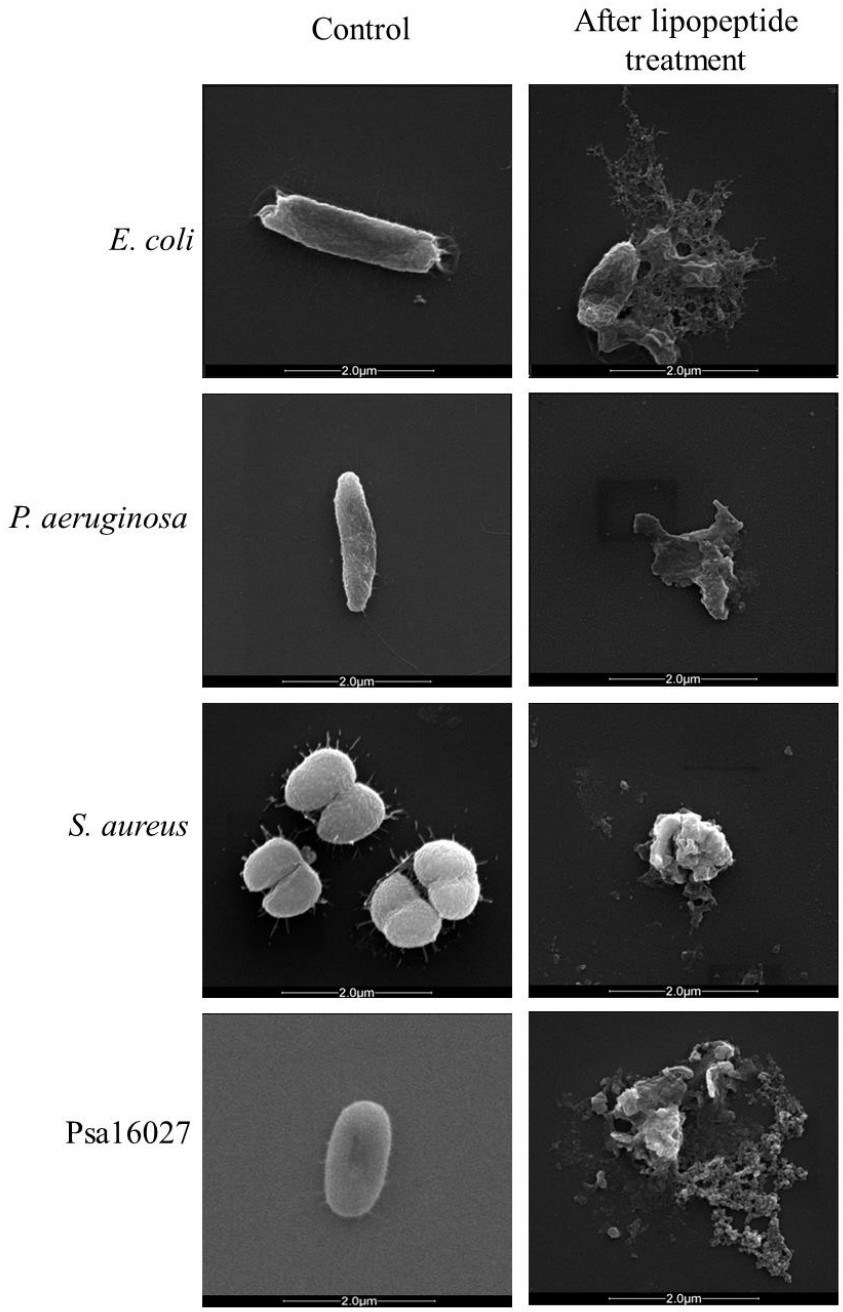

Figure 4.13 SEM images of *E. coli*, *P. aeruginosa*, *S. aureus* and Psa before (control) and after treatment with the lipopeptide GZ3.27, at 2 x the respective MICs.

The untreated Gram-negative bacterial cells (Psa, *P. aeruginosa* and *E. coli*) were rod shaped while the Gram-positive bacterium (*S. aureus*) was spherical in shape, with all cells showing smooth intact surfaces. Treatment with the lipopeptide at 2 x MIC severely damaged the cell membranes in all cases, resulting in a corrugated, blistered appearance. In most cases, complete lysis was observed, with cellular remnants scattered across the glass slides. A comparison of the treated cells with the untreated control cells clearly indicated that the lipopeptide caused catastrophic damage to the cell membranes of the pathogens investigated, and supported the idea of a membrane-lytic mechanism of action. Literature results on the antibacterial mechanism of action of octapeptin and polymyxin have shown morphological changes to bacterial membranes similar to that observed with GZ3.27 treatment, indicating a similar (membrane-lytic) mechanism of action to these peptides.[298,332]

4.7.3 Membrane permeabilisation studies

Polymyxin B inhibits bacterial growth by penetrating both the outer and inner bacterial membranes causing membrane disruption which eventually leads to bacterial cell death.[28] The ability of GZ3.27 to penetrate the outer and inner membranes of bacteria was studied using two different fluorescent dyes, *N*-phenyl-naphthylamine (NPN) and propidium iodide (PI).

4.7.3.1 Outer membrane permeabilisation studies using NPN

N-phenyl-naphthylamine (NPN) is a chemical dye that fluoresces weakly in an aqueous environment but strongly in a hydrophobic environment, such as in the outer bacterial membrane.[333]

The addition of the lipopeptide GZ3.27 to *P. aeruginosa* suspensions, in the presence of NPN, caused an increase in fluorescence intensity, within one minute, which plateaued at a lipopeptide concentration of 32 μM (Figure 4.14), with no further increase in fluorescence intensity observed up to 100 μM. This indicated that all the available surface area on the cell membrane had been permeated by the lipopeptide at a concentration of 32 μM. High fluorescent intensity of NPN in the presence of the peptide demonstrated the ability of the peptide to penetrate the outer membranes of Gram-negative bacteria.

Qian *et al.* also reported a similar increase in NPN fluorescence in the presence of battacin, in a concentration-dependent manner, thus confirming that the synthetic peptide derivative, GZ3.27, behaved like the natural product with respect to outer bacterial membrane permeability. [177]

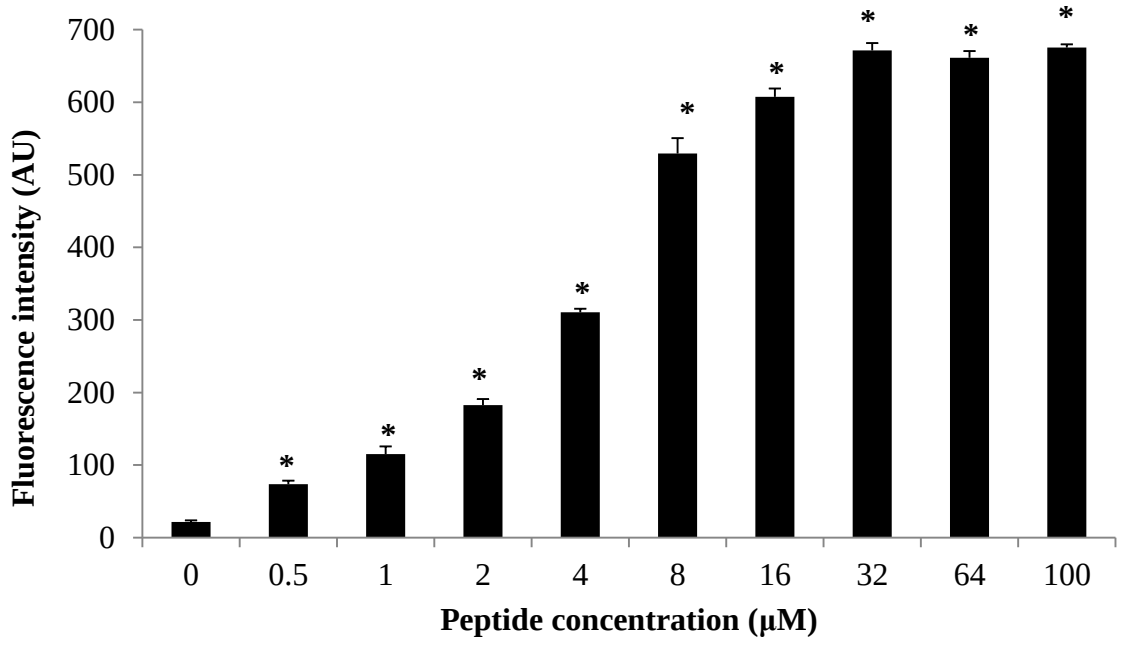

Figure 4.14 Intensity of fluorescence observed at different peptide concentration for the NPN uptake outer membrane assay for *P. aeruginosa*.* Indicates $p < 0.05$.

4.7.3.2 Inner membrane permeabilisation studies using PI

The ability of the lipopeptide to permeabilise the inner membranes of *P. aeruginosa* and *S. aureus* was evaluated using the propidium iodide (PI) uptake assay. Upon binding to DNA, propidium iodide fluoresces strongly, which is indicative of a compromised inner membrane integrity.[334] An increase in PI fluorescence was observed with increasing lipopeptide concentrations, upon incubation with *P. aeruginosa* and *S. aureus* (Figure 4.15), indicating the ability of this lipopeptide to disrupt the cytoplasmic membranes of these bacteria. The damaged *P. aeruginosa* cells fluoresced much more than *S. aureus*, which can be attributed to the larger genome size of *P. aeruginosa*, which is approximately 6.3 million base pairs long[335] and is up to three times larger than that of *S. aureus*, which is approximately 2.1 million base pairs long.[336]

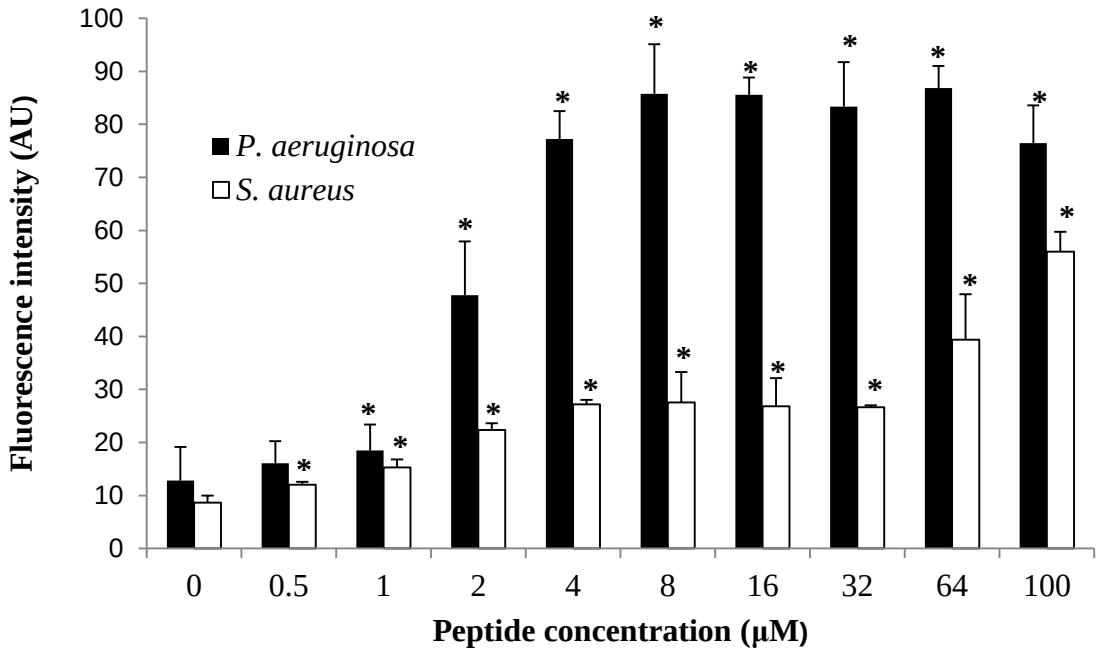

Figure 4.15 Intensity of fluorescence observed at different peptide concentration for the PI uptake of inner membrane assay for *P. aeruginosa* and *S. aureus.** Indicates $p < 0.05$.

4.7.3.3 Influence of high salt concentration on GZ3.27

One of the limitations to the clinical use of AMPs is their loss of antibacterial activity under high salt conditions. Divalent cations such as Ca^{2+} and Mg^{2+} bind to the deeper binding sites of the head groups of the lipids in the outer membrane of the LPS.[70] This cationic interaction allows the lipids to complex with each other and pack closer to each other, which in turn helps to stabilise the outer membrane.[70,337] The cAMPs occupy the same binding pockets in lipids as these cations, and compete for access to these binding sites. At high salt concentrations, monovalent and divalent cations will bind to the lipid binding pockets more frequently than the competing AMPs, leading to diminished antibacterial activity.

The human defensin peptide, β-defensin-I was inactive against *P. aeruginosa* under high salt conditions in the epithelial cells of the lungs of patients with cystic fibrosis.[338] Other AMPs with reduced antibacterial activity in the presence of high salt include LL-37, magainin, bactenecin and gramicidin.[118,339] Antibacterial activity of tachyplesin and polyphemusin are independent of the salt concentration. The high salt tolerability of tachyplesin can be correlated to a stable β-sheet structure due to the presence of six Cys residues and six cationic amino acids.[340] The antibacterial activity of the peptides under high salt conditions can be retained by manipulating the α-helicity, hydrophobicity, amphiphilicity and cationicity of the peptides.

The effect of high salt conditions on the antibacterial activity of GZ3.27 against *S. aureus*, *P. aeruginosa* and *E. coli* was determined by an MIC assay, in the presence of 120 mM NaCl and 2 mM $MgCl_2$ to mimic physiological salt concentrations (Table 4.5).

Table 4.5 Antibacterial activity of GZ3.27 under normal growth conditions and high salt (120 mM NaCl and 2 mM $MgCl_2$) conditions.

	MIC of GZ3.27 (µM)	
Bacteria	**Normal growth conditions**	**High salt conditions**
S. aureus	1-2.5	50-100
P. aeruginosa	1-2.5	5-10
E. coli	2.5-5	25-50

The MICs of GZ3.27, under high salt conditions, were 50-100 µM, 5-10 µM and 25-50 µM against *S. aureus*, *P. aeruginosa* and *E. coli* respectively. Thus, the antibacterial potency of the lipopeptide did not significantly change in the presence of high salt against *P. aeruginosa,* but showed moderate loss of activity against *E. coli* (MIC was 5 times higher than under non-salt conditions). However, with *S. aureus,* the MIC of GZ3.27 was 50 times higher under high salt conditions compared to normal conditions.

The outer membrane NPN uptake assay was repeated in the presence of 10 mM $MgCl_2$ to understand the mechanism of action of GZ3.27 further. As evident from the Figure 4.16, the uptake of GZ3.27 is significantly reduced in the presence of excess Mg^{2+} ions. In fact, no significant changes in NPN fluorescence were observed up to a peptide concentration of 100 µM.

Similar results were reported for battacin under high salt concentration by Qian *et al.*, where the MIC of battacin against *P. aeruginosa* increased from 4 µg/mL to >128 µg/mL in the presence of 10 mM $CaCl_2$.[177] Qian *et al*. also reported reduced NPN fluorescence uptake for the isolated battacin under high calcium ion concentration.[177] These results strongly indicate that both the isolated battacin and GZ3.27 interact with the cationic binding pockets in LPS.

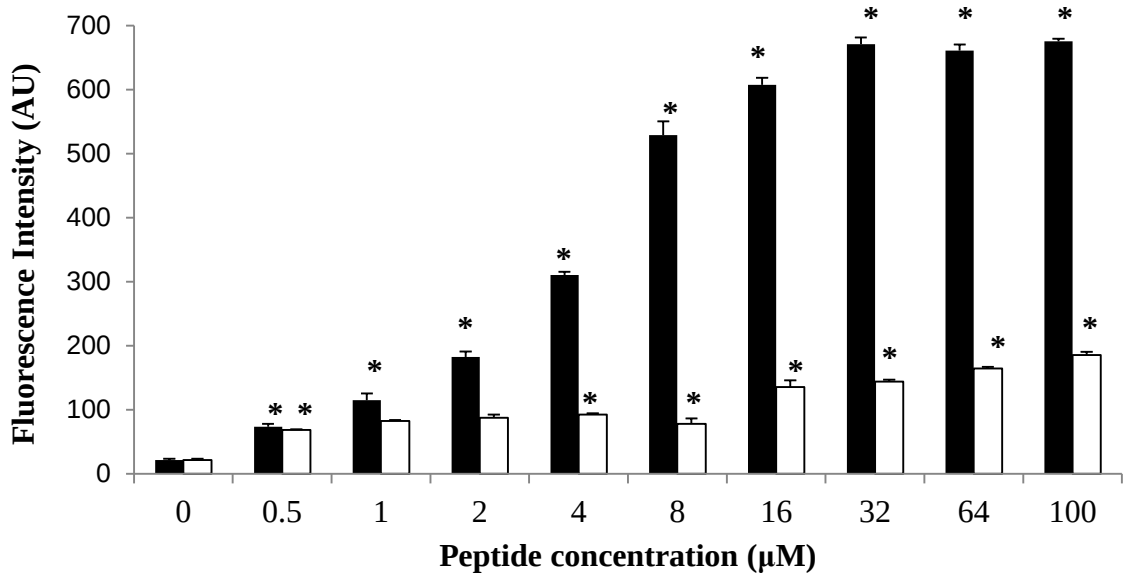

Figure 4.16 Outer membrane NPN assay: fluorescence intensity, at different peptide concentrations, in the absence (black bar) and presence (clear bar) of 10mM $MgCl_2$, for *P. aeruginosa*. * Indicates $p < 0.05$.

4.8 Solution conformation of GZ3.27

4.8.1 Circular dichroism (CD) spectra of GZ3.27 under different conditions

The secondary structure of GZ3.27 was investigated using CD spectroscopy, under different conditions (Figure 4.17).

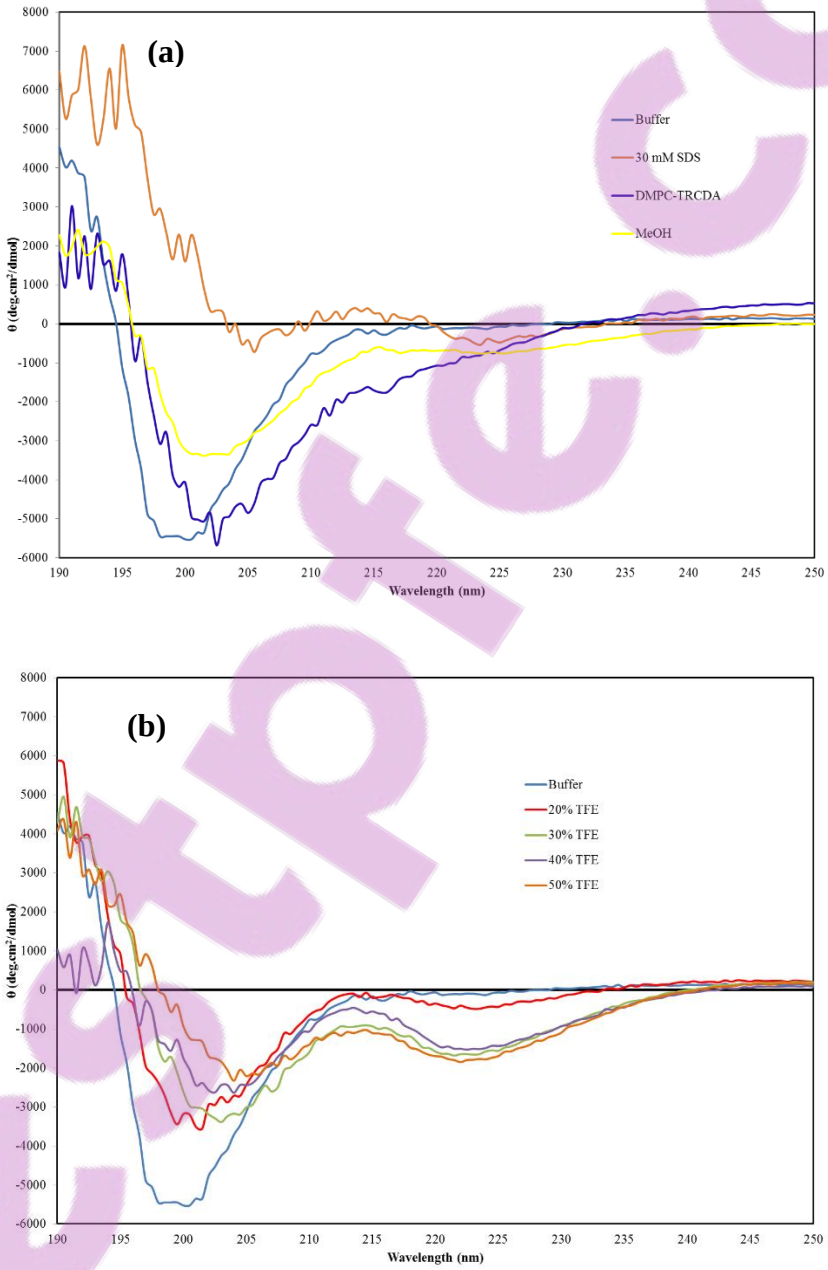

Figure 4.17 Circular dichroism spectra of GZ3.27 **(a)** under different solvent conditions and **(b)** in presence of varying concentrations of TFE.

In phosphate buffer, GZ3.27 adopted a random coil confirmation, with a single minimum close to 200 nm. In methanol, there was a decrease in intensity of this band with a slight shift towards 202 nm, which is indicative of a small structural change in the peptide, in this solvent.

The CD spectra of the lipopeptide were also recorded under the following membrane mimetic conditions: a range of concentrations with the helix-inducing organic solvent 2,2,2-trifluoroethanol (TFE) and in presence of sodium dodecyl sulfate (SDS) micelles and DMPC-TRCDA vesicles. Molar ellipticity values at 222 nm are reported in Table 4.6.

Table 4.6 Molar ellipticity at 222 nm of GZ3.27, under different conditions.

Solvent	**$[\theta]_{222}$(deg.cm^2/dmol)***
Phosphate buffer	-109.36
Methanol	-958.00
20% TFE	-403.72
30% TFE	-1646.44
40% TFE	-1563.33
50% TFE	-1850.91
SDS micelles	-352.10
DMPC-TRCDA vesicles	-851.23

*The following equation has been used in the literature to calculate the percentage helicity of longer peptides and proteins. However, given the lack of helical nature of this peptide even in 50% TFE as judged by the ($[\theta]_{222}$), percentage helicity calculation was not done in the current situation.

% helicity = ($[\theta]_{222}$ - $[\theta]_{222}^{0}$)/($[\theta]_{222}^{100}$). Values for $[\theta]_{222}^{0}$ and $[\theta]_{222}^{100}$ corresponding to 0 and 100% helix content at 222 nm, were estimated to be -2,000 and −30,000.[341-342]

TFE is a solvent commonly used to mimic the hydrophobic environment of the microbial membrane. Although the exact mechanism of action by which TFE induces helicity in potential α-helical peptides is not clearly understood, few plausible explanations have been reported in the literature. TFE can induce helicity by lowering the dielectric constant or by removing the hydrogen bonds of the peptide with surrounding water molecules, stabilising the interaction between the peptide groups.[343-345]

With increasing TFE concentration, the single minimum at 200 nm decreased in intensity and shifted to 205 nm, with the appearance of a second minimum at 222 nm indicating a shift from a random coil conformation in aqueous solution to a more ordered (helical) conformation in TFE. However, TFE titration of GZ3.27 did not induce significant helicity even at 50% TFE. Overall, the CD spectra of GZ3.27 in the aqueous buffer and varying TFE concentrations resemble that of polymyxin B, where the peptide showed a transition from random structure in aqueous buffer to a more ordered structure with increasing concentrations of TFE.[346-347]

SDS micelles and DMPC-TRCDA vesicles are routinely used to mimic the anionic nature of bacterial membranes. In the presence of 30 mM of SDS micelles, the single minimum at 200 nm decreased and also shifted to 205 nm with the appearance of a very weak band at 222 nm indicating small structural changes to the peptide in vicinity of the micelles.

In the presence of the DMPC-TRCDA vesicles, the single minimum at 200 nm shifted to 202 nm with no decrease in the intensity also indicative of a small structural change induced by the vesicles. DMPC-TRCDA vesicles nor SDS induced significant helicity in the peptide. CD spectra of GZ3.27 in the presence of these artificial membranes may suggest, GZ3.27 undergoes small structural changes without any well-defined secondary structure in the vicinity of the bacterial membrane to exert antibacterial activity.

4.8.2 NMR characterisation of GZ3.27 in methanol

4.8.2.1 ^{1}H NMR spectrum

NMR characterisation of GZ3.27 was initially performed in methanol (Figure 4.18) and the spectra showed sharp resonances.

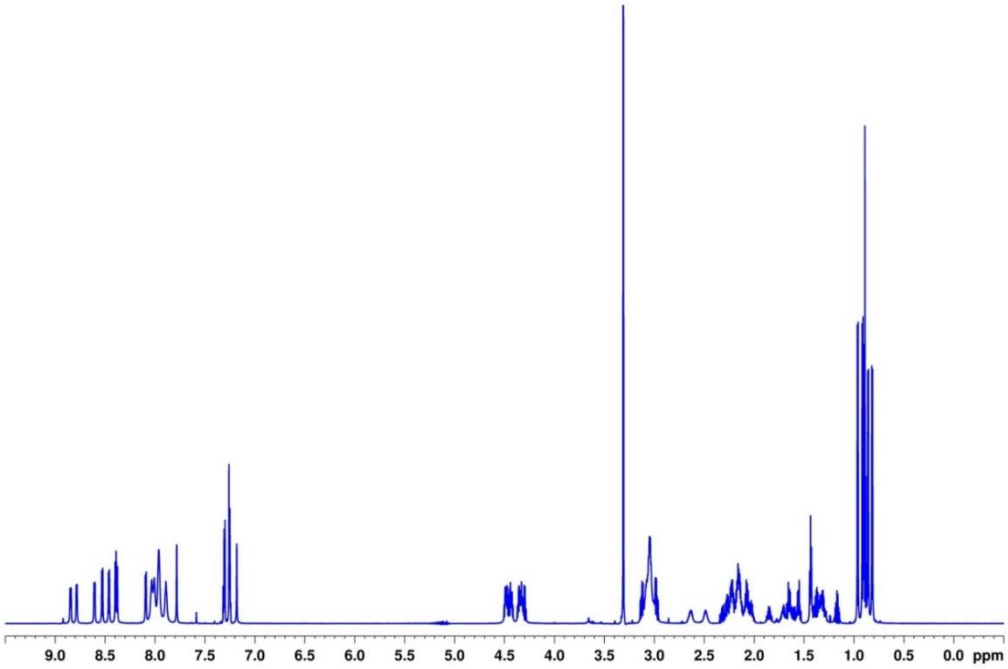

Figure 4.18 800 MHz ^{1}H NMR spectrum of GZ3.27 in CD_3OH at 278 K.

Table 4.7 ^{1}H NMR chemical shifts (ppm), vicinal coupling constants (Hz) and temperature coefficient values (ppb/K) of GZ3.27 in CD_3OH at 278 K.

Residue	**Chemical shift (ppm)**						**$^{3}J_{NHC\alpha H}$ (Hz)**	**dδ/dT (ppb/K)**
	NH	**$C^{\alpha}H$**	**$C^{\beta}H$**	**$C^{\gamma}H$**	**$C^{\delta}H$**	**Other**		
Fatty acid		2.27/1.60	1.37/1.33	$C^{\gamma}H_1$: 1.17 $C^{\gamma}H_3$: 0.90	2.34.2.23	$C^{\varepsilon}H_3$: 0.89		
dab 1 (X1)	8.60	4.32	2.03/2.14	3.03		8.03	6.1	-5.9
Dab 2 (X2)	8.64	4.43	2.08/2.22	3.06		8.01	7.1	-5.2
Dab 3 (X3)	8.46	4.49	2.04/2.13	3.07		7.97	7.5	-3.2
Leu 4 (L4)	8.09	4.30	1.43	1.31	0.86/0.82		7.0	-3.7
phe 5 (F5)	8.78	4.45	3.12/2.98			$C^{\delta}H_2$: 7.25: $C^{\gamma}H_2/C^{\zeta}H$: 7.32	6.9	-8.4
Dab 6 (X6)	8.53	4.36	1.85/2.11	2.63/2.48		7.89	8.0	-4.3
Dab 7 (X7)	8.38	4.48	2.23/2.06	3.08		7.96	7.9	-3.6
Leu 8 (L8)	8.39	4.34	1.71/1.65	1.55	0.96/0.91		7.4	-6.6
C-ter NH_2						7.78/7.18		-5.3

The NMR parameters are summarised in Table 4.7. The values of vicinal coupling constants, $^{3}J_{NH,C\alpha H}$ reported in Table 4.7 range between 6.1-8 Hz, indicating random coil structure.[228]

4.8.2.2 Temperature dependence of NH shifts of GZ3.27

The temperature dependence of the amide proton chemical shift was studied from 278 K to 318 K (Figure 4.19).

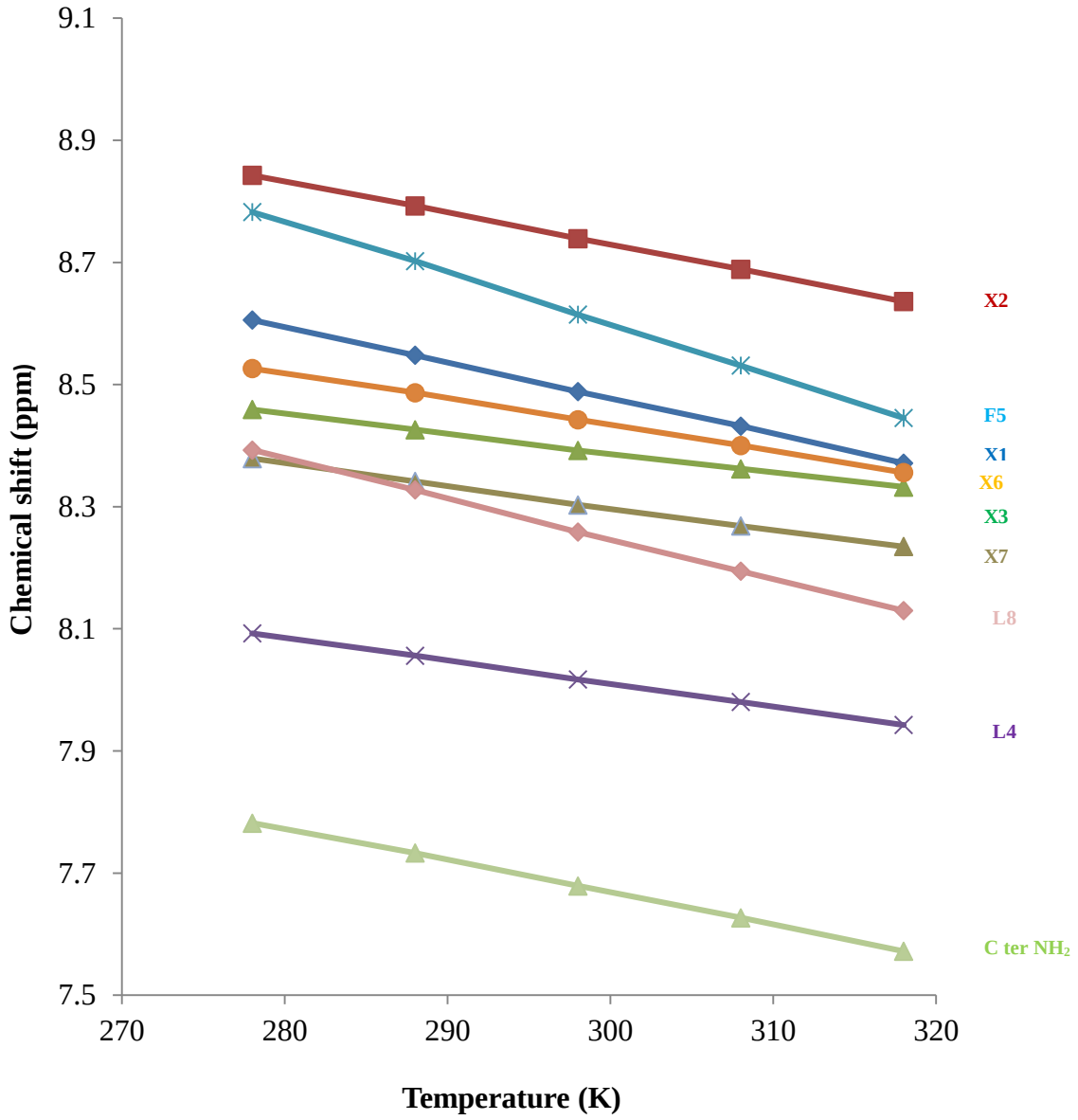

Figure 4.19 Plot of temperature dependence of amide proton chemical shifts for GZ3.27 in CD_3OH.

The results showed that Dab^3, Leu^4 and Dab^7 had low dδ/dT (< 4 ppb/K) indicating that these amino acids were partially shielded from the solvent, due to intramolecular hydrogen bonding. The remaining amino acids showed larger dδ/dT values (> 4 ppb/K), indicating that these amino acids were exposed to the solvent.

4.8.2.3 2D NMR

Sequence specific assignments were obtained using a combination of TOCSY (Figure 4.20) and ROESY (Figure 4.21) spectra.

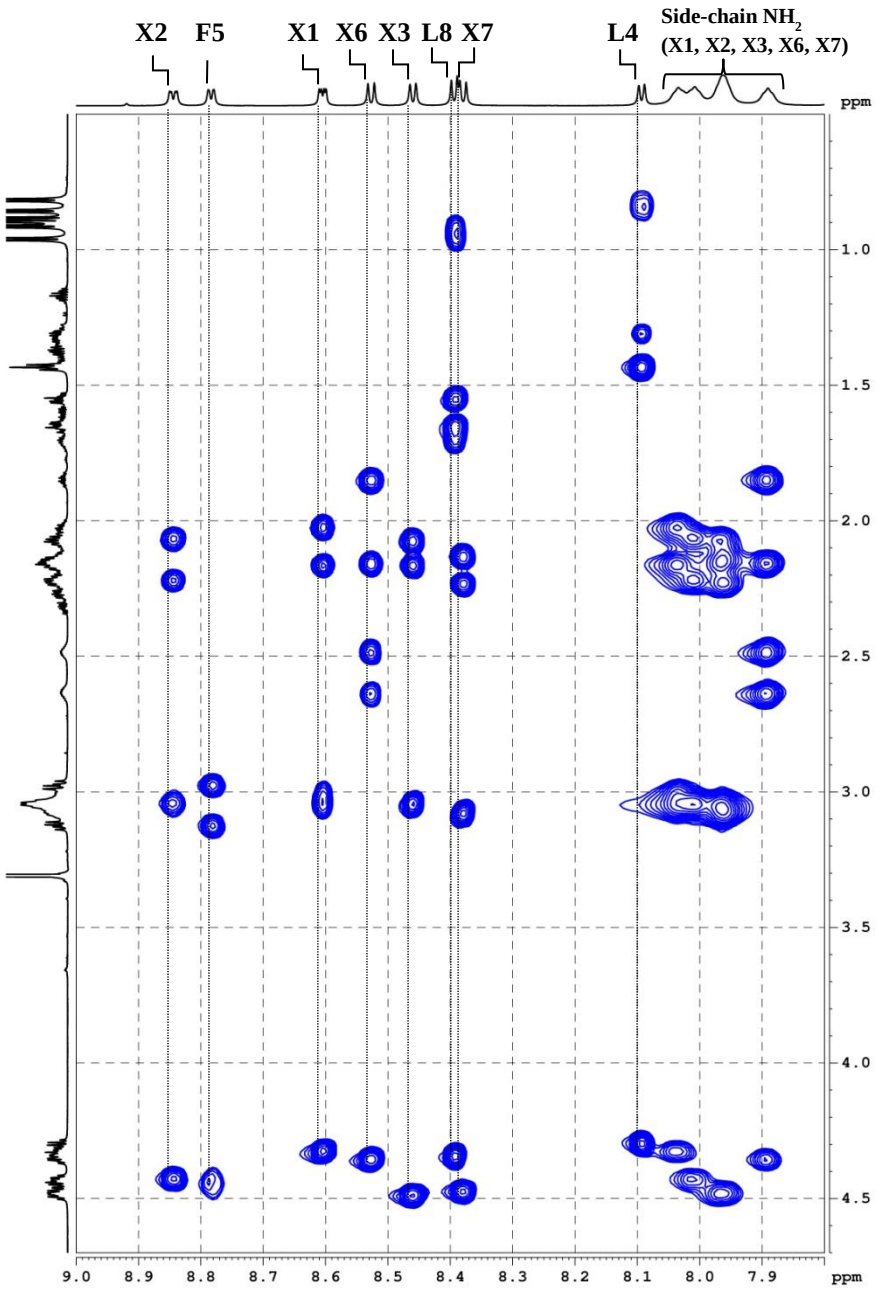

Figure 4.20 Partial 800 MHz TOCSY spectrum of GZ3.27, in CD_3OH, at 278 K. Letters X, F and L refer to Dab, Phe and Leu.

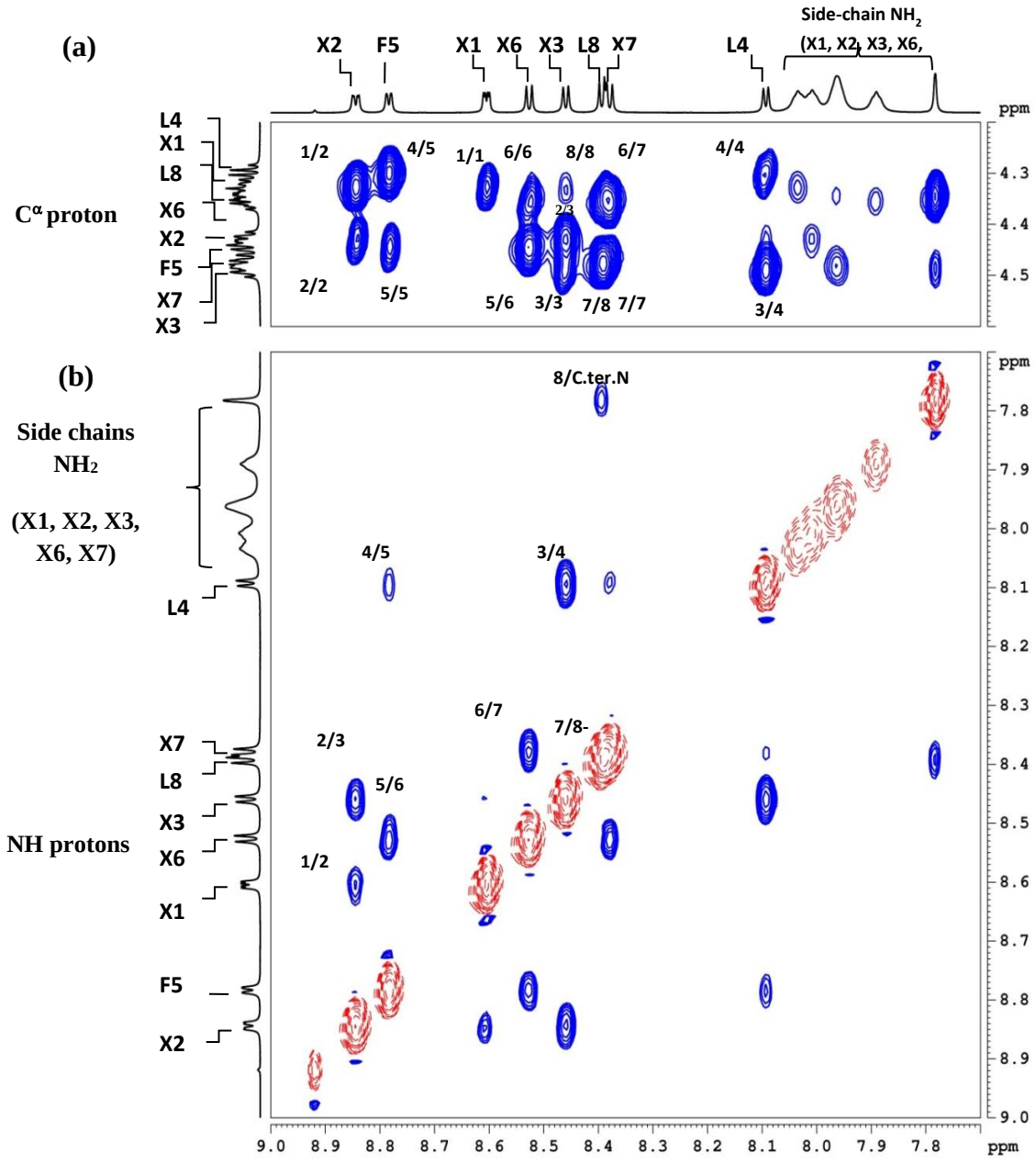

Figure 4.21 Partial 800 MHz ROESY spectrum of GZ3.27 in methanol showing **(a)** $C^{\alpha}H$-NH and **(b)** NH-NH NOEs. Letters X, F and L refer to Dab, Phe and Leu.

The ROESY spectrum of the peptide in methanol showed relatively weaker sequential $N_iH \leftrightarrow N_{i+1}H$ NOEs over the entire length of the peptide. Comparatively, the sequential $C^{\alpha}{}_iH \leftrightarrow N_{i+1}H$ NOEs were stronger. The observed NOE pattern is indicative of the absence of definite secondary structure for the lipopeptide in CD_3OH, and is in agreement with the

CD spectrum in methanol. Lack of NOEs to the N-terminal alkyl chain is indicative of the extensive molecular motion of the N-terminus.

4.8.3 NMR characterisation of GZ3.27 in H_2O-TFE (70:30)

4.8.3.1 ^1H NMR spectrum

NMR structure of GZ3.27 was then resolved in 30% TFE, in order to determine if any structural changes occurred under helix-inducing conditions. This solvent system was also chosen to be able to better compare the NMR structure with that of polymyxin B reported in the literature which was measured under similar measurement conditions.[346] The ^1H NMR spectrum (Figure 4.22) showed sharp signals, similar to the methanol spectrum of GZ3.27.

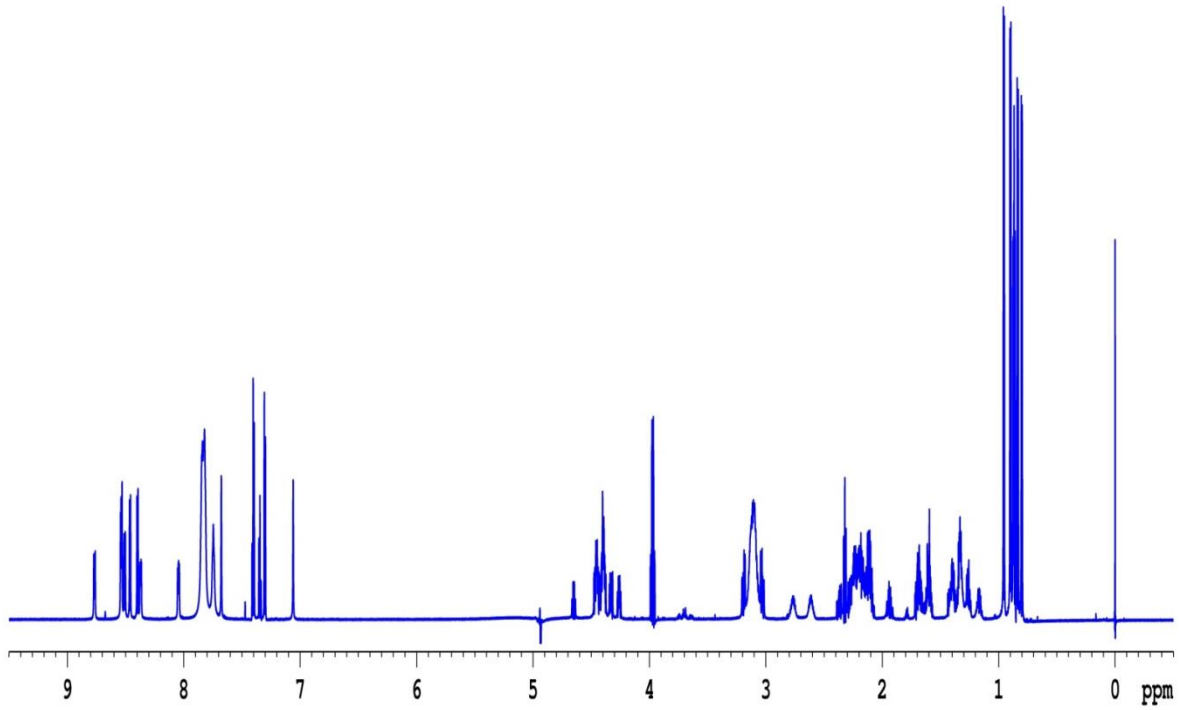

Figure 4.22 800 MHz ^1H NMR spectrum of GZ3.27 in water (70%) and TFE (30%) at 278K.

Table 4.8 ^{1}H NMR chemical shifts (ppm), vicinal coupling constants (Hz) and temperature coefficient values (ppb/K) of GZ3.27 in 30% TFE at 278 K.

Residue	**Chemical shift (ppm)**						**$^{3}J_{NHC\alpha H}$ (Hz)**	**dδ/dT (ppb/K)**
	NH	$C^{\alpha}H$	$C^{\beta}H$	$C^{\gamma}H$	$C^{\delta}H$	Others		
Fatty acid		2.32	1.61	$C^{\gamma}H$:1.17	1.33 / 1.40 $C^{\delta}H_3$: 0.87	$C^{\varepsilon}H_3$: 0.85		
dab 1 (X1)	8.46	4.38	2.20 /2.10	3.13 /3.08		7.83	6.6	-4.8
Dab 2 (X2)	8.76	4.45	2.13 / 2.25	3.09		7.83	7.0	-6.1
Dab 3 (X3)	8.51	4.40	2.22 / 2.13	3.12		7.83	7.6	-8.3
Leu 4 (L4)	8.04	4.26	1.39, 1.33, 1.27		0.84 / 0.80		7.0	-7.0
phe 5 (F5)	8.37	4.65	3.19 / 3.03		Aromatic: $C^{\delta}H_2$: 7.30; $C^{\gamma}H_2$:7.40, $C^{\zeta}H$: 7.35: 7.35		7.0	-9.0
Dab 6 (X6)	8.53	4.46	2.77 / 2.61	2.16 / 1.93		7.74	7.6	-4.1
Dab 7 (X7)	8.54	4.39	3.12	2.23		7.83	7.3	-6.7
Leu 8 (L8)	8.39	4.33	1.71,1.67, 1.60		0.95 / 0.90		7.2	-6.9
C-ter NH_2						7.67 / 7.05		

The relative NMR parameters are summarised in Table 4.8. The values for vicinal coupling constants, $^{3}J_{NH,C}\alpha_{H}$ reported in Table 4.8 range between 6.6-7.6 Hz, also indicating random coil conformation.

4.8.3.2 Temperature dependence of NH shifts in the presence of TFE

The temperature induced changes in the NH chemical shifts of GZ3.27, in the water-TFE mixture, were monitored by increasing the temperature from 278 K to 318 K, and the results are summarised in Figure 4.23 and Table 4.8. A larger $d\delta/dT$ ($\geq$ 4.1 ppb/K) was recorded for the entire peptide indicating that all the amide protons in the peptide were exposed to the solvent.

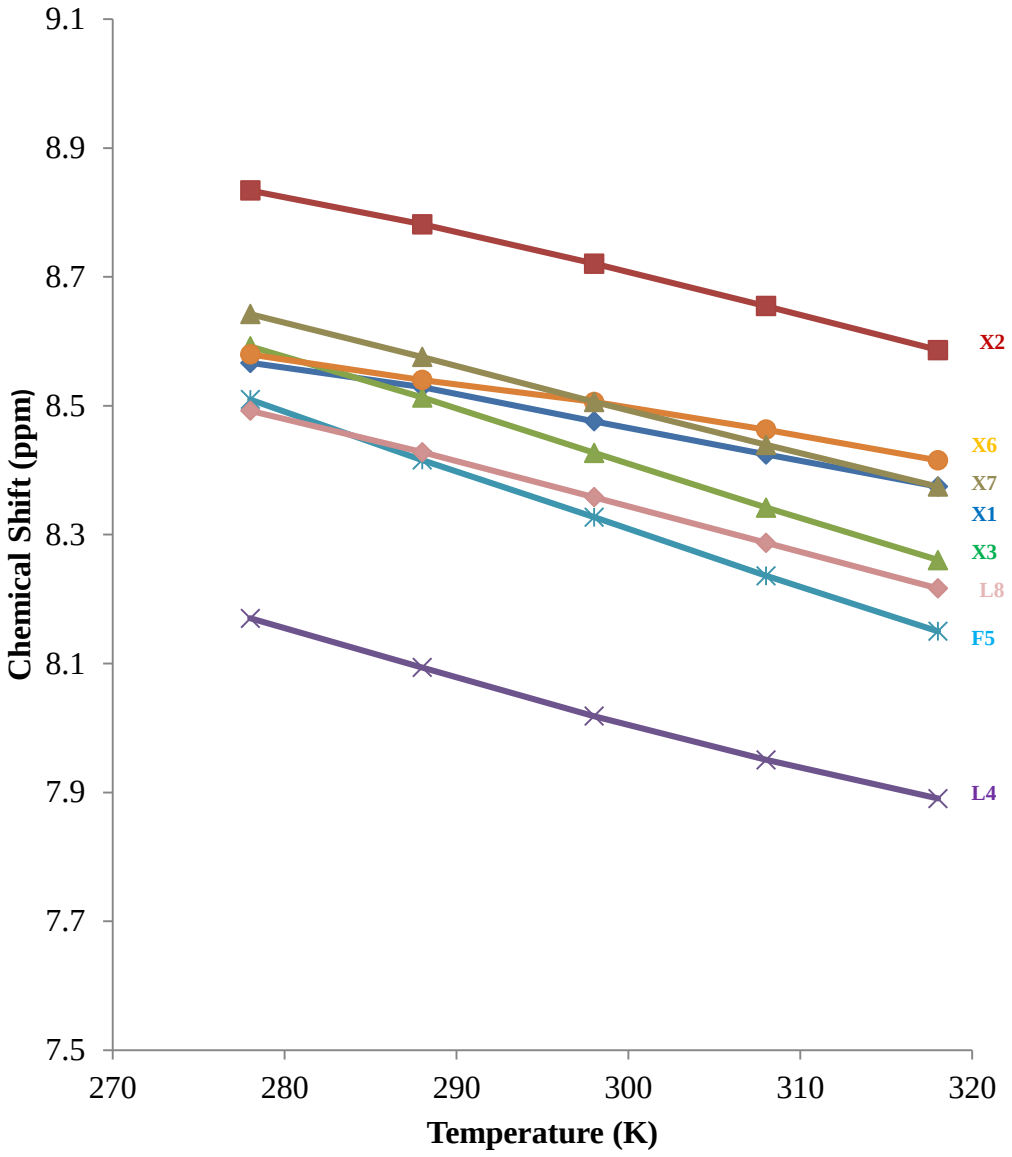

Figure 4.23 Plot of temperature dependence of amide proton chemical shifts for GZ3.27 in in H_2O (70%) and TFE (30%).

4.8.3.3 2D NMR

The sequence specific assignments of GZ3.27 in TFE were also resolved using a combination of TOCSY (Figure 4.24) and ROESY (Figure 4.25).

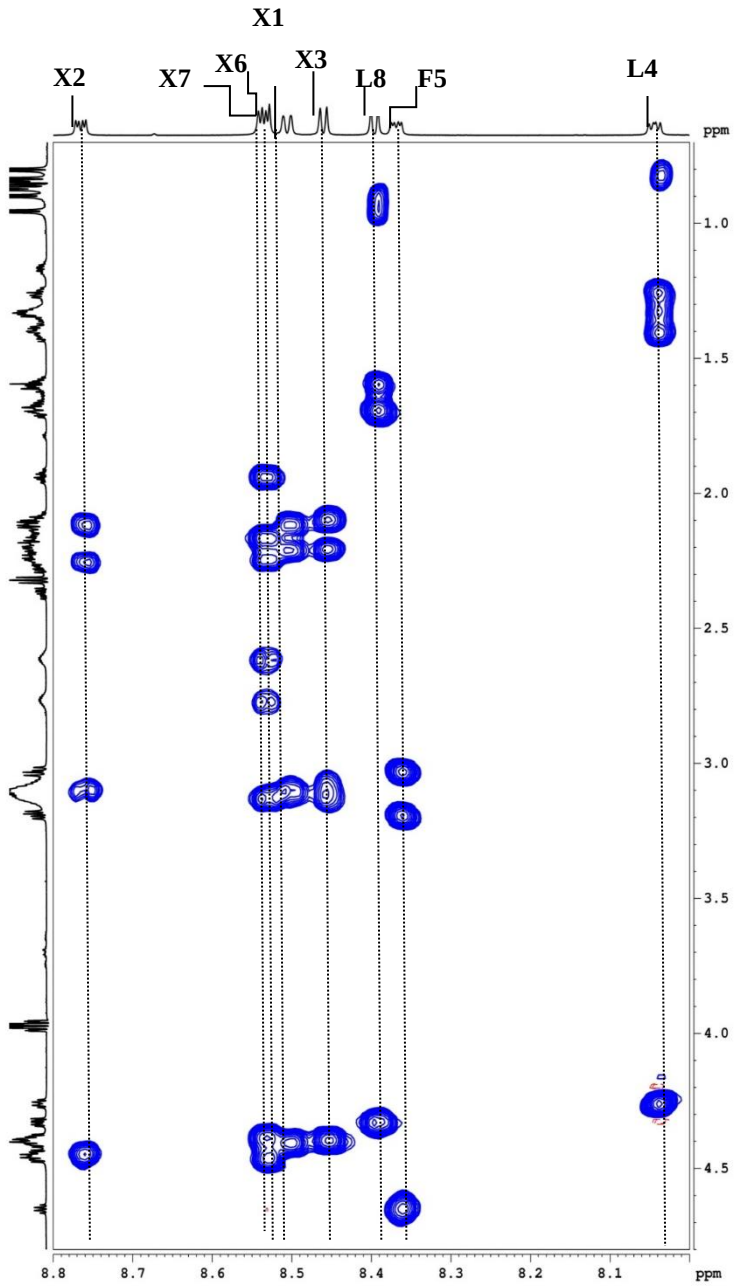

Figure 4.24 Partial 800 MHz TOCSY spectrum of GZ3.27 in H_2O (70%) and TFE (30%) at 278 K. Letters X, F and L refer to Dab, Phe and Leu.

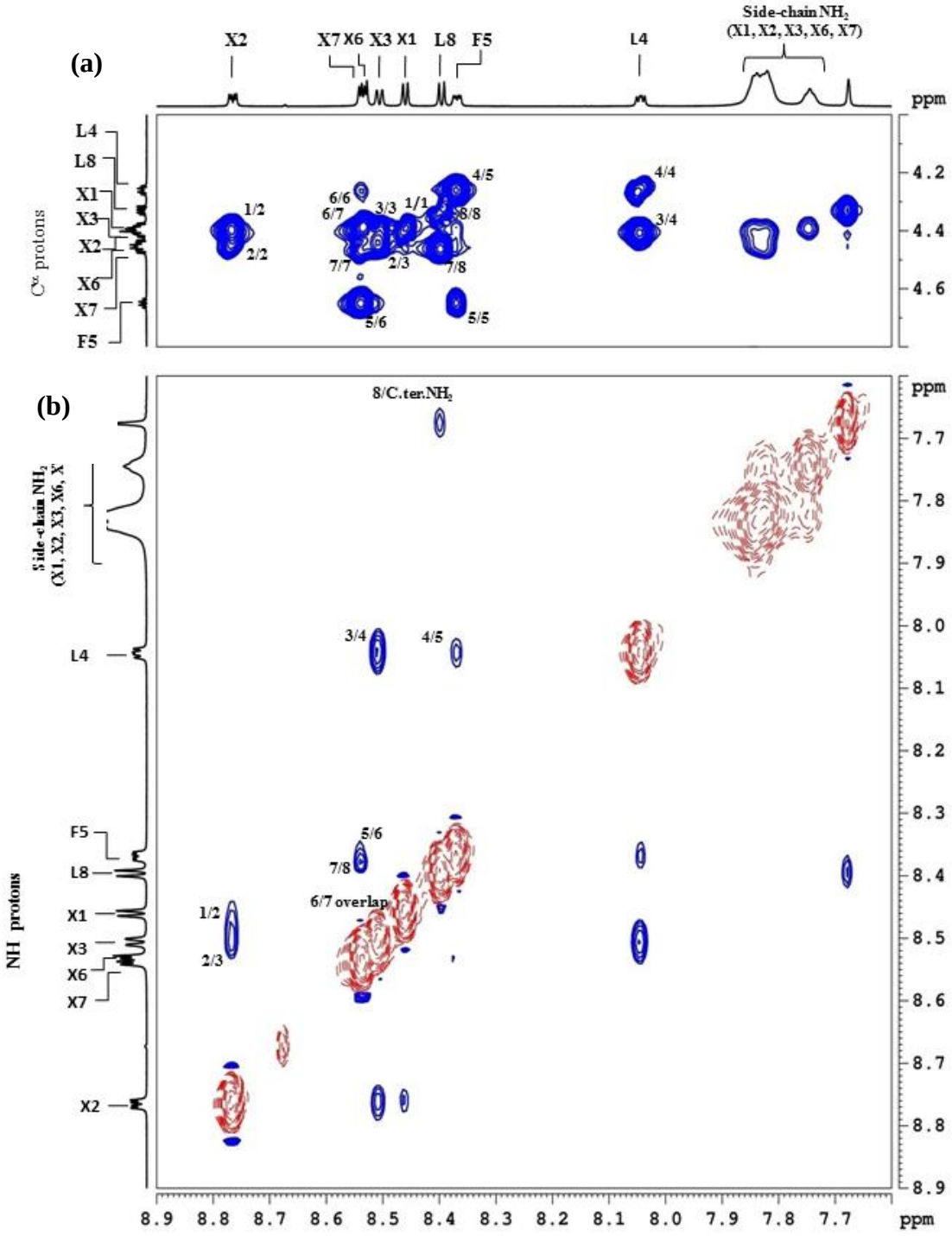

Figure 4.25 Partial 800 MHz ROESY spectrum of GZ3.27 in H_2O (70%) and TFE (30%) showing **(a)** $C^{\alpha}H$-NH and **(b)** NH-NH NOE. Letters X, F and L refer to Dab, Phe and Leu.

The ROESY spectrum showed strong sequential $C^{\alpha}{}_iH \leftrightarrow N_{i+1}H$ NOEs. Surprisingly, a comparatively less intense $N_iH \leftrightarrow N_{i+1}H$ NOEs than in methanol (See Figure 4.21b) was

observed in the water-TFE mixture, despite the fact that 30% of the solvent was helix inducing. As in methanol, the peptide did not show a well-defined secondary structure in water-TFE.

4.8.4 Energy-minimised model of GZ3.27

An energy-minimised model, based on NOE distances and torsion constraints, of GZ3.27, in methanol, was generated using Discovery Studio (Figure 4.26).[348] The model shows that residues from the N-terminal fatty acid to Dab^3 adopt an extended structure, followed by a curved structure from Leu^4 to Dab^7. The floppy N-terminus, solvent exposed nature and large coupling constants of several of the amide protons, as well as the lack of a rigid overall structure for GZ3.27 agree well with the structure reported for polymyxin B.[346]

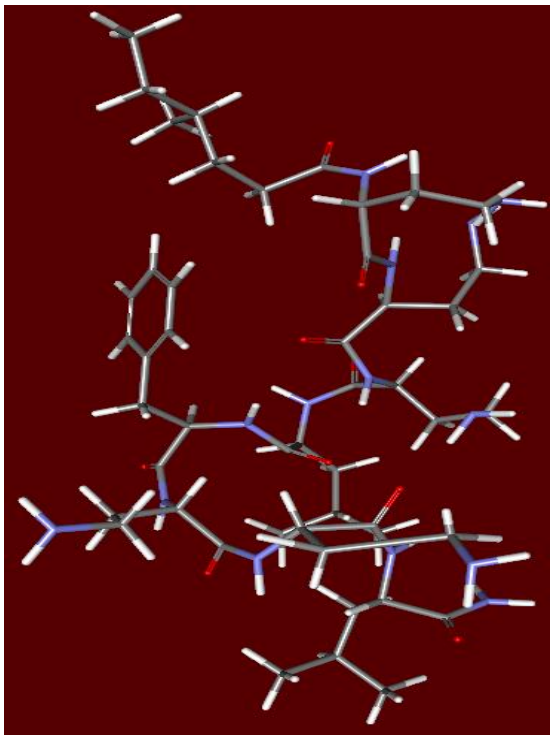

Figure 4.26 Restrained energy-minimized model of GZ3.27 generated using Discovery Studio.

However, it is to be acknowledged that because of the limitations of the algorithms used, the protocol did not conduct an exhaustive analysis of the available conformational space. The current model merely shows one possibility for an average structure, and is unlikely to be representative of any of the individual structures the peptide may be sampling between in solution.

The derived dihedral angles, ϕ, ψ (Figure 4.27a) when mapped onto the Ramachandran plot (Figure 4.27b) were scattered, but within the allowed limits. The D-residue (D-Phe^5) around the centre takes the Leu^4 and DPhe^5 ϕ, ψ values to the positive side, nevertheless remains within the allowed Ramachandran limits.

(a)

Residue	**ϕ**	**Ψ**
^{D}X1	-140	-176
X2	-134	+105
X3	-78	-37
L4	+100	+56
^{D}F5	+34	+27
X6	-144	-172
X7	-97	-3
L8	-104	-45

(b)

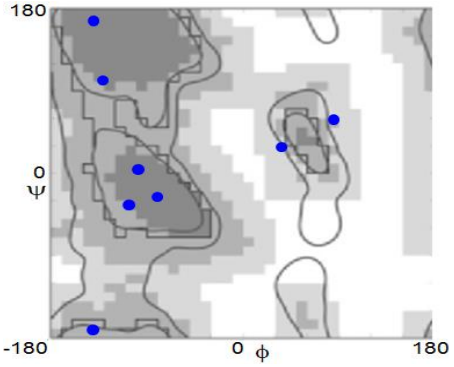

Figure 4.27 (a) Dihedral angles and **(b)** their locations on the Ramachandran map.

4.9 Mechanism of action of GZ3.27

Based on the membrane-binding studies (section 4.7), CD and NMR studies (section 4.8) the following generalised and evidence based mechanisms of action can be proposed.

Based on the NMR and CD data, the unstructured GZ3.27 may be undergoing small, folded structural transitions, near bacterial cell membranes. However, this solvent induced conformation lacks a well-defined secondary structure and is likely to be the average of an assembly of helical and extended conformations in both solvents, due to the structural flexibility. The energy-minimised model of GZ3.27 (Figure 4.26) shows an extended structure between the N-terminal fatty acid to Dab^3, followed by a curved structure from Leu^4 to Dab^7.

For Gram-negative bacteria, the following mechanism of action can be proposed. The Dab side chains of partially folded GZ3.27 interact with the LPS in the outer membrane, binding to the divalent cation binding pockets of lipid A, and displacing the cations. Generally, AMPs have a higher affinity to LPS compared to divalent cations because they carry a greater total positive charge, and they are also stabilised by hydrophobic interactions.[69] This initial interaction was validated by the observed decrease in fluorescence of NPN at high salt concentration, indicating that divalent cations at high concentration competitively inhibit this electrostatic binding interaction between the peptide and lipid A.

Once bound to the LPS, the hydrophobic dipeptide core (D-Phe-Leu) and the fatty acyl chain most likely interact with the lipid tails, to penetrate and damage the outer membrane indicated by the increase in NPN fluorescence in the absence of high salt conditions. Following the outer membrane penetration, the lipopeptide will most likely traverse into the inner membrane via a "self-uptake" mechanism.[166] The propidium iodide

assay described above for *P. aeruginosa* confirms that the peptide does indeed disrupt the inner membrane, in a manner sufficient to cause leakage, allowing the PI to reach the DNA. Perturbation of the outer and inner membranes leads to leakage of intracellular ions and membrane lysis as validated by SEM with the ultimate outcome of bacterial cell death.

For Gram-positive bacteria, the following mechanism of action can be proposed. The Dab side chains of GZ3.27 potentially interacts with the anionic teichoic acid in the peptidoglycan layer of the cell wall.[68] This interaction most likely helps to account for the peptide's affinity and selectivity towards Gram-positive bacteria. However these studies have not investigated a direct correlation to its antimicrobial mechanism. After probably diffusing through the thick peptidoglycan layer, the hydrophobic domains of GZ3.27 could interact with the inner membrane, leading to membrane disruption and subsequent membrane lysis, which was again validated by PI assay and SEM imaging.

4.10 Summary

The antibacterial activity of the battacin library was tested against a series of plant and human pathogenic bacteria. The MIC analysis showed that the N-terminal fatty acid could significantly influence the antibacterial activity of the peptide. The absence of the fatty acid (GZ3.130) or conjugation of a longer chain fatty acid (GZ3.40 and GZ3.55) to the sequence was detrimental to the observed antibacterial activity, possibly due to lack of membrane interaction and the increased steric hindrance observed with the longer chain.

However, GZ3.130 is highly active towards the *Pseudomonas* species. These observations were similar to those reported for polymyxin B nonapeptide and octapeptins.[260,298] In contrast to the polymyxin analogues, linearisation was beneficial to the antibacterial activity in this series of peptides. This is encouraging for the

development of clinically relevant antimicrobial peptides, since it simplifies their synthesis significantly and thereby reduces manufacturing costs.

The *Pseudomonas* species (*P. aeruginosa* and Psa) were highly sensitive to the battacin library, possibly due to the weak packing of the lipid A of LPS of the outer membrane in these strains.[300] A synthetic analogue- the 4-methyl-hexanoyl conjugated linear lipopeptide GZ3.27, was discovered in this study, which showed potency against the Gram-positive human pathogen, *S. aureus*, unlike polymyxin and the natural product battacin reported by Qian *et al*., and was therefore, chosen as the lead molecule for further development as a broad-spectrum antimicrobial peptide.

The kinetic assay revealed that GZ3.27 exhibits bactericidal killing in a concentration-dependant manner. However, the rate of inhibition of bacteria by GZ3.27 was slower than that of polymyxin B, but the bactericidal effect was more prolonged.

GZ3.27 inhibited initial biofilm formation and dispersed mature biofilms of Psa, *P. aeruginosa* and *S. aureus*, quite possibly by penetrating the exopolysaccharide matrix. Inhibition of Psa biofilms has not been previously reported in the literature and this is the first time that the use of lipopeptides to inhibit biofilm formation has been demonstrated. However, an increased concentration of GZ3.27 (10-50 μM) is required to disperse mature biofilms of *P. aeruginosa*, possibly due to the formation of anionic alginate polymers, which can trap the cAMPs before they reach the cells within the biofilm.[315] A higher peptide concentration (10-25 μM) is also required to disrupt biofilm formation of *S. aureus*, possibly due to the secretion of cationic polysaccharide intercellular adhesion polymer matrix, which causes electrostatic repulsion between the matrix and the peptide.[317]

SAR studies of GZ3.27 were carried out by designing an alanine-scanned peptide library via combinatorial synthesis using SynPhase lanterns. The SAR study helped identify the pentapeptide core of GZ3.27 that is crucial for the observed activity. This key pentapeptide core, GZ3.159 maintained similar antibacterial potency to the parent peptide.

A haemolytic assay, using mouse blood cells, showed that the myristoyl-conjugated (GZ3.26) and Fmoc conjugated battacin analogues (GZ3.21) were haemolytic, as shown by their increased affinity towards the RBC. The lead compound GZ3.27 and the truncated peptide, GZ3.159 did not show any hemolysis up to a concentration of 1 mM. These results have revealed that the conjugation of a short-chained fatty acid not only improves the antibacterial activity, but also shows a promising trend in the improved therapeutic potential.

The mechanism of action of the active lipopeptide GZ3.27 was proposed using a combination of a colorimetric assay, scanning electron microscopy and outer and inner membrane permeabilisation assays. Many of the active battacin analogues showed a blue to red colour transition in the presence of DMPC-TRCDA vesicles. The rapid colour change occurs due to the rearrangement of this vesicle system, caused by the strain on the TRCDA backbone by the lipopeptide, an interaction which is comparable to a bacterial membrane lysis event.[326]

The effect of GZ3.27 on the bacterial cell morphologies of *P. aeruginosa*, *E. coli*, *S. aureus* and Psa, in the presence of GZ3.27, as seen in the SEM images, are similar to those caused by membrane-lytic peptides reported in the literature.[298]

The results from the NPN assay and PI assay revealed that GZ3.27 induces membrane-lytic action by disrupting both the outer and inner bacterial membranes.

Finally, a moderate loss of antibacterial activity was observed for GZ3.27 against Gram-negative pathogens, and a higher loss of activity was observed for *S. aureus*, under high salt concentrations (120 mM of NaCl and 2 mM $MgCl_2$). GZ3.27 also lost its ability to perturb the outer bacterial membrane with 10 mM of $MgCl_2$, indicated by decreased NPN fluorescence. These observations indicated that GZ3.27 competed with cations at the binding site of lipid A of LPS in the outer membrane of Gram-negative bacteria. The overall results from the mechanistic studies indicated that GZ3.27 has a similar mechanism of action to polymyxin B.

The overall structure of GZ3.27 was resolved using CD and NMR spectroscopy to understand the importance, if any, of secondary structure, on the observed membrane-lytic antibacterial activity. CD spectroscopy revealed that GZ3.27 did not adopt any characteristic secondary structures under different non-membrane mimicking (methanol and phosphate buffer) or membrane-mimicking (TFE titration, SDS micelles and DMPC-TRCDA vesicles) conditions. However, under membrane mimetic conditions, GZ3.27 shifted slightly from random coil structure towards ordered structural conformation.

The ROESY spectrum of the peptide under both of these conditions showed weak sequential $N_iH \leftrightarrow N_{i+1}H$ NOEs and strong sequential $C^{\alpha}{}_iH \leftrightarrow N_{i+1}H$ NOEs for the entire length of the peptide. The observed NOE pattern is indicative of no definite secondary structure for GZ3.27 in methanol or helix-inducing conditions (30% TFE). In fact, the intensities of the sequential $N_iH \leftrightarrow N_{i+1}H$ NOEs of GZ3.27 in TFE were weaker compared to the same NOEs observed in methanol. The CD and NMR data, together with the antibacterial activity studies, indicate that a well-defined secondary structure is not crucial for the observed antibacterial activity and mechanism of action of this lipopeptide. The membrane-lytic action of GZ3.27 may occur in accordance with either the carpet model

or the SMH model, since secondary structure formation is not a requisite for these models.

The shorter fatty-acid chain conjugated linear battacin analogue GZ3.27, could be superior to both battacin and polymyxin, based on its potent antibacterial activity against both Gram-negative and positive pathogens. In addition to low micromolar activity, GZ3.27 is non-haemolytic up to 1 mM and capable of inhibiting biofilms formation and dispersing pre-formed biofilms. GZ3.27 and the pentapeptide GZ3.159 have shown promise to be developed further as therapeutics to combat multi-drug resistant pathogens.

Furthermore, the ability of GZ3.27 to be immobilised onto solid materials that are used frequently in implant industry will be discussed in Chapter 5. This could pose as an attractive alternative to combat bacterial colonisation of these medical implants.

4.11 Experimental

4.11.1 General details

All chemicals were of reagent grade quality and used without any further purification. Yeast extract, select agar, Luria broth and Live/Dead staining kit (L34856) were purchased from Invitrogen (New Zealand). D-series SynPhase lanterns were obtained from Mimtopes (Australia). Dimyristoylphosphatidylcholine (DMPC) was obtained from Avanti Polar Lipids, Inc. (Alabama, USA) and 10, 12-tricosadiynoic acid (TRCDA) from Alfa Aesar (Heysham, England).

Ea1501 was obtained from the International Collection of Microorganisms for Plants (Landcare Research, New Zealand). E. *coli* DH5α, *P. aeruginosa* and *S. aureus* were obtained from the microbial culture collection of School of Biological Sciences, at the University of Auckland. Str4Ea and Psa16027 were gifted by Dr Vanneste, at the New Zealand Institute for Plant & Food Research. The strains were stored in 50% glycerol at -20 °C and -80 °C. For routine use, bacteria were plated on nutrient agar plates containing Proteose Peptone #3 (0.5%), yeast extract (0.3%), NaCl (0.5%) and agar (2.5%), dissolved in 500 mL of sterilised Milli-Q water (Sartorius Arium, 18.2 Ω) and stored in a refrigerator. Single colonies were re-plated every two weeks. All media for bacterial growth and glassware were autoclaved at 120 °C for 1 hour using a Tomy SX 500E high-pressure steam steriliser.

4.11.2 Determination of minimal inhibitory concentration (MIC)

Luria broth (1.25%) was dissolved in 100 mL sterilised Milli-Q water and autoclaved at 120 °C for 1 hour, then cooled to room temperature. A single colony of the bacterial strain was transferred to 20 mL of the Luria broth and grown at either 28 °C (Ea1501, Str4Ea and Psa16027) or 37 °C (*E. coli*, *P. aeruginosa* and *S. aureus*), overnight. The optical density (OD) of the overnight culture was measured at 600 nm and adjusted to be 0.6 (OD_{600}: 0.6) by dilution with Luria broth. Peptides and the antibiotic controls were dissolved in Luria broth, and a dilution series was made. The assay was performed by adding 50 µL each of the peptide solutions, at various concentrations, and the diluted bacterial culture, to the different wells of a 96-well microtiter plate. Three replicates of each peptide concentration were tested against each bacterial strain. Optical density (OD_{600}) measurements for the MIC assay were conducted using an EnSpire Multimode plate reader at the Faculty of Medical and Health Sciences, University of Auckland.

4.11.2.1 MIC under high salt concentration (120 mM of NaCl and 2 mM $MgCl_2$)

High salt assay was carried out by dissolving Luria broth (1.5%) supplemented with 120 mM NaCl (0.7 g) and 2 mM $MgCl_2$ (0.02 g) in 100 mL and autoclaved at 120 °C for 1 hour then cooled to room temperature. The MIC activity of the peptides, under high salt concentrations was carried out as described in the section 4.11.2.

4.11.3 Time-kill assay

An overnight bacterial culture was diluted to mid-logarithmic phase with Luria broth to yield 10^5 to 10^8 CFU/mL. The diluted bacterial solution (100 µL) was added to 10 mL of the antibacterial peptide solution sterile Luria broth at 1 x, 2 x, 4 x and 20 x MIC. The solutions were incubated at either 28 °C (Ea1501 and Psa16027) or 37 °C (*E. coli*, *P.*

aeruginosa and *S. aureus*), with shaking (100 rpm). 100 µL of the solution was pipetted onto Luria broth agar plates at 0, 0.5, 1, 3, 6, 9, and 24 hours, with appropriate serial dilutions in 0.9% sterilised saline, to result in approximately 20 to 300 colonies. After 24 hours of incubation, the surviving colonies were counted. The experiment was done in duplicate.

4.11.4 Inhibition of bacterial biofilm

4.11.4.1 Inhibition of Psa16027 biofilm formation - Semi-quantitative estimation and visualisation of crystal violet stained biofilms

For semi-quantitative estimation, biofilms of Psa16027 were prepared in 96 well plates, using an overnight culture of Psa16027 (OD_{600}: 0.3) grown at 28 °C in Luria broth medium, with a sufficient number of GZ3.27 test samples, positive and negative controls. The assay was performed by adding 50 µL of GZ3.27 solution, in sterile Luria broth at various concentrations (1 to 100 µM), and 50 µL of the diluted bacterial culture to the different wells of the 96-well Microtiter plate. The positive control comprised of 50 µL of the diluted bacterial culture and 50 µL of Luria broth medium. The negative control comprised of sterile Luria broth medium (100 µL). Three replicates of each peptide concentration were tested. The plates were incubated for 48 hours at 28 °C, at 50 rpm. At appropriate time intervals, the supernatant from each well was discarded and the wells stained with 100 µL of 1% crystal violet for 5 minutes, following standard protocols.[349] The stain was removed carefully and the wells washed twice with 100 µL Milli-Q water. Crystal violet-stained biofilms at the bottom of each well were solubilised with 96% ethanol and the absorbance of this ethanol solution measured at 560 nm, for a semi-quantitative estimation of biofilm biomass.

For imaging purposes, biofilms of Psa16027 were prepared in 12 well plates, as described above. GZ3.27 (50 μL) at 1, 5 and 50 μM concentrations were incubated with the Psa16027 culture (50 μL) and Luria broth medium (900 μL) for 48 hours, at which time, the supernatant from each well was removed, the wells gently washed twice with Milli-Q water and stained with 1% crystal violet for five minutes. The dye was removed by decantation and the wells were gently rinsed twice with 1 mL water. The stained biofilms in individual wells were viewed at 400 x magnification, under the microscope (Nikon Eclipse TE2000) at the Faculty of Medical and Health Sciences, University of Auckland,

4.11.4.2 Effect of GZ3.27 on Psa16027 preformed biofilms

The ability of GZ3.27 to disperse preformed biofilms of Psa16027 was also investigated by crystal violet staining, in 96 well Microtiter plates. After an initial 48 hour of biofilm formation as described above, in the absence of test peptides, the supernatant from each well was carefully removed, without damaging the preformed biofilm architecture. Each well was washed twice gently with sterile water (1 mL) and supplemented with 100 μL of fresh Luria broth alone (control wells) or 100 μL of 1, 5 and 50 μM concentrations of GZ3.27 in sterile Luria broth medium, and incubated for a further 24 hours at 28 °C. These treated pre-formed biofilms were then subjected to crystal violet staining, imaging and semi-quantitative estimation of the biofilm mass, as described above.

4.11.4.3 Inhibition of *P. aeruginosa* and *S. aureus* biofilm formation- Live/Dead staining

Biofilms of *P. aeruginosa* and *S. aureus* were prepared in 12 well plates, as described above, using a sufficient number of positive and negative controls, and GZ3.27 at various concentrations. To provide a surface for biofilm formation, which was amenable for microscopy at higher magnification, circular coverslips (15 mm diameter, 1 mm thick)

were inserted into each well at the start of bacterial inoculation. GZ3.27 (50 µL) at 5, 10, 25, 50 and 100 µM concentrations were incubated with the diluted bacterial cultures (50 µL) and Luria broth medium (900 µL) for 48 hours. The coverslips were removed from the wells, rinsed with sterile water to remove any planktonic cells and dried at 50 °C for 20 minutes. A solution of Live/Dead bacterial stain was used to stain the biofilm. Live/Dead stain was prepared (3:1000 dilution) using 1.5 µL each of SYTO 9 (green-fluorescent nucleic acid stain) and propidium iodide (red-fluorescent nucleic acid stain) solution in 997 µL of sterile water. 60 µL of this solution was dispensed onto each of the coverslips and incubated, in the dark for 25 minutes, at room temperature. After this, the excess stain was washed off with sterile water and the coverslips were air-dried. The dried coverslips were inverted onto a drop of mounting oil (supplied with Live/Dead kit), on a fresh glass slide for examination of biofilms at 1000 x magnification, using a Nikon Eclipse E600 microscope. The stained biofilms were viewed separately using FITC 2 and Texas Red filters and the images were captured using an in-built digital sight DS-U1 camera. The images were merged using the in-built ACT-2U software.

4.11.4.4 Eradication of *P. aeruginosa* and *S. aureus* preformed biofilms

The ability of GZ3.27 to disperse pre-formed biofilms of *P. aeruginosa* and *S. aureus* was also investigated using a Live/Dead staining experiment. After an initial 48 hour of biofilm formation as described above, but without the addition of the test peptides to the wells, the supernatant from each well was carefully removed without damaging the preformed biofilm architecture. Each well was washed twice with sterilised water (1 mL), and supplemented with 100 µL of GZ3.27 at 10, 50 and 100 µM concentrations and sterile Luria broth medium, and incubated for a further 24 hours at 37 °C. The preformed biofilm was subjected to Live/Dead staining as described above.

4.11.5 Alanine-scanned library using D-series lanterns

D-series trityl alcohol SynPhase lanterns (5 μmol) were treated with 5 mL of 10% acetyl chloride in dry DCM, at room temperature for 3 hours, to produce trityl chloride lanterns.[322] The excess solution was decanted and the lanterns washed with DCM (3 x, 3 min), and used immediately in the next reaction.

A mixture of 120 mM Fmoc-amino acid and 240 mM DIPEA (0.21 mL), in DMF (15 mL), was added to the lanterns and was allowed to react for 90 minutes. Lanterns sharing common amino acids at the same position were kept in the same reaction vessel, whereas the lanterns in which amino acids at specific positions were replaced with alanine were suspended in separate reaction vessels. All lanterns were then pooled together and washed with DMF and methanol. The Fmoc group from the lanterns was removed by submerging the lanterns in 20% piperidine in DMF for 30 minutes, followed by washing with DMF and methanol. The lanterns were sorted as required, and the subsequent Fmoc amino acid (120 mM) coupled using 240 mM of TBTU and DIPEA for 90 minutes.[350] Fmoc deprotection, coupling and washing steps were repeated until the desired sequences were obtained. On completion of syntheses, the lanterns were washed with DCM thoroughly, and dried under vacuum, overnight. The lanterns were separated into eight reaction vessels, and the peptides cleaved off the lanterns with a TFA cocktail mixture (TFA-TIS-H_2O - 95:2.5:2.5; 10 mL) for 3 hours. The TFA mixtures were then evaporated separately under a stream of N_2, and the peptides precipitated using excess cold diethyl ether. The peptides were centrifuged thrice, resulting in white pellets, which were dissolved in water and lyophilised, to recover the crude peptides as white fluffy solids. The crude peptide structures were confirmed by ESI-MS, and were used for biological testing without any further purification.

4.11.6 Haemolytic Assay[351]

The haemolytic activity of the lipopeptides was tested by determining the extent of haemoglobin release from erythrocyte suspensions of fresh mouse blood cells (2% v/v) obtained at the Vernon Jensen Unit, Faculty of Medical and Health Sciences, University of Auckland. Freshly collected mouse blood cells were centrifuged at 1000 x for 5 minutes to remove the buffy coat. The blood cells were washed thrice in Tris buffer (10 mM Tris, 150 mM NaCl, pH 7.4), and re-suspended in 2% (v/v) Tris buffer. The peptides were dissolved in Tris buffer at concentrations ranging from 1 mM to 1 µM. The peptide solution (100 µL) was added to the re-suspended blood cells (100 µL) in 96 well plates, and the plates incubated for 1 hour, at 37 °C without agitation. The buffer solution and 0.1% Triton X-100 were used as the negative and positive controls respectively. All of the samples and controls were tested in triplicate. The plates were centrifuged at 3500 x g for 10 min. The supernatant from each sample (100 µL) was transferred to new 96 well plates, and the absorbance at 540 nm was measured. Percentage haemolysis, at each peptide concentration, was calculated using the following equation 4.1,

$$\%\text{haemolysis} = (A_{exp} - A_{Tris}) / (A_{100\%} - A_{Tris}) \times 100 \quad (4.1)$$

Where, A_{exp} is the experimental absorbance at 540 nm measurement, A_{Tris} is the absorbance of the negative control, where only Tris buffer was added to mouse blood cells and $A_{100\%,}$ is the absorbance of the positive control, where 0.1% Triton X-100 was used to cause lysis of 100% mouse blood cells present.

4.11.7 Colorimetric assay[326]

Dimyristoylphosphatidylcholine (DMPC) and 10, 12-tricosadiynoic acid (TRCDA) were dissolved, in a 4:6 ratio in DCM, and dried together under nitrogen, to yield a thin white film. This film was dissolved in Milli-Q water, to obtain a total lipid concentration of 2

mM. This solution was then probe sonicated for 10 minutes, at 80-90 °C, and cooled to room temperature before being kept overnight at 4 °C. Prior to polymerisation, the vesicles were warmed to room temperature and then polymerised by irradiation with UV light (254 nm), until a deep blue colour was formed. The assay was performed in 96-well plates, by the immediate addition of 150 µL of 2 mM DMPC-TRCDA vesicles and the compounds were dissolved to 0.2 mM in 4 mM tris buffer (pH 8.5).

4.11.8 Scanning electron microscopy

E. coli, *P. aeruginosa*, *S. aureus* and Psa16027 were grown to an OD_{600}: 0.3 in Luria broth on glass slides (10 mm) for 24 hours. Excess bacteria were removed by washing with 10 mM sodium phosphate buffer (pH 7.4). The glass slides were treated with the peptide dissolved in Luria broth, at twice the upper-limit of its MIC, for 20 minutes. The excess peptide was removed by washing with 10 mM PBS. The slides were fixed with 4% glutaraldehyde in 10 mM phosphate buffer (pH 7.4), for 1 hour and then washed with 10 mM sodium phosphate buffer and dehydrated with a graded ethanol series (25-100%), prior to drying at 60 °C for 10 minutes. The dried slides were sputter- coated with platinum, for 2 minutes, at 20 mA, before viewing under high vacuum, using an FEI Quanta 200 F ESEM microscope, at 10 kV at the Faculty of Engineering, University of Auckland.

4.11.9 N-phenylnaphthylamine (NPN) uptake assay[333,352-353]

A *P. aeruginosa* strain was grown overnight in Luria broth at 37 °C. The overnight culture was incubated for another 3-6 hours in fresh Luria broth to obtain an OD_{600}: 0.5. The bacterial cells were centrifuged at 4600 rpm for 10 min and washed thrice with 10 mM phosphate buffer (pH 7.0), before re-suspension in the same buffer to obtain an OD_{600} of 0.5. Then, 2.94 mL of the bacterial suspension was added to various peptide

concentrations (30 μL, 0.5-100 μM) in the absence or presence of 10 mM $MgCl_2$ (60 μL), followed by the addition of 60 μL of 0.5 mM N-phenylnaphthylamine, to attain a final NPN concentration of 10 μM. Fluorescence measurements of the samples at an excitation wavelength of 350 nm, emission wavelength of 420 nm and slit width of 5.0 nm, were acquired using a SpectraMax M2 fluorescence spectrometer at the Faculty of Medical and Health Sciences, University of Auckland. Fluorescence measurements were taken in triplicate, and averaged.

4.11.10 Propidium iodide (PI) uptake assay[352-353]

P. aeruginosa and *S. aureus* were grown overnight in Luria broth at 37 °C. The cells were then re-incubated in fresh Luria broth for 3 hours to obtain an OD_{600}: 0.35. The bacterial cells were harvested by centrifugation at 4600 rpm for 10 min and washed with 10 mM phosphate buffer (pH 7) thrice. They were then re-suspended in phosphate buffer to a final concentration of 1 x 10^8 CFU/mL. 50 μL of the cell suspension was incubated with 50 μL of peptide solutions, of various concentrations (0.5-100 μM) in phosphate buffer, for 60 min at 37 °C. 5 μL of PI at 1 μM concentration was added to the cell suspension and the fluorescence was measured, using a multi-mode microplate reader, at excitation and emission wavelengths of 520 nm and 620 nm respectively.

4.11.11 Circular dichroism

Circular dichroism spectra were recorded on an Applied Photophysics ð-Star 180 spectrometer at the Faculty of Biological Sciences, the University of Auckland, at 20 °C in a 0.1 cm path-length cuvette, from 190-250 nm at 0.5 nm intervals with a 5 s response time. Six scans per sample were averaged. Data were expressed as mean residue ellipticities [θ] in degrees × cm^2 $dmol^{-1}$. Peptide stock solutions were prepared in 10 mM

sodium phosphate buffer (pH 7.0), methanol, 2,2,2 trifluoroethanol (TFE) or 2 mM DMPC-TRCDA vesicles and the final peptide concentration was made up to 500 μM.

4.11.12 Nuclear magnetic resonance spectroscopy

All 1D and 2D NMR experiments on GZ3.27 were carried out on either a Bruker 800 MHz or 700 MHz spectrometer, equipped with a cryoprobe, at the NMR research centre, Indian Institute of Science. For GZ3.27, a series of 1D spectra were recorded at five different temperatures, between 278 and 318 K at 10 K intervals. These spectra were used to calculate amide-proton temperature coefficients (Δδ/T). At 278 K, in addition to good dispersion, there was also a sharpening of side-chain amide resonances, due to slow exchange rates. Hence, all 2D spectra, for further resonance assignments and analysis, were recorded at 278 K. The spectral width was set to 9600 Hz (12 ppm). 2k time domain points were used in direct dimension (t2) with 400 points in the indirect dimension (t1). The data were zero filled into 1k points in the t1 dimension, to improve the resolution. TOCSY and ROESY mixing times were 100 and 250 ms respectively. All data processing was done, using TopSpin (version 2.1, Bruker Corp., 2015). Shifted sine bell window functions were used for processing 2D data.

4.11.13 Molecular modelling

A model of the peptide was generated using Accelrys Discovery Studio version 3.5 (*Dassault Systèmes, 2015)*.[348]A restrained energy minimisation was carried out, in vacuum, using NMR-derived distances and torsion constraints, as described in detail below. The linear model peptide was built using HyperChem (HyperCube Inc., 2007) or ChemDraw (Cambridge Scientific Computing Inc.), and converted to *.mol or *.pdb files. From NMR data, distances and dihedral constraints were obtained. The distance constraints were from NOE data, which were broadly classified into three categories as

strong, medium, and weak, and the corresponding upper limit set was 2.5, 3.5, and 5.0 Å, respectively, while the lower limit in all cases were fixed at 1.9 Å. A strong NOE across the Dab[6] $C^{\gamma}H_2$ geminal protons, resonating at 2.63 and 2.48 ppm, was considered the reference. A loose ϕ dihedral constraint of 0° to −180° was used for all L-residues, as their $^{3}J_{NHC\alpha H}$ values were around 7 Hz. The NMR-derived distances and dihedral constraints were then applied. The structure was refined by energy minimisation, using CHARMm in Discovery Studio 3.5.[354] The Accelrys CHARMm force field was used throughout the simulation. Approximately 2000 cycles of steepest descent gradient were applied during minimisation, to clean the geometry of the peptide, followed by 500−1000 steps of conjugate gradient. The refined model was validated with a Ramachandran plot.

Chapter 5

Surface immobilisation studies of GZ3.27

This page has been intentionally left blank

Chapter 5: Surface immobilisation studies of GZ3.27

This chapter describes the immobilisation of the most potent antibacterial lipopeptide GZ3.27, identified from the studies so far, onto glass, silicon and titanium surfaces. Both silicon and titanium are extensively used in medical implants and the coating of antimicrobial compounds on to these surfaces could prevent bacterial colonisation. GZ3.27 was modified by incorporating a Cys residue into the peptide sequence, to facilitate the immobilisation of the peptide onto the surfaces via selective covalent interaction. The Cys modified lipopeptide was attached to the surfaces via the heterobifunctionalised PEG linker. The success of each of the steps in the peptide immobilisation process was verified by water-contact angle measurements, ellipsometry and X-Ray photoelectron spectroscopy. Finally, the immobilised surfaces were evaluated for antibacterial activity using Live/Dead stained biofilm assay of *P. aeruginosa* and by studying the morphology of *P. aeruginosa* in the absence and presence of the immobilised peptide, using scanning electron microscopy.

5.1. Immobilisation of antimicrobial compounds to surfaces

Coating the surfaces of medical implants with antimicrobial compounds, to prevent bacterial colonisation, is an attractive alternative to the expensive surgical procedures currently being used to remove colonised bacteria from them. Figure 5.1 illustrates four possible strategies for designing antimicrobial surfaces.

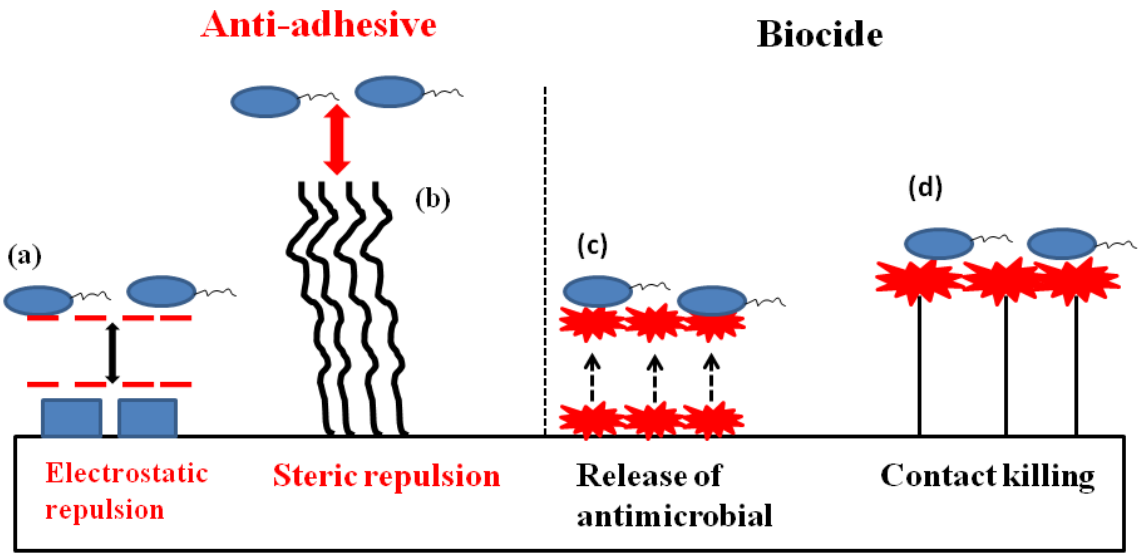

Figure 5.1 Designing antibacterial surfaces using anti-adhesive and biocidal methodologies. Creating an anti-adhesive surface by coating surfaces with **(a)** negatively charged biomaterials such as albumin and heparin or **(b)** sterically hindered polymers such as PEG. Creating an antimicrobial surface by **(c)** slowly releasing antibiotics and quaternary salts or **(d)** conjugation of these antibiotics and salts to a linker attached to the surface, to initiate bacterial killing upon contact with the biocide. Adopted from Siedenbiedel *et al.*[355]

As evident from Figure 5.1, antimicrobial substances can be coated to prevent the initial attachment of bacteria (anti-adhesive) or antibacterial activity can be initiated once the bacteria have colonised the surfaces (biocidal). These biocidal coatings can be slow-releasing antimicrobial compounds from the surface that target the planktonic bacteria, or surface attachments that initiate antibacterial activity as soon as bacteria make contact with the coated surface.[19,355-356]

Anti-adhesive or non-fouling surfaces can be created, either by generating extremely hydrophobic surfaces, or by coating the surfaces with negatively charged biomaterials such as albumin and heparin, causing an electrostatic repulsion between the negatively charged surface and the anionic bacteria.[356-357] Another popular approach to creating non-fouling surfaces involves coating them with polyethylene glycol (PEG) (see section 5.2.1.3), to prevent the attachment of the conditioning film of proteins that can facilitate the bacterial attachment to the implant surface, as well as prevent bacteria from adhering onto the surface directly. The anti-adhesive property of PEG can be attributed to its high mobility and steric hindrance.[356,358] These anti-adhesive properties of PEG ensure that bacteria are kept at a distance from the implant surface leading to a lower van der Waals attraction between the two, eventually causing lower bacterial adsorption onto the implant surface.[19] PEG linkers are also safe for use in medical implants since they produce low host immune responses.[358]

Antibiotics such as cefazolin,[359] teicoplanin[360] and vancomycin[361] have been successfully coated onto catheters, either with a slow-release strategy or as a covalent attachment. The slow-release strategy, however, only has a short-term antibacterial effect, and the leaching of antibiotics to the surrounding tissues can cause unwanted side effects. This can be minimised by the covalent attachment of antibiotics to the surface, which also prolongs antibacterial activity.[19,356] However, antibiotic-immobilised surfaces are still ineffective against antibiotic-resistant pathogens. It is also necessary to sterilise implants before implantation, to reduce the bacterial contamination; however, surface immobilised antibiotics are unstable at the high temperatures required for the sterilisation process, leading to a loss in their antibacterial activity.[362]

Silver,[363] salicylic acid,[364] quaternary ammonium compounds,[365] and chlorhexidine[366] have also been immobilised onto implant surfaces. However, evidence suggests that silver and chlorhexidine coated surfaces did not offer any additional advantages compared to the

uncoated surfaces.[367] Additionally, silver and ammonium compounds can be cytotoxic while chlorhexidine, in some cases, led to anaphylaxis.[368]

5.2 Immobilisation of antimicrobial peptides onto surfaces

Surface attachment of AMPs can help to overcome some of the inherent limitations of AMPs themselves, such as short serum half-life and high haemolytic, and can facilitate a higher, localised concentration at the source of infection.[19,369] Table 5.1 provides a comprehensive summary of antimicrobial peptides that have been immobilised on to different surfaces, in the past.

Table 5.1 Immobilisation of AMPs onto various surfaces.

Peptide	Surface	Immobilisation Technique	Tested pathogen(s)	Ref
Melimine	Glass	Covalent linkage via azide linker (4-azidobenzoic acid and 4-fluoro-3-nitrophenyl azide).	*P. aeruginosa, S. aureus*	362
	Contact lenses	Physical (evaporation of a saturated solution) and covalent linkage using EDC as the coupling agent.	*P. aeruginosa, S. aureus*	370
LL37	Titanium	Covalent linkage, either using bifunctional PEG linkers where cysteine-containing peptides are attached to the maleimide group, or direct linkage of the peptide to epoxy-coated surfaces.	*E. coli*	371
	Magnetic nickel nanoparticles	Covalent linkage between coated polyacrylic acid and the peptide.	*E. coli*	372
Magainin I	Titanium	Covalent linkage, using EDC as the coupling agent.	*L. ivanovii*	373
	Silicon dioxide beads	Covalent linkage, where cysteine modified magainin was grafted onto the hydroxyl group of the methacrylate polymer.	*L. ivanovii*	374

	Silicon wafers	Same as silicon beads.	*L. ivanovii*, *B. cereus*, *E. coli*	375-376
	Glass	Side-chain amines of magainin I were selectively coupled to immobilised succinimide ester.	*E. coli*, *S. typhimurium*	377
	Gold surface	Covalent linkage, where magainin I was grown on a self-assembling monolayer of mercaptoundecanoic acid and mercaptohexanol.	*L. ivanovii*, *E. faecalis*, *S. aureus*	378
Magainin 2 and analogues	Polyamide resin (pepsynK)	C-terminal end of the peptide was selectively immobilised onto the pepsynK resin using TBTU/DIPEA as the coupling agent.	*E. coli*, *S. aureus*, *K. pneumoniae*, *B. subtilis*, *C. albicans*, *P. aeruginosa*, *A. niger*	379
β-sheet peptide	PEG-PS resin	Chemical immobilisation using standard Fmoc-peptide chemistry.	*S. aureus*, *M. luteus*, *P. aeruginosa*, *E. coli*	380
Melittin	Tentagel S-NH_2 resin beads	Covalent linkage, where aminooxyacetic acid modified terminal end was coupled via oxime forming ligation.	*E. coli*, *B. subtilis*	381
Buforin 2	Tentagel S- NH_2 resin beads	Covalent linkage via oxime formed ligation.	*E. coli*, *B. subtilis*	381

Ponericin G1	Silicon	Physical adsorption using layer-by-layer methodology. Ponericin G1 was sandwiched between a poly anionic solution of poly (β-amino ester), chondroitin sulphate, alginic acid and dextran sulphate.	*S. aureus*	[382]
Cathelicidin library (Tet-20 & Tet-213)	Titanium and quartz slides	Covalent interaction using bifunctionalised PEG linker selectively reacting with the cysteine-modified cathelicidin.	*P. aeruginosa, S. aureus*	[383-384]
CWR11	Polydimethylsiloxane	Same immobilisation protocol as cathelicidin.	*P. aeruginosa, S. aureus, E. coli*	[352]
Bovine lactoferrin (L5)	Silicon wafers	Physical adsorption where saturated solution of peptide was deposited onto poly-lysine coated PEG surface.	*S. epidermidis*	[385]
Nisin	Stainless steel	Physical adsorption using layer-by-layer methodology, where negatively charged mixture of heparin and mucins is sandwiched between the peptide.	*E. coli, B. subtilis*	[386]
Tritrpticin	Stainless steel	Same protocol as nisin.	*E. coli, B. subtilis*	[386]
	Tentagel S-NH_2 resin beads	Covalent linkage via oxime formed ligation.	*E. coli, B. subtilis*	[381]

Lipopeptide 4K-C16	Stainless steel	Same procedure as nisin.	*E. coli, B. subtilis*	386
Polymyxins B and E	Glass	Side chain amines of PMB were coupled to immobilised succinimide ester.	*E. coli, S. typhimurium*	377
		Side chains of PMB coupled to immobilised epoxide ring.	*E. coli*	387
	Indium tin oxide coated glass	Covalent linkage of peptide to surface coated epoxide rings.	*E. coli*	388
Cecropin A	Glass	Covalent linkage using succinimide ester.	*E. coli, S. typhimurium*	377
Parasin	Glass	Covalent linkage using succinimide ester.	*E. coli, S. typhimurium*	377
Defensin	Poly electrolyte films	Physical adsorption using layer-by-layer method.	*M. luteus, E. coli*	388
Short lipopeptides	Glass slides	Covalent linkage via dopamine coated surfaces.	*E. coli, S. aureus*	389
	Polyolefin slides	Same linkage as the glass slides.	*E. coli, S. aureus*	389
Chrysophsin-I	Silicon dioxide crystals	Covalent linkage, where Cys-modified peptide was immobilised to PEG linker and physical adsorption where AMP was deposited for 30 min, in PBS buffer.	*E. coli*	390

Lys and Leu rich AMP (6K8L)	Surface modified polystyrene PEG-PS	Chemical linkage using SPPS.	*E. coli, L. monocytogenes, S. aureus, P. fluorescens, K. marxianus*	[391]
Lasioglossin-III	Silicon wafer	Covalent linkage using bifunctionalised PEG linker reacting with cysteine modified peptide	*E. coli*	[353]

5.2.1 Factors influencing the activity of AMP-immobilised surfaces:

In order to immobilise AMPs onto solid surfaces, factors such as the type of peptide immobilisation (either physical or covalent), peptide orientation after immobilisation and influence of the spacer need to be considered and will be summarised in the following sections.[19,392]

5.2.1.1 Types of peptide immobilisation

As evident from Table 5.1, AMPs can be immobilised onto surfaces either by physical adsorption or by covalent interactions. The layer–by-layer method is the most common physical adsorption technique used to immobilise AMPs onto solid surfaces. In this method, AMPs are embedded between two polyanionic layers.[392] The amount of the peptide immobilised onto the surface can be controlled. However, some of the embedded AMP layers may not be in contact with the bacteria and, as a result, this may require the peptide to diffuse out to initiate the bacterial killing. At the same time bound bacteria on the upper layers of the AMP may act as a barrier and prevent the diffusion of peptides which may be trapped within the multi-layer embedded structure.[392] Also haemolytic and cytotoxic peptides such as melittin, pexiganan and LL-37 may not be suitable for the layer-by-layer methodology, as leaching of these peptides from the immobilised surface onto the surrounding tissues can cause harm to the host tissues.[356] Finally, the long-term stability of the layer-by-layer methodology has not been well-documented.[356]

As evident from Table 5.1, most of the AMPs reported in the literature are immobilised onto surfaces using covalent interactions. Covalent immobilisation of AMPs can prevent peptide leaching and enhance the long-term stability of the immobilisation due to the strong covalent interactions of the reactive group(s) on AMPs with the surface.[19,356] Willcox *et al.* compared the efficiency of physical and covalent immobilisation of the AMP melimine onto

commercial contact lenses, and showed that covalent immobilisation resulted in 70% greater reduction in bacterial colonisation than physical adsorption.[370] The authors suggested that the diminished antibacterial activity of the physically adsorbed AMP could possibly be attributed to peptide aggregation, uneven distribution of the peptide on the surface or the leaching of the peptides from the surface. Figure 5.2 represents the common covalent immobilisation strategies used in the literature to couple AMPs onto surfaces.[19,392-393]

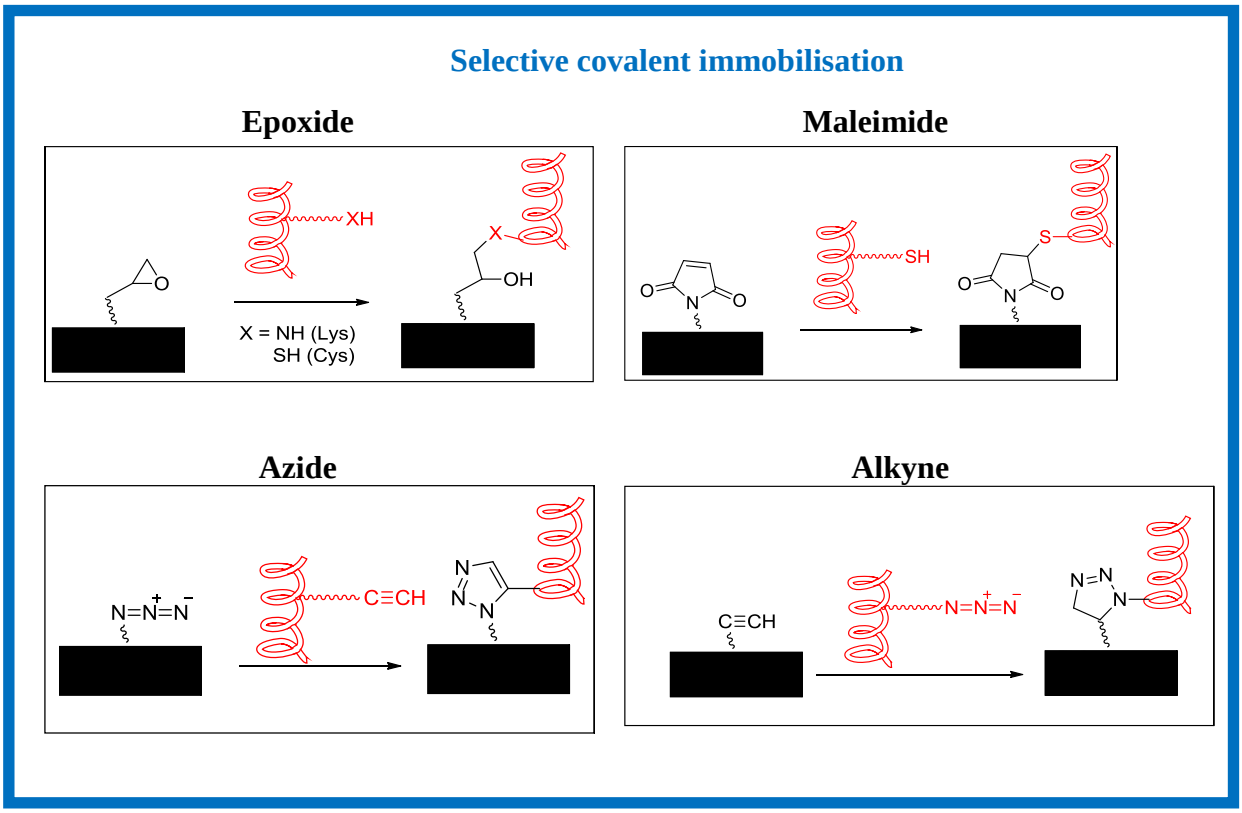

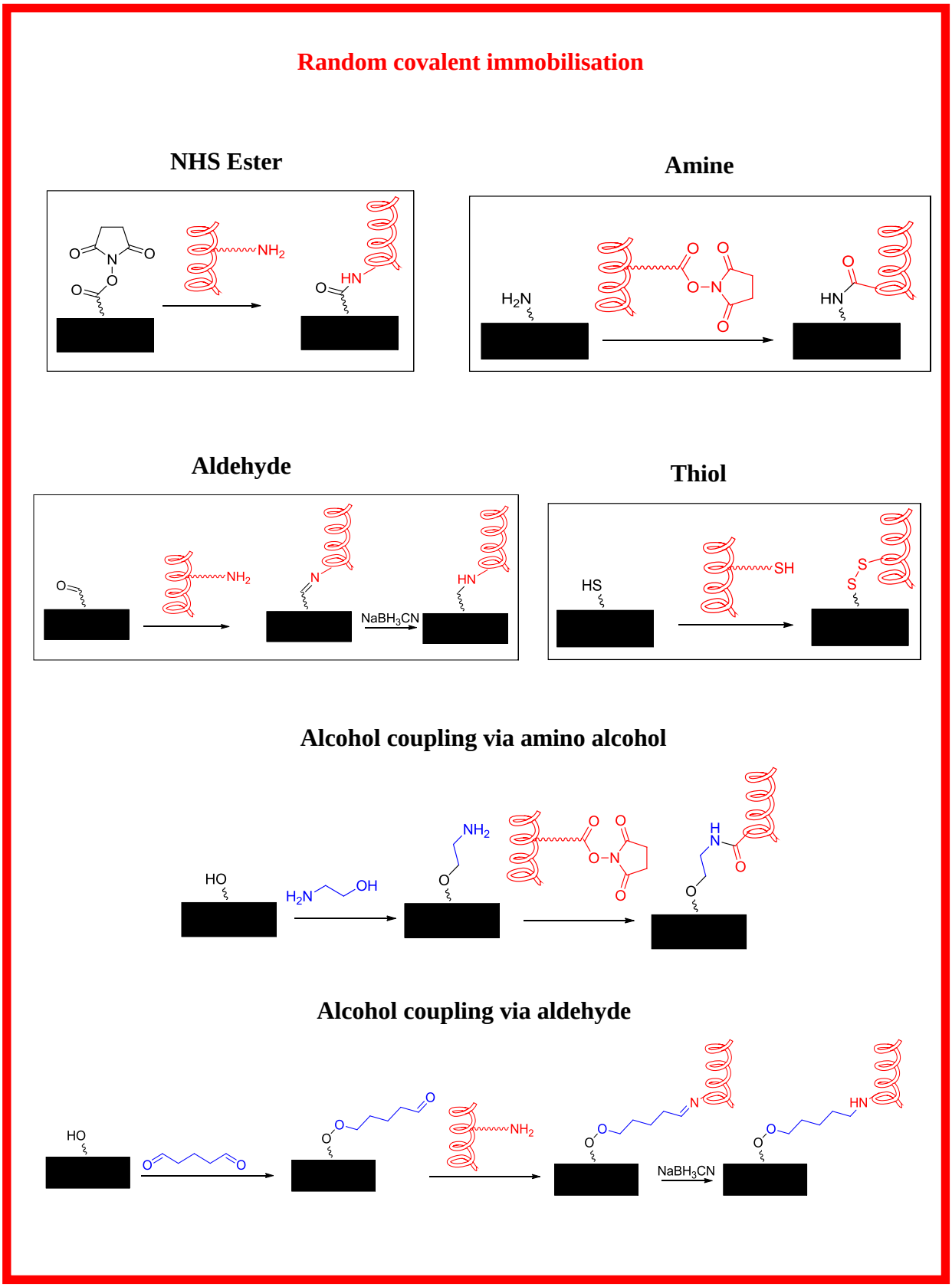

Figure 5.2 Common covalent coupling reactions of AMPs onto solid surfaces. Covalent immobilisation can be categorised as selective (blue bordered box) or random (red bordered box).

5.2.1.2 Peptide orientation after surface immobilisation

Peptide orientation is an important parameter that needs to be considered for efficient AMP immobilisation onto surfaces.[19,392] Peptides can be randomly oriented onto the surface via physical adsorption or via random covalent linkage, as shown in the red box in Figure 5.2. Random covalent linkage involves the reaction of any or all of the amines or carboxylic acid reactive groups of the AMP, with the complementary reactive groups present on the surface. Controlled immobilisation of AMPs (blue box highlighted in Figure 5.2) involves the modification of the peptide, either by cysteine or azide reactive groups reacting with the functionalised surface, in a chemo-selective manner, by sulfhydryl linkage or by click chemistry.[392-393] However, caution must be taken during peptide modification, since it could possibly lead to reduced antibacterial activity.

Native peptide conformations are most likely to be preserved during chemo-selective immobilisation, unlike with random covalent immobilisation, where cationic acids, which are crucial to antibacterial activity, may be immobilised onto the surface.[19,392] In addition, membrane-lytic AMPs, which act either via carpet, toroidal pore or barrel-stave models, require peptides to orient themselves in a favourable position before inserting themselves into the bacterial membrane.[392]

5.2.1.3 Influence of a spacer

The antibacterial activity of immobilised AMPs is heavily influenced by the presence of a spacer, which acts as a bridge between the peptide sequence and the surface.[19,392] It has been reported that AMPs such as nisin, LL-37 and chrysophsin-I lost antibacterial activity upon surface conjugation without a spacer.[371,390] The flexibility of the spacer allows the immobilised AMP to maintain a similar level of mobility as the native peptide in solution, which in turn helps to preserve its original mechanism of action.[19,392]

Even though literature agrees on the necessity of a spacer to retain antimicrobial activity in the immobilised state, reports on the effect of the spacer length on the antibacterial activity is contradictory. Bagheri *et al*. have reported a four-fold decrease in the antibacterial activity of the immobilised KLKL AMP against *E. coli* and *B. subtilis*, with a decrease in the ethylene oxide units in the PEG linker from 10 repeats to 5 repeats.[394] The superior antibacterial activity of KLKL in the presence of a longer PEG linker could be attributed to enhanced peptide insertion into bacterial cell.[394] Haynie *et al*. suggested that long spacer is not a pre-requisite for antibacterial activity, as magainin immobilised using two to six carbon chains as spacers showed antibacterial activity against several bacterial pathogens.[379] Since the length of the spacer used would not be long enough (2 to 6 carbons long) to allow the immobilised AMP to penetrate deep into the bacterial membrane, Haynie *et al*. have suggested that the observed antibacterial activity is probably due to the displacement of divalent cations from the bacterial outer membrane by the AMP.[379] This will result in an electrochemical imbalance on the membrane surface and the cytoplasmic membrane by altering the Donnan potential and would trigger fatal cellular events such as the activation of autolytic enzymes, eventually leading to cell death.[379,395]

Based on the above observations the battacin analogue GZ3.27 was immobilised onto solid surfaces following chemo-selective reaction in the presence of a flexible spacer molecule.

5.3 Immobilisation of battacin analogue, GZ3.27

Hilpert *et al*. have reported that the antibacterial activity of immobilised peptides is not influenced by the type of surface used for immobilisation.[395] Three different surfaces-glass, silicon and titanium were chosen to explore the surface immobilisation of the most potent lipopeptide GZ3.27. Glass was used initially, to standardise and optimise the immobilisation conditions. Both titanium and silicon coated materials are used in the medical implant industry extensively, due to their mechanical flexibility, excellent biocompatibility and long-term stability.[20,396]

Three versions of GZ3.27 were synthesised by incorporating a cysteine amino acid into the peptide sequence (Figure 5.3). The lipopeptide was immobilised onto the surface using a PEG spacer, following selective thiol chemistry, in order to preserve the structural features crucial for the observed antibacterial activity.[19,392]

GZ3.27	FA-D-Dab-Dab-Dab-Leu-D-Phe-Dab-Dab-Leu-NH_2
GZ3.163	FA-**Cys**-D-Dab-Dab-Dab-Leu-D-Phe-Dab-Dab-Leu-NH_2
GZ3.160	FA-D-Dab-Dab-Dab-Leu-D-Phe-Dab-Dab-Leu-**Cys**-NH_2
GZ3.155	FA-D-Dab-Dab**(Cys)**-Dab-Leu-D-Phe-Dab-Dab-Leu-NH_2

Figure 5.3 Amino acid sequences of cysteine-modified lipopeptides. FA denotes the fatty acid, 4-methyl-hexanoyl.

The strategic placement of cysteine in the lipopeptide sequence is important to maintain the observed antibacterial activity.[371] The lipopeptide GZ3.27 was modified by placing cysteine at the N-terminus (GZ3.163), C-terminus (GZ3.160) and branching onto the side chain amine of Dab^2 (GZ3.155). As reported in section 4.5.2.1, alanine scanning studies of GZ3.27 showed that Dab^2 was not crucial for the antimicrobial activity.[397] Therefore, it was presumed

that the conjugation of cysteine to this side chain would not lead to a dramatic reduction in antibacterial activity.

5.3.1 Antimicrobial activity and haemolytic activity of cysteine-modified lipopeptides, in solution

5.3.1.1 Antimicrobial activity

The MICs of cysteine-modified lipopeptides, against three Gram- negative pathogens (*E. coli*, Psa16027 and *P. aeruginosa*) and one Gram-positive pathogen (*S. aureus*), were evaluated following the Microtiter plate assay reported in Chapter 4 (see section 4.2). Results are shown in Table 5.2.

Table 5.2 Antibacterial activities of cysteine modified lipopeptides*

Sequence	**MIC (μM)**			
	E. coli	Psa16027	*P. aeruginosa*	*S. aureus*
GZ3.27	2.5-5	1-2.5	1-2.5	1-2.5
Ala^2	25-50	2.5-5	2.5-5	2.5-5
GZ3.163	10-15	1-2.5	1-2.5	2.5-5
GZ3.160	10-15	1-2.5	1-2.5	2.5-5
GZ3.155	25-50	2.5-5	1-2.5	5-10

* Average of three independent experiments, performed in triplicate

The N- and C-terminal cysteine-conjugated lipopeptides retained similar potency to GZ3.27, against Psa and *P. aeruginosa*, while a slight loss of activity (2-fold decrease) was observed against *S. aureus* and *E. coli*. Conjugation of cysteine to the side chain of Dab^2 (GZ3.155) led to a 10 x, 5 x and 2 x decrease in activity against *E. coli*, *S. aureus* and Psa respectively, while its potency against *P. aeruginosa* remained unaffected. GZ3.155 and the Ala^2 analogue

showed potency validating the results generated from the alanine scanning experiment mentioned in section 4.5.2.1.[397]

5.3.1.2 Haemolysis of mouse blood cells by cysteine-modified battacin analogues

The haemolytic assay of the cysteine-modified peptides was conducted using the same protocol discussed in section 4.6 (Table 5.3).

Table 5.3 Percentage of haemolysis of mouse blood cells at 100 μM of peptide concentration.

Peptide	**%haemolysis at 100 μM**
GZ3.27	1.8 ± 0.45
GZ3.163	4.3 ± 0.42
GZ3.160	2.8 ± 0.30
GZ3.155	2.2 ± 0.93

As evident from Table 5.3, the cysteine modified lipopeptides showed a negligible increase in haemolytic activity against mouse RBCs, compared to GZ3.27.

These results show that the addition of cysteine to the linear peptide sequence at the N- and C- termini, as well as the side chain amine of Dab^2, is not detrimental to the antibacterial and haemolytic activity. Although both N-terminally and C-terminally Cys-conjugated analogues showed similar potency against all of the tested pathogens, the lipopeptide GZ3.163 was chosen for immobilisation studies due to the better overall yield of this peptide (See Appendix A).

5.4 Surface immobilisation of GZ3.163

The overall strategy followed for the immobilisation of GZ3.163 on to glass, silicon and titanium surfaces is highlighted in scheme 5.1.

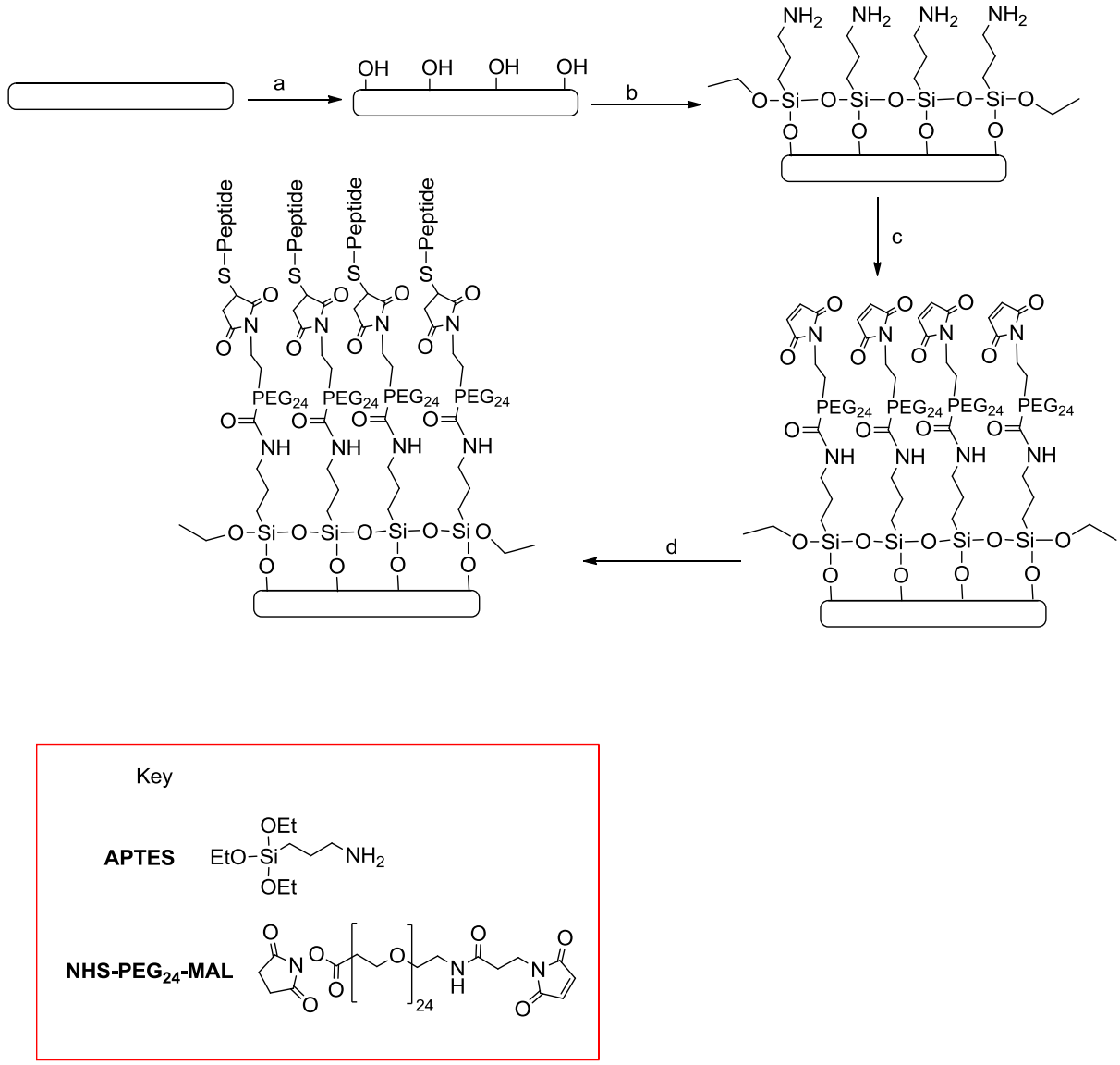

Scheme 5.1 Selective covalent immobilisation of lipopeptide GZ3.163 onto solid surfaces. Reagents and conditions: **(a)** piranha treatment: H_2O_2-H_2SO_4 (30:70 v/v), 30 min; **(b)** silanization: 1% APTES in toluene, 18 h; **(c)** attachment of the spacer: NHS-PEG_{24}-MAL (0.2 mg/mL) in DMF, 4 h; **(d)** peptide conjugation; GZ3.163 (1 mg/mL) in PBS buffer, pH 7, 16 h.

5.4.1 Piranha treatment of the surface

As evident from scheme 5.1, the first step involved the cleaning of the surfaces with a piranha solution, which consists of H_2O_2-conc.H_2SO_4 (30:70), for 30 min. Piranha treatment is expected to remove any organic residues and contaminants on the surface, and to expose the reactive hydroxyl groups of the oxide layer of the glass surface. Piranha-treated titanium slides have a rough, yellowish appearance compared to the untreated slides (Figure 5.4a and b top panels). The rough surface produced by the piranha solution (Figure 5.4b bottom panel) enhances the available surface area, subsequently allowing increased amounts of the lipopeptide to be attached to the surface.[398]

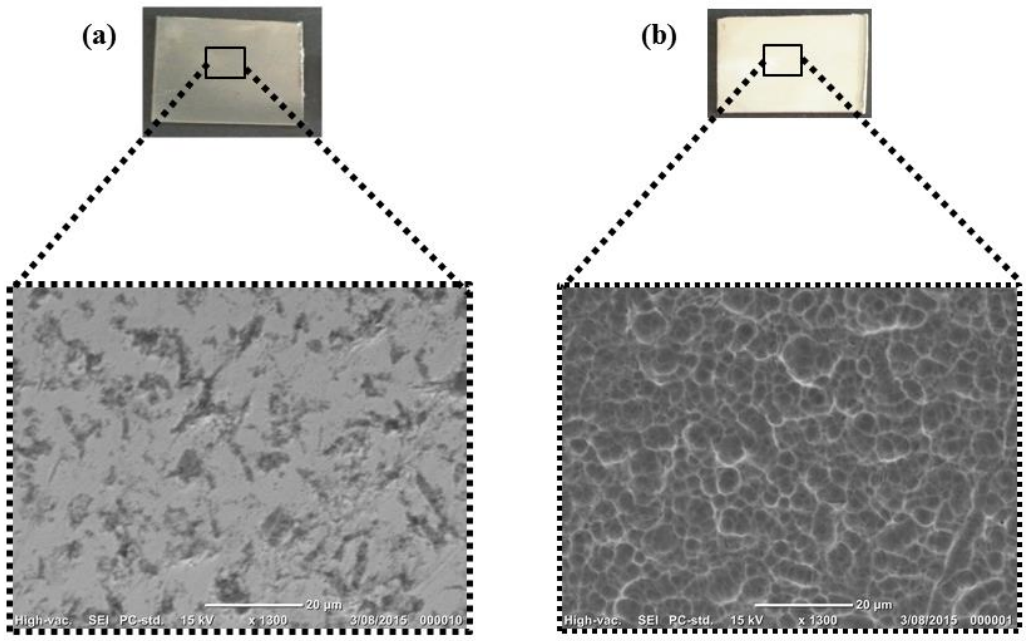

Figure 5.4 Photograph (top panel) of **(a)** untreated and **(b**) piranha-treated titanium plates. SEM image (bottom panel) of untreated **(a)** and **(b)** piranha-treated titanium plates.

5.4.2 Silanization of the surface with aminopropyltriethoxysilane (APTES)

Following piranha treatment, the solid surfaces were silanized by submerging the solid sample in a 1% solution of 3-aminopropyltriethoxysilane (APTES) in dry toluene, for 24 hours, to achieve a high surface concentration of APTES, as well as facilitating more stable

covalent interactions with the surface.[399] APTES is widely used both, in industry and in research settings, to promote the adhesion of polymers and proteins films onto glass and other surfaces, for cell growth and lab-on-a-chip applications.[398,400] In addition silanization with APTES has been shown to prevent the deposition of biological moieties such as proteins and peptides onto titanium implants which would otherwise facilitates bacterial colonisation.[398] APTES acts as an intermediate spacer by facilitating the attachment of organic substances to inorganic materials.[400] The silane group in APTES is generally unreactive with organic molecules but reactive towards inorganic substrates, while the terminal amines can react with organic substances, allowing their conjugation on the surface.[400] The mechanism of APTES surface attachment is highlighted in scheme 5.2.

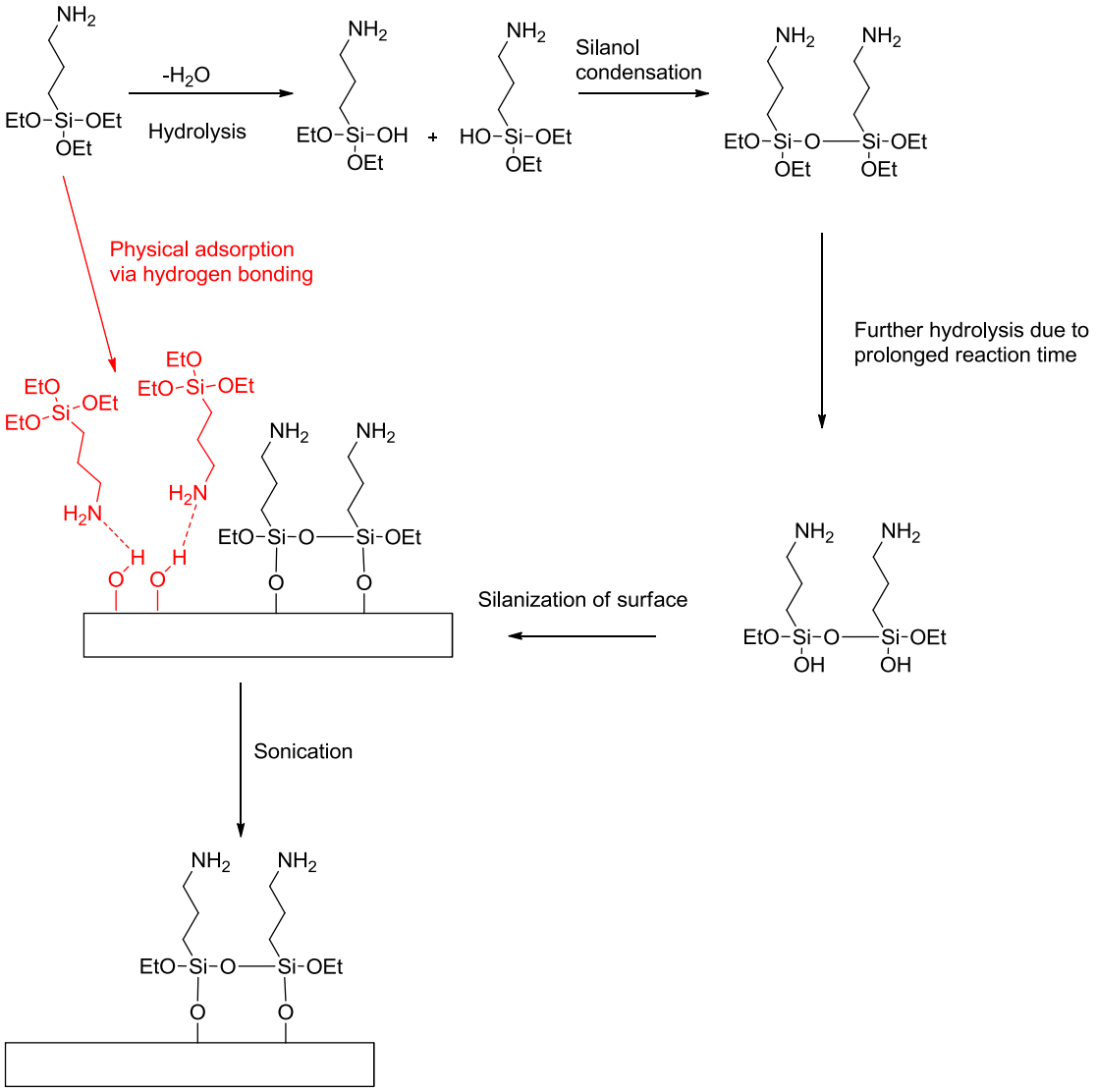

Scheme 5.2 Silanization with APTES onto a solid surface.

The initial reaction involves hydrolysis of the ethoxy groups in APTES, in presence of water, to form reactive silanols.[400-402] However, only a partial hydrolysis of the ethoxy chain is observed in the presence of dry toluene, and is facilitated by the presence of trace amounts of surface bound water particles as well as the base catalytic ability of the terminal amines.[400-402] Following hydrolysis, the reactive silanol groups of APTES undergo condensation, either with adjacent silanol groups by forming Si-O-Si bonds, or with surface-bound hydroxyl groups forming a stable Si-O bond between APTES and the surface.[400-402] The silanol

condensation reaction is slow, mainly due to the absence of water, thus a prolonged reaction time is necessary.[402]

The amine group in APTES (highlighted in red) can form hydrogen bonds with the hydroxyl groups of the surface, and deposit onto the surface via physical adsorption.[401-402] Therefore, APTES can be deposited onto the solid surface as a mixture of covalently linked or a physically adsorbed, thick films. However, physically adsorbed APTES layers can be removed by sonication and curing processes. leading to formation of a covalently attached APTES layer.[401-402]

5.4.3 Attachment of the bifunctional PEG linker

The silanized surfaces were further functionalised with the bifunctional PEG linker, which served as a spacer molecule between the peptide and the surface.[19,392] Mishra *et al.* reported increased antibacterial activity upon immobilisation of active lasioglossin-III to a PEG spacer consisting of 24 ethylene oxide repeats, compared to a 12 ethylene oxide repeat.[353] Based on this observation, a PEG spacer with 24 ethylene oxide repeats was used for the immobilisation studies.

The selective immobilisation of the cysteine-modified lipopeptide to the PEG linker was achieved using a heterobifunctional PEG linker (NHS-PEG_{24}-MAL). The linker had *N*-hydroxy succinimide (NHS) and maleimide (MAL) functional groups at either end, separated by the ethylene glycol spacer. The NHS of the PEG linker formed a selective amide bond with the silanized surface, while the MAL moiety formed a selective thiol linkage with the cysteine residue in the peptide.[19,392-393] The chemo-selectivity of the system minimises any non-specific reactions between the peptide and the solid surface.[352,393]

5.4.4 Peptide immobilisation onto the PEG coated surface

The Cys-modified lipopeptide, GZ3.163, was coupled to the maleimide group of the PEGylated surface, using selective sulfhydryl chemistry.[352-353] The cysteine group, in the peptide, and the maleimide underwent a selective Michael-type reaction, to form a thioether bond.[371,393] The thiol group then underwent a nucleophilic addition, with the carbon adjacent to the double bond in the maleimide group, to form the irreversible thiol ether bond, as shown in scheme 5.3.

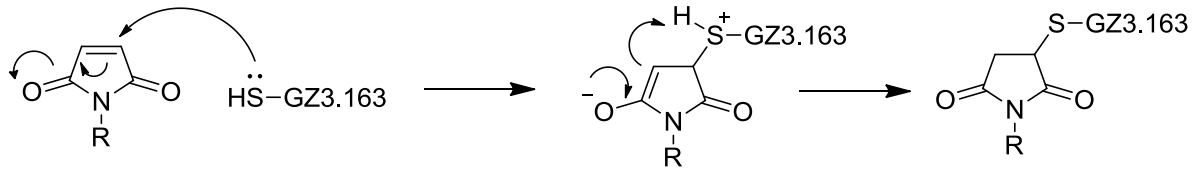

Scheme 5.3 Proposed mechanism of action of Cys peptide reacting with the maleimide group.

Generally, the optimum reaction conditions for the formation of the selective thioether bond occurred between pH 6.5-7.5. In this pH range, the reaction of the maleimide group, with the thiol group in the peptide occurred 1000 times faster than with the adjacent amine groups.[393] At a higher pH (>8.5) the maleimide group has a higher affinity towards primary amine groups, which could lead to hydrolysis.[393]

5.5 Surface characterisation of immobilised peptide

At each stage of immobilisation, the surfaces were characterised by water-contact angle measurements, ellipsometry and X-Ray photoelectron spectroscopy (XPS).

5.5.1 Water-contact angle measurements

The water contact angles, for each step of the functionalisation process, on three different surfaces are listed in Table 5.4. During each of the functionalisation steps, a snapshot was

taken of the water droplet deposited on the surface (Figure 5.5). The changes in the water contact angle during each of the immobilisation steps can be used to assess the success of the immobilisation process indirectly.

Table 5.4 Values of water contact angles, for the various stages of the immobilisation of the lipopeptide GZ3.163, on glass, silicon and titanium.

Surface	**Water-contact angle (°)***		
	Glass	**Silicon**	**Titanium**
SS	32.19 ± 6.3	55.07 ± 2.9	62.5 ± 6.3
SS^1	20.37± 3.0	46.7 ± 2.3	36.4 ± 6.1
SS^1--APTES	95.2 ± 6.3	79.3 ± 4.3	64.7 ± 5.2
SS^1--APTES--PEG	76.9 ± 7.0	66.6 ± 8.0	55.9 ± 5.2
SS^1--APTES--PEG--GZ3.163	59.8 ± 4.5	59.8 ± 1.2	43.3 ± 5.2

SS = solid surface, SS^1 = piranha-treated solid surface, APTES = 3-aminopropyl triethoxysilane, PEG = bifunctional polyethylene glycol spacer. * Angles are reported as average ± standard deviation.

Surface	Water droplet morphology		
	Glass	**Silicon**	**Titanium**
SS	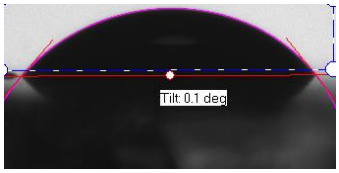	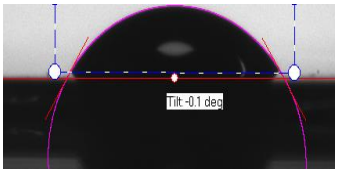	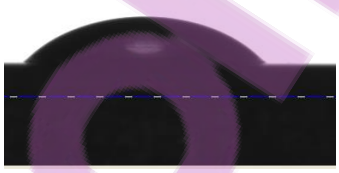
SS^1	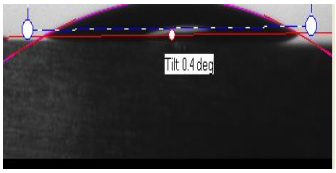	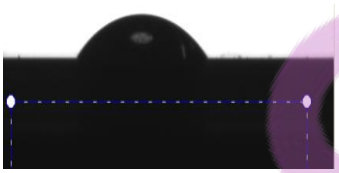	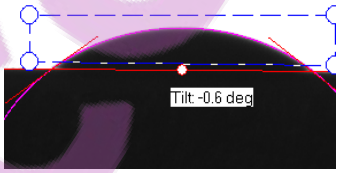
SS^1--APTES	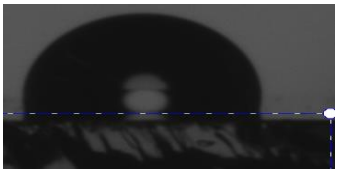	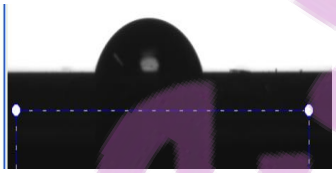	
SS^1--APTES--PEG	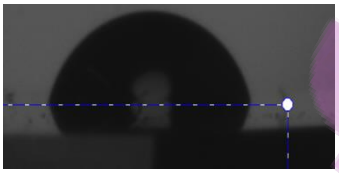	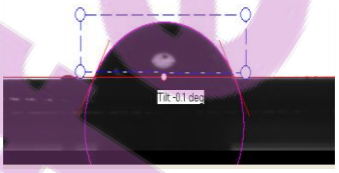	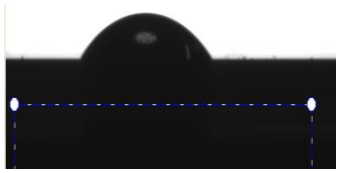
SS^1--APTES--PEG--GZ3.163	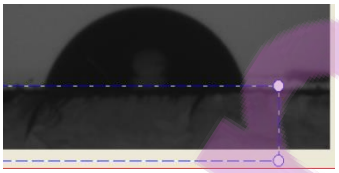	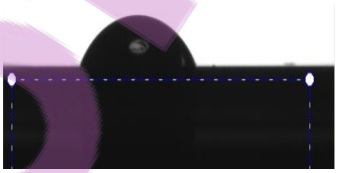	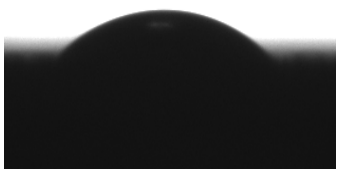

Figure 5.5 Images of water droplet under different functionalised surfaces.

The water droplets adopt a dome-shaped morphology on a hydrophobic surface (SS^1--APTES of all the three surfaces) due to the weak affinity of the liquid towards the surface. On a hydrophilic surface (SS^1 of all the three surfaces); the water droplets spread over a larger surface area, exhibiting a flatter, pancake-morphology.

As evident from Table 5.4, piranha treatment led to a reduction in the contact angles, as compared to the untreated samples for all three surfaces. This is due to the increased

exposure of the reactive hydroxyl groups, resulting in the creation of a more hydrophilic surface.[352-353] As can be seen in Figure 5.5, the water droplets on the piranha-treated surfaces (SS^1) are more spread out which is indicative of the more hydrophilic nature of the surface.

Silanization led to increased hydrophobicity of the surfaces, due to the presence of the propyl hydrocarbon chains, resulting in an increase in the water-contact angle values for all of the three surfaces.[352-353] The water droplet on the silanized surfaces exhibited a dome-shaped morphology, indicative of a hydrophobic surface.

Successful PEGylation of the silanized surfaces, upon reaction with the bifunctional NHS-PEG-MAL linker, was demonstrated by a moderate reduction in the contact angle values. The PEGylation of glass, silicon and titanium surfaces led to reduction of the contact angle values by 18°, 13° and 9°, respectively (Table 5.4). The linker has an amphiphilic nature, due to the presence of the polyethylene oxide units and the maleimide group.[352-353] The lipopeptide GZ3.163 also has an amphiphilic nature, due to the presence of multiple Dab residues, which are hydrophilic, together with the hydrophobic residues, Leu and Phe, and the fatty acid.

After peptide immobilisation, the contact angles on glass, silicon and titanium reduced by 17°, 6.8° and 12.6° respectively. The observed changes during each of the functionalisation steps indicate successful completion.

5.5.2 Ellipsometry

The thicknesses of the different coated layers on silicon, measured using ellipsometry, are shown in Table 5.5.

Table 5.5 Thickness (Å) of conjugated layers onto silicon surface

Layer	Thickness (Å)
Si	17 ± 4
APTES	107 ± 3
PEG[a]	41 ± 6
GZ3.163[b]	26 ± 7

[a] Thickness of the PEG linker, [b] Thickness of the coated peptide

The APTES coated silicon wafer produced a uniform layer 10 nm (107 Å) thick, and was within the values, reported in the literature, for 24-hour treatment with APTES.[402] PEGylation of the APTES coated silicon surface produced a layer 4.1 nm (41 Å) thick. Mishra *et al.* reported similar thicknesses (34 Å) when a 24 carbon long hetero-functional PEG layer was coated to the APTES-functionalised silicon wafer.[353]

The immobilised lipopeptide layer had a thickness of 2.6 nm (26 Å). A thickness of 15 Å has been reported, for the immobilisation of the 15 residue AMP lasioglossin-III to PEG functionalised silicon surface, by Mishra *et al*.[353]

The surface concentration of the immobilised peptide on the silicon wafer was calculated using the modified Lorentz-Lorenz equation shown below:[403]

$$\sigma = d\,\rho^{\circ} = \frac{0.01 d M_w}{A}\,\frac{n^2 - 1}{n^2 + 2} \qquad (5.1)$$

where,
σ = Mass/ unit area (μg cm^{-2})
ρ°= Density (mass per unit volume)
d= Thickness of adhered layer (Å)
M_w = Molecular weight of the peptide (kDa)
A = Molar refractivity of absorbed surface, set at 0.414
n = Refractive index of peptide, set at 1.460

Using this equation, the concentration of the peptide, deposited on the silicon surface, was calculated to be 190 ± 51 ng cm^{-2}, and was similar to the reported immobilised concentration for lasioglossin-III (180 ± 15 ng cm^{-2}).[353] The immobilised peptide concentration of GZ3.163 is also within the expected monolayer peptide concentration deposited onto silicon wafer and indicates no peptide aggregation has occurred.[404]

5.5.3 X-Ray photoelectron spectroscopy (XPS)

5.5.3.1 XPS of silicon wafer

5.5.3.1.1 Survey spectra

The immobilisation of GZ3.163 onto silicon and titanium surfaces was further characterised using XPS. Figure 5.6 shows the XPS survey spectra for the step-by-step immobilisation of GZ3.163 onto a silicon surface. Quantification was carried out on the elements present on the immobilised surface and is summarised in Table 5.6.

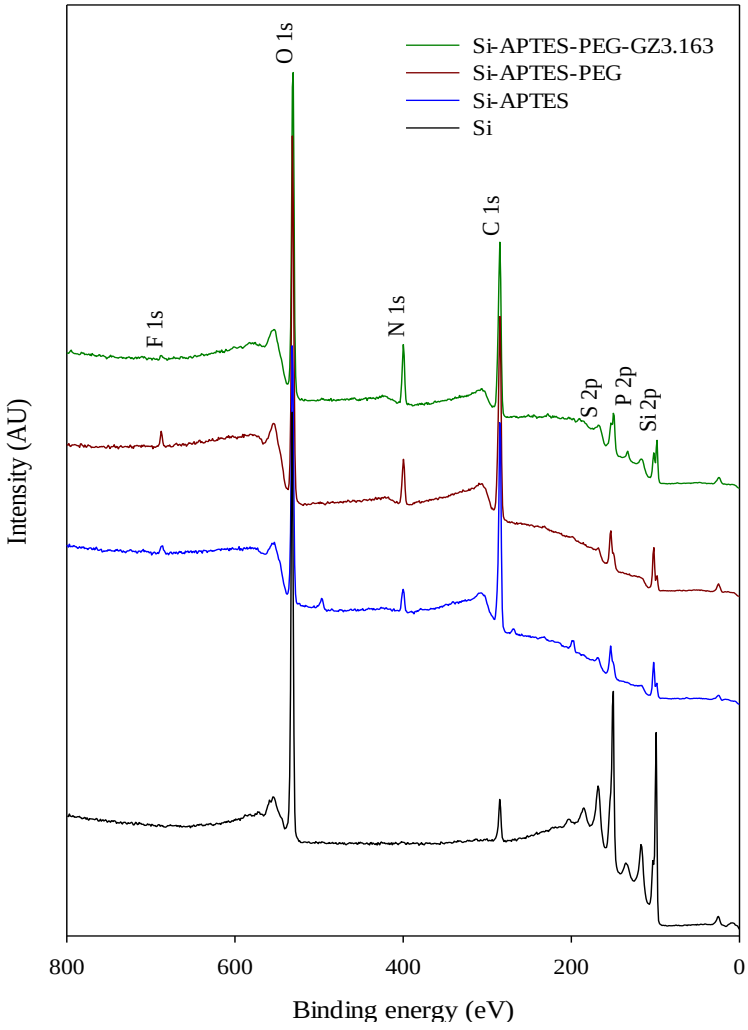

Figure 5.6 XPS survey spectra for the systematic selective immobilisation of the lipopeptide onto silicon.

Table 5.6 XPS quantification (atomic %) for the various stages of peptide immobilisation on the silicon surface.

Surface	Atomic %composition			
	C	**O**	**N**	**Si**
Piranha-treated Si wafer	9.58	24.90	0.00	48.40
Si---APTES	57.98	21.02	3.51	14.07
Si---APTES---PEG	54.94	24.24	5.67	14.10
Si---APTES---PEG---GZ3.163	49.26	24.49	6.89	16.75

XPS survey spectra revealed characteristic peaks for carbon, oxygen, nitrogen and silicon. Small traces of fluorine, sulphur and phosphorus were also observed.[405] The presence of sulphur and phosphorus were attributed to sulphuric acid in the piranha solution and phosphate buffer washings, respectively.

The piranha-cleaned silicon wafer mainly contained silicon (48.4%) and oxygen (24.9%) and, to a smaller extent, carbon (9.6%). A high proportion of silicon and oxygen indicated that a clean silicon oxide layer was created after the piranha treatment. However, it should be noted that there will always be small contributions of C and O from adventitious atmospheric hydrocarbons adsorbed on to the surface of the sample.

Successful APTES treatment of the piranha-cleaned silicon wafer was demonstrated by a significant increase in the percentage of elemental carbon from 9.6% to 58.0% and by the presence of nitrogen (3.5%) on the silanized surface.[406] The increase in the concentration of elemental carbon was due to the presence of the propyl chain. The presence of nitrogen could possibly be attributed either to the deposition of nitrogen molecules during the drying of the APTES surface with nitrogen gas, or to the terminal amines of the APTES molecule. The significant decrease in the percentage of silicon from 48.4% to 14.1% after silanization indicated the successful coverage of the piranha-treated silicon dioxide layer with the APTES group.

Successful attachment of the bifunctional PEG linker to the APTES coated surface was shown by increases in elemental oxygen, from 21.0% to 24.2%, and nitrogen, from 3.5% to 5.7%. This was mainly due to the ethylene oxide repeat units of PEG, and the terminal maleimide functionality.

The successful immobilisation of the lipopeptide onto the PEGylated silicon wafer was characterised by an increase in the percentage of elemental nitrogen from 5.7% to 6.9%, due to the presence of the side-chain amines and the peptide bonds. Overall, the results from the survey spectra indicated successful immobilisation of the lipopeptide onto the silicon surface. Core level scans were also carried out over the O 1s, N 1s, C 1s, and Si 2p regions, to analyse the chemical environments surrounding each element.

5.5.3.1.2 O 1s XPS core level spectra

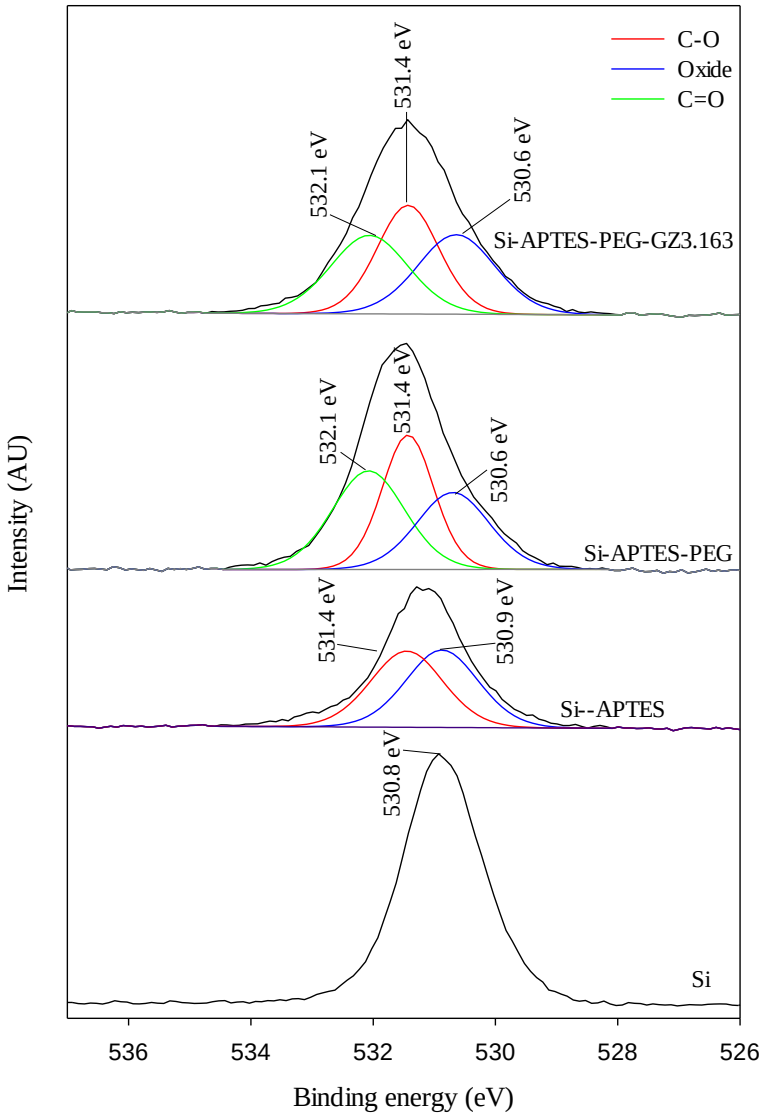

Figure 5.7 XPS core level scans over the O 1s region from each step of the systematic selective immobilisation of GZ3.163 onto the silicon substrate. The black line in each spectrum is the raw data while the coloured peaks correspond to the fitted Gaussian-Lorentzian peaks (30% Lorentzian).

The O 1s core level spectrum of the piranha-treated silicon surface showed a single peak at 530.8 eV, which was attributed to the oxide layer on the surface of the silicon substrate. During APTES treatment, two peaks were observed at, 530.9 eV and 531.4 eV; the latter of which corresponded to the C-O bond from the ethoxy functional groups of APTES.[407]

The PEGylated surface showed three peaks at 530.6 eV, 531.4 eV and 532.1 eV. The peak at 531.4 eV (C-O) had a greater intensity in the PEGylated surface spectrum as compared to the APTES, due to the presence of the ethylene oxide moiety of the PEG linker. The new peak at 532.1 eV arose from the carbonyl (C=O) groups of the peptide bond between APTES and the PEG linker. The intensity of this new peak was higher than the intensity of the silicon oxide (530.6 eV) in the PEGylated surface, which indicated the successful conjugation of the PEG linker to the APTES functionalised surface.[373,407]

In the presence of the immobilised peptide no new peaks were observed, however three peaks at 530.6 eV, 531.4 eV and 532.1 eV were identified corresponding to the native oxide layer, C-O from the PEG linker and carbonyl groups from the peptide bonds of the immobilised peptide respectively.[373]

5.5.3.1.3 N 1s XPS core level spectra

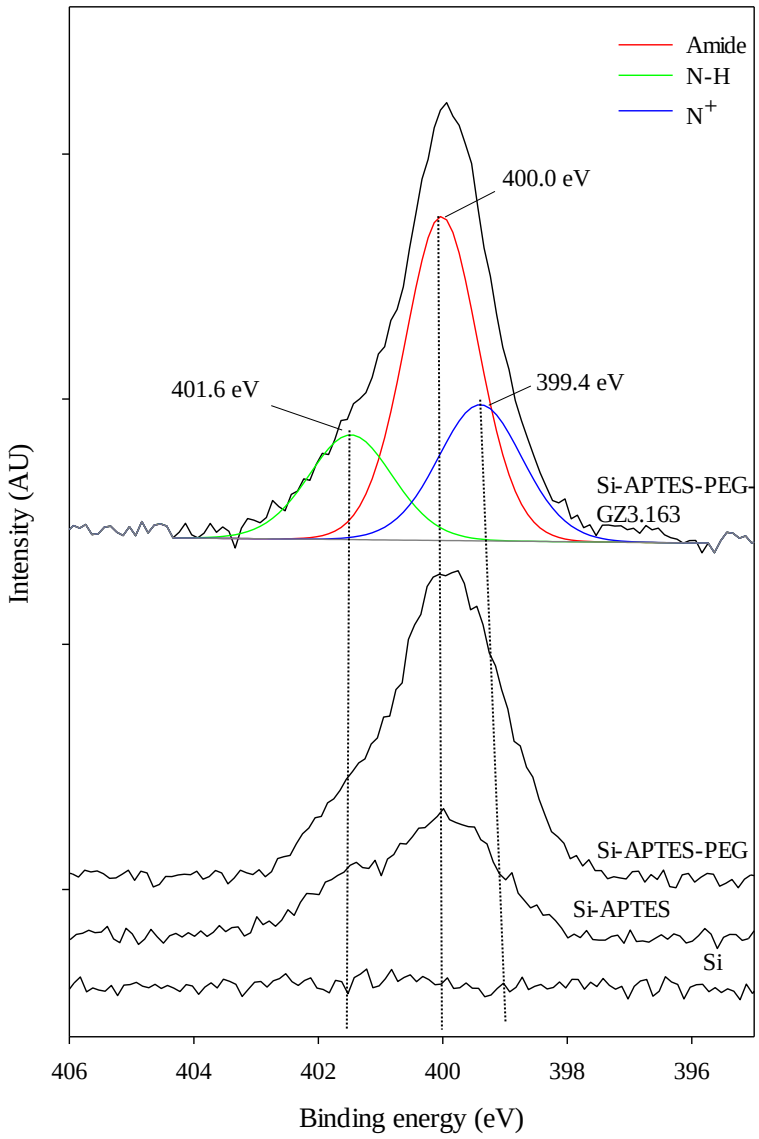

Figure 5.8 XPS core level scans over the N 1s region from each step of the selective immobilisation of GZ3.163 onto silicon.

The piranha-treated silicon surface did not show any traces of elemental nitrogen, as indicated by the absence of observable peaks in N 1s core level spectrum.

The sharp signal at 400 eV in Si-APTES was attributed to the terminal amine group in APTES, in the non-protonated and protonated forms, whereas, the intense peak at 400 eV

observed for the PEGylated surface was due to the formation of an amide bond between the silanized surface and the PEG molecule.[373,407]

The N 1s core level spectrum for the lipopeptide GZ3.163 showed three peaks fitted at 399.4 eV, 400.0 eV and 401.6 eV, which were assigned to the nitrogen in the side-chain amines of Dab, the amide bonds of the peptide and the protonated Dab side chains, respectively.[373,407] The peak at 400.0 eV had the greatest intensity of the three, because the majority of the nitrogen in the peptide was present as amide bonds.

The non-protonated peak at 399.4 eV was slightly more intense than the protonated peak at 401.6 eV. This could be because several Dabs in the peptide sequence were deprotonated, since the peptide was coupled to the PEGylated surface at a pH of 7.4.

5.5.3.1.4 C 1s XPS core level spectra

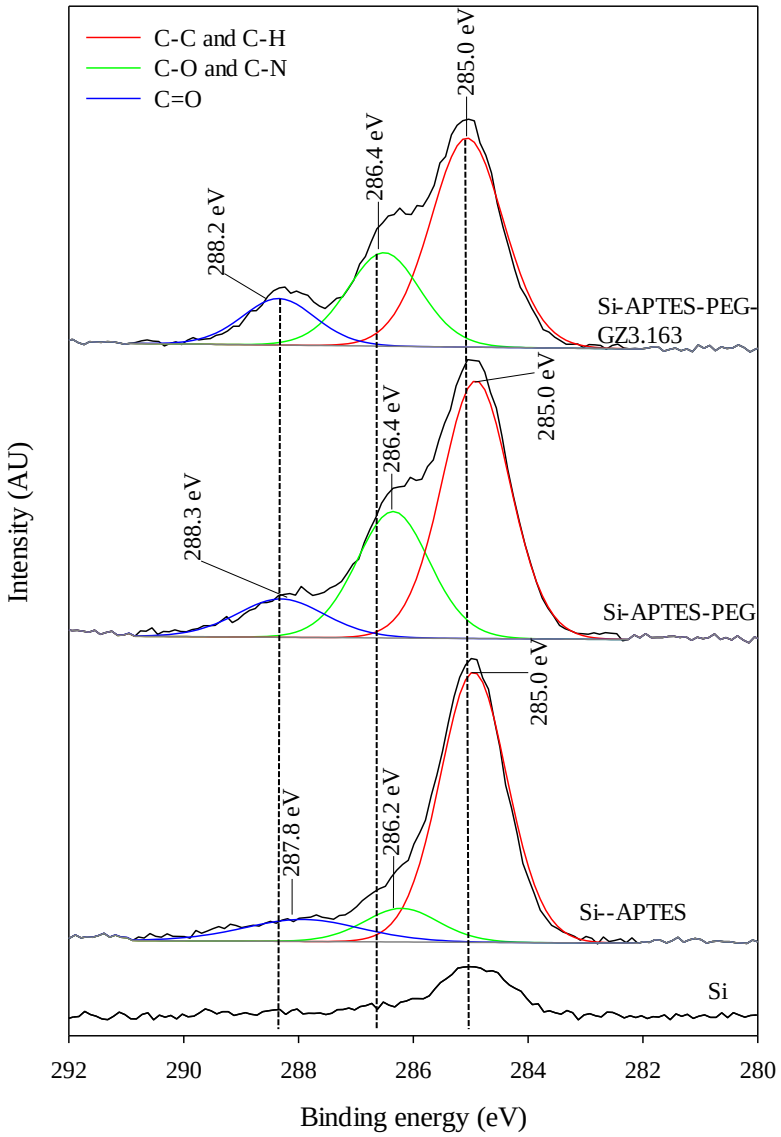

Figure 5.9 XPS core level scans over the C 1s region from each step of the systematic selective immobilisation of GZ3.163 onto silicon.

The C 1s core level spectrum for the piranha-treated silicon surface was not fitted, as it was solely attributed to the presence of adventitious hydrocarbons.

In the APTES-treated surface, the C 1s narrow scans showed three carbon environments, fitted at 285.0 eV, 286.2 eV and 287.8 eV which correspond to C-C and C-H, C-O and C-N and C=O, respectively.[373,407] The main peak, observed at 285 eV, was due to the

presence of the propyl chain of APTES as well as adventitious hydrocarbons. The less intense peak at 286.2 eV was attributed to the presence of ether bonds of the tri-ethoxy functional groups and the carbon-nitrogen bond of the terminal amine group of APTES. The carbonyl peak at 287.8 eV was possibly caused by contamination.

The C 1s narrow scans for the PEGylated surface were also fitted, with three peaks at 285.0 eV, 286.4 eV and 288.3 eV, which were attributed to C-C and C-H, C-O and C-N and C=O respectively. However, the intensities of the peaks at 286.4 eV and 288.3 eV for the PEGylated surface were greater than the corresponding two peaks observed for the silanized surface.[373] The increase in peak intensity at 286.4 eV was mainly due to the presence of ether functional groups from the ethylene oxide repeat units of the PEG moiety and carbon-nitrogen bonds from the terminal maleimide group in the PEG linker. The increase in intensity of the 288.3 eV peak was mainly due to the carbonyl group of the maleimide group in the PEG linker.[373]

The immobilised lipopeptide was also fitted with three peaks at similar peak intensities as the PEG linker at 285.0 eV, 286.4 eV and 288.2 eV, which corresponded to C-C and C-H, C-O and C-N and C=O, respectively. In this case, the peak at 286.4 eV was mainly due to the ether functional groups from ethylene oxide repeats units of the PEG molecule and the C-N bond of the side chain amines of Dab and the peptide bond. The peak at 288.2 eV was mainly due to the presence of carbonyl groups from the peptide bonds in the immobilised lipopeptide.[373]

5.5.3.1.5 Si 2p XPS core level spectra

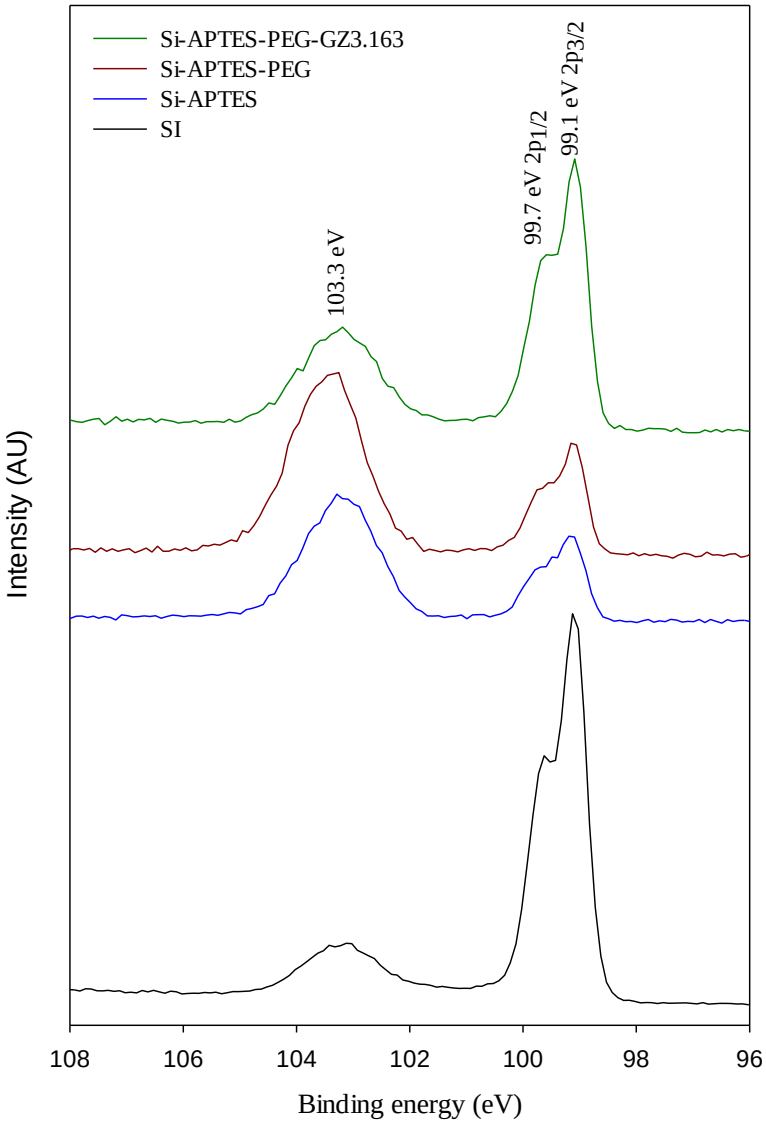

Figure 5.10 XPS core level scans over the Si 2p region from each step of the systematic selective immobilisation of GZ3.163 onto silicon.

The Si 2p narrow region spectrum for all samples showed two distinct peaks, at a 1:2 peak ratio, located at binding energies of 99.1 eV and 99.7 eV (spin orbit splitting = 0.6 eV), which corresponded to Si $2p_{3/2}$ and Si $2p_{1/2}$ lines, of Si. Another peak was present at a binding energy of 103.3 eV which was attributed to the oxide layer on the Si substrate.[405,407] The ratio of the intensity of silicon-oxide to Si, in the piranha-treated

surface, was 1:10. During each of the functionalisation steps, the ratio of the peak intensity of the silicon oxide layer to elemental Si increased.

The Si 2p core level spectra for the APTES-treated, the PEGylated and the immobilised lipopeptide samples had their Si $2p_{3/2}$ and Si $2p_{1/2}$ lines at lower binding energies of 99.1 eV and 99.7 eV, respectively, compared to the piranha-treated silicon surface. The oxide was also at a lower binding energy of 103.3 eV. This is because in this case, Si-C and Si-O bonds within the APTES group contribute to the peaks to a greater extent, compared to the Si substrate.

The PEGylated surface had the greatest silicon oxide to elemental Si peak ratio, at 2:1. This increase was due to an increase in oxygen on to the silicon surface, from different oxygen-containing environments, during each of the functionalisation steps. However, as expected, in the presence of the immobilised peptide, the intensity of the silicon oxide layer (103.3 eV) was less than that of elemental silicon. This is because the oxygen content in the peptide is lower than that of the PEG linker is, and because surface coverage of the PEG linker by the peptide causes a reduction in the intensity of the silicon oxide layer.

5.5.3.2 XPS of titanium surface

5.5.3.2.1 Survey spectra

The survey spectrum for the systematic immobilisation of GZ3.163 onto titanium and the semi-quantitative analysis of elements present on the immobilised surface are summarised in Figure 5.11 and Table 5.7.

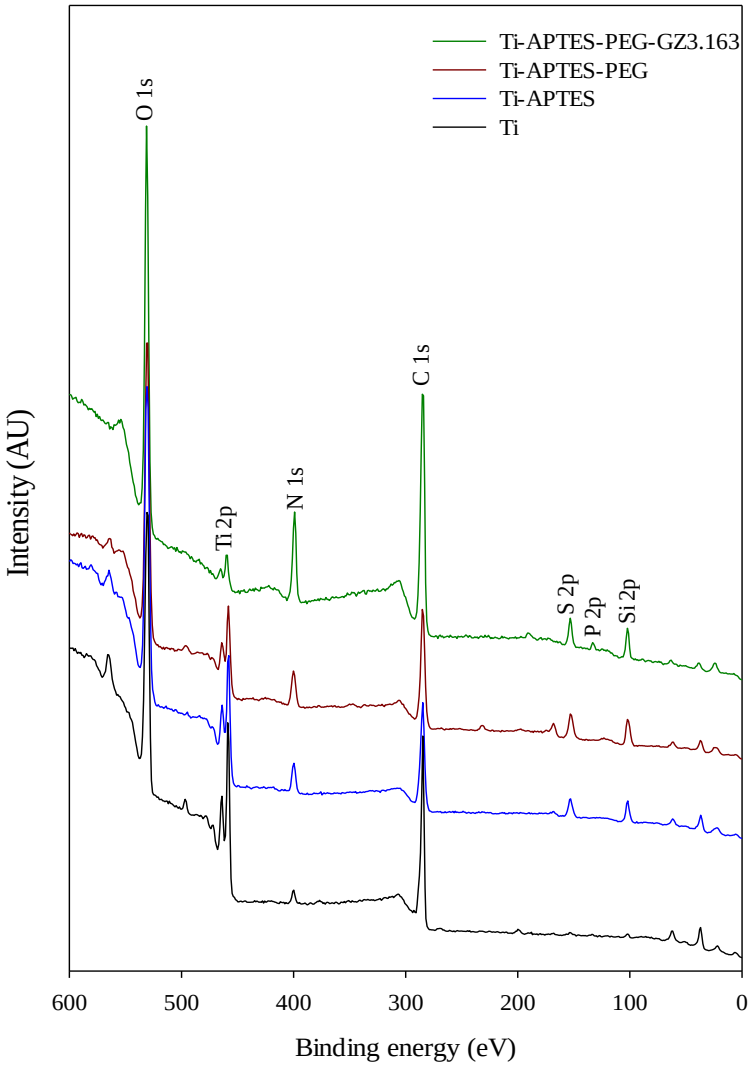

Figure 5.11 XPS survey spectra of each step of the systematic selective immobilisation of GZ3.163 onto titanium.

Table 5.7 XPS quantification (atomic %) for the peptide immobilised titanium surface.

Surface	Atomic %composition				
	C	**O**	**N**	**Ti**	**Si**
Piranha-treated titanium slide	53.31	30.38	2.02	6.74	1.36
Ti---APTES	40.48	37.09	5.01	5.56	9.19
Ti---APTES---PEG	41.51	31.52	6.22	3.54	11.52
Ti---APTES---PEG---GZ3.163	57.80	25.00	9.60	0.90	6.30

The survey spectra revealed characteristic peaks for carbon, oxygen, nitrogen, titanium and silicon. Traces of sodium, chlorine and sulphur were also detected. The piranha-treated titanium surface showed very high proportions of adventitious carbon (53%) and nitrogen (2.02%) contamination. The high proportion of oxygen present in the piranha treated sample can be attributed to coverage of small layer (2-3 nm) of TiO_2 upon exposure of titanium to the air.[398] The presence of nitrogen could be from drying the surface with a stream of N_2 during each of the immobilisation steps.

Successful silanization with APTES was indicated by the increase in the percentage of oxygen from 30% to 37% and of nitrogen from 2% to 5% on the silanized titanium surface, which was mainly due to the presence of the ethoxy and terminal amine groups, respectively. In addition, the increase in silicon concentration from 1.4% to 9.2%, in the silanized surface, indicated successful formation of silicon-oxygen bonds between APTES and the titanium surface.[406]

Successful PEGylation of the titanium surface was indicated by the increase in the concentration of nitrogen from 5.0% to 6.2%, from the nitrogen in the maleimide group.[373]

The increased nitrogen content, from 6.2% to 9.6%, is attributed to the successful immobilisation of the peptide.[373] This nitrogen is presumed to be arising from the peptide bond and the terminal amines of the Dab residues.

Lastly, the systematic reduction in elemental titanium, suggested successful surface coverage, during each of the immobilisation steps. Core level scans were carried out over the O 1s, Ti 2p, N 1s, and C 1s regions, to analyse the chemical environments surrounding each element, in detail.

5.5.3.2.2 O 1s XPS core level spectra

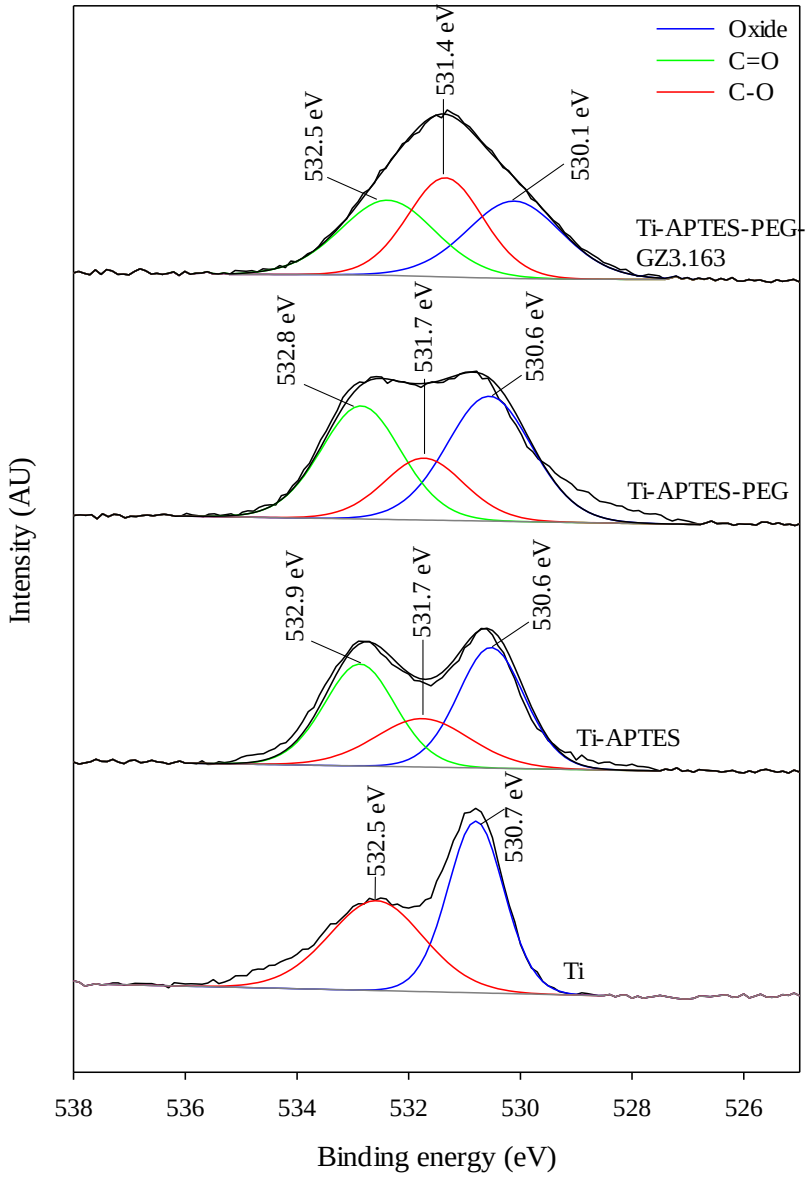

Figure 5.12 XPS core level scans over the O 1s region for each step of the systematic selective immobilisation of GZ3.163 onto titanium.

The O 1s narrow scans for the piranha-treated titanium surface was fitted with two chemical environments at 530.7 eV and 532.5 eV, attributed to the oxygen in the oxide layer and the hydroxyl groups of Ti-OH, respectively. [373,407-408]

During the silanization, process an additional peak was fitted, at 531.7 eV, which was attributed to the ethoxy functional groups in APTES.[373,407]

The O 1s core level spectrum for the PEGylated titanium surface was fitted with three peaks at 530.6, 531.7 eV and 532.8 eV. The peaks at 530.6 and 531.7 eV were due to the oxide layer of the titanium surface and the ether bonds arising from the ethylene oxide moiety of the PEG molecule. The peak at 532.8 eV corresponded to the carbonyl group from the peptide bond formed between the PEG linker and APTES coated surface.[373]

In the presence of the immobilised peptide, three peaks at 530.1 eV, 531.4 eV and 532.5 eV were fitted in the O 1s core level spectrum, which corresponded to the oxide layer, C-O from the PEG linker and the carbonyl groups from the peptide bonds respectively.[373]

5.5.3.2.3 Ti 2p XPS core level spectra

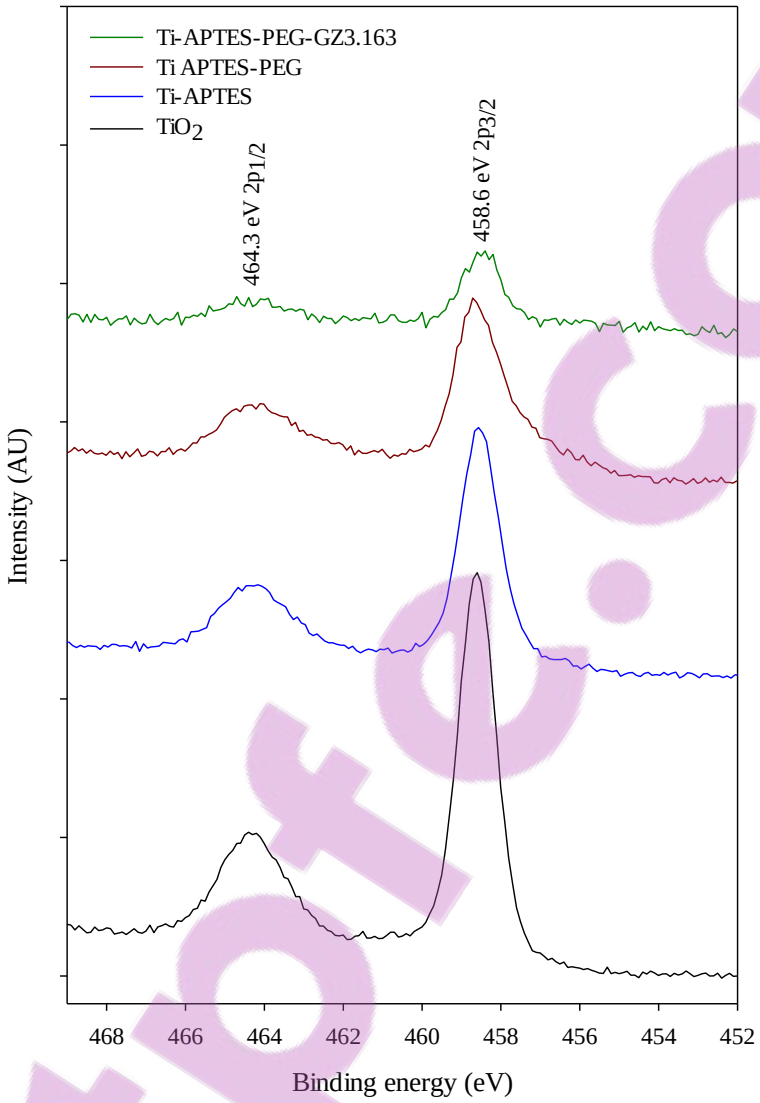

Figure 5.13 XPS core level scans over the Ti 2p region for each step of the systematic selective immobilisation of GZ3.163 onto titanium.

Narrow scans over the Ti 2p region showed two peaks of interest with a 1:2 area ratio at binding energies of 464.3 eV and 458.6 eV (spin orbital splitting of 5.7 eV). The peaks corresponded to Ti $2p_{1/2}$ and Ti $2p_{3/2}$ lines. These values correlated with the presence of Ti^{4+} species in TiO_2.[405] During each of the immobilisation steps, the intensity of Ti 2p decreased, which indirectly corresponded to the successful grafting of each layer during the systematic immobilisation procedure.[373]

5.5.3.2.4 N 1s XPS core level spectra

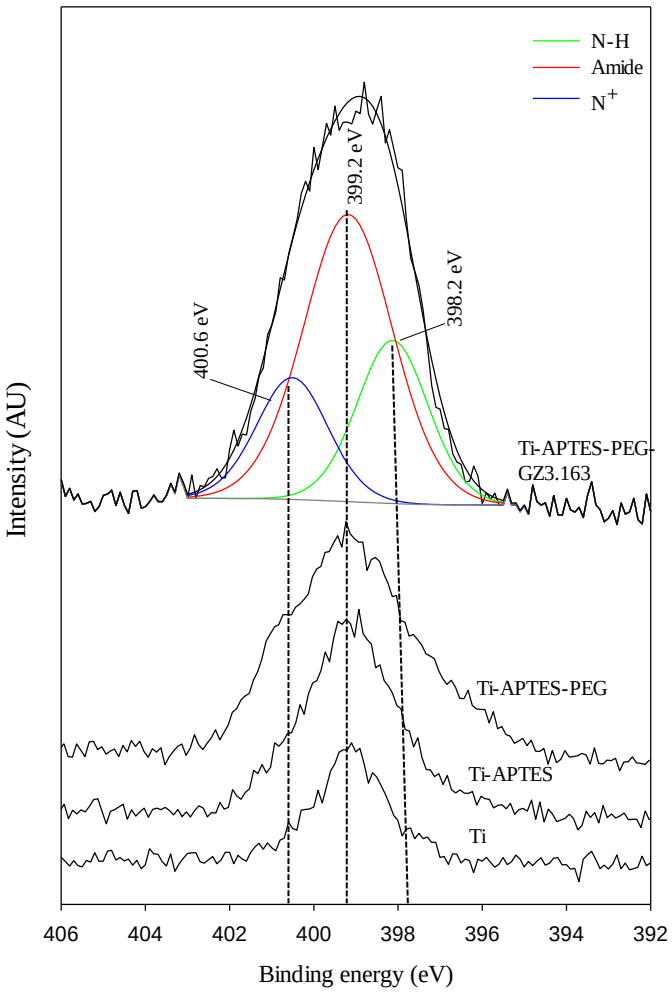

Figure 5.14 XPS core level scans over the N 1s region for each step of the systematic selective immobilisation of GZ3.163 onto titanium.

The N 1s peak for the piranha-treated titanium surface could be due to trace amounts of nitrogen left on the sample surface during the drying of the surface with N_2 gas.

Nitrogen present in the silanized titanium surface was mainly due to the terminal amines arising from the APTES molecule. Successful PEGylation of the titanium surface was identified by the presence of the amide peak at 399.2 eV, which arose due to the formation of the peptide bond between the terminal amines of APTES and carboxylic moiety of the bifunctional linker.[373,407]

The N 1s core level spectrum for the immobilised peptide was fitted with three main nitrogen environments at 398.1 eV, 400.1 eV and 400.6 eV, corresponding to side-chain amines of the Dab in the lipopeptide, the amide bonds of the peptide and the protonated Dab side chains, respectively.[373,407]

5.5.3.2.5 C 1s XPS core level spectra

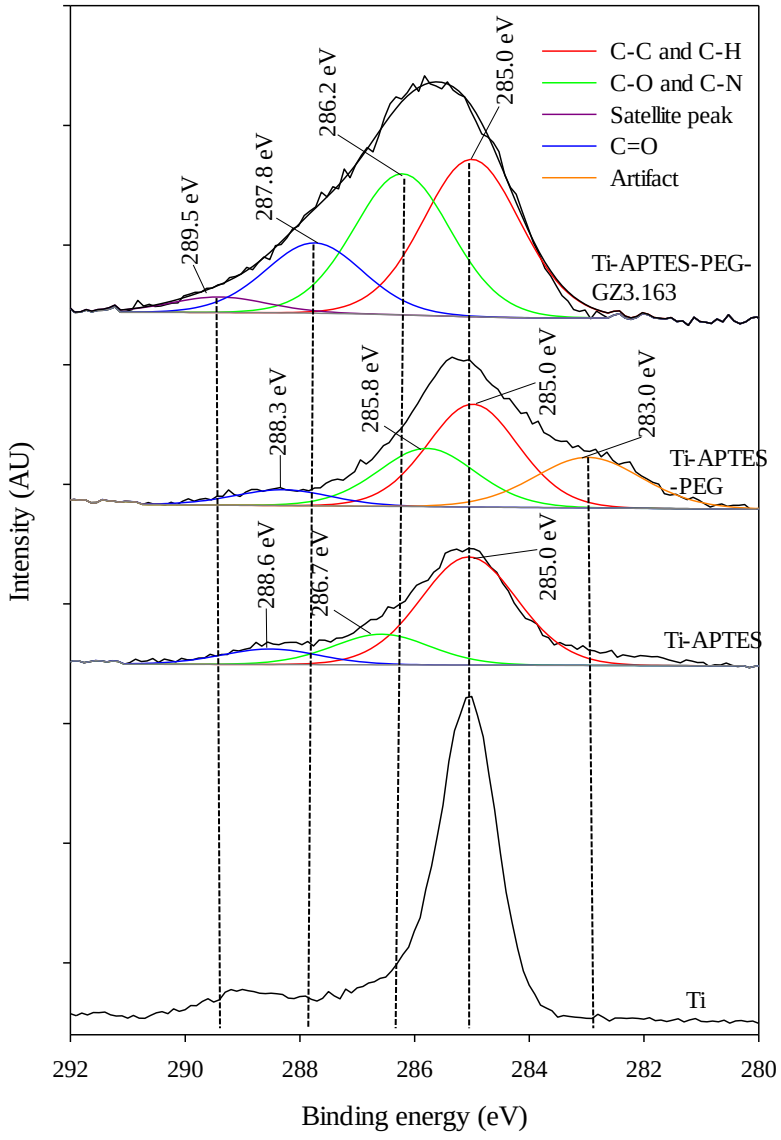

Figure 5.15 XPS core level scans over the C 1s region for each step of the systematic selective immobilisation of GZ3.163 onto titanium.

The C 1s core level spectrum for the piranha-treated titanium surface showed a peak at 285 eV due to adventitious hydrocarbons.

The C 1s narrow scan spectrum for APTES treated titanium surface was fitted with three peaks located at 285 eV, 286.7 eV and 288.6 eV. The intense peak at 285 eV was attributed to hydrocarbons (C-C and C-H), and was due to the alkyl chain of APTES.[373,407] The less intense peak at 286 eV was mainly due to ether bonds of the ethoxy side chains on the APTES molecules. Small traces of carbonyl contamination (288.6 eV) were also observed.

The PEGylated titanium surface C 1s spectrum was fitted with four peaks at binding energies of 283.0 eV, 285.0 eV, 285.8 eV and 288.3 eV which were attributed to contamination, C-C and C-H, C-O and C-N, and C=O, respectively.[373,407] The successful PEGylation was demonstrated by the increased intensity of the C-O peak at 285.8 eV, caused by the ethylene oxide moieties of the PEG molecule and the carbonyl peak at 288.3 eV from the peptide bond formed between the bifunctional PEG linker and the APTES coated titanium surface.

The artefact (orange peak) in the Ti-APTES-PEG sample was a result of differential charging. It correlated to the adventitious hydrocarbon directly attached to the Ti substrate. The APTES-PEG is unlikely to cover the Ti substrate fully, therefore there are likely to be parts, which are not coated, onto which adventitious carbon can attach. The Ti substrate itself is a conductor whereas APTES-PEG is an insulator. In insulators, positive charge can build up as photoelectrons are lost during XPS measurements, which causes the kinetic energy of the emitted photoelectrons to decrease, resulting in peaks being shifted to higher binding energies. One way around this is to use a charge neutraliser, which provides low energy electrons to replace the emitted photoelectrons, stopping the

build-up of positive charge on the surface of the sample and shifting the peak back to a lower binding energy. The Ti-APTES-PEG sample, contained some areas which were insulating and others which were conducting, giving rise to different levels of charging, which the charge neutraliser would compensates for. However the kinetic energies would be dependent on which part of the sample the photoelectrons were emitted from, and so be compensated by the charge neutraliser accordingly, causing the peaks to shift and broaden. The artefact peak is a result of the over-compensation by the charge neutraliser for the conducting component of the sample, so the adventitious hydrocarbon on the Ti substrate have been shifted to lower binding energies.[409]

In the presence of the immobilised peptide, the C 1s core level spectrum was fitted with four chemical environments at 285.0 eV, 286.2 eV, 287.8 eV and 289.5 eV corresponding to C-C and C-H, the C-O and C-N, the C=O and a satellite peak, respectively.[373] The C-C and C-O peaks were the two dominant peaks, since these functional groups were present in abundance during each of the functionalisation steps of the immobilisation procedure. The C=O peak was at 1:2 peak ratio to the C-C and C-O peaks since this peak was predominately the contribution of the carbonyl groups in the peptide sequence. The small satellite peak at 289 eV was due to a characteristic $\pi \rightarrow \pi^*$ transition arising from the benzyl group of phenylalanine in the peptide sequence.[410]

5.6 Antibacterial activity of immobilised peptide

The antibacterial activity of the immobilised GZ3.163, on glass, silicon and titanium surfaces, was characterised by biofilm inhibitory assays and scanning electron microscopy against *P. aeruginosa* since the Cys modified lipopeptides showed the most potent activity against it.

5.6.1 Biofilm inhibitory assay of immobilised lipopeptide

The ability of the immobilised lipopeptide to prevent biofilm formation of *P. aeruginosa* was studied using a Live/Dead staining assay (Figure 5.16). The biofilm assay was monitored up to 48 hours, which was the same period as for the biofilm assay studies discussed in the section 4.4.

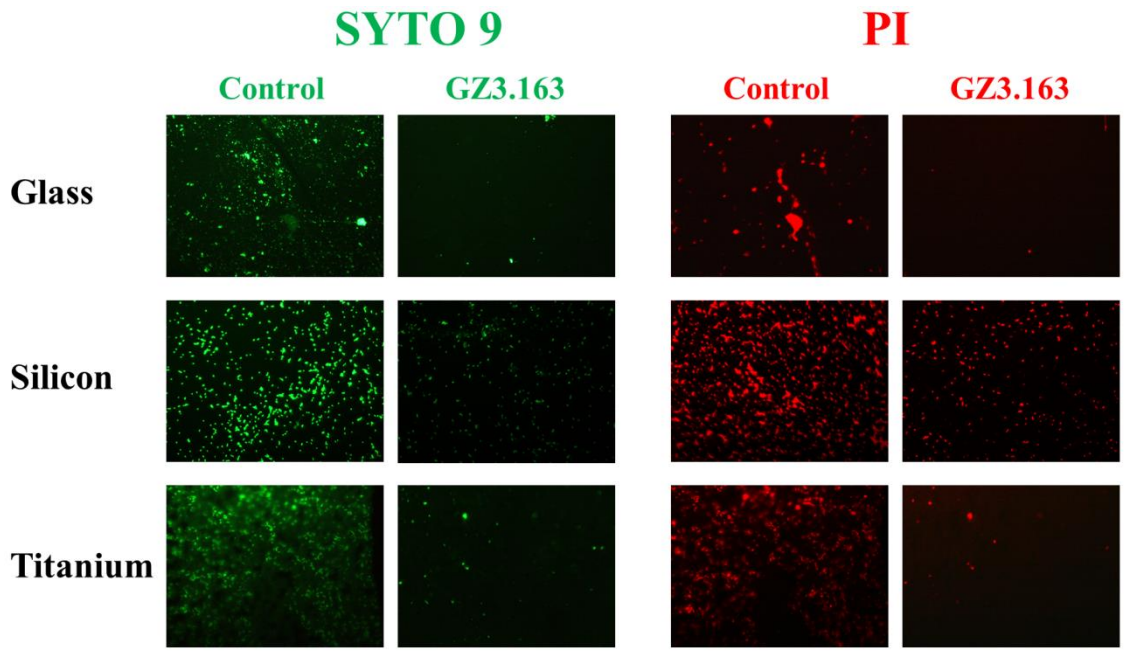

Figure 5.16 Representative images of biofilms formation of *P. aeruginosa* in the absence (control) and presence of GZ3.163 immobilised on glass, silicon and titanium surface. The biofilms were visualised using Live/Dead staining.

The uncoated glass, silicon and titanium surfaces retained the biofilms architecture, as shown by the increase in SYTO 9 and PI fluorescence. However, in the presence of the immobilised peptide, fewer bacterial cells managed to adhere to the three surfaces, resulting in a reduction in biofilms formation. These observations prove, that the immobilisation of GZ3.163 on glass, silicon and titanium maintained the same anti-biofilms activity observed in solution.

Live/Dead stained biofilm images of *P. aeruginosa* were quantified using ImageJ (U.S. National Institutes of Health, Bethesda) software. ImageJ measures the total fluorescence of the image by calculating the total value of the pixels in the image based on the equation mentioned in section 5.8.5.2 and the total fluorescence was calculated for three images per sample, to show a fair representation (Figure 5.17).

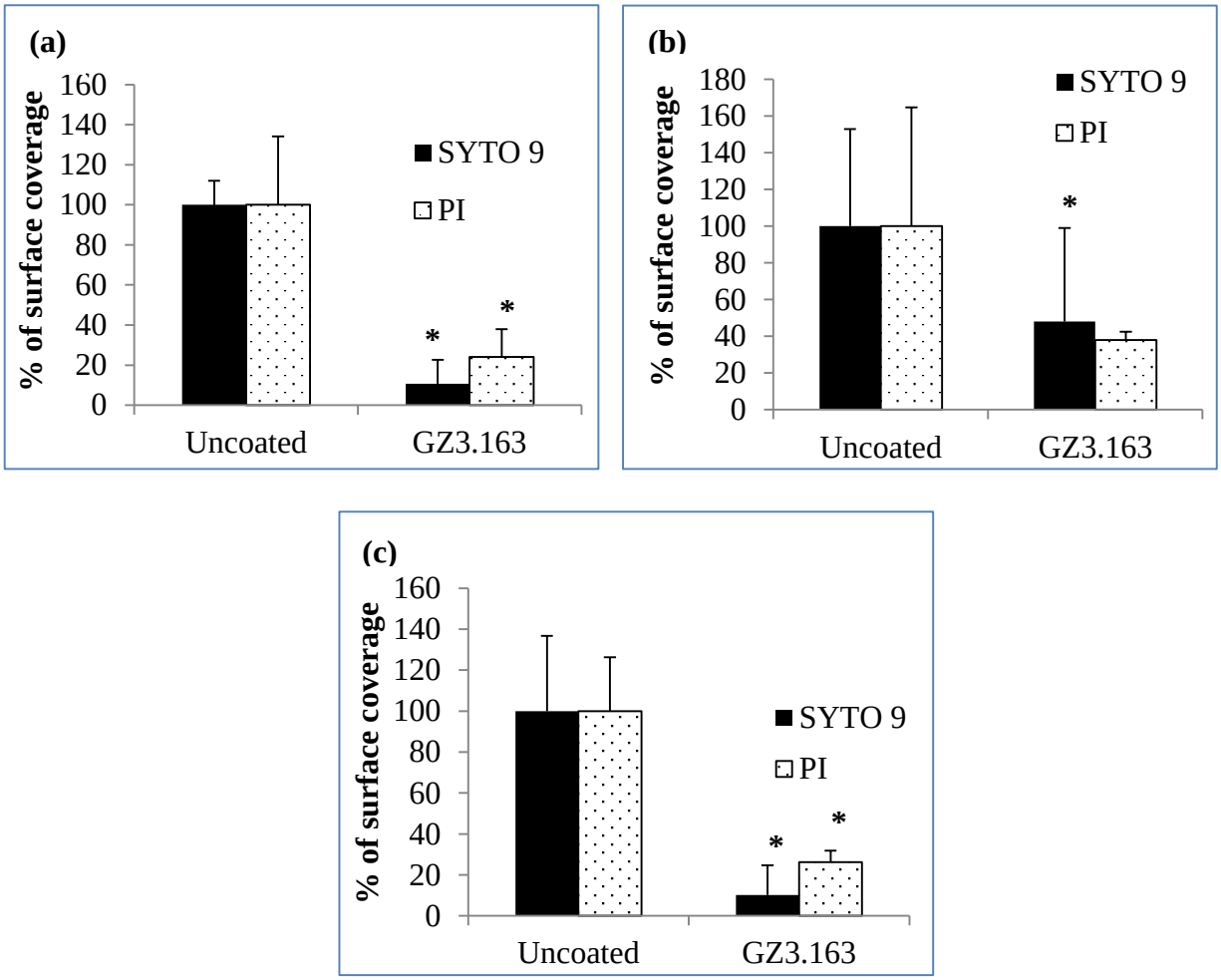

Figure 5.17 Percentage of surface coverage by *P. aeruginosa*, in the absence and presence of immobilised GZ3.163 on **(a)** glass **(b)**, silicon and **(c)** titanium surfaces. Error bars represent the standard deviation. * Indicates $p < 0.05$.

Surface coverage of *P. aeruginosa* is reported as a percentage, where, 100% indicates the total surface coverage by bacteria and 0% indicates the total inhibition of *P. aeruginosa* colonisation, on the surfaces, calculated separately for SYTO 9 and PI images. In the presence of the immobilised peptide on glass (Figure 5.17a), a significant reduction in

both SYTO 9 (90%) and PI (75%) fluorescence was observed. The immobilised peptide on silicon surface (Figure 5.17b) led to a moderate reduction in SYTO 9 (50%) and PI (72%) fluorescence. As evident from Figure 5.17c, the immobilisation of GZ3.163 on titanium surface also lead to a significant reduction in SYTO 9 (90%) and PI (74%) fluorescence.

5.6.2 Scanning electron microscopy of the immobilised lipopeptide

The immobilised lipopeptide on three different surfaces showed the ability to prevent colonisation and subsequent biofilm formation of *P. aeruginosa*. Scanning electron microscopy images of the lipopeptide, immobilised on the glass, silicon and titanium surfaces, were taken, to gain insight into its mechanism of action in the immobilised state, (Figure 5.18).

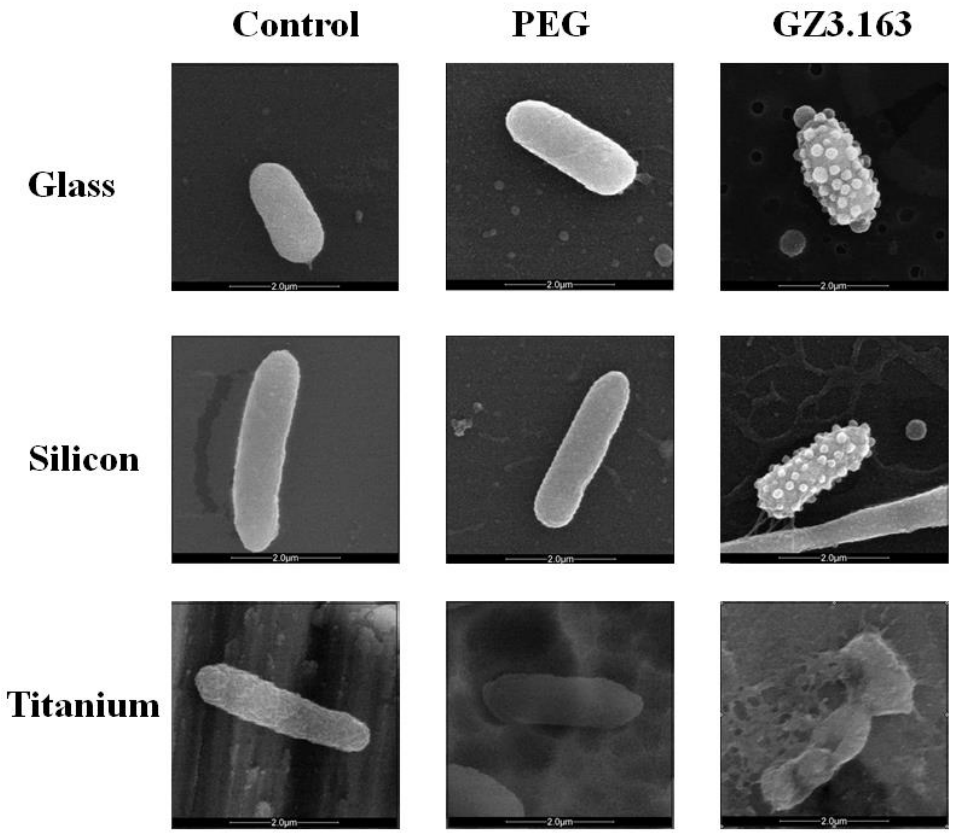

Figure 5.18 SEM image of *P. aeruginosa* in the absence (control) and presence of PEGylated and GZ3.163 immobilised on glass, silicon and titanium surfaces.

The rod-shaped *P. aeruginosa* maintained a smooth cell surface on all of the uncoated surfaces. In the presence of the PEGylated surfaces (middle row), the bacteria also retained similar cell morphology to the control cell, indicating the inability of the linker to induce any damage to bacterial cells. In the presence of the immobilised peptide, bacterial cells were corrugated, with small blisters appearing throughout the membrane, demonstrating that the immobilised peptide on glass, silicon and titanium retained the same membrane-lytic mechanism of action as the lipopeptide GZ3.27, in solution.[397] Hilpert *et al.* reported similar morphological changes in *P. aeruginosa* cells, in the presence of a series of immobilised cationic AMPs from the cathelicidin family.[395]

The membrane-lytic mechanism of action of the immobilised peptide is most likely attributed to enhanced peptide penetration into the bacterial cell due to the presence of PEG spacer with 24 ethylene oxide repeats. The effect of the spacer length on the immobilised peptide activity will have to be explored in future by incorporating a shorter spacer for conjugation.

5.7 Summary

This chapter described the attempts made to immobilise the novel battacin analogue, GZ3.27, successfully onto the model solid surfaces, silicon and titanium, which are used, in medical implants. Glass was also included in the study.

GZ3.27 lipopeptide was modified by conjugation with cysteine to its N-terminus (GZ3.163), C-terminus (GZ3.160) and the side chain of Dab^2 (GZ3.155), to allow selective covalent immobilisation, using thiol chemistry. The Cys modified lipopeptides did not lead to significant loss of antibacterial activity and so GZ3.163 was selected for the immobilisation studies.

The modified lipopeptide was immobilised on the surfaces using a heterobifunctional PEG linker. Each step of the immobilisation process was extensively characterised by water-contact angle measurements, ellipsometry and XPS. The changes in water contact angle during each of the immobilisation steps indicated successful grafting of the different layers onto the surfaces. Ellipsometry measurements identified that a thin monolayer of the peptide (190 ng cm^{-2}) was sufficient to inhibit bacterial adhesion. XPS measurements confirmed successful grafting of the peptide onto the silicon and titanium surfaces by measuring the change in the percentage atomic compositions of the surfaces.

The ability of the immobilised peptide to retain its antibacterial and anti-biofilm activities was validated by Live/Dead biofilm assay and SEM imaging of *P. aeruginosa*, immobilised on the surfaces. Immobilisation of the peptide on glass, silicon and titanium surfaces successfully inhibited the formation of *P. aeruginosa* biofilms, for 48 hours, as determined by qualitative (Live/Dead staining) and quantitative (ImageJ) analysis. Scanning electron microscopy revealed that the immobilisation of the lipopeptide maintained the same membrane-lytic mechanism of action as GZ3.27, since the bacterial cells were similarly corrugated and blistered in the presence of the immobilised peptide.

5.8 Experimental

5.8.1 Chemicals and Reagents

All solvents were of analytical grade and were used without further purification. Fmoc-Cys(Trt)-OH was purchased from GL Biochem (Shanghai, China). The NHS-PEG_{24}-MAL linker was purchased from Fisher Scientific. 3-aminopropyltriethoxysilane (APTES) was purchased from Sigma Aldrich. Glass slides (25 mm x 75 mm, 1 mm thick) were supplied by the stores at the School of Chemical Sciences, The University of Auckland. Silicon wafers (76 mm diameter, 0.4 mm thickness) were purchased from EL-CAT Inc. (New Jersey, USA). Titanium (99.2%) foil (100 mm x 100 mm, 2 mm thick) was purchased from Alfa Aesar (Heysham, England). Titanium surface was polished with silicon carbide and washed thoroughly with Milli-Q water. The titanium surface was further polished using a diamond-polishing disk and was then cut into 10 mm x 10 mm square pieces, using a diamond-cutting saw, for the immobilisation studies.

5.8.2 Synthesis of cysteine branched lipopeptide GZ3.155

The peptide was assembled on Tentagel-S-NH_2 resin as a C-terminal amide using a rink amide linker, following the same protocol as described in section 3.4.4. The side chain amine of Dab^2 was protected with Mtt protecting group and the remaining amine side chains in the peptide sequence were protected with Boc groups. The Mtt group was removed from the resin using 1.8% TFA in DCM for 3 minutes, at room temperature, and the filtrate was collected.[253] The resin was repeatedly submerged in this cleavage cocktail every three minutes, until a yellow filtrate was obtained. The intense yellow colour of the filtrate was due to presence of the trityl chloride cations and indicated successful removal of the Mtt protecting group from the resin. The resin mixture was thoroughly washed with DCM and DMF to remove any excess TFA bound to the resin. The Fmoc-Cys(Trt)-OH

was coupled to the side chain amine of Dab^2 followed by cleavage of the branched peptide using the same protocol as described in section 3.4.4.

5.8.3 Peptide immobilisation procedures to the surface

5.8.3.1 Piranha treatment of surface

All of the three different surfaces were thoroughly washed with Milli-Q water prior to piranha treatment. The surfaces were placed in a piranha solution (150 mL) consisting of 30% hydrogen peroxide and 70% concentrated sulphuric acid for 30 minutes. The temperature of the piranha solution was maintained between 80-130 °C during the cleaning. After piranha treatment, the substrates were soaked in Milli-Q water and thoroughly rinsed with it. The samples were then dried under nitrogen.[406]

5.8.3.2 Silanization with APTES

Piranha-treated glass slides and silicon wafers were silanized in 1% APTES in dry toluene (20 mL), for 24 hours. The APTES treatment of titanium slides was carried out under a glove box, to ensure a dry environment to facilitate the silanization. The silanized samples were washed thoroughly with acetone and ethanol, soaked in toluene (20 mL) and sonicated for 10 minutes. The soaked surfaces were thoroughly washed with ethanol to remove any traces of toluene, and dried at 121 °C for one hour to stabilise the APTES monolayer on the surface.[399,406] The silanized surfaces were dried under nitrogen.

5.8.3.3 PEGylation of NHS-PEG_{24}-MAL

The APTES coated surfaces were functionalised with succinimidyl-[N-maleimidopropionamido]-polyethylene glycol ester (NHS-PEG_{24}-MAL). The NHS-PEG_{24}-MAL ester at 0.2 mg/mL was dissolved in dry DMF. The dissolved ester (1 mL)

was reacted with the silanized surface for 4 hours at room temperature. The surfaces were then thoroughly washed with DMF, PBS buffer and Milli-Q water and dried under nitrogen.[352-353]

5.8.3.4 Conjugation of GZ3.163 on to the PEGylated surface

The cysteine-modified lipopeptide GZ3.163 was coupled to the PEG functionalised surface using selective sulfhydryl chemistry. GZ3.163 at 2 mg/mL was dissolved in PBS buffer at pH 7.4. The PEGylated surface was immersed in the solution (1 mL) and left for 16 hours at room temperature. The coated surface was thoroughly washed with PBS buffer and Milli-Q water and dried under nitrogen. The peptide-coated surfaces were stored at -20 °C for further use.[352,371]

5.8.4 Surface characterisation

5.8.4.1 Water-contact angle

Contact angle measurements were collected with a KSV Cam 100 Goniometer (Biolin Scientific) at the School of Chemical Sciences, University of Auckland with Attension Theta analysis software (Biolin Scientific, 2014) for contact angle calculations. A water droplet with uniform size (0.5 μL) was deposited on to the surface using a Hamilton syringe. Droplets were allowed to stand for 10 seconds before measurements were taken using an in-built planar CCD camera. The water contact angle was calculated using the in-built CAM 100 software and the measurement was repeated in three different regions, to gain a representative sample. The contact angle values are reported as average ± standard deviation.

5.8.4.2 Ellipsometry

The thickness of the immobilised peptide coated on the silicon wafer was measured using a Beaglehole Ellipsometer (Beaglehole Instruments, 2009) at variable angles (80°-60°) at 4° increments, at 632 nm. The film thickness was determined using the Thin Film Companion (SemiconSoft Inc., USA) software. A refractive index of 1.457 was used for the uncoated SiO_2 layer. The refractive index for APTES was set up at 1.422 and 1.460 was fixed for PEG and the peptide layer.[411]

5.8.4.3 X-Ray photoelectron spectroscopy (XPS)

A Kratos Axis UltraDLD equipped with a hemispherical electron energy analyser was utilised to collect XPS data at Faculty of Engineering, University of Auckland. XPS analyses were conducted using monochromatic Al Kα X-Rays (1486.69 eV) with the X-Ray source working at 10 mA and 15 kV (analysis area 300 × 700 μm spot). All measurements were collected in normal emission geometry in chamber pressures of approximately 10^{-9} Torr. For the survey scans, an energy step of 0.1 eV and pass energy of 160 eV was used, whereas for core level scans, a pass energy of 20 eV was used. The C 1s signal from saturated hydrocarbons (285.0 eV) was used as an internal standard, to correct the binding energy scale for charging specimen and the neutraliser shift. Data was analysed using CasaXPS (Casa software, 2009) with Shirley backgrounds and relative sensitivity factors provided by the instrument. In some cases, where required, XPS peaks were fitted with Gaussian-Lorentzian peaks (30% Lorentzian).

5.8.5 Antibacterial activity of immobilised peptide

5.8.5.1 Inhibition of *P. aeruginosa* biofilms formation using Live/Dead staining

Overnight grown *P. aeruginosa* culture was diluted to OD_{600}: 0.3. The peptide-free and immobilised glass and silicon were cut into 10 mm x 10 mm squares with a diamond cutter, and inserted into 12 well plates. Titanium-coated surfaces were placed in a large petri dish. The surfaces were covered with 1 mL of Luria broth, and 50 µL of diluted bacteria was added. The substrates were incubated for 48 hours, without shaking, at 37 °C. They were then carefully washed with Milli-Q water to remove any planktonic bacteria, and dried at 50 °C for 20 minutes. The same Live/Dead staining protocol reported in section 4.11.4.3 was used for the immobilised peptides. The biofilms were visualised at 1000 x magnification using a Nikon Eclipse E600 microscope. The stained biofilms were viewed separately using FITC 2 and Texas Red filters, and the images were captured using an in-built digital sight DS-U1 camera.

5.8.5.2 Quantitative analysis of biofilms inhibition by using ImageJ software

Quantitative analyses of biofilms inhibition of the Live/Dead stained images were analysed using ImageJ (U. S. National Institutes of Health, Bethesda, USA) software. ImageJ software measured the amount of fluorescence in the image by using the following formula:[412]

Total cell fluorescence = Integrated density – (area of the selected cell x mean background florescence reading) (5.2)

Where, the integrated density was the total value of the pixels in the selected area, and was calculated by the product of the mean grey value (sum of the grey values of all pixels in selected area divided by the number of pixels) and selected cell area. The mean

background fluorescence reading was the mean grey value of the selected area, without any fluorescence. The total cell fluorescence was calculated separately for SYTO 9 and PI stained images, and three representative images were used for each calculation. Total cell fluorescence was expressed as a percentage where 100% corresponded to mature biofilm architecture (immobilised free sample) and 0% represented total biofilm inhibition.

5.8.5.3 Scanning electron microscopy

Overnight culture of *P. aeruginosa* was diluted to OD_{600}: 0.3 and 1 mL of the diluted sample was incubated with the peptide-free and immobilised surfaces for 4 hours, at 37 °C, without any shaking. Excess bacteria were removed by washing with 10 mM phosphate buffer (pH 7.4). The immobilised slides were fixed with 4% glutaraldehyde in 10 mM phosphate buffer (pH 7.4) for 1 hour. Sample preparation for SEM imaging was followed using the same protocol as reported in section 4.11.8.

Chapter 6

Overall summary and future work

This page has been intentionally left blank

Chapter 6: Overall summary and future work

6.1 Overall summary

This thesis described the synthesis of battacin, a series of cyclic and linear lipopeptide battacin analogues (Chapter 3) and evaluation of antibacterial activity against human (*P. aeruginosa*, *S. aureus* and *E. coli*) and plant (*E. amylovora* and *Pseudomonas syringae pv. actinidiae*) pathogens to identify potent lipopeptides with therapeutic potential (Chapter 4). The most potent lipopeptide GZ3.27 was then extensively analysed, by conducting a series of mechanistic studies and evaluating structural characteristics to understand the importance of structure and the mechanism of action on the observed antibacterial activity (see Chapter 4). Lastly, the active lipopeptide was immobilised on to surface materials used in the medical implant industry, to determine its use as a viable option to prevent the colonisation of bacteria on implants surfaces (see Chapter 5). The major findings from each of these chapters are discussed below.

Chapter 3 described the first total synthesis of battacin **3.14,** using a combination of solid and solution-phase peptide chemistry. The N-terminal fatty acid of battacin, 3-hydroxy-6-methyl-octanoic acid **3.10,** was synthesised separately from commercially available 4-methyl-hexanoic acid **3.5,** following the protocol reported by Sakura *et al*.[249] The synthesis of the fatty acid **3.10** was followed by the synthesis of the protected linear lipopeptide **3.12,** using acid sensitive 2-chlorotrityl chloride resin. The protected linear lipopeptide **3.12** was selectively cyclised between the side chain amine of Dab^2 and the carboxylic acid of Leu^8, under a dilute peptide concentration (1.5 mM) followed, by global deprotection, to generate battacin.

Following the successful synthesis of battacin, five cyclic (GZ3.21, GZ3.15, GZ3.19, GZ3.40 and GZ3.55) and linear amidated lipopeptides (GZ3.130, GZ3.27, GZ3.38, GZ3.26 and GZ3.37) were synthesised, by varying the fatty acid chain length or by Dab substitution with Lys (GZ3.55 and GZ3.37).

In Chapter 4, the *in vitro* antibacterial activity of this battacin library was evaluated, using a broth dilution minimum inhibitory concentration assay (MIC) against human and plant pathogenic bacteria.

The MIC assay revealed several key observations. Conjugation of the longer myristoyl (GZ3.55 and GZ3.40) and geranyl (GZ3.19) fatty acids to the cyclic lipopeptide led to a significant reduction in the antibacterial activity, against all of the tested pathogens. Contrary to findings in previous literature, the linear lipopeptides showed more potent antibacterial activity than the cyclic lipopeptides.[305] In addition, three out of the five linear lipopeptide analogues (GZ3.27, GZ3.26 and GZ3.37) showed potent antibacterial activity against the Gram-positive *S. aureus*, whereas only one of the five cyclic lipopeptide analogues (GZ3.21) had a low MIC (2-5 µM) against *S. aureus*. This surprising result may indicate that the flexibility of the peptide sequence may be crucial for the observed antibacterial activity. The linear lipopeptide, without the N-terminal fatty acid, GZ3.130, showed potent antibacterial activity against the *Pseudomonas* species, but was completely inactive against other bacterial species. Based on the MIC assay, the 4-methyl-hexanoic conjugated linear lipopeptide analogue, GZ3.27 was the most potent analogue, and unlike battacin and polymyxin, was also active against *S. aureus*.

The haemolytic activity of some of the potent lipopeptides was evaluated, using mouse red-blood cells, and showed the longer fatty acid myristoyl conjugated linear lipopeptide analogue (GZ3.26) being highly haemolytic (76% RBC lyses) at 100 µM concentrations.

However, GZ3.27 showed negligible haemolysis (1.79% of RBC lyses) at 100 μM. This result indicated that shorter fatty acid chain conjugated battacin lipopeptides have a safer therapeutic index since they displayed superior antibacterial activity as well as minimal toxicity.

The linear lipopeptide also displayed anti-biofilm activity against the Psa pathogen, *P. aeruginosa* and *S. aureus*, by preventing bacterial colonisation that eventually form biofilms, and dispersing mature biofilms, by penetrating the exopolysaccharide matrix. However, a high concentration of GZ3.27 (10-50 μM) is required to prevent formation of the biofilms of *P. aeruginosa* and *S. aureus*.

The alanine scanning study of GZ3.27 indicates that a core-pentapeptide moiety is crucial for the observed antibacterial activity. This finding was further corroborated when conjugation of 4-methyl-hexanoic acid to this pentapeptide core (GZ3.159) exhibited similar antibacterial activity as GZ3.27, as well as negligible haemolytic activity.

The mechanism of action of GZ3.27 was evaluated using a combination of colorimetric assays, scanning electron microscopy (SEM), outer and inner membrane permeabilisation assays and a high salt assay. Many of the battacin analogues, including GZ3.27, showed a blue to red colour transition in the presence of anionic dimyristoylphosphatidylcholine: tricosadiynoic acid (DMPC-TRCDA) vesicles, indicating a membrane-lytic mechanism of action, caused by the rearrangement of the TRCDA backbone occurred when the peptide interacted with the vesicles. The SEM images of bacterial cells of *P. aeruginosa*, *S. aureus*, *E. coli* and Psa in presence of GZ3.27 showed that they were blistered and corrugated, with cellular remnants scattered across the surface, which indicated the membrane-lytic action. The addition of the lipopeptide, in a concentration-dependent manner, to *P. aeruginosa*, caused an increase in the fluorescent intensity of *N*-phenyl-

naphthylamine, indicating a damaged outer membrane. The fluorescent intensity of propidium iodide also increased with increasing peptide concentration, upon incubation with *S. aureus* and *P. aeruginosa*, indicating a damaged inner cell membrane. However, moderate reduction of antibacterial activity of GZ3.27 was observed against *S. aureus*, *E. coli* and *P. aeruginosa* under high salt concentrations (120 mM NaCl and 2 mM $MgCl_2$), indicating that GZ3.27 competes with the divalent ions at the cationic binding sites on the outer membrane of Gram-negative bacteria.

Circular dichroism (CD) studies identified that GZ3.27 did not adopt any well-defined secondary structures under non-membrane mimetic conditions (phosphate buffer and methanol) or membrane mimetic conditions (TFE, SDS micelles and DMPC-TRCDA). However, under membrane mimetic conditions, GZ3.27 adopts an ordered structural conformation, rather than its initial random coil structure.

The NMR analysis of GZ3.27 also showed a lack of well-defined secondary structure, in the presence of methanol and 30% TFE. The ROESY spectrum of the peptide showed weak sequential $N_iH \leftrightarrow N_{i+1}H$ NOEs and strong sequential $C^{\alpha}{}_iH \leftrightarrow N_{i+1}H$ NOEs, indicating the absence of definite secondary structure, but the tendency to adopt an ordered conformation.

Thus, the NMR, CD and membrane binding studies investigated in this thesis have suggested, that a well-defined secondary structure is not important for the membrane-lytic antibacterial activity of GZ3.27.

The aforementioned results also suggest that GZ3.27 has a similar mechanism of action to polymyxins, against Gram-negative bacteria. The unstructured GZ3.27 adopts into a more favoured, ordered conformation, near the outer membrane of Gram-negative bacteria. The side chain amines of Dab interact with the cationic binding sites in the lipid A of the

lipopolysaccharide of the outer membrane, causing outer membrane destabilisation. Following this initial electrostatic interaction, the dipeptide core (D-Phe-Leu), and the fatty acyl of GZ3.27 probably interact with the anionic phospholipids, and permeate the outer membrane and GZ3.27 translocates to the inner membrane via a "self-uptake" mechanism, similar to that of polymyxin. This leads to inner membrane disruption and intracellular leakage, ultimately leading to cell death.

In the vicinity of the cell wall, the side chain amines of the lipopeptide most likely interact with the anionic teichoic acids in the Gram-positive *S. aureus*. Subsequently, the peptide may diffuse through the thick peptidoglycan layer, to reach the inner membrane. The hydrophobic domains of GZ3.27 most likely interact with the anionic phospholipids in the inner membrane, leading to membrane destabilisation and subsequent membrane lysis.

Chapter 5 described the immobilisation of the active lipopeptide GZ3.27 onto solid surface materials used in the medical implant industry.

The first part of this chapter described the effective design of immobilised AMP surfaces. Three different surfaces were chosen for immobilisation studies: glass, silicon and titanium. Glass was chosen to optimise the surface chemistry while the two latter surfaces are extensively used in the medical implant industry.

These surfaces were first treated with a piranha solution, to remove any organic surface contaminants and to expose reactive hydroxyl groups to maximise surface attachment. The piranha-treated samples were then silanized with 3-aminopropyltriethoxysilane (APTES), to facilitate the conjugation of the peptides onto the substrate. Then, the APTES treated samples were conjugated with a flexible heterobifunctional PEG linker (NHS-PEG_{24}-MAL), where the *N*-hydroxy succinimide (NHS) reacts with the terminal

amines of APTES, while the maleimide (MAL) forms a selective, covalent thiol-linkage with the cysteine residue in the peptide, thus maintaining the mobility of the peptide, crucial for its antibacterial activity.

In order to conjugate GZ3.27 to the MAL of the PEG linker, GZ3.27 was modified by introducing a Cys amino acid at either the N-terminus (GZ3.163), C-terminus (GZ3.160) or side chain Dab^2 (GZ3.155). The antibacterial activity of the Cys-modified analogues were tested against *E. coli*, *P. aeruginosa*, *S. aureus* and Psa pathogen, to identify a potent analogue for the immobilisation study. The MIC assay revealed that the Cys modification did not cause any significant reduction in antibacterial activity, except for GZ3.155, where a moderate reduction in activity was observed against *E. coli* (25-50 μM). The N-terminally Cys-conjugated GZ3.163 was thus chosen for the immobilisation studies.

The second part of Chapter 5 validated the step-by-step immobilisation of GZ3.163 onto the surface, using techniques such as water-contact angle measurements, ellipsometry and X-Ray photoelectron spectroscopy (XPS). Changes in the contact angle during each of the functionalisation steps, indicated changes in the surface wettability, which indirectly validated the successful grafting of different layers onto the surface. Ellipsometry measurements of the immobilised peptide onto the silicon revealed that a thin monolayer of the peptide (190 ng cm^{-2}) was deposited onto the surface. XPS measurements confirmed the successful immobilisation of GZ3.163 onto silicon and titanium surfaces, as indicated by the increase in nitrogen 1s at 7.2% and 9.6% on the immobilised surfaces, caused by the presence of the side chain amines of Dabs and the amides from the peptide bonds.

The antibacterial activity of the immobilised peptide surfaces was evaluated by a Live/Dead biofilm assay and SEM imaging of *P. aeruginosa* interaction. Immobilisation of the peptide on glass, silicon and titanium surfaces successfully inhibited the formation of *P. aeruginosa* biofilms, for up to 48 hours, as determined by qualitative (Live/Dead staining) and quantitative (ImageJ) analysis. SEM images of the bacteria on the immobilised surfaces showed a similar corrugated and blistered cellular morphology as the solubilised GZ3.27, indicating the retention of the membrane-lytic activity of the peptide upon surface immobilisation.

Overall, the linearisation of battacin (and the truncated pentapeptide) not only improves the therapeutic potential but also simplifies the synthesis of complex lipopeptides. This leads to a reduction in manufacturing cost, thereby further enhancing the development of clinically relevant AMPs. The ability of the linear lipopeptide to prevent bacterial biofilms, both before and after surface immobilisation, is highly desirable. Therefore, the results summarised in this thesis represent an important advancement in the development of novel therapeutics against multi-drug resistant bacteria, and in particular targeting the bacterial biofilm formation and maturation.

6.2 Future Work

The potent linear lipopeptide GZ3.27 could be developed into a novel therapeutic to combat biofilm-forming pathogens. However, further experiments are needed to evaluate its therapeutic potential. The antibacterial and anti-biofilm efficacy of GZ3.27 against multi-drug resistant pathogens is yet to be tested. Even though lipidation and C-terminal amidation is known to increase the peptide stability, this will have to be experimentally verified using serum protease assays.

Preliminary results have shown that the linear lipopeptide, without the N-terminal fatty acid, GZ3.130, is highly selective towards *Pseudomonas* species, and the ability to inhibit these pathogenic bacteria selectively, without inhibiting other beneficial bacteria, could be highly desirable. However, in order to validate the selectivity of GZ3.130 toward *Pseudomonas* spp., antibacterial testing against a broad spectrum of bacterial species, as well as some multi-drug resistant *Pseudomonas* spp., will be required.

The antibacterial activity of the immobilised surface against *S. aureus* is yet to be tested, since this pathogen is capable of colonising numerous medical implants. The long-term stability of these peptide-immobilised surfaces are also yet to be determined.

Appendices

This page has been intentionally left blank

Appendices

Appendix A: Physical characteristics of peptides

Peptide		HPLC gradient (% solvent B; Time)	HPLC R_t(min) and % Purity	Yield (%)[a]	Molecular formula	Calculated $[M+H]^+$	Observed $[M+H]^+$
Cyclic	Battacin	20-45%;25 min	9.50;96.87%	2.9%	$C_{50}H_{88}N_{13}O_{10}$	1030.6772	1030.6743
	GZ3.21	10-60%;30 min	18.09;96.92%	6.3%	$C_{56}H_{82}N_{13}O_{10}$	1096.6302	1096.6268
	GZ3.15	10-60%;30 min	15.68;98.50%	2.2%	$C_{48}H_{84}N_{13}O_{9}$	986.6509	986.6452
	GZ3.19	10-60%;30 min	16.81;96.69%	1.1%	$C_{51}H_{86}N_{13}O_{9}$	1024.6666	1024.6647
	GZ3.40	10-80%;30 min	19.59;95.98%	4.6%	$C_{55}H_{98}N_{13}O_{9}$	1084.7605	1084.7586
	GZ3.55	10-80%;30 min	18.69;97.45%	7.3%	$C_{65}H_{118}N_{13}O_{9}$	1224.9170	1224.9117
Linear	GZ3.27	10-55%;30 min	20.93;99.50%	70.0%	$C_{48}H_{87}N_{14}O_{9}$	1003.6775	1003.6786
	GZ3.38	10-60%;30 min	14.00;98.19%	10.5%	$C_{51}H_{89}N_{14}O_{9}$	1041.6931	1041.6917
	GZ3.26	10-60%;30 min	22.86;98.07%	23.0%	$C_{55}H_{101}N_{14}O_{9}$	1101.7870	1101.7798
	GZ3.37	10-60%;30 min	22.12;98.12%	24.2%	$C_{65}H_{121}N_{14}O_{9}$	1241.9435	1241.9326
	GZ3.130	10-60%;30 min	11.63;99.17%	32.3%	$C_{41}H_{75}N_{14}O_{8}$	891.5887	891.5919
	GZ3.148	10-55%;30 min	16.23;87.38%	8.1%	$C_{89}H_{159}N_{27}O_{17}$[b]	939.1198[b]	939.1123[b]

GZ3.149	10-55%;30 min	16.90;84.23%	6.5%	$C_{130}H_{230}N_{240}O_{25}$ [b]	1375.9024	1375.8972
GZ3.159	10-60%;30 min	17.30;97.44 %	28.9%	$C_{34}H_{60}N_9O_6$	690.4661	690.6484
Ala[1]	10-60%;30 min	17.28;88.12%	65.2% [c]	$C_{47}H_{83}N_{12}O_{10}$	975.6350	975.6351
Ala[2]	10-60%;30 min	16.70;91.49%	72.0%[c]	$C_{47}H_{83}N_{12}O_{10}$	975.6350	975.6385
Ala[3]	10-60%;30 min	16.81;90.14%	95.3% [c]	$C_{47}H_{83}N_{12}O_{10}$	975.6350	975.6383
Ala[4]	10-60%;30 min	13.05;82.08%	59.2% [c]	$C_{45}H_{80}N_{13}O_{10}$	962.6146	962.6174
Ala[5]	10-60%;30 min	20.01;40.76%	92.6% [c]	$C_{42}H_{82}N_{13}O_{10}$	928.6302	928.6330
Ala[6]	10-60%;30 min	17.37;87.92%	20.4% [c]	$C_{47}H_{83}N_{12}O_{10}$	975.6350	975.6375
Ala[7]	10-60%;30 min	16.89;81.99%	91.0%[c]	$C_{47}H_{83}N_{12}O_{10}$	975.6350	975.6386
Ala[8]	10-60%;30 min	13.81;83.97%	27.8% [c]	$C_{45}H_{80}N_{13}O_{10}$	962.6146	962.6158
GZ3.155	10-55%;30 min	15.55;98.50%	4.5%	$C_{51}H_{92}N_{15}O_{10}S$	1106.6867	1106.6883
GZ3.160	10-55%;30 min	17.89;95.26%	13.6%	$C_{51}H_{92}N_{15}O_{10}S$	1106.6867	1106.6875
GZ3.163	10-55%;30 min	18.63;96.47%	22.7%	$C_{51}H_{92}N_{15}O_{10}S$	1106.6867	1106.6885

[a] RP-HPLC purified peptides, [b] $[M+2H]^{2+}$ instead of $[M+H]^+$, [c] % crude yield

Appendix B: HPLC traces

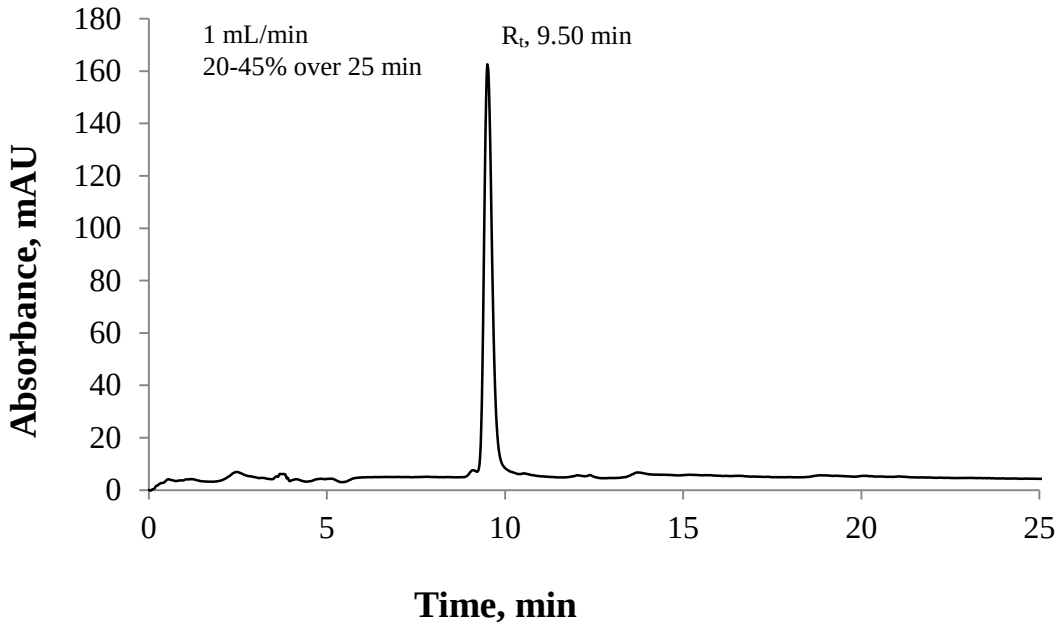

Figure B1 Battacin

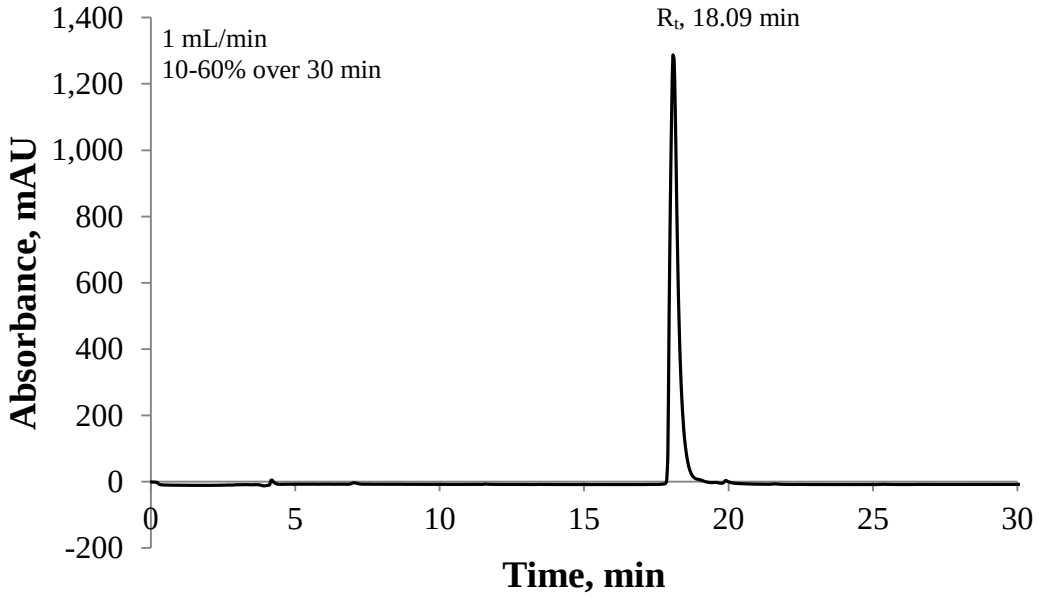

Figure B2 GZ3.21 Fmoc-D-Dab-cyclo[Dab-Dab-Leu-D-Phe-Dab-Dab-Leu]

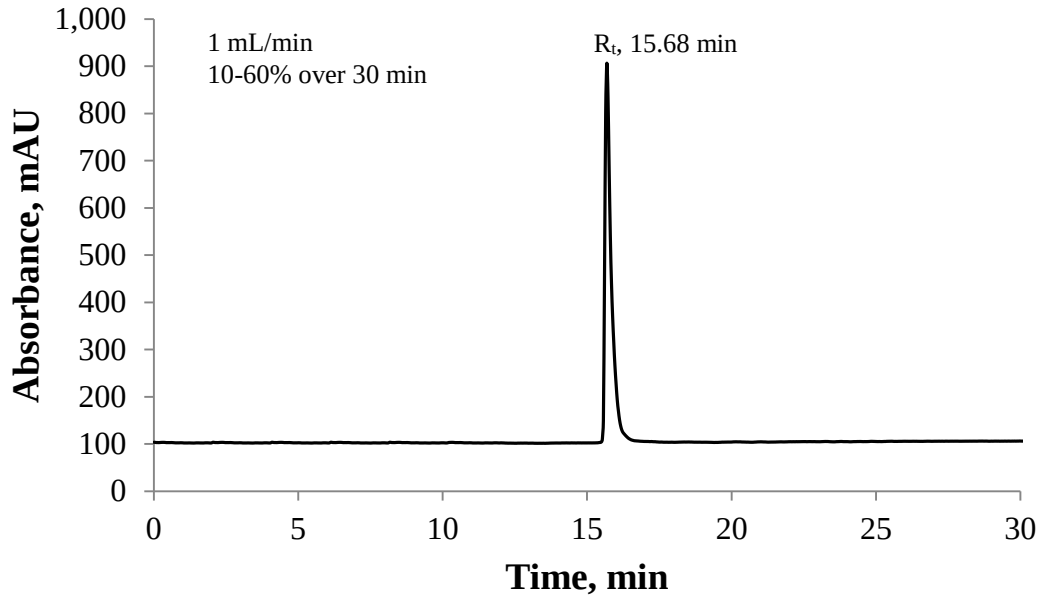

Figure B3 GZ3.15 R^1-D-Dab-*cyclo*[Dab-Dab-Leu-D-Phe-Dab-Dab-Leu] (R_1 = 4-methyl -hexanoyl).

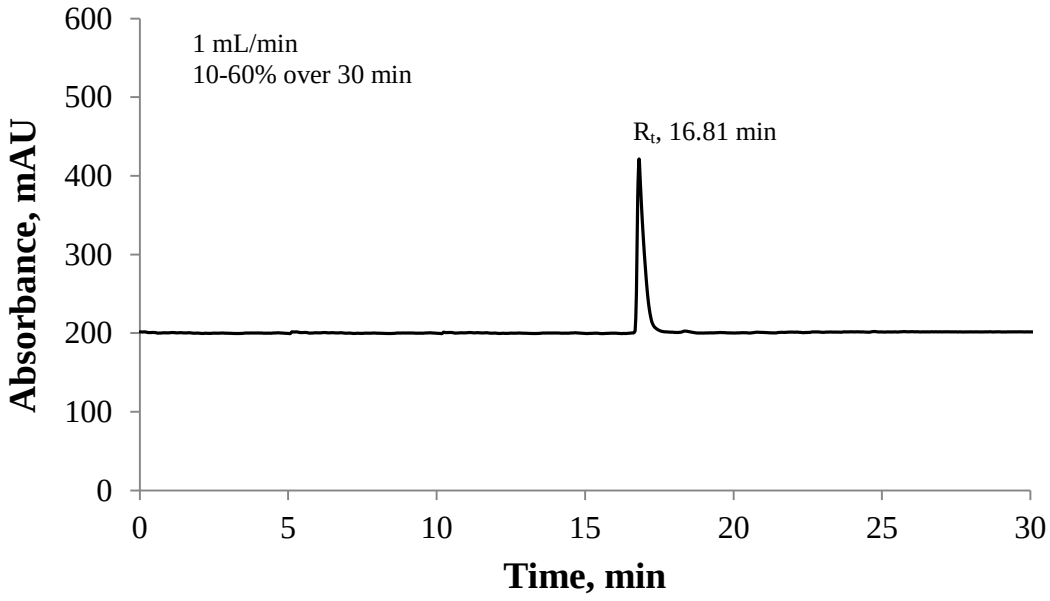

Figure B4 GZ3.19 R^2-D-Dab-*cyclo*[Dab-Dab-Leu-D-Phe-Dab-Dab-Leu] (R_2 = geranyl).

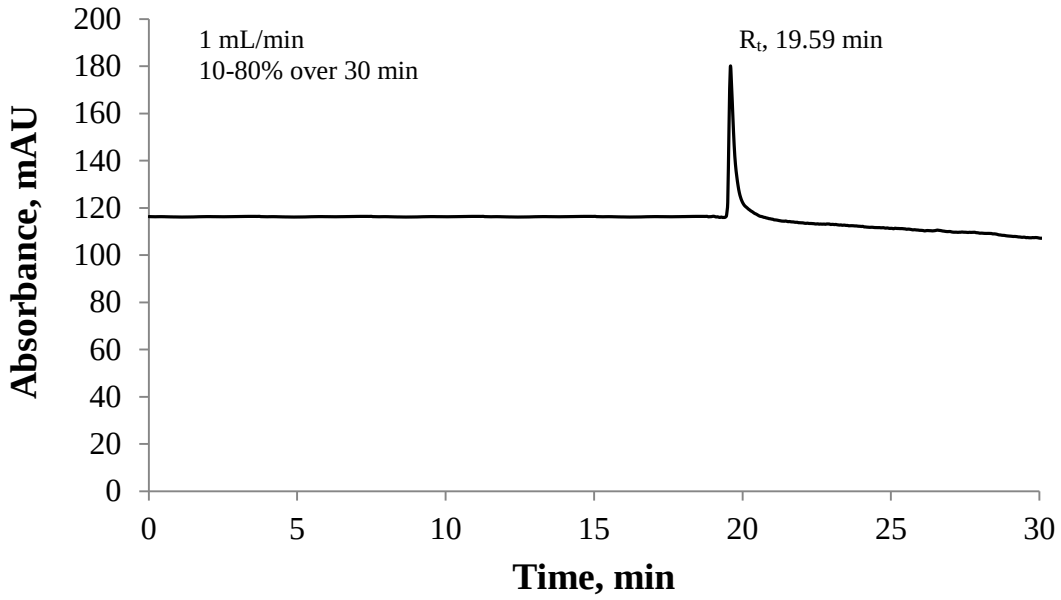

Figure B5 GZ3.40 R^3-D-Dab-*cyclo*[Dab-Dab-Leu-D-Phe-Dab-Dab-Leu] (R_3 = myristoyl)

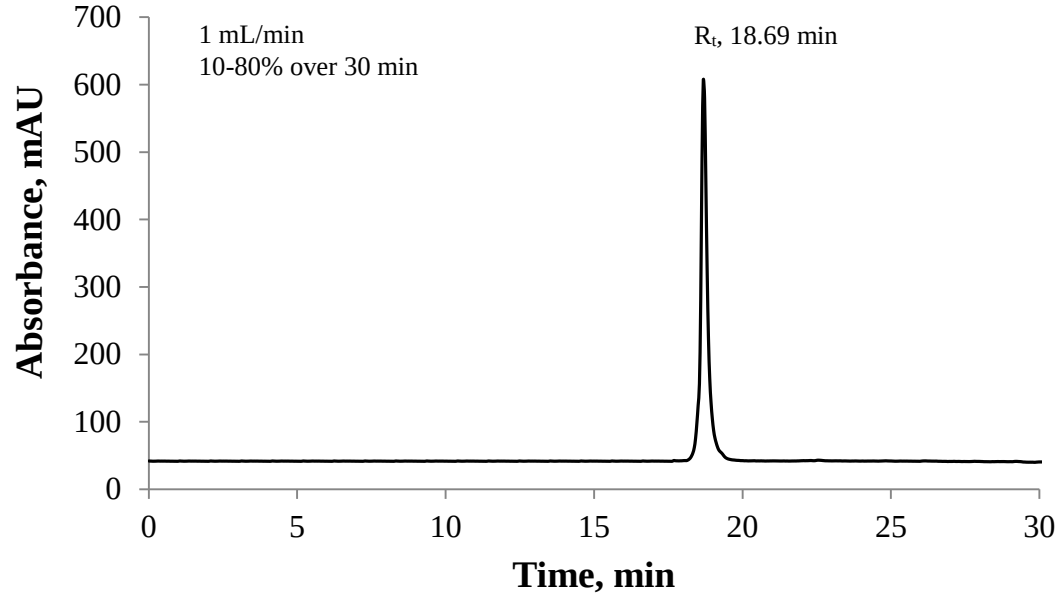

Figure B6 GZ3.55 R^3-D-Lys-*cyclo*[Lys-Lys-Leu-D-Phe-Lys-Lys-Leu] (R_3 = myristoyl)

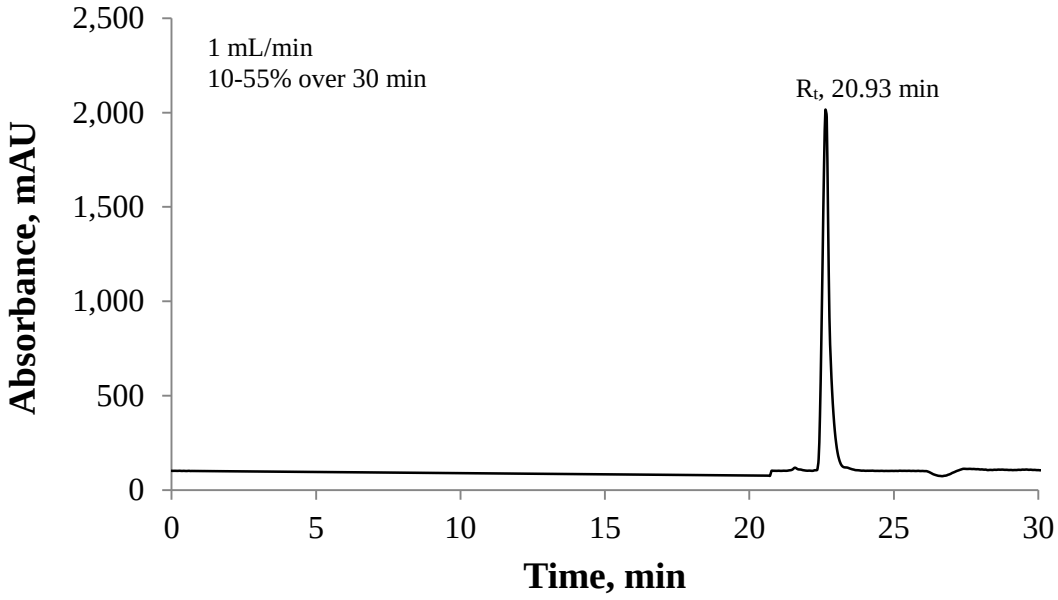

Figure B7 GZ3.27 R^1-D-Dab-Dab-Dab-Leu-D-Phe-Dab-Dab-Leu-NH_2 (R_1 = 4-methyl-hexanoyl).

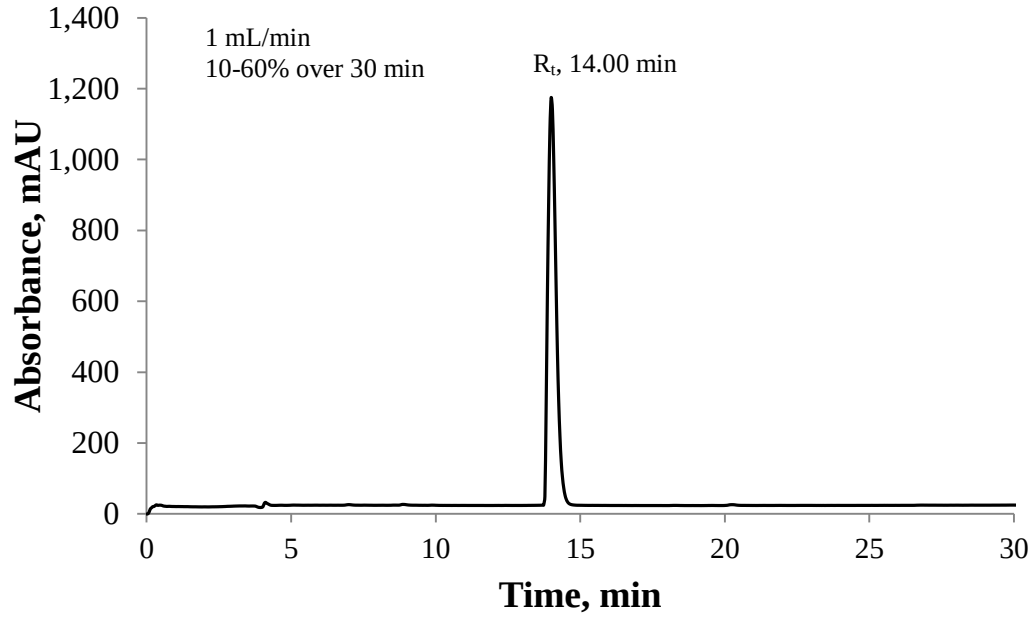

Figure B8 GZ3.38 R^2-D-Dab-Dab-Dab-Leu-D-Phe-Dab-Dab-Leu-NH_2 (R_2 = geranyl).

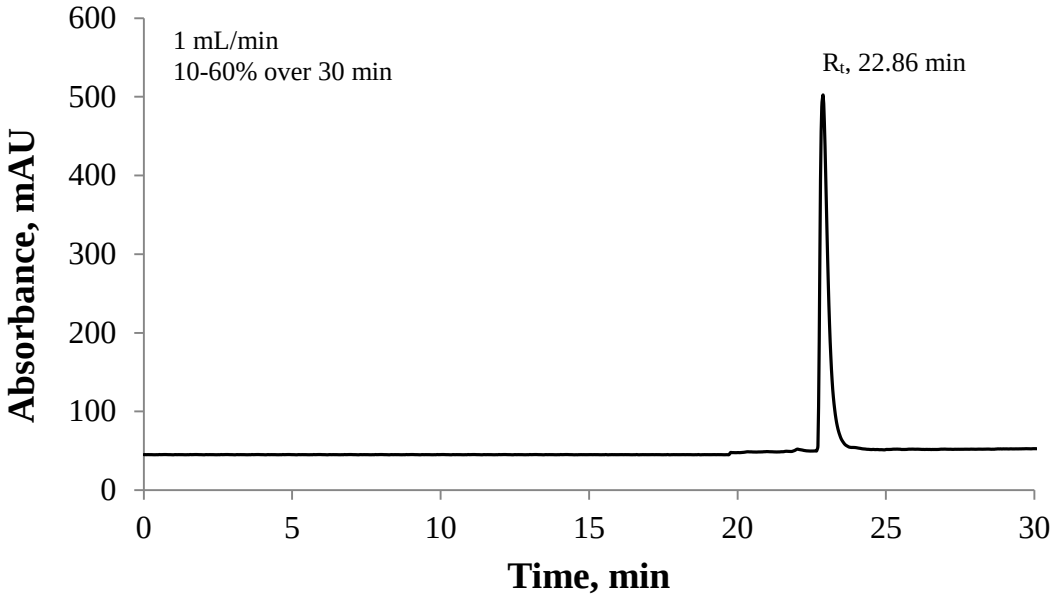

Figure B9 GZ3.26 R^3-D-Dab-Dab-Dab-Leu-D-Phe-Dab-Dab-Leu-NH_2 (R_3 = myristoyl).

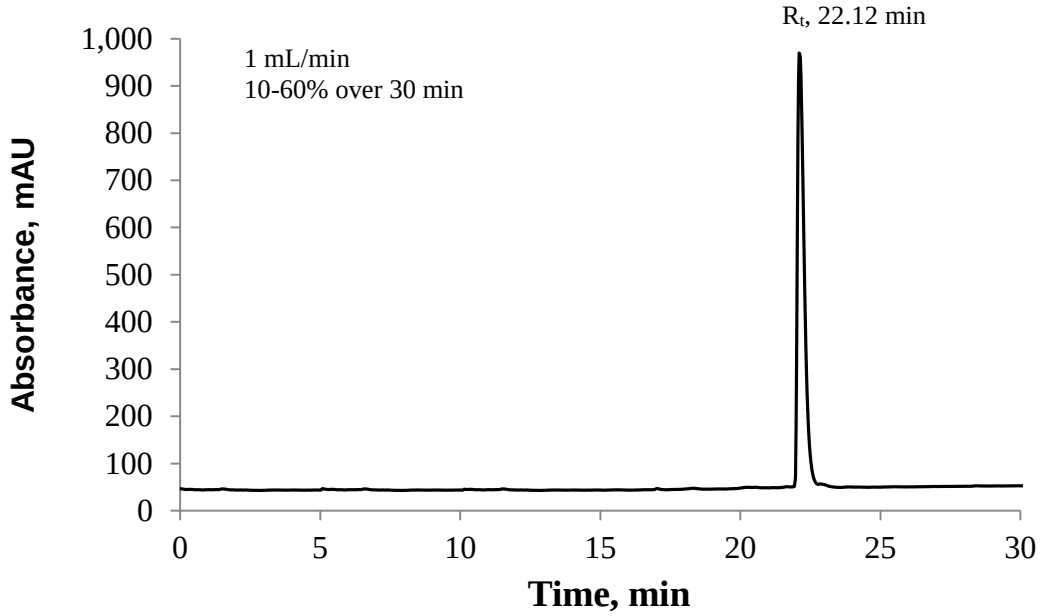

Figure B10 GZ3.37 R^3-D-Lys-Lys-Lys-Leu-D-Phe-Lys-Lys-Leu-NH_2 (R_3 = myristoyl).

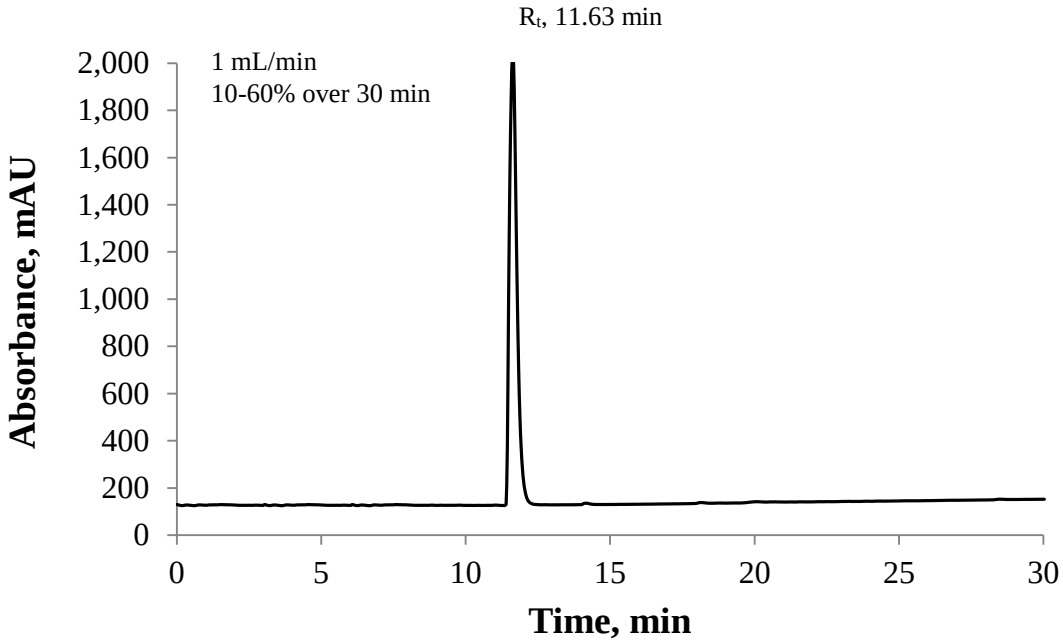

Figure B11 GZ3.130 NH_2-D-Dab-Dab-Dab-Leu-D-Phe-Dab-Dab-Leu-NH_2.

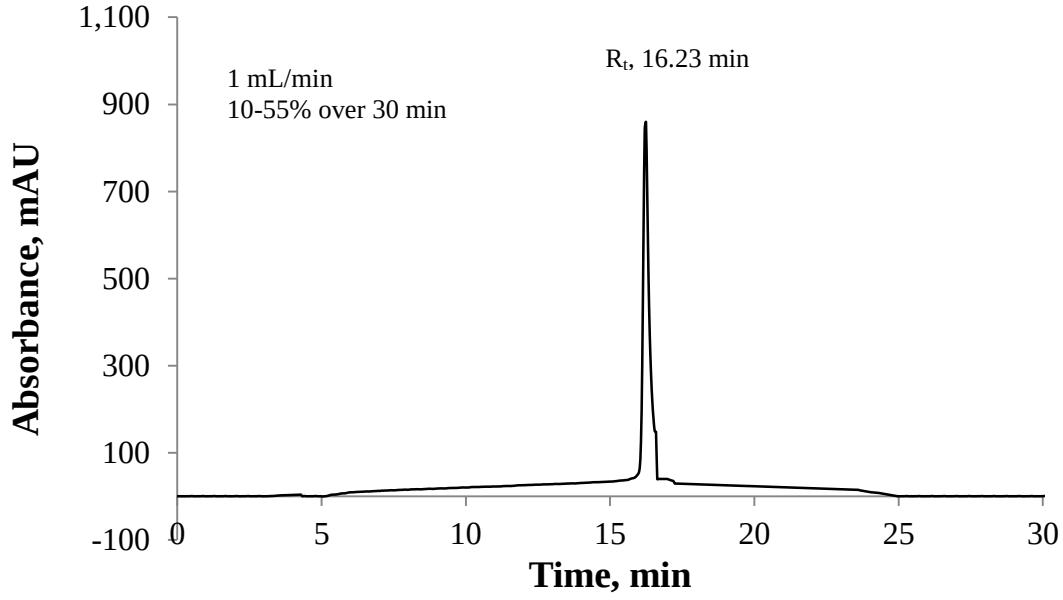

Figure B12 GZ3.148 R_1-D-Dab-Dab-Dab-Leu-D-Phe-Dab-Dab-Leu-D-Dab-Dab-Dab-Leu-D-Phe-Dab-Dab-Leu-NH_2 (R_1 = 4-methyl-hexanoyl).

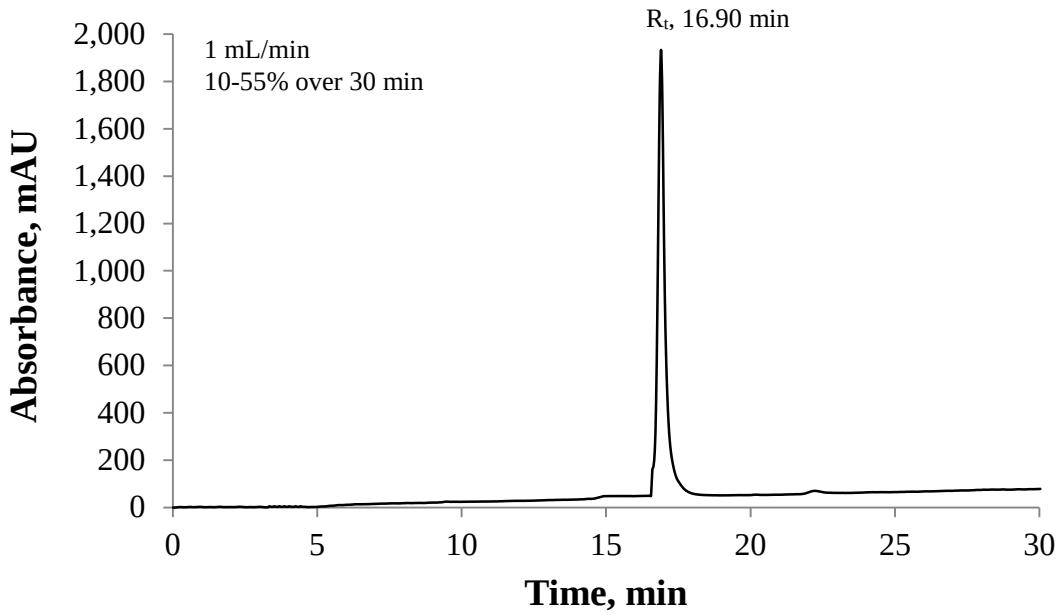

Figure B13 GZ3.149 R_1-D-Dab-Dab-Dab-Leu-D-Phe-Dab-Dab-Leu-D-Dab-Dab-Dab-Leu-D-Phe-Dab-Dab-Leu- D-Dab-Dab-Dab-Leu-D-Phe-Dab-Dab-Leu-NH_2. (R_1 = 4-methyl-hexanoyl).

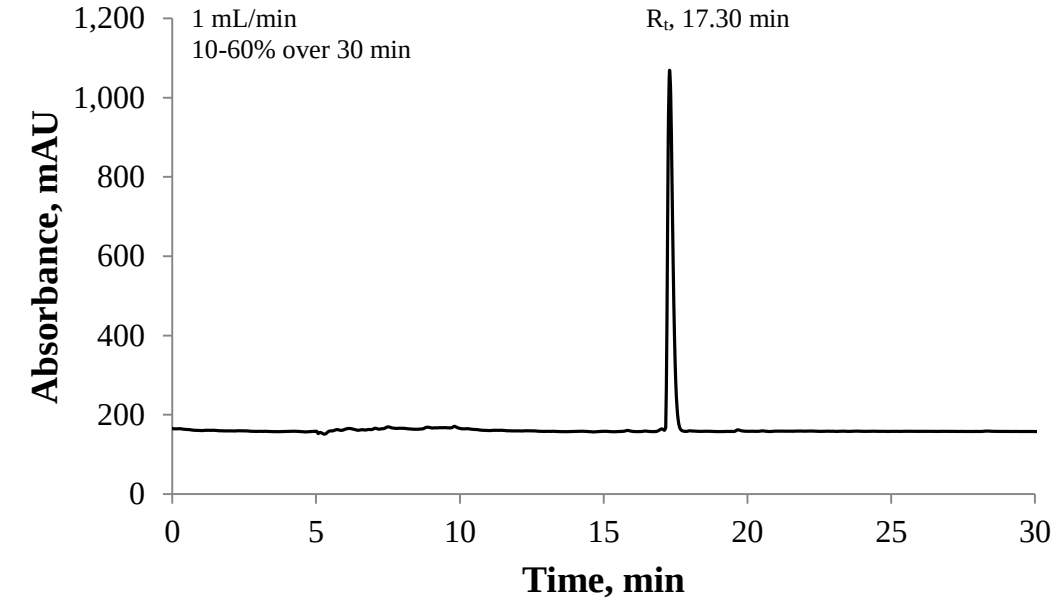

Figure B14 GZ3.159 R^1-D-Dab-Dab-Leu-D-Phe-Dab-NH_2 (R_1 = 4-methyl-hexanoyl).

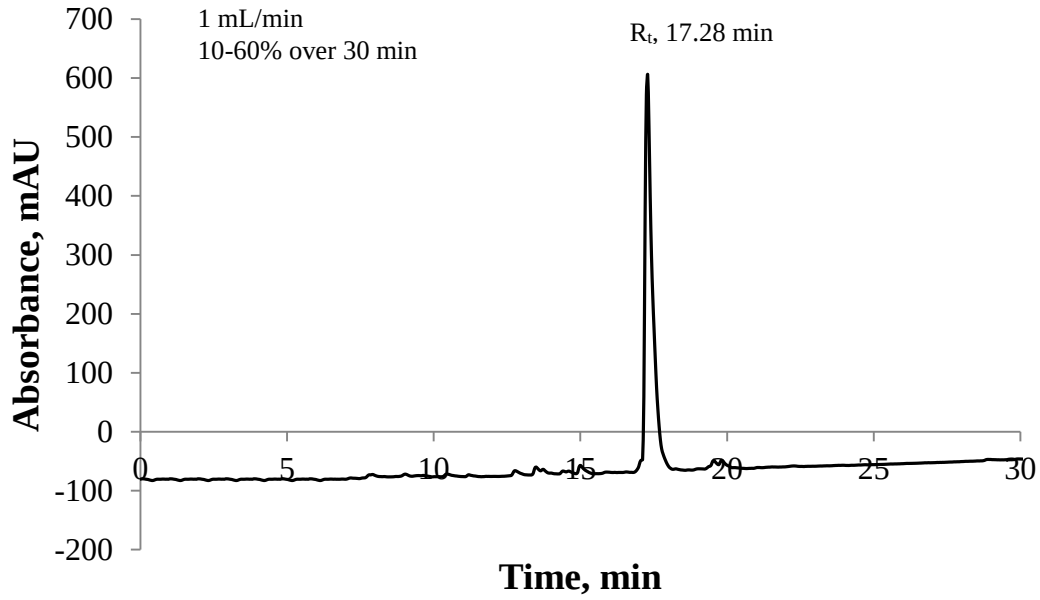

Figure B15 Ala[1] R[1]-Ala-Dab-Dab-Leu-D-Phe-Dab-Dab-Leu-OH (R_1 = 4-methyl-hexanoyl).

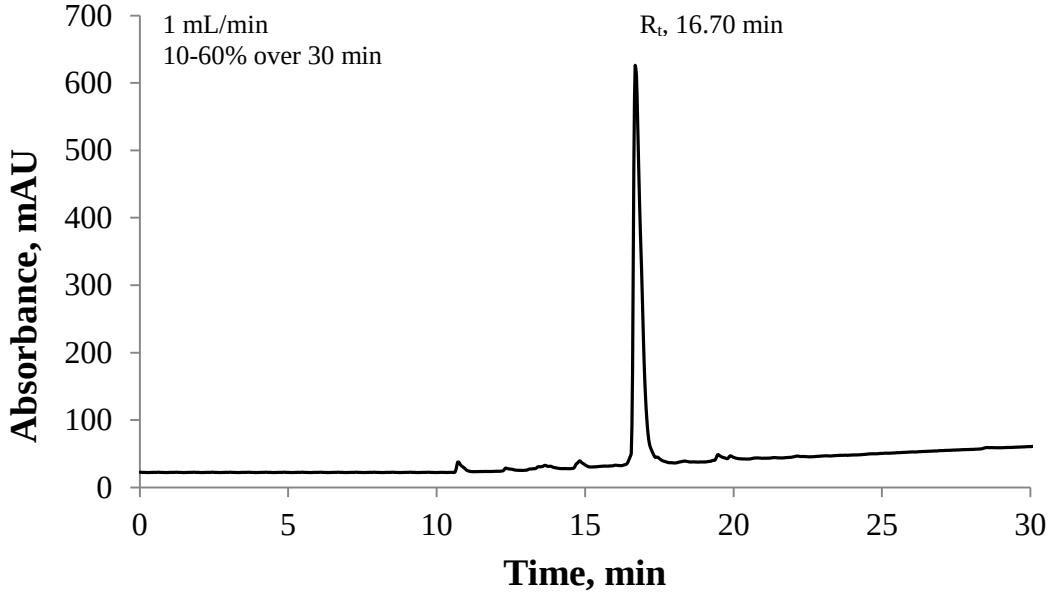

Figure B16 Ala[2] R[1]-D-Dab-Ala-Dab-Leu-D-Phe-Dab-Dab-Leu-OH (R_1 = 4-methyl hexanoyl).

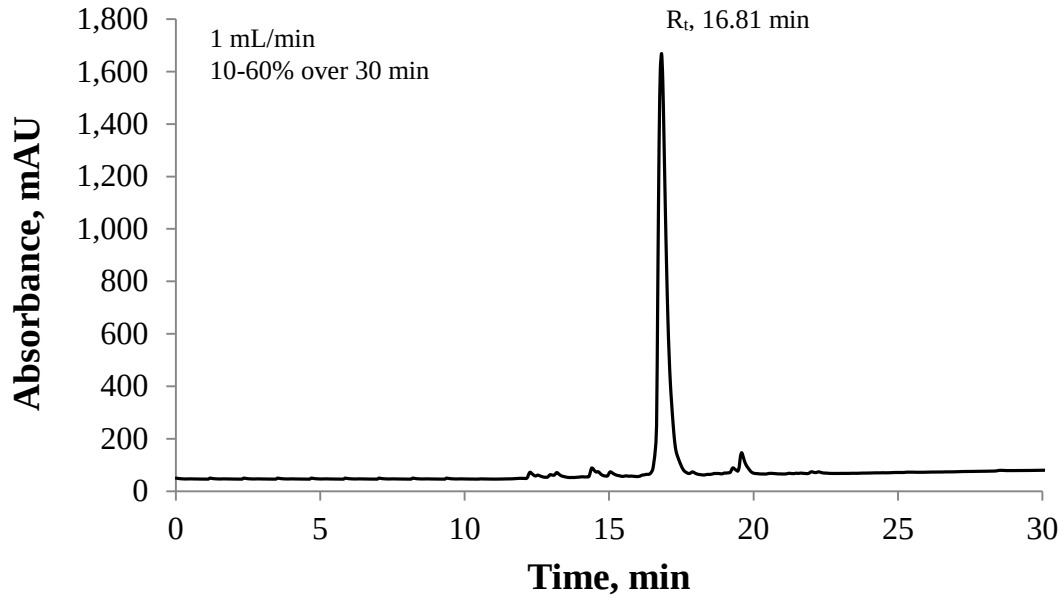

Figure B17 Ala[3] R^1-D-Dab-Dab-Ala-Leu-D-Phe-Dab-Dab-Leu-OH (R_1 = 4-methyl-hexanoyl).

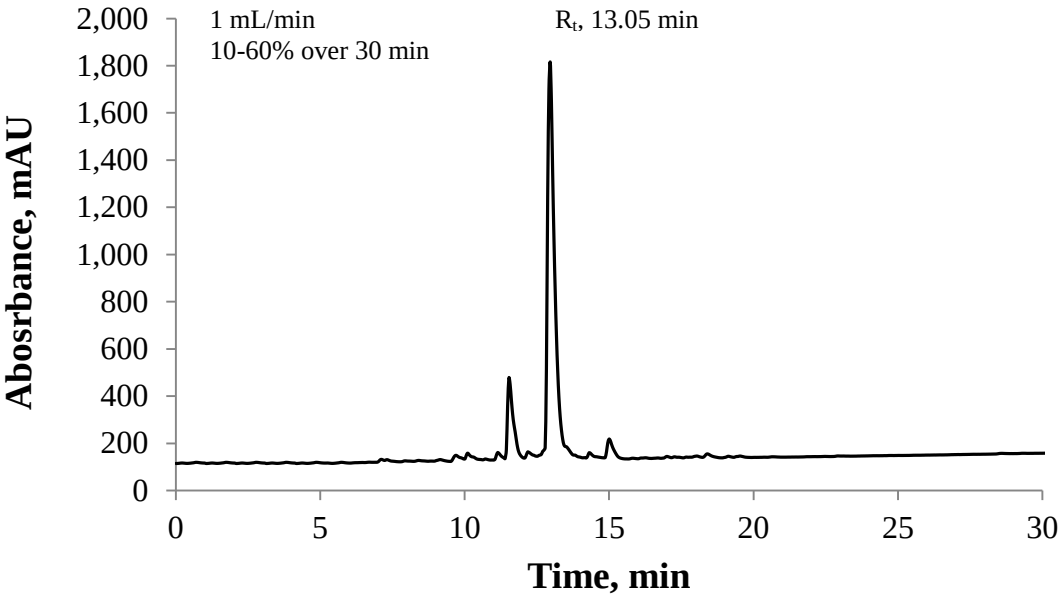

Figure B18 Ala[4] R^1-D-Dab-Dab-Dab-Ala-D-Phe-Dab-Dab-Leu-OH (R_1 = 4-methyl-hexanoyl).

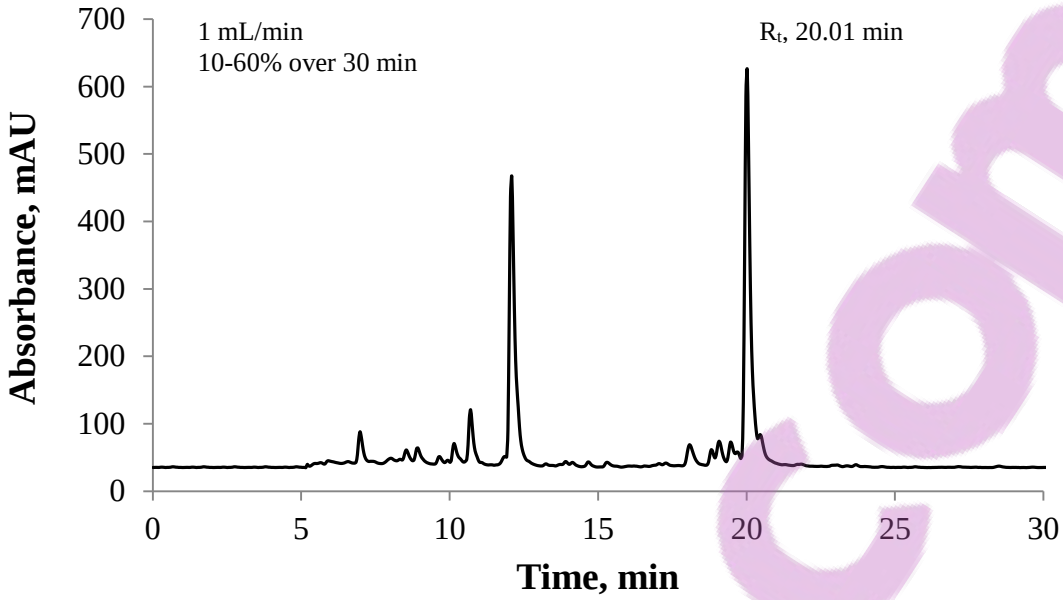

Figure B19 Ala[5] R^1-D-Dab-Dab-Dab-Leu-Ala-Dab-Dab-Leu-OH (R_1 = 4-methyl-hexanoyl).

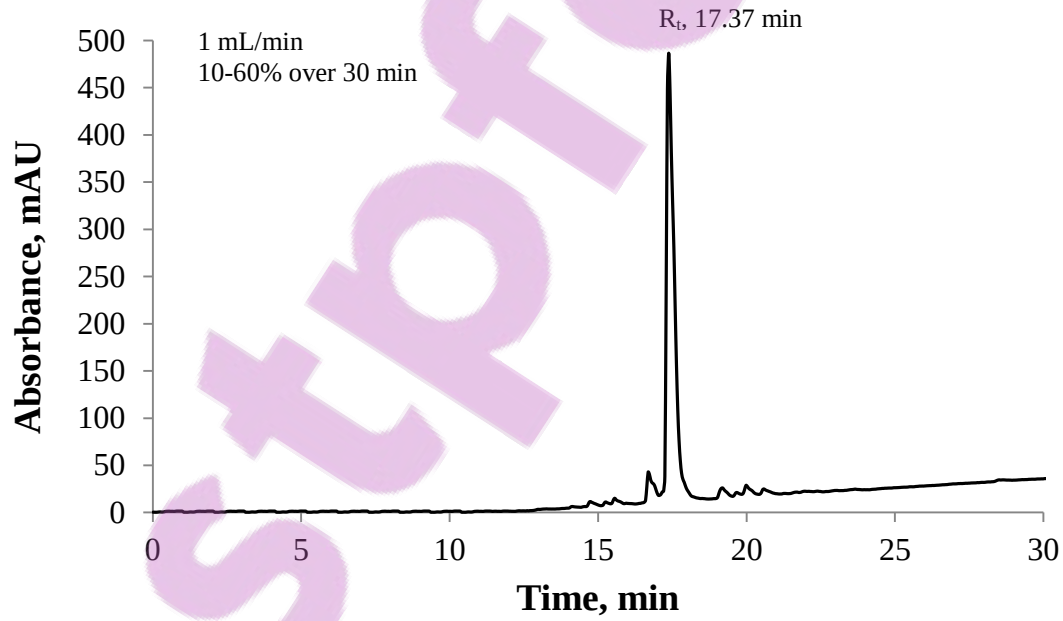

Figure B20 Ala[6] R^1-D-Dab-Dab-Dab-Leu-D-Phe-Ala-Dab-Leu-OH (R_1 = 4-methyl-hexanoyl).

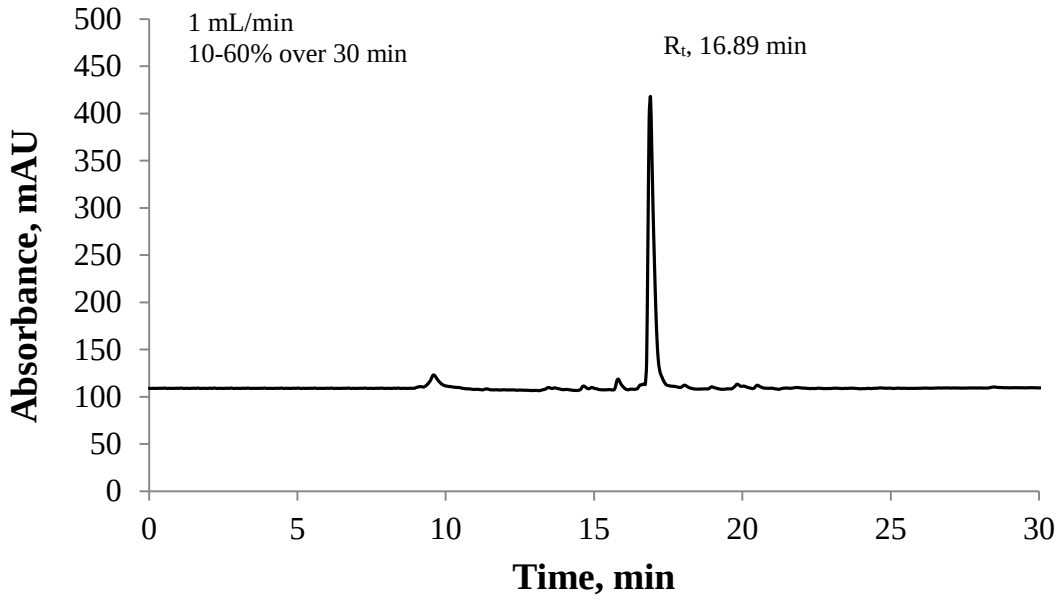

Figure B21 Ala[7] R^1-D-Dab-Dab-Dab-Leu-D-Phe-Dab-Ala-Leu-OH (R_1 = 4-methyl-hexanoyl).

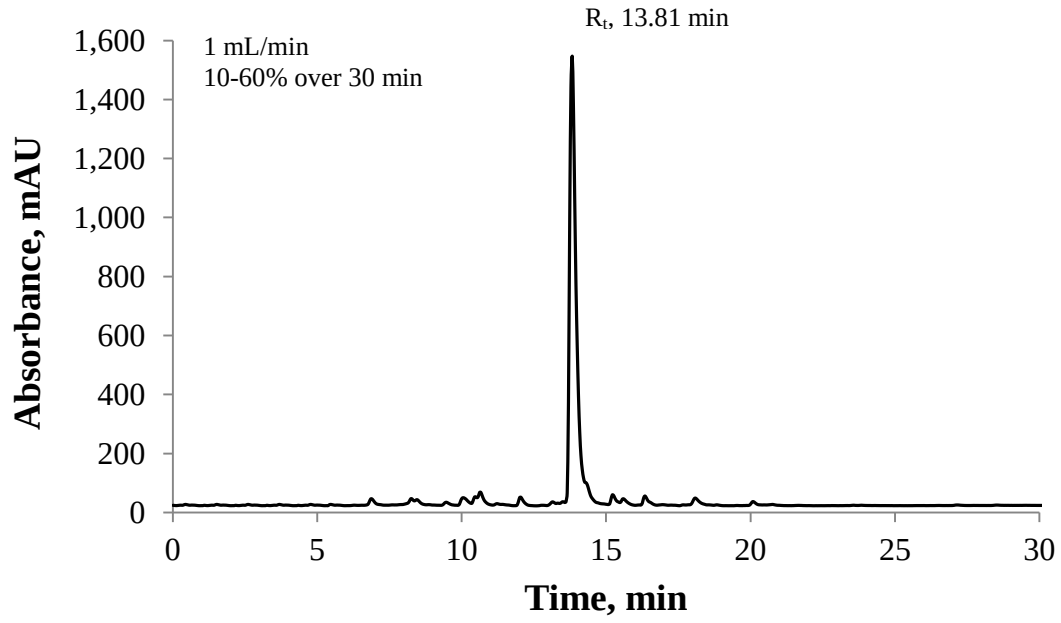

Figure B22 Ala[8] R^1-D-Dab-Dab-Dab-Leu-D-Phe-Dab-Dab-Ala-OH (R_1 = 4-methyl-hexanoyl).

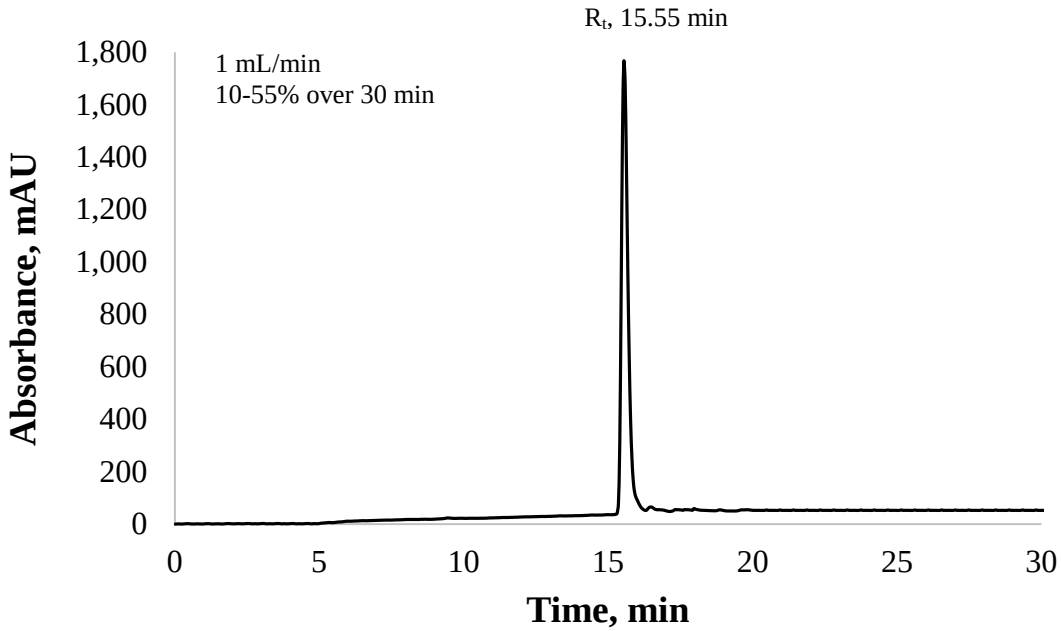

Figure B23 GZ3.155 R_1-D-Dab-Dab(Cys)-Dab-Leu-D-Phe-Dab-Dab-Leu-NH_2

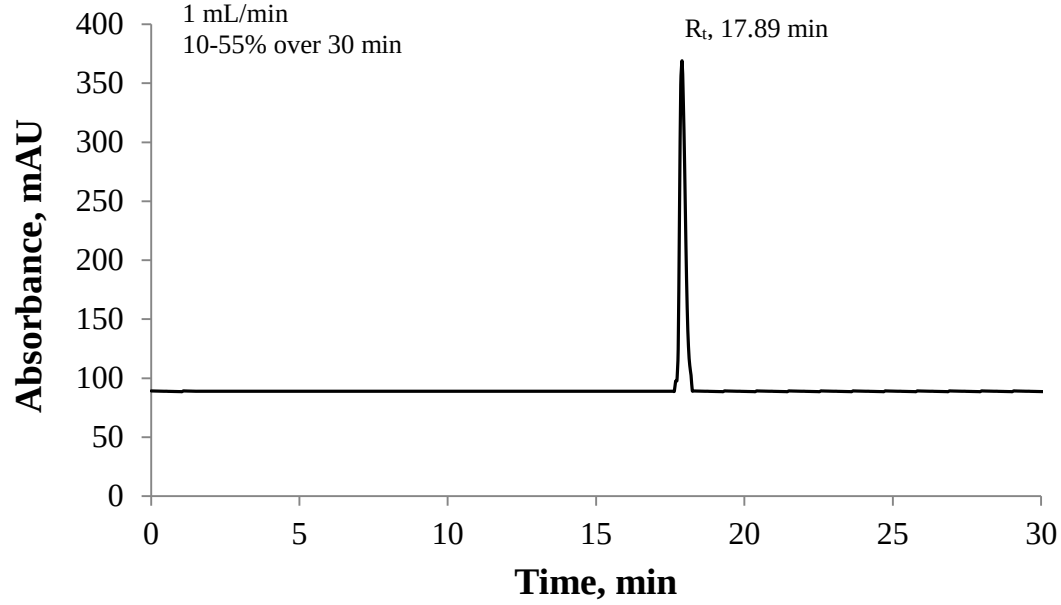

Figure B24 GZ3.160 R_1-D-Dab-Dab-Dab-Leu-D-Phe-Dab-Dab-Leu-Cys-NH_2 (R_1 = 4-methyl-hexanoyl).

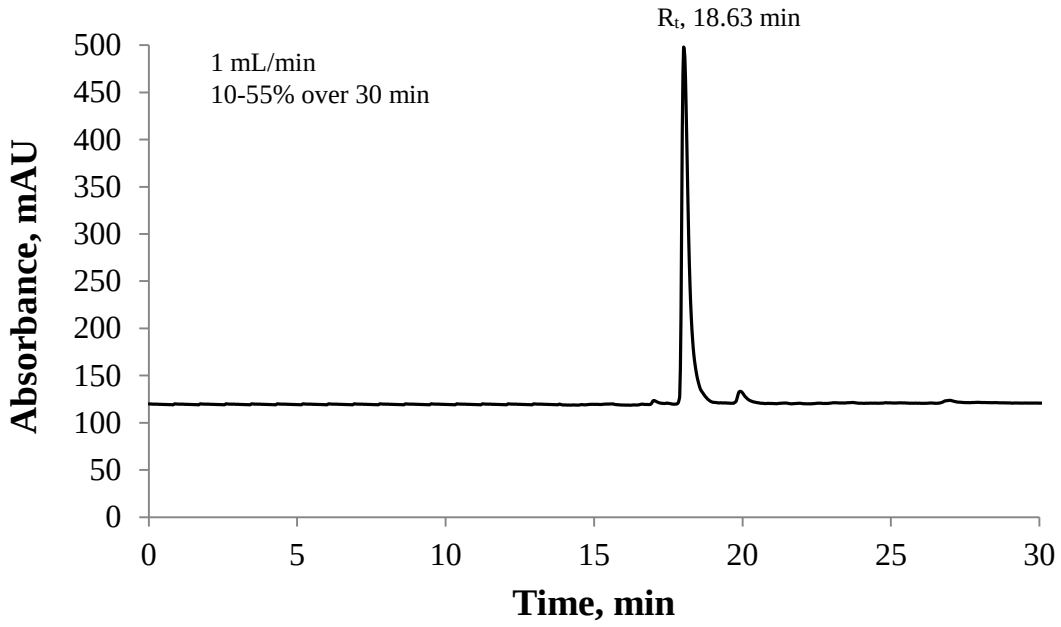

Figure B25 GZ3.163 R_1-Cys-D-Dab-Dab-Dab-Leu-D-Phe-Dab-Dab-Leu-NH_2 (R_1 = 4-methyl-hexanoyl).

Appendix C: HRMS (EI) spectra

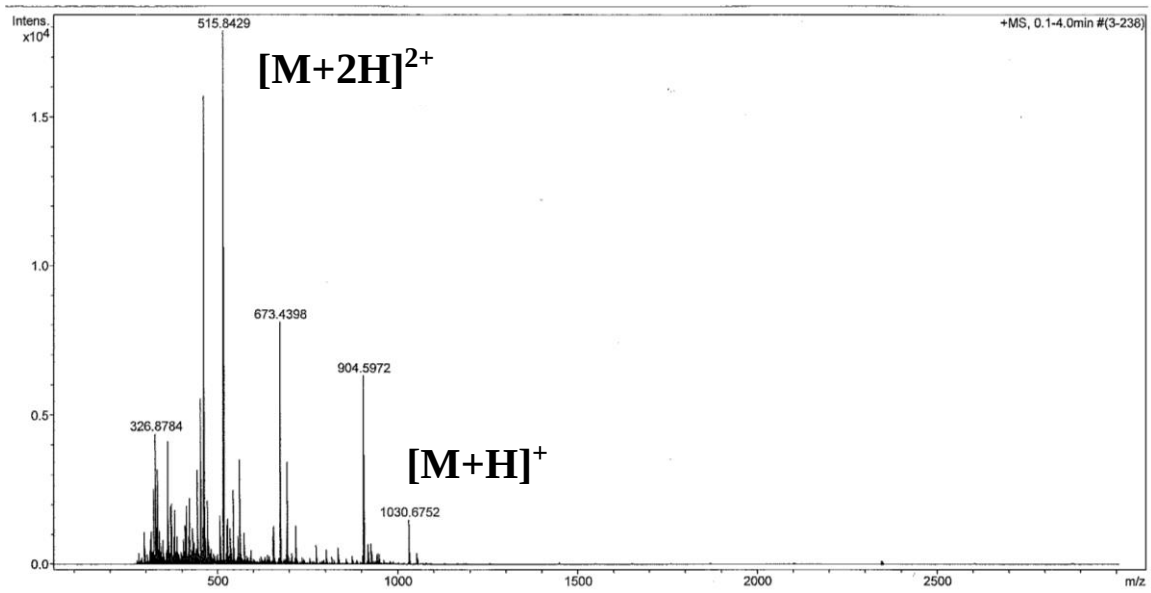

Figure C1 battacin HRMS (EI) (calculated for $[M+H]^+$ = 1030.6772).

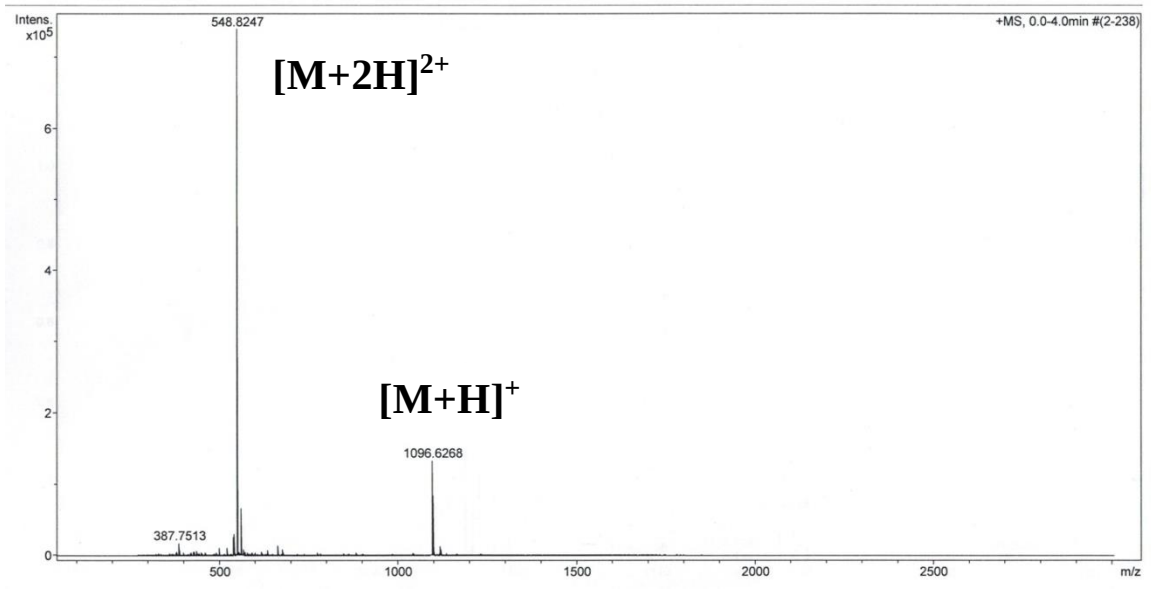

Figure C2 GZ3.21 HRMS (EI) (calculated for $[M+H]^+$ = 1096.6302).

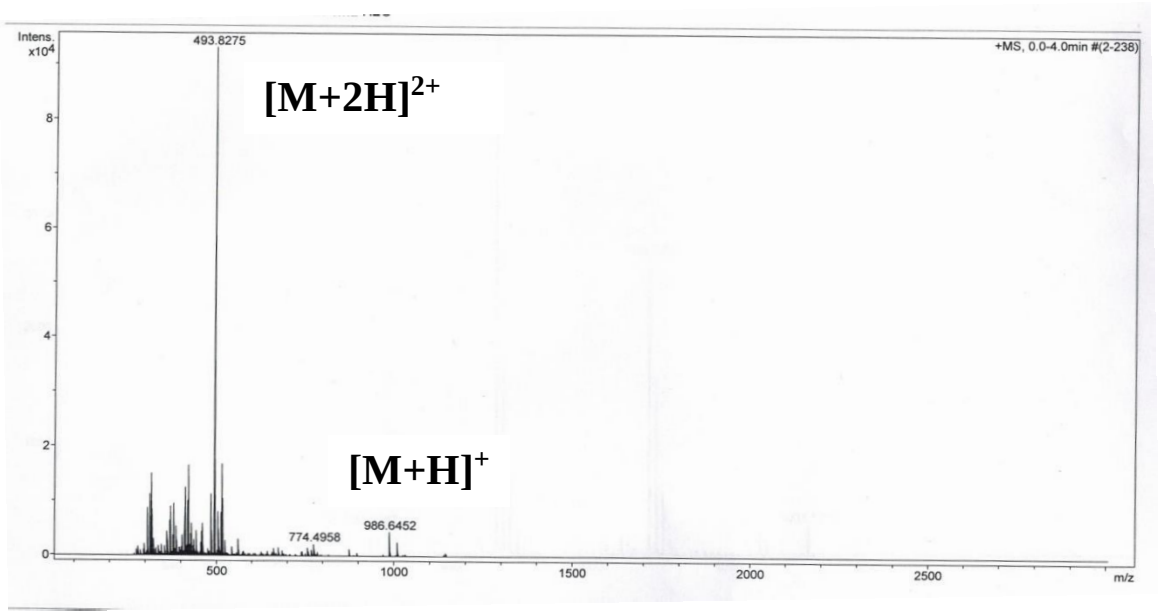

Figure C3 GZ3.15 HRMS (EI) (calculated for $[M+H]^+$ = 986.6509)

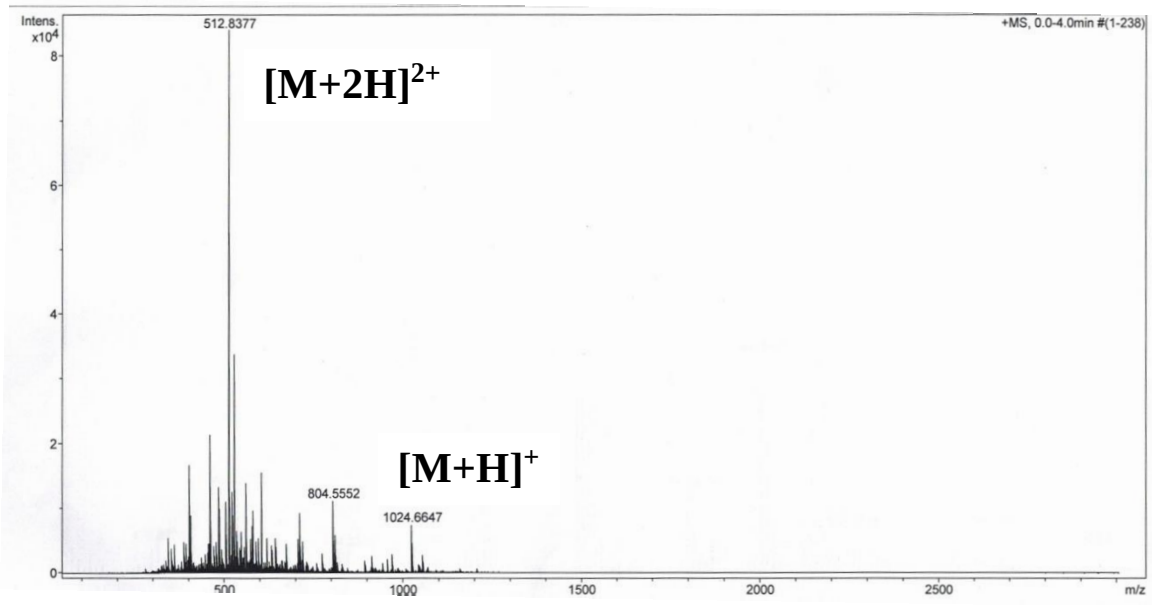

Figure C4 GZ3.19 HRMS (EI) (calculated for $[M+H]^+$ = 1024.6666).

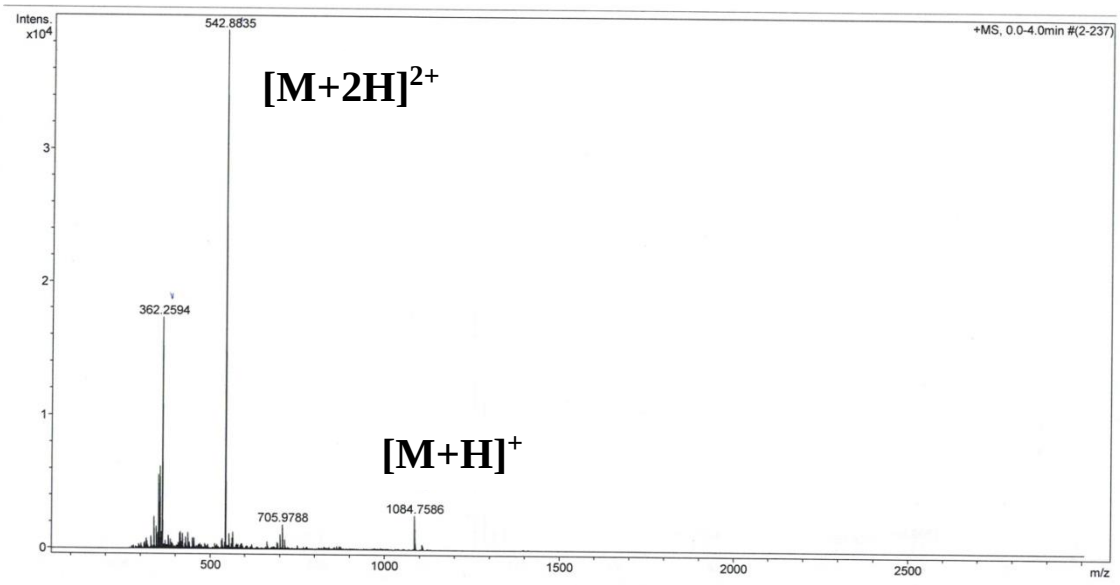

Figure C5 GZ3.40 HRMS (EI) (calculated for $[M+H]^+$ = 1084.7605).

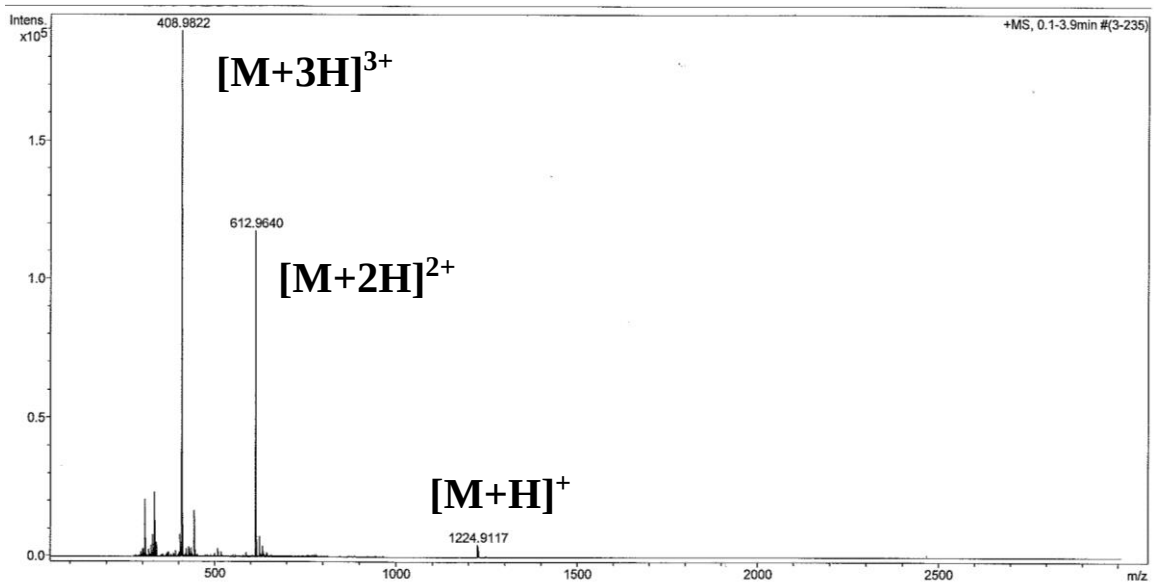

Figure C6 GZ3.55 HRMS (EI) (calculated for $[M+H]^+$ = 1224.9170).

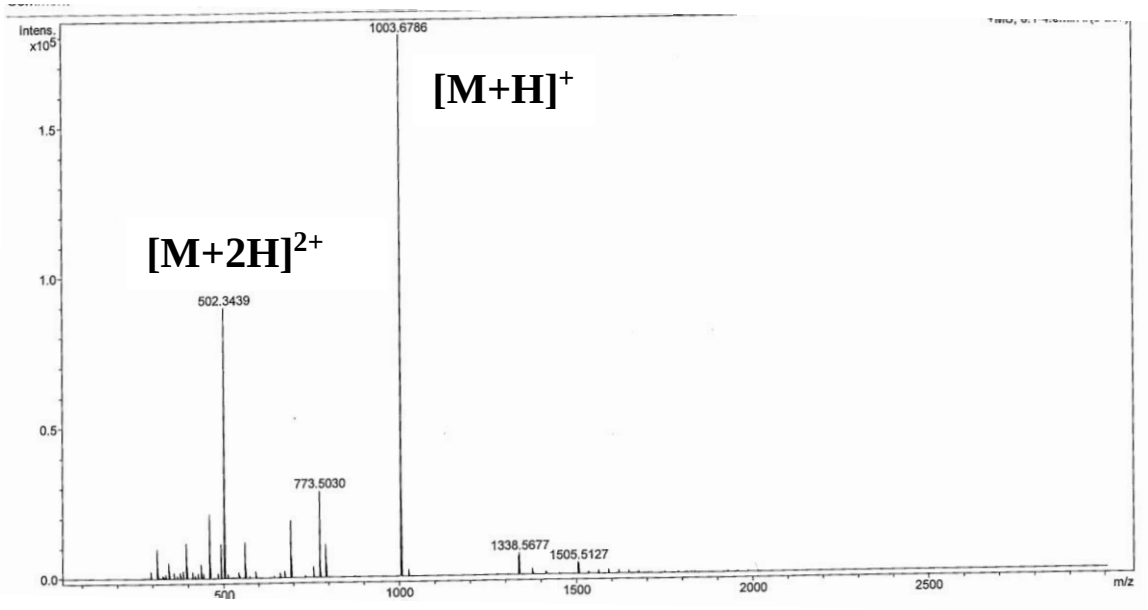

Figure C7 GZ3.27 HRMS (EI) (calculated for $[M+H]^+$ =1003.6775).

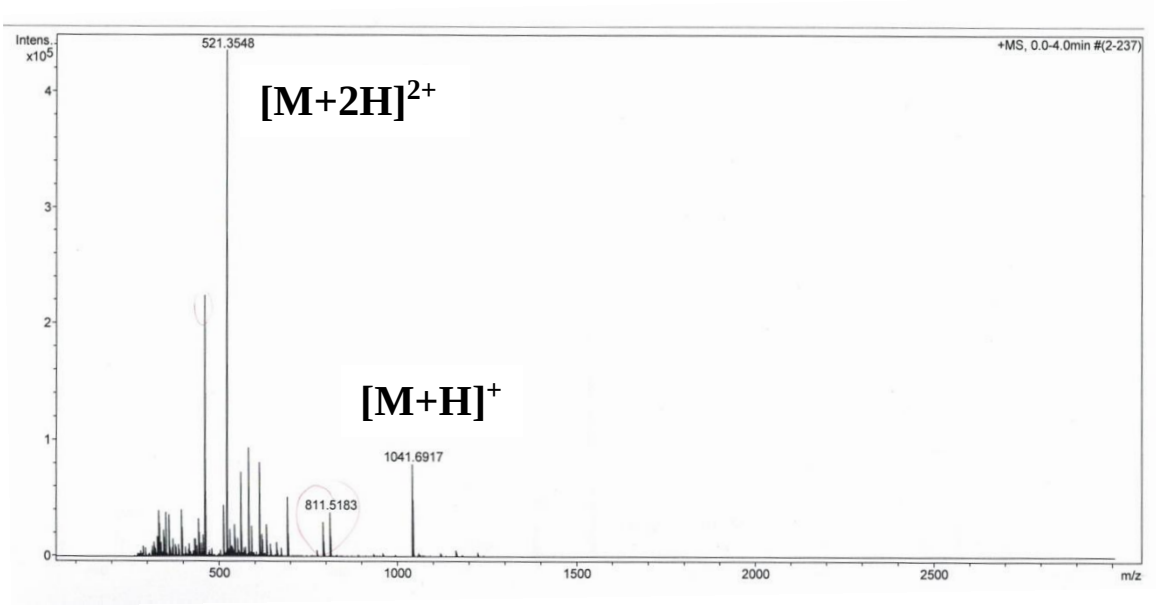

Figure C8 GZ3.38 HRMS (EI) (calculated for $[M+H]^+$ = 1041.6931).

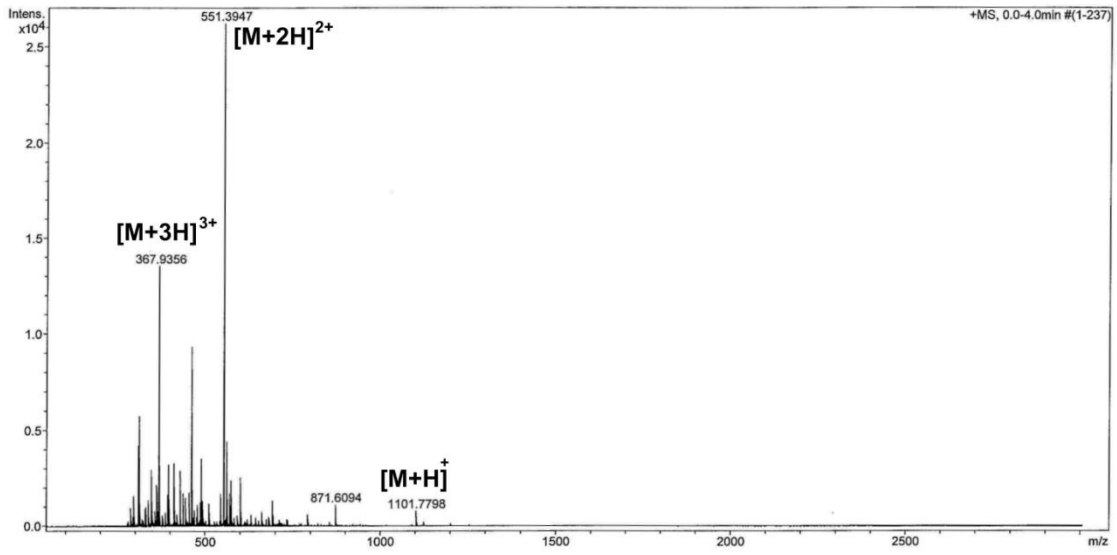

Figure C9 GZ3.26 HRMS (EI) (calculated for $[M+H]^+$ =1101.7870).

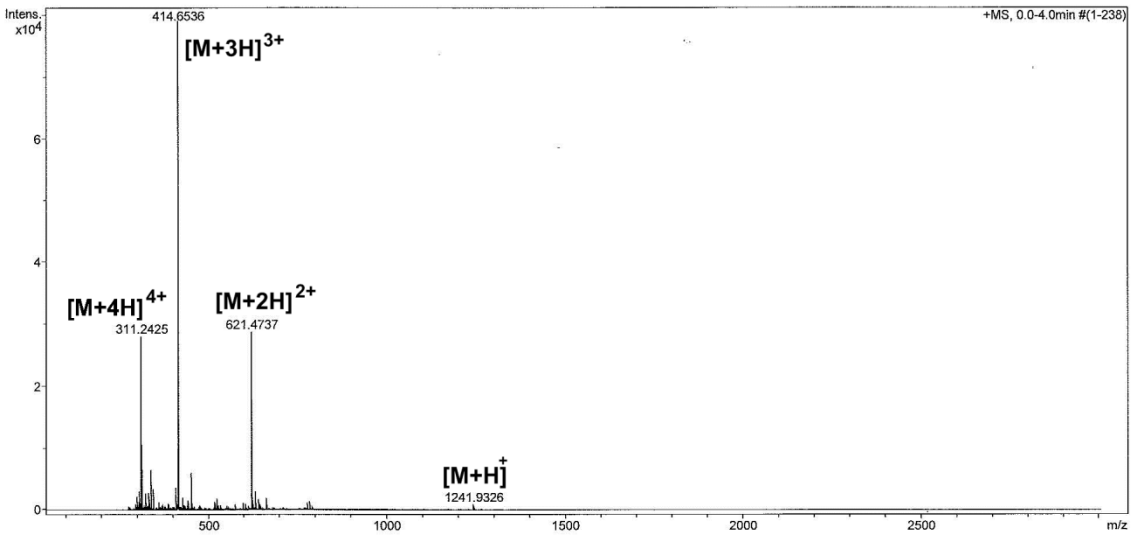

Figure C10 GZ3.37 HRMS (EI) (calculated for $[M+H]^+$ = 1241.9435).

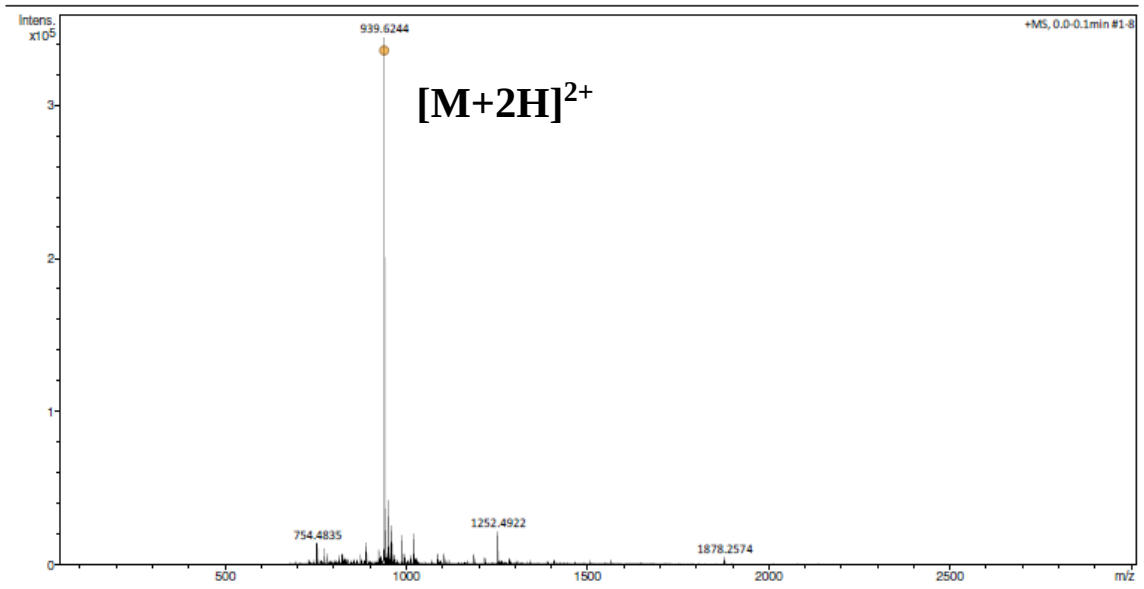

Figure C11 GZ3.148 HRMS (EI) (calculated for $[M+2H]^{2+}$ = 939.1198).

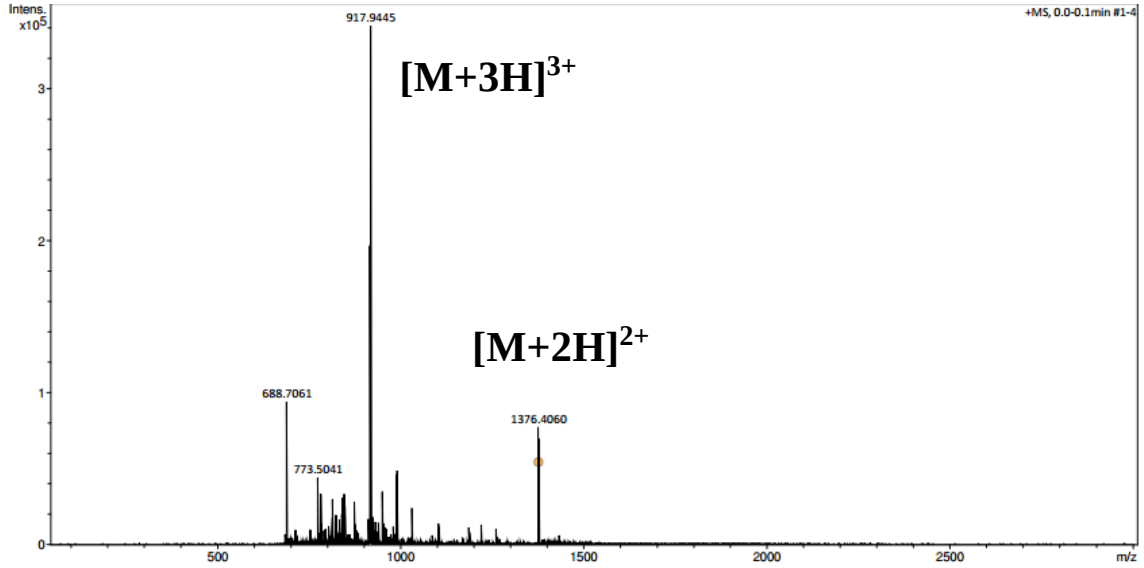

Figure C12 GZ3.149 HRMS (EI) (calculated for $[M+2H]^{2+}$ = 1375.9024).

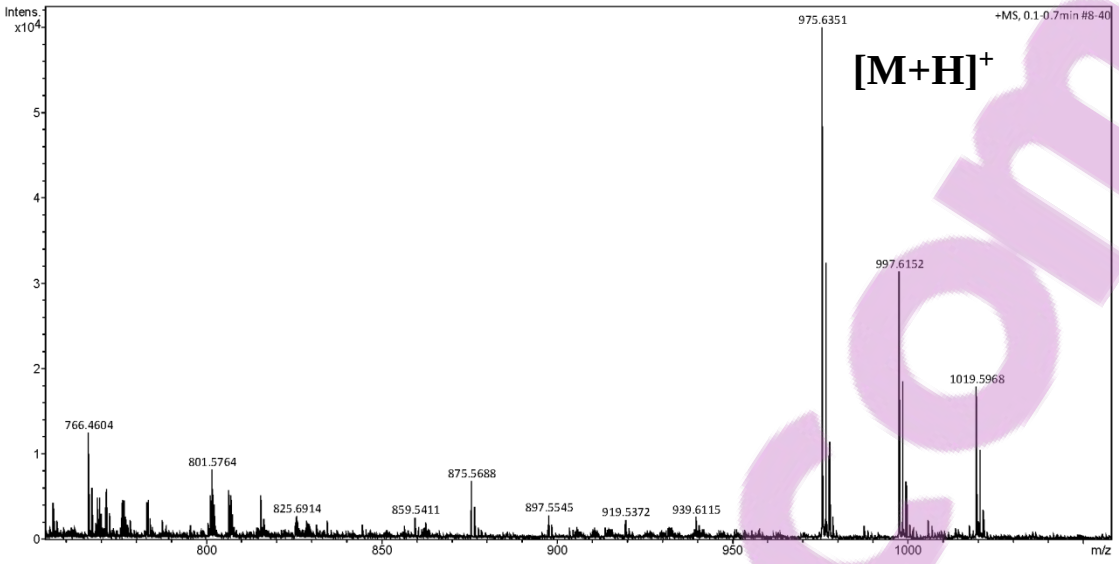

Figure C13 Ala[1] HRMS (EI) (calculated for $[M+H]^+$ = 975.6350).

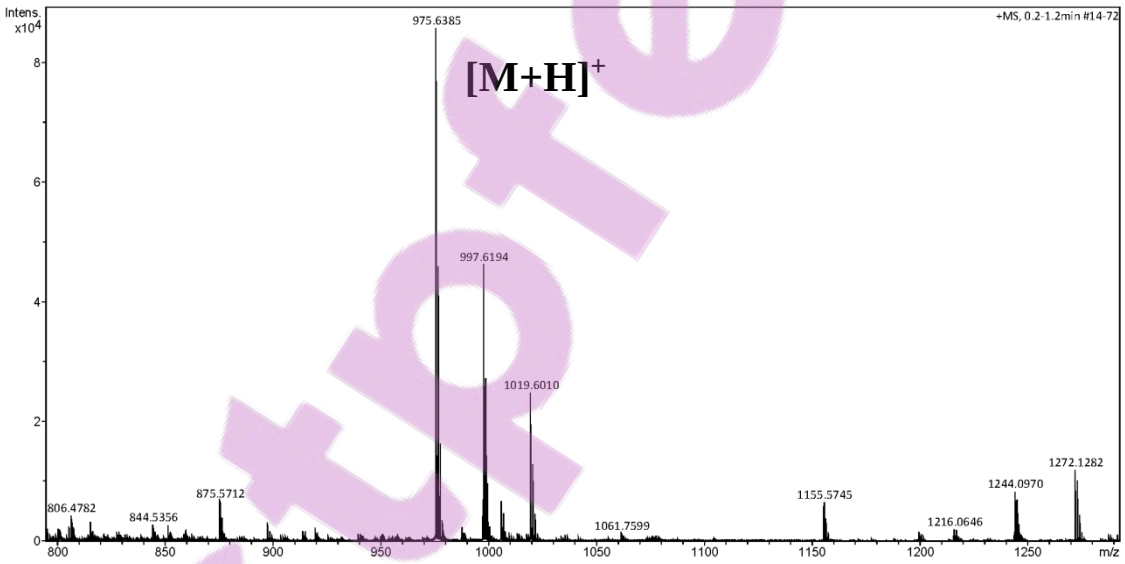

Figure C14 Ala[2] HRMS (EI) (calculated for $[M+H]^+$ = 975.6350).

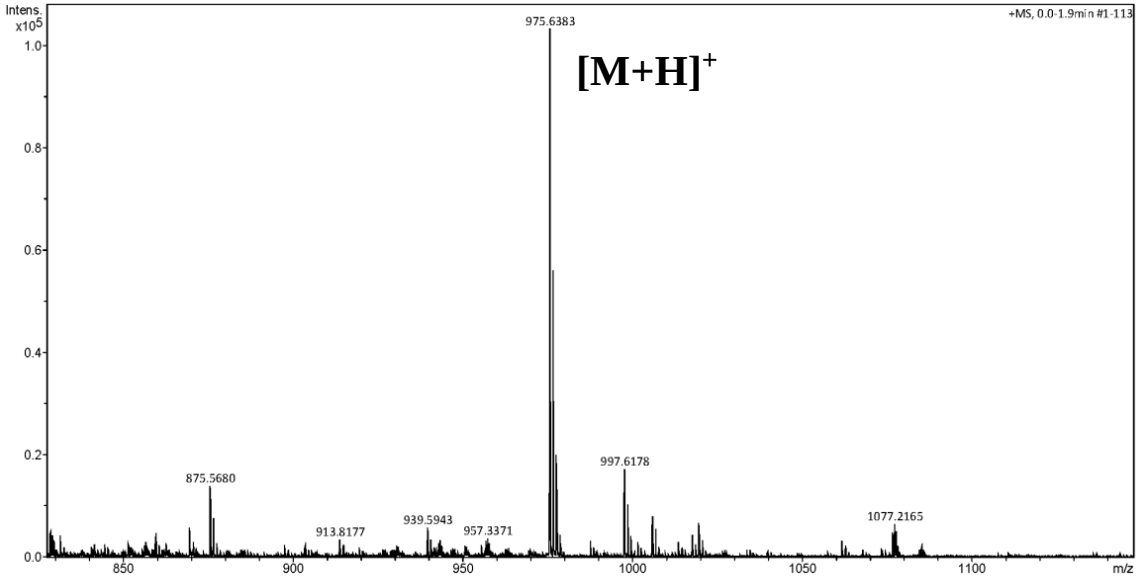

Figure C15 Ala^3 HRMS (EI) (calculated for $[M+H]^+$ = 975.6350).

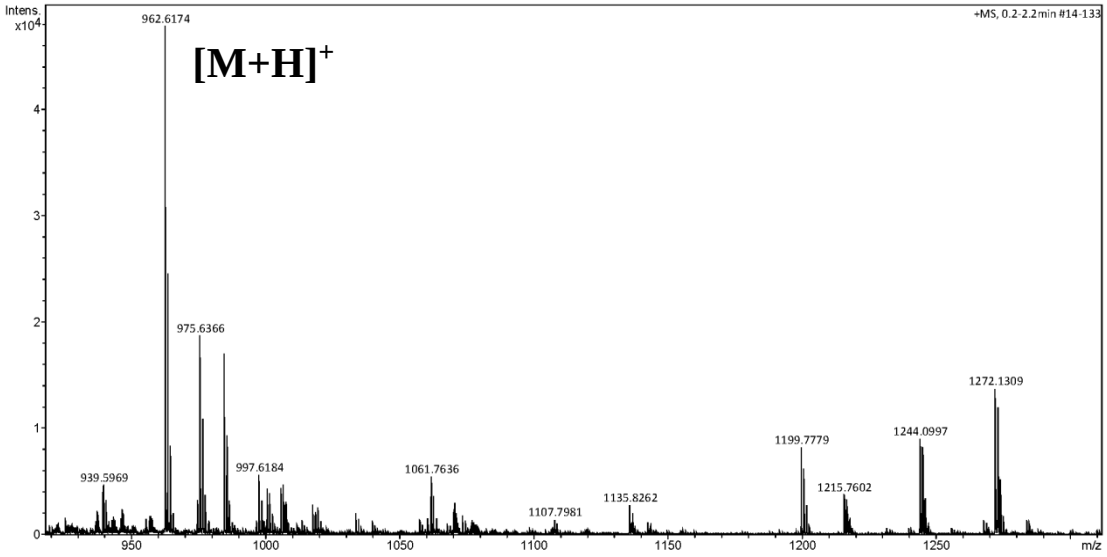

Figure C16 Ala^4 HRMS (EI) (calculated for $[M+H]^+$ = 962.6146).

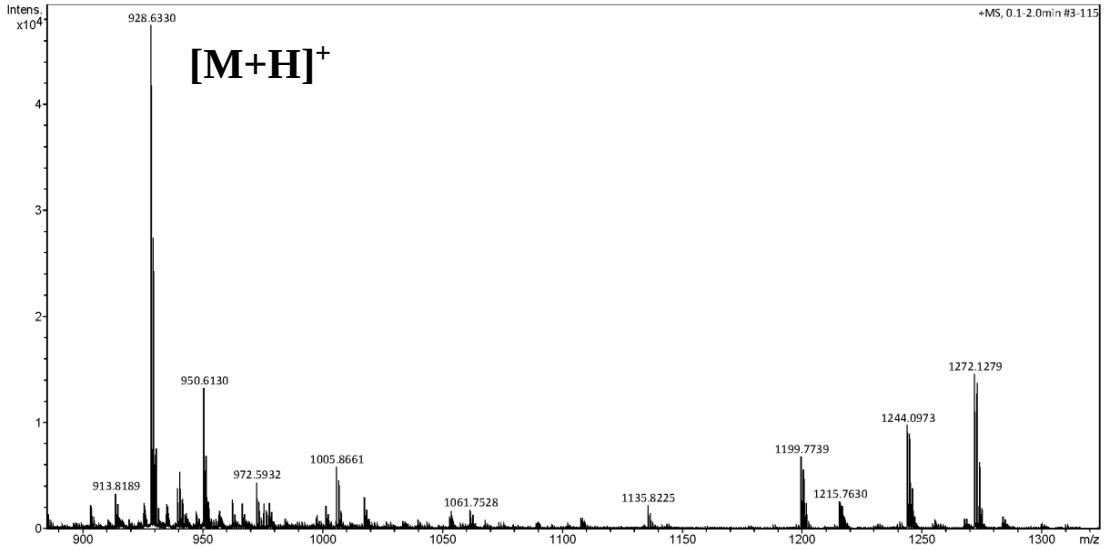

Figure C17 Ala^5 HRMS (EI) (calculated for $[M+H]^+$ = 928.6302).

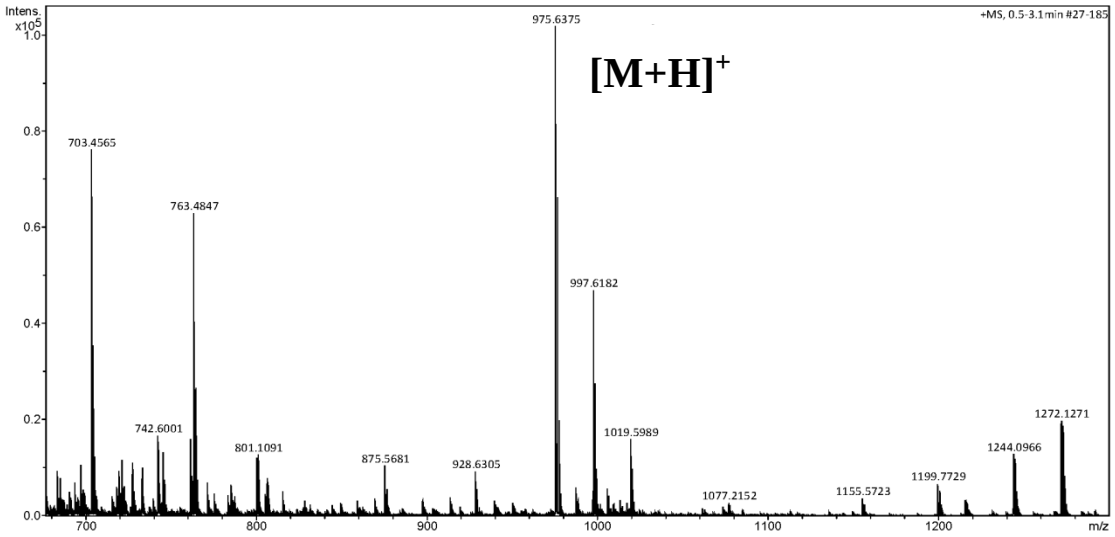

Figure C18 HRMS (EI) Ala^6 ESI-MS (calculated for $[M+H]^+$ = 975.6350).

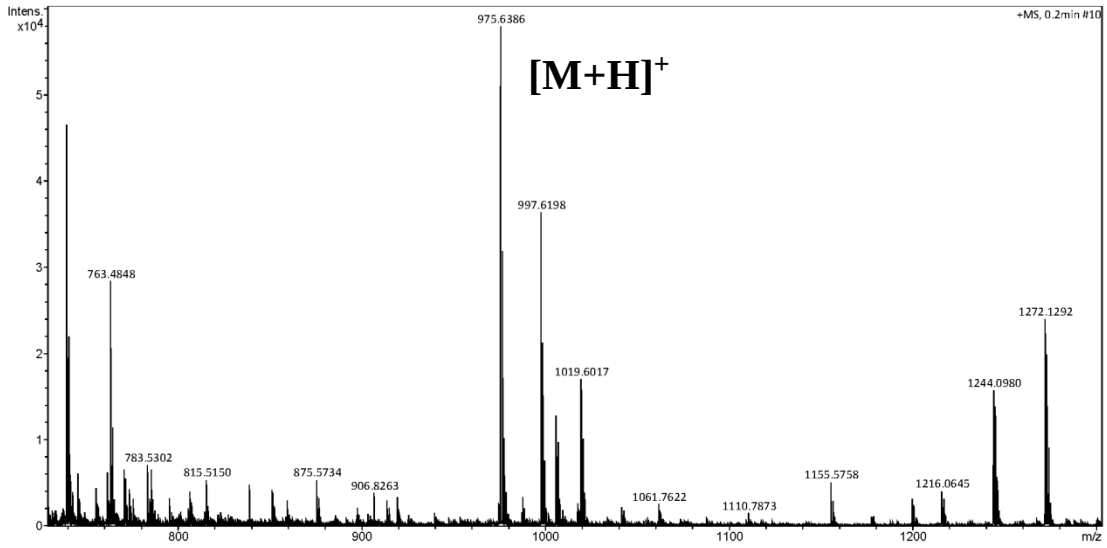

Figure C19 HRMS (EI) Ala^{7} ESI-MS (calculated for $[M+H]^+$ = 975.6350).

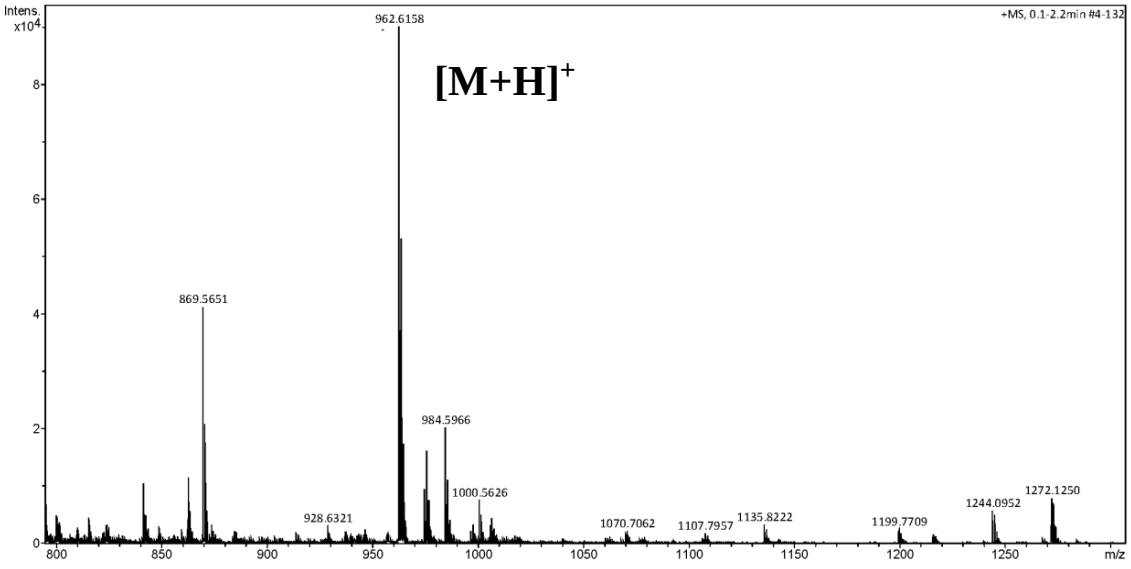

Figure C20 HRMS (EI) Ala^{8} ESI-MS (calculated for $[M+H]^+$ = 962.6146).

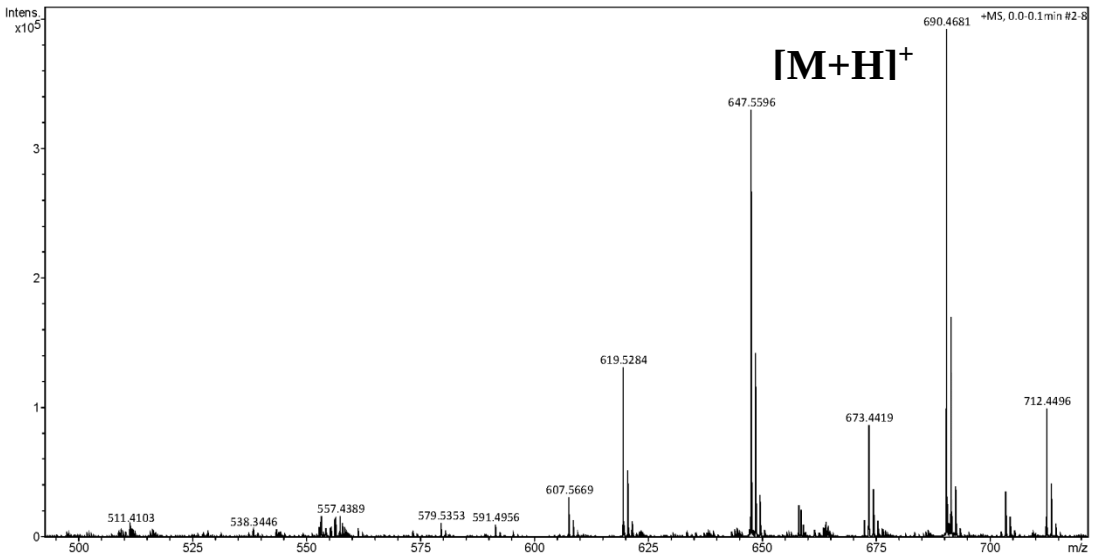

Figure C21 HRMS (EI) GZ3.159 ESI-MS (calculated for $[M+H]^+$ = 690.4661).

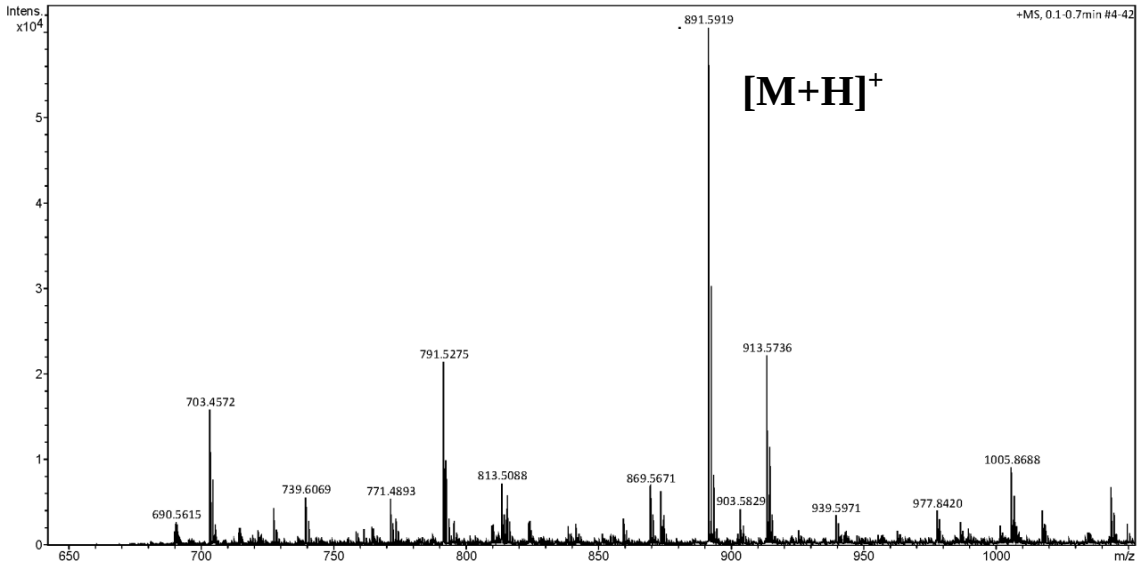

Figure C22 HRMS (EI) GZ3.130 ESI-MS (calculated for $[M+H]^+$ = 891.5887).

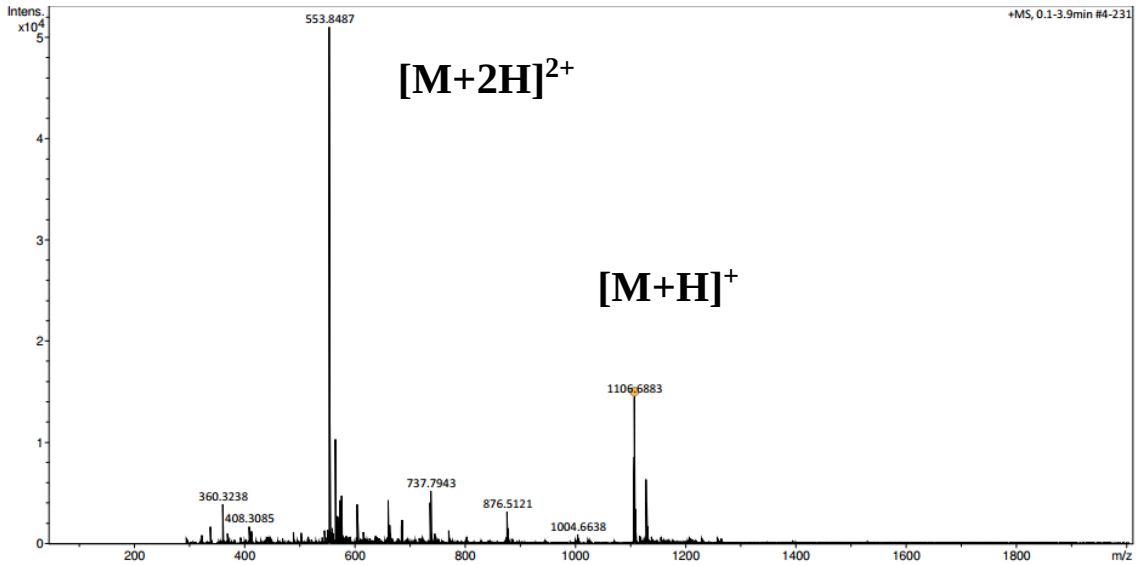

Figure C23 HRMS (EI) GZ3.155 ESI-MS (calculated for $[M+H]^+$ = 1106.6867).

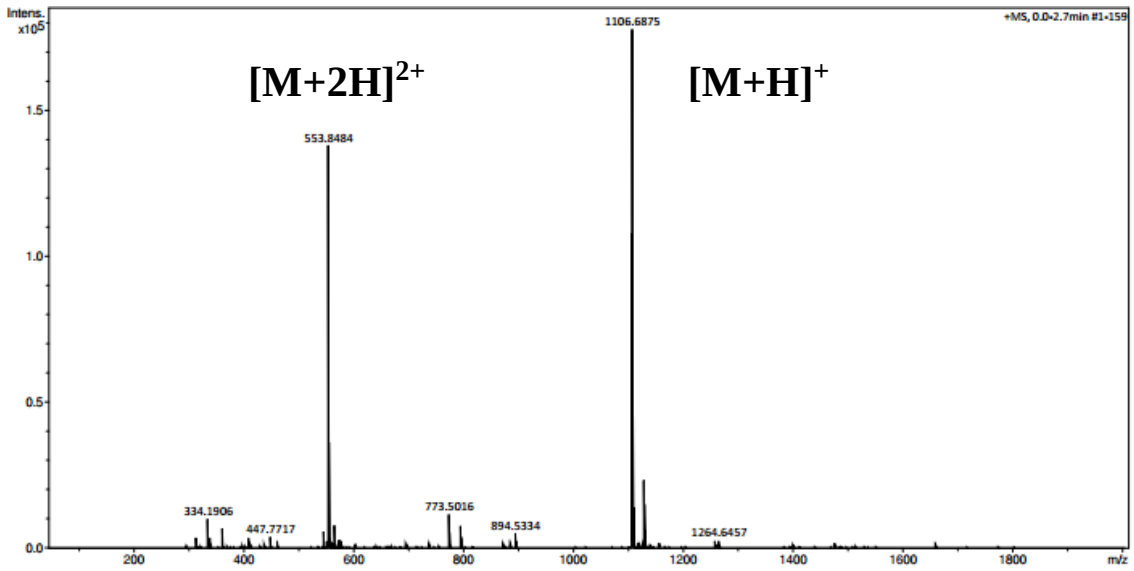

Figure C24 HRMS (EI) GZ3.160 ESI-MS (calculated for $[M+H]^+$ = 1106.6867).

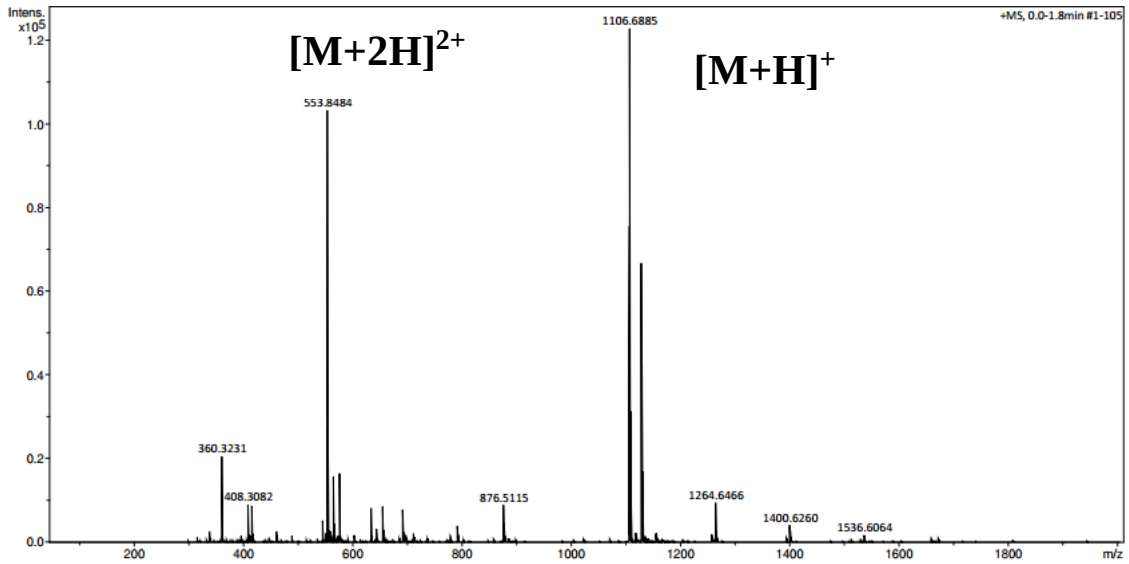

Figure C25 HRMS (EI) GZ3.163 ESI-MS (calculated for $[M+H]^+$ = 1106.6867)

Appendix D: ^{1}H NMR spectra of peptides

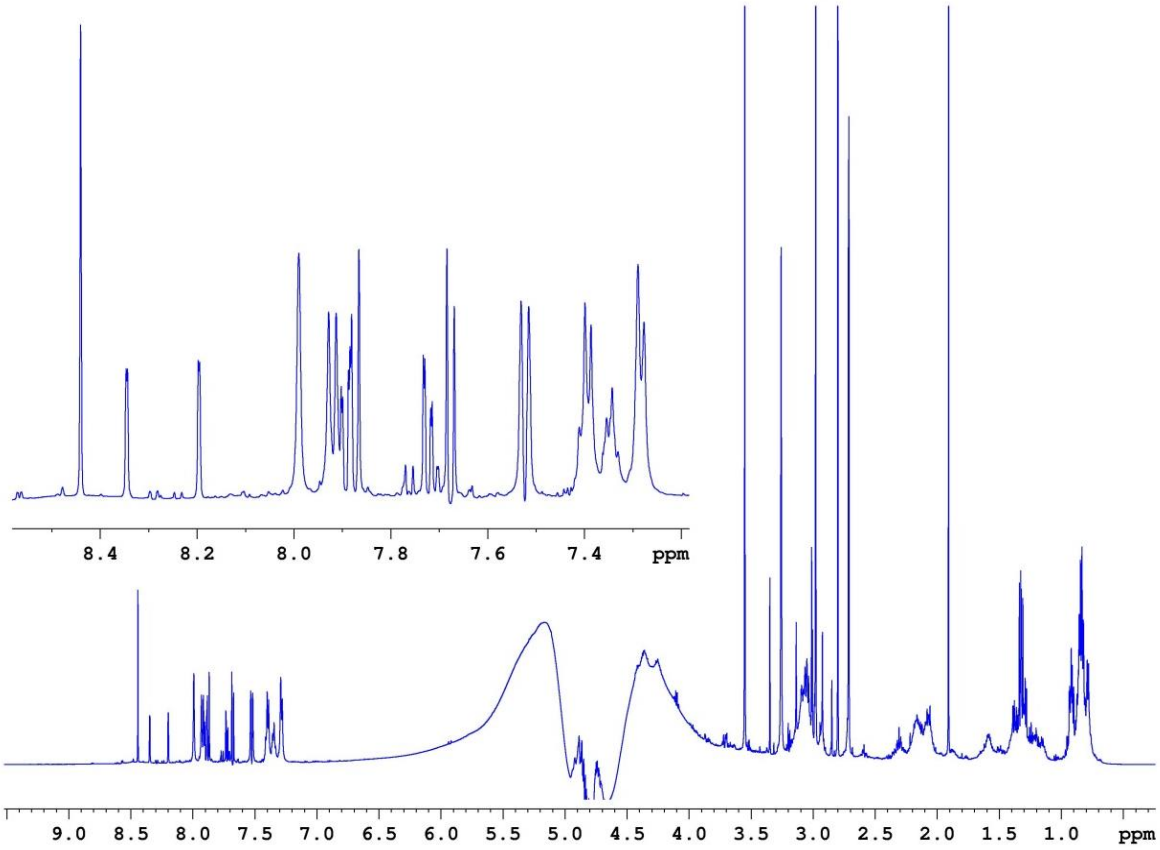

Figure D1 ^{1}H NMR spectrum of battacin in H_2O-D_2O (90:10) at 600 MHz at 300 K.

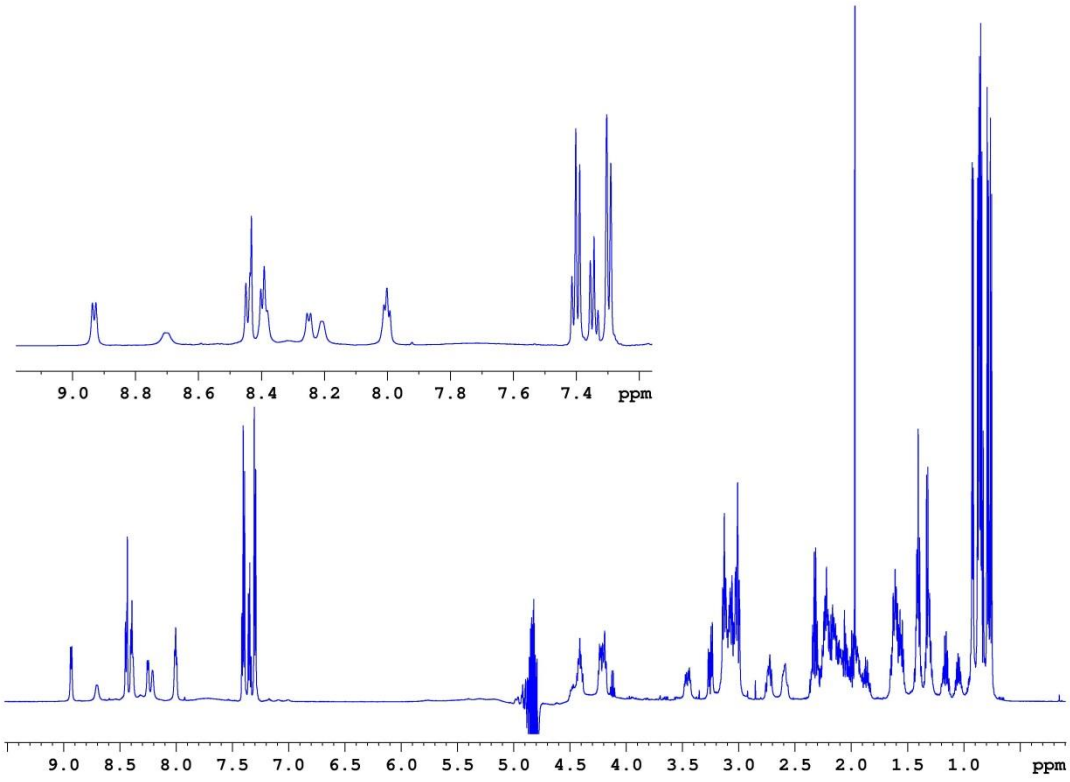

Figure D2 ^{1}H NMR spectrum of GZ3.15 in H_2O-D_2O (90:10) at 600 MHz at 300 K.

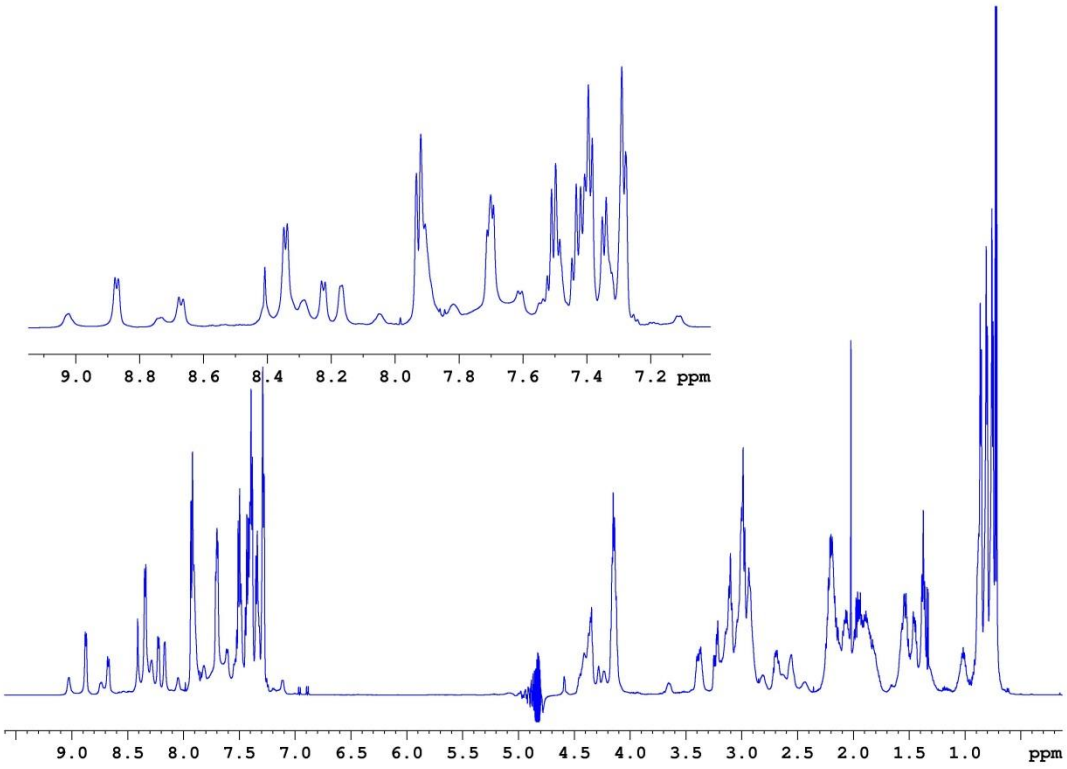

Figure D3 ^{1}H NMR spectrum of GZ3.21 in H_2O-D_2O (90:10) at 600 MHz at 300 K.

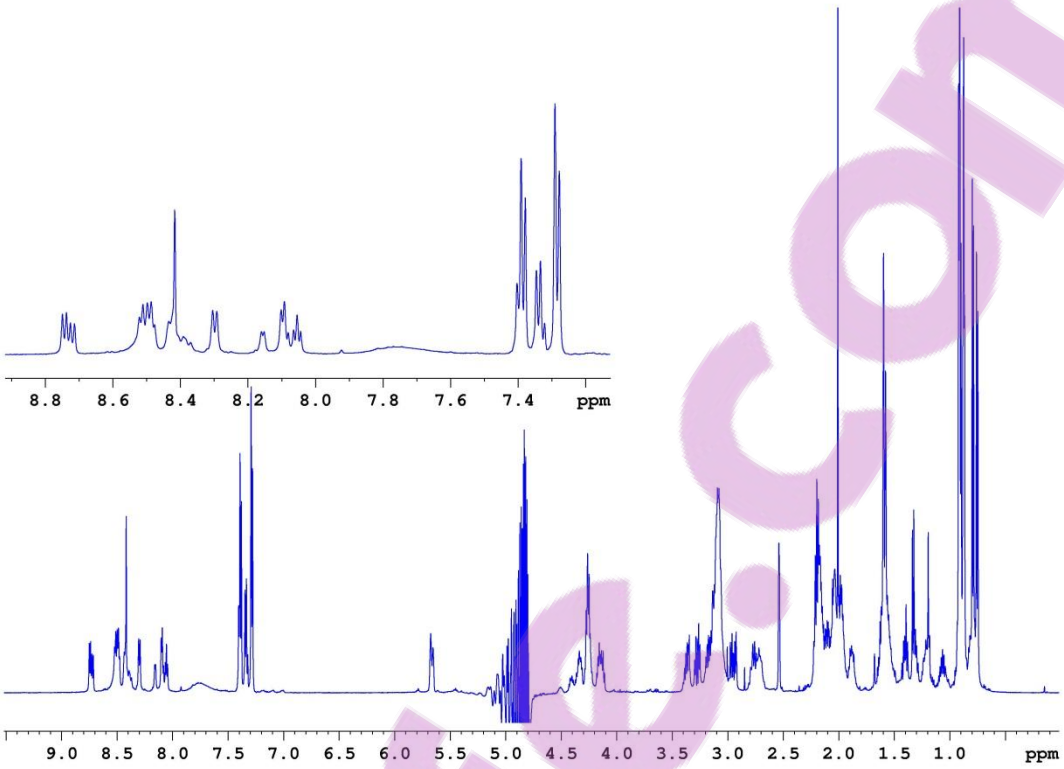

Figure D4 ^{1}H NMR spectrum of GZ3.19 in H_2O-D_2O (90:10) at 600 MHz at 300 K.

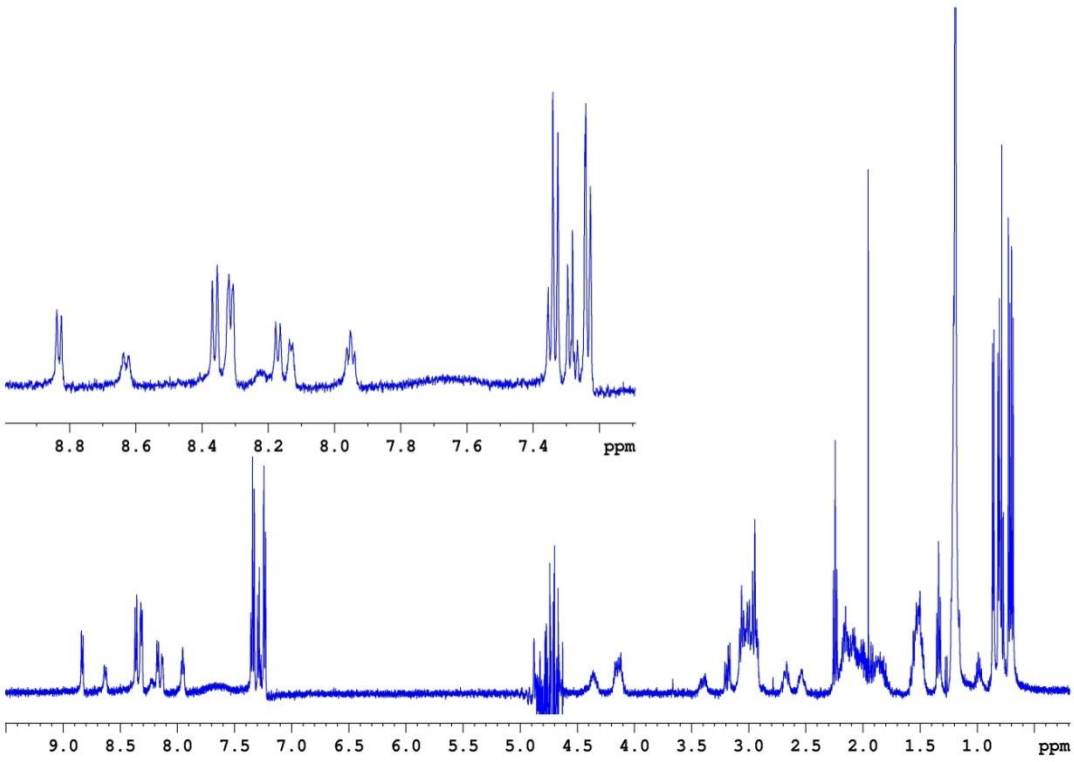

Figure D5 ^{1}H NMR spectrum of GZ3.40 in H_2O-D_2O (90:10) at 500 MHz at 278 K.

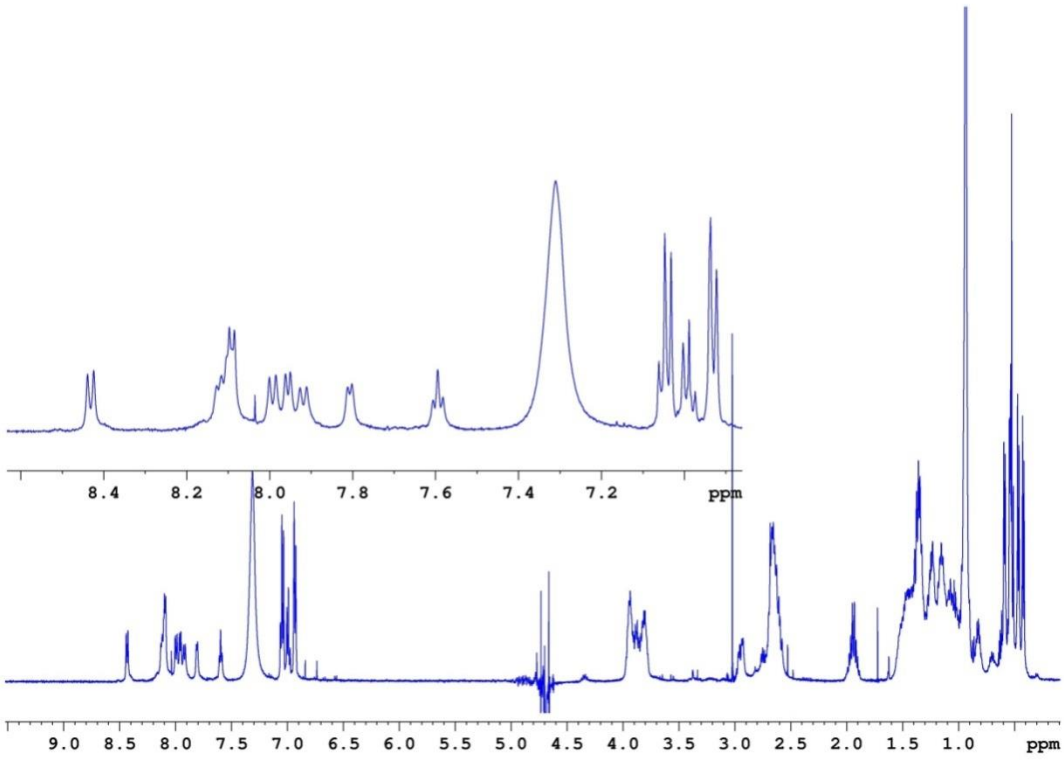

Figure D6 ^{1}H NMR spectrum of GZ3.55 in H_2O-D_2O (90:10) at 500 MHz at 278 K.

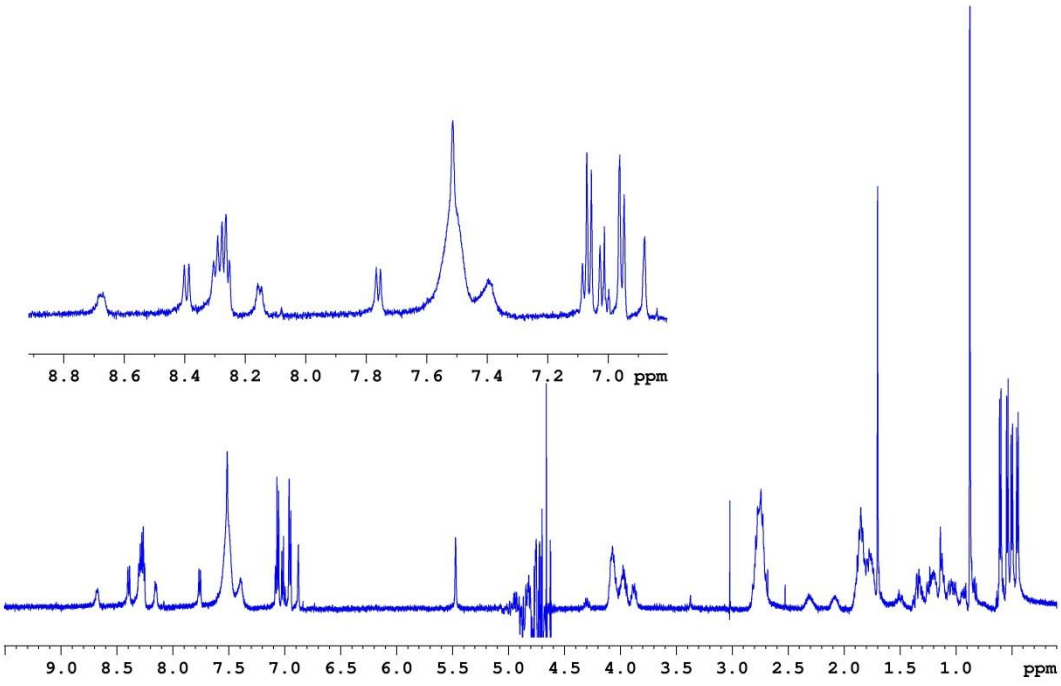

Figure D7 ^{1}H NMR spectrum of GZ3.38 in H_2O-D_2O (90:10) at 500 MHz at 278 K.

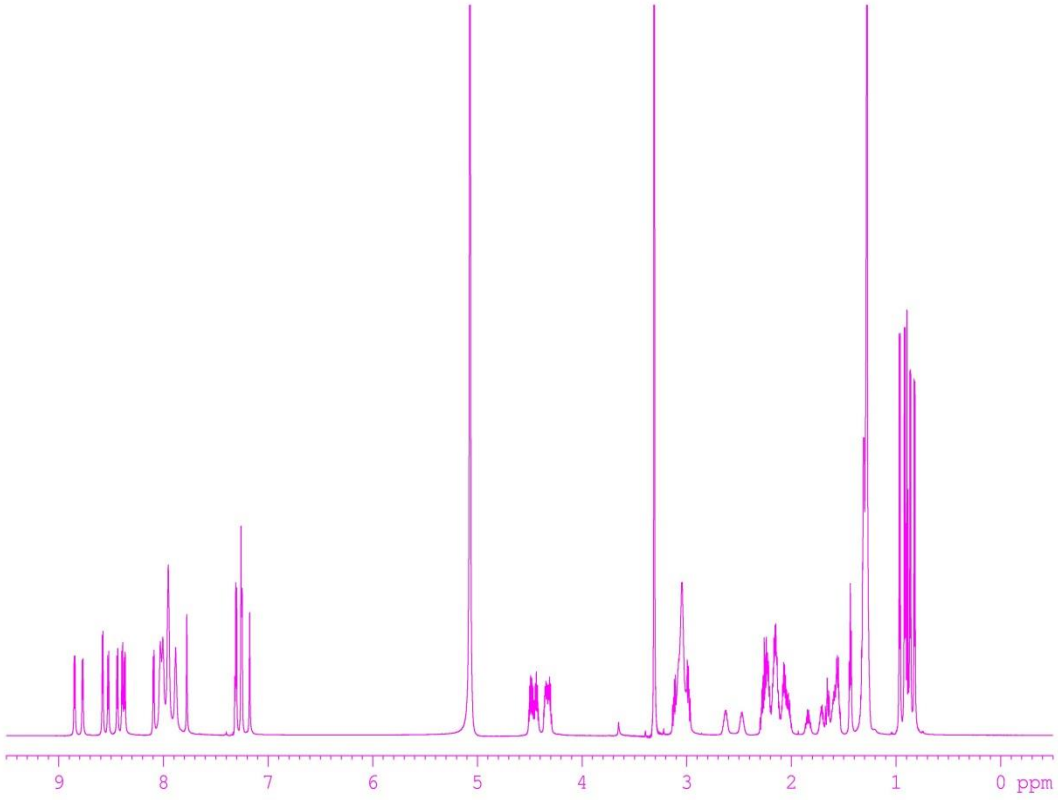

Figure D8 ^{1}H NMR spectrum of GZ3.26 in CD_3OH at 800 MHz at 278 K.

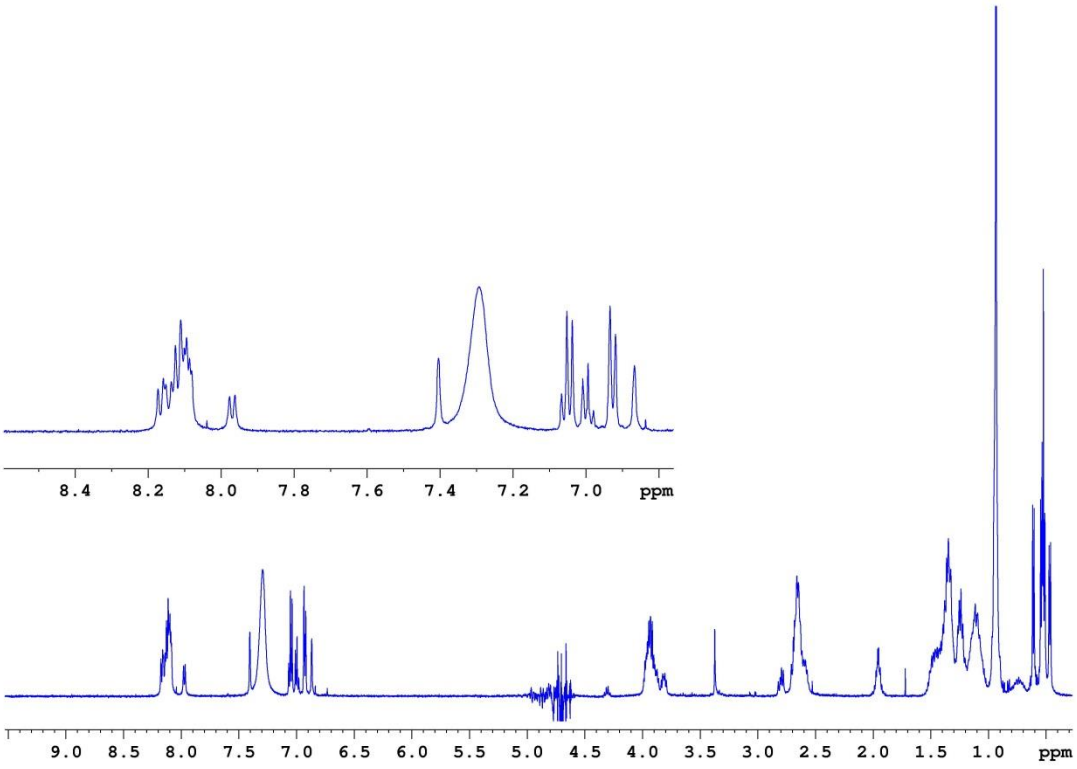

Figure D9 ^{1}H NMR spectrum of GZ3.37 in H_2O-D_2O (90:10) at 500 MHz at 278 K.

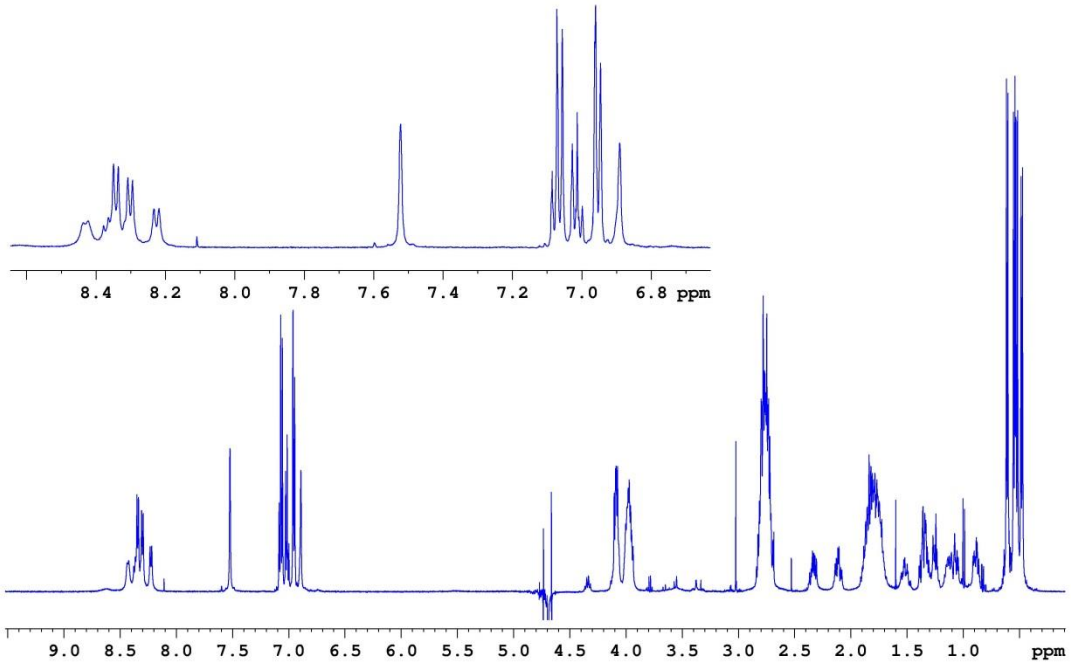

Figure D10 ^{1}H NMR spectrum of GZ3.130 in H_2O-D_2O (90:10) at 500 MHz at 278 K.

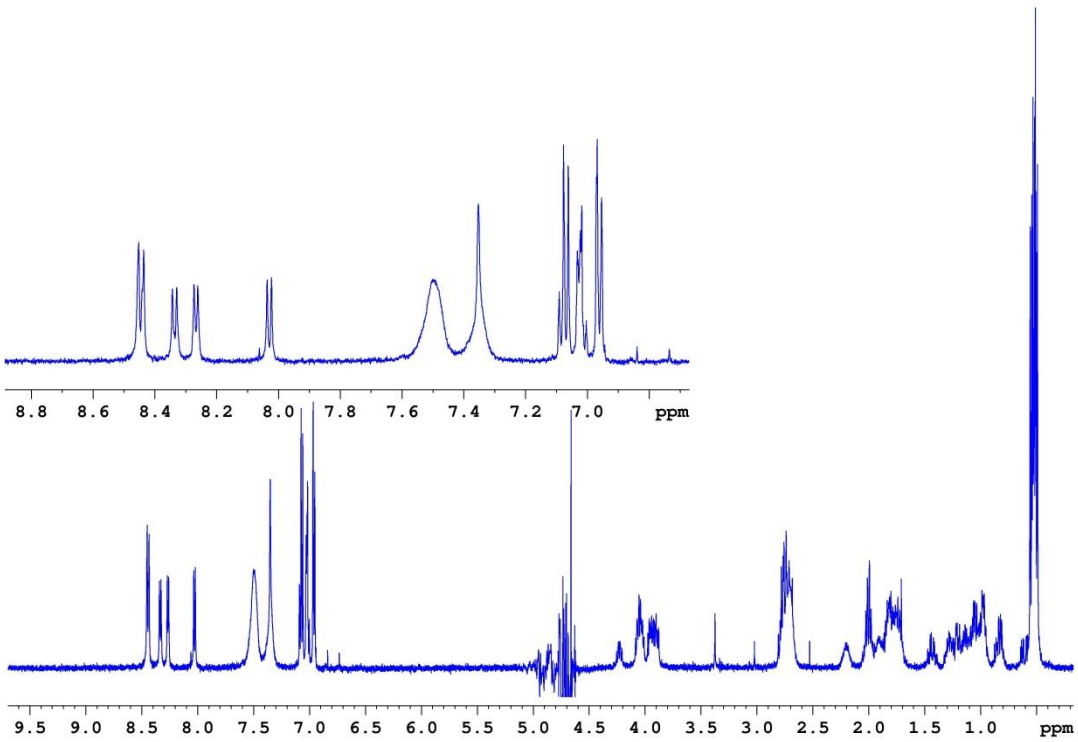

Figure D11 ^{1}H NMR spectrum of GZ3.159 in H_2O-D_2O (90:10) at 500 MHz at 278 K.

References

This page has been intentionally left blank

References

(1) Lewis, K. *Nat. Rev. Drug Discovery.* **2013**, *12*, 371-387.

(2) von Nussbaum, F.; Brands, M.; Hinzen, B.; Weigand, S.; Häbich, D. *Angew. Chem. Int. Ed.* **2006**, *45*, 5072-5129.

(3) Wright, G. D. *Nat. Rev. Microbiol.* **2007**, *5*, 175-186.

(4) Van Boeckel, T. P.; Gandra, S.; Ashok, A.; Caudron, Q.; Grenfell, B. T.; Levin, S. A.; Laxminarayan, R. *Lancet Infect. Dis.* **2014**, *14*, 742-750.

(5) Kümmerer, K. *Chemosphere.* **2009**, *75*, 417-434.

(6) WHO, *Antimicrobial resistance: global report on surveillance*. World Health Organization: **2014**.

(7) Overbye, K. M.; Barrett, J. F. *Drug Discovery Today.* **2005**, *10*, 45-52.

(8) Davies, J. *Science.* **1994**, *264*, 375-382.

(9) Berdy, J. *J. Antibiot.* **2012**, *65*, 385-395.

(10) Rasmussen, B. *Nature.* **2000**, *405*, 676-679.

(11) Stoodley, P.; Sauer, K.; Davies, D. G.; Costerton, J. W. *Annu. Rev. Microbiol.* **2002**, *56*, 187-209.

(12) Davies, D. G.; Parsek, M. R.; Pearson, J. P.; Iglewski, B. H.; Costerton, J. W.; Greenberg, E. P. *Science.* **1998**, *280*, 295-298.

(13) Waters, C. M.; Bassler, B. L. *Annu. Rev. Cell Dev. Biol.* **2005**, *21*, 319-346.

(14) Lewis, K. *Antimicrob. Agents Chemother.* **2001**, *45*, 999-1007.

(15) Costerton, J. W.; Stewart, P. S.; Greenberg, E. P. *Science.* **1999**, *284*, 1318-1322.

(16) Spoering, A. L.; Lewis, K. *J. Bacteriol.* **2001**, *183*, 6746-6751.

(17) Hetrick, E. M.; Schoenfisch, M. H. *Chem. Soc. Rev.* **2006**, *35*, 780-789.

(18) Schierholz, J. M.; Beuth, J. *J. Hosp. Infect.* **2001**, *49*, 87-93.

(19) Costa, F.; Carvalho, I. F.; Montelaro, R. C.; Gomes, P.; Martins, M. C. *Acta Biomater.* **2011**, *7*, 1431-1440.

(20) Zhao, L.; Chu, P. K.; Zhang, Y.; Wu, Z. *J. Biomed. Mater. Res.* **2009**, *91*, 470-480.

(21) Darouiche, R. O. *N. Engl. J. Med.* **2004**, *350*, 1422-1429.

(22) Bandyk, D. F.; Esses, G. E. *Surg. Clin. N. Am.* **1994**, *74*, 571-90.

(23) Hall-Stoodley, L.; Costerton, J. W.; Stoodley, P. *Nat. Rev. Microbiol.* **2004**, *2*, 95-108.

(24) Sutherland, I. W. *Trends Microbiol.* **2001**, *9*, 222-227.

(25) Stewart, P. S. *Int. J. Med. Microbiol.* **2002**, *292*, 107-13.

(26) Dibdin, G. H.; Assinder, S. J.; Nichols, W. W.; Lambert, P. A. *J. Antimicrob. Chemother.* **1996**, *38*, 757-769.

(27) Zasloff, M. *Nature.* **2002**, *415*, 389-95.

(28) Hancock, R. E. W.; Chapple, D. S. *Antimicrob. Agents Chemother.* **1999**, *43*, 1317-1323.

(29) van 't Hof, W.; Veerman, E. C. I.; Helmerhorst, E. J.; Amerongen, A. V. N. *Biol. Chem.* **2001**, *382*, 597-619.

(30) Brogden, K. A. *Nat. Rev. Microbiol.* **2005**, *3*, 238-250.

(31) Wang, G. S.; Li, X.; Wang, Z. *Nucleic Acids Res.* **2009**, *37*, D933-D937.

(32) Hwang, P. M.; Vogel, H. J. *Biochem. Cell Biol.* **1998**, *76*, 235-46.

(33) Marahiel, M. A.; Stachelhaus, T.; Mootz, H. D. *Chem. Rev.* **1997**, *97*, 2651-2674.

(34) Perlman, D.; Bodanszky, M. *Annu. Rev. Biochem.* **1971**, *40*, 449-464.

(35) Kleinkauf, H.; von Dohren, H. *Annu. Rev. Microbiol.* **1987**, *41*, 259-289.

(36) Koczulla, A. R.; Bals, R. *Drugs.* **2003**, *63*, 389-406.

(37) Brogden, K. A.; De Lucca, A. J.; Bland, J.; Elliott, S. *Proc. Natl. Acad. Sci. U. S. A.* **1996**, *93*, 412-416.

(38) Gesell, J.; Zasloff, M.; Opella, S. J. *J. Biomol. NMR.* **1997**, *9*, 127-135.

(39) Hoover, D. M.; Chertov, O.; Lubkowski, J. *J. Biol. Chem.* **2001**, *276*, 39021-39026.

(40) Mandard, N.; Sodano, P.; Labbe, H.; Bonmatin, J. M.; Bulet, P.; Hetru, C.; Ptak, M.; Vovelle, F. *Eur. J. Biochem.* **1998**, *256*, 404-410.

(41) Zahn, M.; Kieslich, B.; Berthold, N.; Knappe, D.; Hoffmann, R.; Strater, N. *Protein Pept. Lett.* **2014**, *21*, 407-412.

(42) Jung, H.-H.; Yang, S.-T.; Sim, J.-Y.; Lee, S.-K.; Lee, J.-Y.; Kim, H.-H.; Shin, S.-Y.; Kim, J.-I. *BMB rep.* **2010**, *43*, 362-368.

(43) Hultmark, D.; Steiner, H.; Rasmuson, T.; Boman, H. G. *Eur. J. Biochem.* **1980**, *106*, 7-16.

(44) Zasloff, M. *Proc. Natl. Acad. Sci. U. S. A.* **1987**, *84*, 5449-5453.

(45) Dempsey, C. E. *Biochim. Biophys. Acta, Rev. Biomembr.* **1990**, *1031*, 143-161.

(46) Pollock, J. J.; Denepitiya, L.; MacKay, B. J.; Iacono, V. J. *Infect. Immun.* **1984**, *44*, 702-707.

(47) Selsted, M. E.; Novotny, M. J.; Morris, W. L.; Tang, Y. Q.; Smith, W.; Cullor, J. S. *J. Biol. Chem.* **1992**, *267*, 4292-4295.

(48) Zanetti, M.; Del Sal, G.; Storici, P.; Schneider, C.; Romeo, D. *J. Biol. Chem.* **1993**, *268*, 522-526.

(49) Simmaco, M.; Mignogna, G.; Barra, D.; Bossa, F. *J. Biol. Chem.* **1994**, *269*, 11956-11961.

(50) Fehlbaum, P.; Bulet, P.; Chernysh, S.; Briand, J.-P.; Roussel, J.-P.; Letellier, L.; Hetru, C.; Hoffmann, J. A. *Proc. Natl. Acad. Sci. U. S. A.* **1996**, *93*, 1221-1225.

(51) Ganz, T.; Selsted, M. E.; Szklarek, D.; Harwig, S. S.; Daher, K.; Bainton, D. F.; Lehrer, R. I. *J. Clin. Invest.* **1985**, *76*, 1427-1435.

(52) Kokryakov, V. N.; Harwig, S. S. L.; Panyutich, E. A.; Shevchenko, A. A.; Aleshina, G. M.; Shamova, O. V.; Korneva, H. A.; Lehrer, R. I. *FEBS Lett.* **1993**, *327*, 231-236.

(53) Nakamura, T.; Furunaka, H.; Miyata, T.; Tokunaga, F.; Muta, T.; Iwanaga, S.; Niwa, M.; Takao, T.; Shimonishi, Y. *J. Biol. Chem.* **1988**, *263*, 16709-16713.

(54) Debono, M.; Barnhart, M.; Carrell, C. B.; Hoffmann, J. A.; Occolowitz, J. L.; Abbott, B. J.; Fukuda, D. S.; Hamill, R. L.; Biemann, K.; Herlihy, W. C. *J. Antibiot.* **1987**, *40*, 761-777.

(55) Goumon, Y.; Strub, J.-M.; Moniatte, M.; Nullans, G.; Poteur, L.; Hubert, P.; Van Dorsselaer, A.; Aunis, D.; Metz-Boutigue, M.-H. *Eur. J. Biochem.* **1996**, *235*, 516-525.

(56) Schittek, B.; Hipfel, R.; Sauer, B.; Bauer, J.; Kalbacher, H.; Stevanovic, S.; Schirle, M.; Schroeder, K.; Blin, N.; Meier, F. *Nat. Immunol.* **2001**, *2*, 1133-1137.

(57) Jones, T. S. *Ann. N. Y. Acad. Sci.* **1949**, *51*, 909-916.

(58) Benedict, R. G.; Langlykke, A. F. *J. Bacteriol.* **1947**, *54*, 24-25.

(59) Rogers, L. A. *J. Bacteriol.* **1928**, *16*, 321-325.

(60) Dubos, R. J. *J. Exp. Med.* **1939**, *70*, 1-10.

(61) Dubos, R. J. *J. Exp. Med.* **1939**, *70*, 11-17.

(62) Remade, J., The cell wall and metal binding. In *Biosorption of heavy metals*, CRC Press Boca Raton: **1990**; pp 83-92.

(63) Heijenoort, J. v. *Glycobiology.* **2001**, *11*, 25R-36R.

(64) Schleifer, K. H.; Kandler, O. *Bacteriol. Rev.* **1972**, *36*, 407-477.

(65) Ward, J. *Microbiol. Rev.* **1981**, *45*, 211-243.

(66) Archibald, A.; Baddiley, J. *Adv. Carbohydr. Chem. Biochem.* **1966**, *21*, 323.

(67) Rahman, O.; Dover, L. G.; Sutcliffe, I. C. *Trends Microbiol.* **2009**, *17*, 219-225.

(68) Swoboda, J. G.; Campbell, J.; Meredith, T. C.; Walker, S. *Chembiochem.* **2010**, *11*, 35-45.

(69) Hancock, R. E. W. *Trends Microbiol.* **1997**, *5*, 37-42.

(70) Nikaido, H. *Microbiol. Mol. Biol. Rev.* **2003**, *67*, 593-656.

(71) Hancock, R. E. *Lancet Infect. Dis.* **2001**, *1*, 156-64.

(72) Simons, K.; Ikonen, E. *Science.* **2000**, *290*, 1721-1726.

(73) Matsuzaki, K. *Biochim. Biophys. Acta, Biomembr.* **1999**, *1462*, 1-10.

(74) Lohner, K. *Gen. Physiol. Biophys.* **2009**, *28*, 105-116.

(75) Yoneyama, F.; Imura, Y.; Ohno, K.; Zendo, T.; Nakayama, J.; Matsuzaki, K.; Sonomoto, K. *Antimicrob. Agents Chemother.* **2009**, *53*, 3211-3217.

(76) Yang, L.; Weiss, T. M.; Lehrer, R. I.; Huang, H. W. *Biophys. J.* **2000**, *79*, 2002-2009.

(77) Batoni, G.; Maisetta, G.; Lisa Brancatisano, F.; Esin, S.; Campa, M. *Curr. Med. Chem.* **2011**, *18*, 256-279.

(78) Overhage, J.; Campisano, A.; Bains, M.; Torfs, E. C.; Rehm, B. H.; Hancock, R. E. *Infect. Immun.* **2008**, *76*, 4176-4182.

(79) Kai-Larsen, Y.; Luthje, P.; Chromek, M.; Peters, V.; Wang, X.; Holm, Å.; Kádas, L.; Hedlund, K.-O.; Johansson, J.; Chapman, M. R. *PLoS Pathog.* **2010**, *6*, e1001010-e1001010.

(80) Hell, E.; Giske, C.; Nelson, A.; Römling, U.; Marchini, G. *Lett. Appl. Microbiol.* **2010**, *50*, 211-215.

(81) Chennupati, S. K.; Chiu, A. G.; Tamashiro, E.; Banks, C. A.; Cohen, M. B.; Bleier, B. S.; Kofonow, J. M.; Tam, E.; Cohen, N. A. *Am J Rhinol Allergy.* **2009**, *23*, 46-51.

(82) Mataraci, E.; Dosler, S. *Antimicrob. Agents Chemother.* **2012**, *56*, 6366-6371.

(83) Zhu, C.; Tan, H.; Cheng, T.; Shen, H.; Shao, J.; Guo, Y.; Shi, S.; Zhang, X. *J. Surg. Res.* **2013**, *183*, 204-213.

(84) Martinez, L. R.; Casadevall, A. *Infect. Immun.* **2006**, *74*, 6118-6123.

(85) Zhu, C.; He, N.; Cheng, T.; Tan, H.; Guo, Y.; Chen, D.; Cheng, M.; Yang, Z.; Zhang, X. *Inflammation.* **2013**, *36*, 983-996.

(86) Minardi, D.; Ghiselli, R.; Cirioni, O.; Giacometti, A.; Kamysz, W.; Orlando, F.; Silvestri, C.; Parri, G.; Kamysz, E.; Scalise, G. *Peptides.* **2007**, *28*, 2293-2298.

(87) Gordon, Y. J.; Romanowski, E. G.; McDermott, A. M. *Curr. Eye Res.* **2005**, *30*, 505-515.

(88) De Zoysa, G. H.; Sarojini, V. *Chem. N. Z.* **2015**, 94-101.

(89) Gause, G.; Brazhnikova, M. *Nature.* **1944**, *154*, 703-703.

(90) Barrett, J. *Curr. Opin. Invest. Drugs.* **2001**, *2*, 1039-1044.

(91) Goldstein, B. P.; Candiani, G.; Arain, T. M.; Romano, G.; Ciciliato, I.; Berti, M.; Abbondi, M.; Scotti, R.; Mainini, M.; Ripamonti, F. *Antimicrob. Agents Chemother.* **1995**, *39*, 1580-1588.

(92) McCormick, M. H.; McGuire, J.; Pittenger, G.; Pittenger, R.; Stark, W. *Antibiot. Annu.* **1954**, *3*, 606-611.

(93) Koyama, Y.; Kurosasa, A.; Tsuchiya, A.; Takakuta, K. *J Antibiot (Tokyo).* **1950**, *3*, 457-458.

(94) Hirsch, A.; Grinstead, E.; Chapman, H. R.; Mattick, A. *J. Dairy Res.* **1951**, *18*, 205-206.

(95) McNicol, P.; Rubinchik, E.; Pasetka, C.; Barger, R.; Lopez, J.; Friedland, H. Abstracts of the 41st Interscience Conference on Antimicrobial Agents and Chemotherapy, **2001**; p 205.

(96) Isaacson, R. *Curr. Opin. Invest. Drugs.* **2003**, *4*, 999-1003.

(97) Rothstein, D. M.; Spacciapoli, P.; Tran, L. T.; Xu, T.; Roberts, F. D.; Dalla Serra, M.; Buxton, D. K.; Oppenheim, F. G.; Friden, P. *Antimicrob. Agents Chemother.* **2001**, *45*, 1367-1373.

(98) Toney, J. *Curr. Opin. Invest. Drugs.* **2002**, *3*, 225-228.

(99) Marr, A. K.; Gooderham, W. J.; Hancock, R. E. W. *Curr. Opin. Pharmacol.* **2006**, *6*, 468-472.

(100) Vlieghe, P.; Lisowski, V.; Martinez, J.; Khrestchatisky, M. *Drug Discovery Today.* **2010**, *15*, 40-56.

(101) Werle, M.; Bernkop-Schnürch, A. *Amino Acids.* **2006**, *30*, 351-367.

(102) Pernot, M.; Vanderesse, R.; Frochot, C.; Guillemin, F.; Barberi-Heyob, M. *Expert Opin. Drug Metab. Toxicol.* **2011**, *7*, 793-802.

(103) Andreu, D.; Rivas, L. *Biopolymers.* **1998**, *47*, 415-433.

(104) Ong, Z. Y.; Wiradharma, N.; Yang, Y. Y. *Adv. Drug Delivery Rev.* **2014**, *78*, 28-45.

(105) Adessi, C.; Soto, C. *Curr. Med. Chem.* **2002**, *9*, 963-978.

(106) Shai, Y.; Oren, Z. *J. Biol. Chem.* **1996**, *271*, 7305-7308.

(107) Lee, D. L.; Powers, J. P. S.; Pflegerl, K.; Vasil, M. L.; Hancock, R. E. W.; Hodges, R. S. *The Journal of Peptide Research.* **2004**, *63*, 69-84.

(108) Oren, Z.; Shai, Y. *Biochemistry.* **1997**, *36*, 1826-1835.

(109) Hong, S. Y.; Oh, J. E.; Lee, K.-H. *Biochem. Pharmacol.* **1999**, *58*, 1775-1780.

(110) Grauer, A.; Koenig, B. *Eur. J. Org. Chem.* **2009**, *2009*, 5099-5111.

(111) Gracia, S. R.; Gaus, K.; Sewald, N. *Future Med. Chem.* **2009**, *1*, 1289-1310.

(112) Tossi, A.; Sandri, L.; Giangaspero, A. *Biopolymers.* **2000**, *55*, 4-30.

(113) Agerberth, B.; Lee, J. Y.; Bergman, T.; Carlquist, M.; Boman, H. G.; Mutt, V.; Jörnvall, H. *Eur. J. Biochem.* **1991**, *202*, 849-854.

(114) Gallis, B.; Mehl, J.; Prickett, K.; Martin, J.; Merriam, J.; March, C.; Cerretti, D. *Biotechnol. Ther.* **1988**, *1*, 335-346.

(115) Nakajima, Y.; Qu, X.; Natori, S. *J. Biol. Chem.* **1987**, *262*, 1665-1669.

(116) Mor, A.; Nicolas, P. *J. Biol. Chem.* **1994**, *269*, 1934-1939.

(117) Pasupuleti, M.; Schmidtchen, A.; Chalupka, A.; Ringstad, L.; Malmsten, M. *PLoS One.* **2009**, *4*, e5285.

(118) Chu, H.-L.; Yu, H.-Y.; Yip, B.-S.; Chih, Y.-H.; Liang, C.-W.; Cheng, H.-T.; Cheng, J.-W. *Antimicrob. Agents Chemother.* **2013**, *57*, 4050-4052.

(119) Zhang, L.; Bulaj, G. *Curr. Med. Chem.* **2012**, *19*, 1602-1618.

(120) Laverty, G.; McLaughlin, M.; Shaw, C.; Gorman, S. P.; Gilmore, B. F. *Chem. Biol. Drug Des.* **2010**, *75*, 563-569.

(121) Schneider, T.; Müller, A.; Miess, H.; Gross, H. *Int. J. Med. Microbiol.* **2014**, *304*, 37-43.

(122) Jerala, R. **2007**, *16*, 1159-1169.

(123) Kanlayavattanakul, M.; Lourith, N. *Int. J. Cosmet. Sci.* **2010**, *32*, 1-8.

(124) Mandal, S. M.; Barbosa, A. E. A. D.; Franco, O. L. *Biotechnol. Adv.* **2013**, *31*, 338-345.

(125) Meyers, E.; Parker, W. L.; Brown, W. E.; Linnett, P.; Stroming, J. L. *Ann. N. Y. Acad. Sci.* **1974**, *235*, 493-501.

(126) Howell, S. F. *J Biol Chem.* **1950**, *186*, 863-77.

(127) Aretz, W.; Meiwes, J.; Seibert, G.; Vobis, G.; Wink, J. *J. Antibiot.* **2000**, *53*, 807-815.

(128) Liu, R. F.; Zhang, D. J.; Li, Y. G.; Tao, L. M.; Tian, L. *Helv. Chim. Acta.* **2010**, *93*, 2419-2425.

(129) Naganawa, H.; Hamada, M.; Maeda, K.; Okami, Y.; Takeuchi, T.; Umezawa, H. *J. Antibiot.* **1968**, *21*, 55-62.

(130) Nyfeler, R.; Keller-Schierlein, W. *Helv Chim Acta.* **1974**, *57*, 2459-2477.

(131) Peypoux, F.; Guinand, M.; Michel, G.; Delcambe, L.; Das, B. C.; Lederer, E. *Biochemistry.* **1978**, *17*, 3992-3996.

(132) Peypoux, F.; Pommier, M. T.; Das, B. C.; Besson, F.; Delcambe, L.; Michel, G. *J. Antibiot.* **1984**, *37*, 1600-1604.

(133) Arima, K.; Kakinuma, A.; Tamura, G. *Biochem. Biophys. Res. Commun.* **1968**, *31*, 488-494.

(134) Vanittanakom, N.; Loeffler, W.; Koch, U.; Jung, G. *J. Antibiot.* **1986**, *39*, 888-901.

(135) Konishi, M.; Sugawara, K.; Hanada, M.; Tomita, K.; Tomatsu, K.; Miyaki, T.; Kawaguchi, H.; Buck, R. E.; More, C.; Rossomano, V. Z. *J. Antibiot.* **1984**, *37*, 949-957.

(136) Hashizume, H.; Igarashi, M.; Hattori, S.; Hori, M.; Hamada, M.; Takeuchi, T. *J. Antibiot.* **2001**, *54*, 1054-1059.

(137) Lakey, J. H.; Lea, E. J. A.; Rudd, B. A. M.; Wright, H. M.; Hopwood, D. A. *J. Gen. Microbiol.* **1983**, *129*, 3565-3573.

(138) Shoji, J.; Kato, T. *J. Antibiot.* **1976**, *29*, 380-389.

(139) Kajimura, Y.; Kaneda, M. *J. Antibiot.* **1996**, *49*, 129-135.

(140) Shoji, J.; Hinoo, H. *J. Antibiot.* **1975**, *28*, 60-63.

(141) Kato, T.; Hinoo, H.; Shoji, J. *J Antibiot (Tokyo).* **1978**, *31*, 652-661.

(142) Desjardine, K.; Pereira, A.; Wright, H.; Matainaho, T.; Kelly, M.; Andersen, R. J. *J. Nat. Prod.* **2007**, *70*, 1850-1853.

(143) Balunas, M. J.; Linington, R. G.; Tidgewell, K.; Fenner, A. M.; Urena, L. D.; Della Togna, G.; Kyle, D. E.; Gerwick, W. H. *J. Nat. Prod.* **2010**, *73*, 60-66.

(144) Cochrane, S. A.; Vederas, J. C. *Med. Res. Rev.* **2014**, 1-28.

(145) Steenbergen, J. N.; Alder, J.; Thorne, G. M.; Tally, F. P. *J. Antimicrob. Chemother.* **2005**, *55*, 283-288.

(146) Lamp, K.; Rybak, M.; Bailey, E.; Kaatz, G. *Antimicrob. Agents Chemother.* **1992**, *36*, 2709-2714.

(147) Edmiston Jr, C. E.; Goheen, M. P.; Seabrook, G. R.; Johnson, C. P.; Lewis, B. D.; Brown, K. R.; Towne, J. B. *Am. J. Surg.* **2006**, *192*, 344-354.

(148) LaPlante, K. L.; Mermel, L. A. *Nephrol., Dial., Transplant.* **2007**, *22*, 2239-2246.

(149) Jung, D.; Rozek, A.; Okon, M.; Hancock, R. E. *Chem. Biol.* **2004**, *11*, 949-957.

(150) Mascio, C. T.; Mortin, L. I.; Howland, K. T.; Van Praagh, A. D.; Zhang, S.; Arya, A.; Chuong, C. L.; Kang, C.; Li, T.; Silverman, J. A. *Antimicrob. Agents Chemother.* **2012**, *56*, 5023-5030.

(151) Eliopoulos, G. M.; Willey, S.; Reiszner, E.; Spitzer, P.; Caputo, G.; Moellering, R. *Antimicrob. Agents Chemother.* **1986**, *30*, 532-535.

(152) Jones, R. N.; Barry, A. L. *Antimicrob. Agents Chemother.* **1987**, *31*, 625-629.

(153) Straus, S. K.; Hancock, R. E. *Biochim. Biophys. Acta, Biomembr.* **2006**, *1758*, 1215-1223.

(154) Silverman, J. A.; Perlmutter, N. G.; Shapiro, H. M. *Antimicrob. Agents Chemother.* **2003**, *47*, 2538-2544.

(155) Baltz, R. H.; Miao, V.; Wrigley, S. K. *Nat. Prod. Rep.* **2005**, *22*, 717-741.

(156) Raetz, C. R.; Whitfield, C. *Annu Rev Biochem.* **2002**, *71*, 635-700.

(157) Rifkind, D. *J. Bacteriol.* **1967**, *93*, 1463-1464.

(158) Bergen, P. J.; Li, J.; Rayner, C. R.; Nation, R. L. *Antimicrob. Agents Chemother.* **2006**, *50*, 1953-1958.

(159) Suzuki, T.; Hayashi, K.; Fujikawa, K.; Tsukamoto, K. *J. Biochem.* **1965**, *57*, 226-227.

(160) Velkov, T.; Thompson, P. E.; Nation, R. L.; Li, J. *J. Med. Chem.* **2010**, *53*, 1898-1916.

(161) Barnett, M.; Bushby, S.; Wilkinson, S. *Br. J. Pharmacol. Chemother.* **1964**, *23*, 552-574.

(162) Marumo, K.; Komukai, D.; Hirose, M.; Nakamura, H.; Tanaka, H.; Ugajin, K.; Nagashima, G.; Yoshimura, A. *J. Infect. Chemother.* **2013**, *19*, 348-351.

(163) Herrmann, G.; Yang, L.; Wu, H.; Song, Z.; Wang, H.; Høiby, N.; Ulrich, M.; Molin, S.; Riethmüller, J.; Döring, G. *J. Infect. Dis.* **2010**, *202*, 1585-1592.

(164) Jass, J.; Lappin-Scott, H. M. *J. Antimicrob. Chemother.* **1996**, *38*, 987-1000.

(165) Liu, M.-C.; Lin, S.-B.; Chien, H.-F.; Wang, W.-B.; Yuan, Y.-H.; Hsueh, P.-R.; Liaw, S.-J. *PLoS One*, **2012**, *7*, e45563.

(166) Hancock, R. E. *The Lancet.* **1997**, *349*, 418-422.

(167) Danner, R. L.; Joiner, K.; Rubin, M.; Patterson, W.; Johnson, N.; Ayers, K.; Parrillo, J. *Antimicrob. Agents Chemother.* **1989**, *33*, 1428-1434.

(168) Jerala, R.; Porro, M. *Curr. Top. Med. Chem.* **2004**, *4*, 1173-1184.

(169) Storm, D. R.; Rosenthal, K. S.; Swanson, P. E. *Annu. Rev. Biochem.* **1977**, *46*, 723-763.

(170) Vaara, M.; Vaara, T. *Nature.* **1983**, *303*, 526-528.

(171) Moestrup, S. K.; Cui, S.; Vorum, H.; Bregengård, C.; Bjørn, S.; Norris, K.; Gliemann, J.; Christensen, E. I. *J. Clin. Invest.* **1995**, *96*, 1404-1413.

(172) Falagas, M. E.; Kasiakou, S. K. *Crit. Care.* **2006**, *10*, R27-R40.

(173) Azad, M. A.; Finnin, B. A.; Poudyal, A.; Davis, K.; Li, J.; Hill, P. A.; Nation, R. L.; Velkov, T.; Li, J. *Antimicrob. Agents Chemother.* **2013**, *57*, 4329-4335.

(174) Vaara, M.; Sader, H. S.; Rhomberg, P. R.; Jones, R. N.; Vaara, T. *J. Antimicrob. Chemother.* **2012**, dks438-dks442.

(175) Vaara, M.; Fox, J.; Loidl, G.; Siikanen, O.; Apajalahti, J.; Hansen, F.; Frimodt-Møller, N.; Nagai, J.; Takano, M.; Vaara, T. *Antimicrob. Agents Chemother.* **2008**, *52*, 3229-3236.

(176) Meyers, E.; Parker, W. L.; Brown, W. E.; Shoji, J. I.; Wakiska, Y. *J. Antibiot.* **1976**, *29*, 1241-1242.

(177) Qian, C. D.; Wu, X. C.; Teng, Y.; Zhao, W. P.; Li, O.; Fang, S. G.; Huang, Z. H.; Gao, H. C. *Antimicrob. Agents Chemother.* **2012**, *56*, 1458-1465.

(178) Vigneaud, V. d.; Ressler, C.; Swan, C. J. M.; Roberts, C. W.; Katsoyannis, P. G.; Gordon, S. *J. Am. Chem. Soc.* **1953**, *75*, 4879-4880.

(179) Yajima, H.; Fujii, N. *J. Chem. Soc., Chem. Commun.* **1980**, 115-116.

(180) Kent, S. B. *Annu. Rev. Biochem.* **1988**, *57*, 957-989.

(181) Merrifield, R. B. *J. Am. Chem. Soc.* **1963**, *85*, 2149-2154.

(182) Merrifield, B. *Biosci. Rep.* **1985**, *5*, 353-376.

(183) Atherton, E.; Fox, H.; Harkiss, D.; Sheppard, R. *J. Chem. Soc., Chem. Commun.* **1978**, 539-540.

(184) Chan, W. C.; White, P. D., *Fmoc solid phase peptide synthesis A practical approach*. Oxford University Press: Nottingham, **2000**.

(185) Sarin, V. K.; Kent, S. B. H.; Merrifield, R. B. *J. Am. Chem. Soc.* **1980**, *102*, 5463-5470.

(186) Pugh, K. C.; York, E. J.; Stewart, J. M. *Int. J. Pept. Protein Res.* **1992**, *40*, 208-213.

(187) Fields, G. B.; Noble, R. L. *Int. J. Pept. Protein Res.* **1990**, *35*, 161-214.

(188) Zalipsky, S.; Chang, J. L.; Albericio, F.; Barany, G. *React. Polym.* **1994**, *22*, 243-258.

(189) Barlos, K.; Chatzi, O.; Gatos, D.; Stavropoulos, G. *Int. J. Pept. Protein Res.* **1991**, *37*, 513-520.

(190) Chatzi, K. B.; Gatos, D.; Stavropoulos, G. *Int. J. Pept. Protein Res.* **1991**, *37*, 513-520.

(191) Rink, H. *Tetrahedron Lett.* **1987**, *28*, 3787-3790.

(192) Jursic, B. S.; Zdravkovski, Z. *Synth. Commun.* **1993**, *23*, 2761-2770.

(193) Sheehan, J. C.; Hess, G. P. *J. Am. Chem. Soc.* **1955**, *77*, 1067-1068.

(194) El-Faham, A.; Albericio, F. *Chem. Rev.* **2011**, *111*, 6557-6602.

(195) Valeur, E.; Bradley, M. *Chem. Soc. Rev.* **2009**, *38*, 606-631.

(196) Koning, W.; Geiger, R. *Chem. Ber.* **1970**, *103*, 2024-2034.

(197) Carpino, L. A. *J. Am. Chem. Soc.* **1993**, *115*, 4397-4398.

(198) Montalbetti, C. A. G. N.; Falque, V. *Tetrahedron.* **2005**, *61*, 10827-10852.

(199) Gawne, G.; Kenner, G. W.; Sheppard, R. C. *J. Am. Chem. Soc.* **1969**, *91*, 5669-5671.

(200) Carpino, L. A.; El-Faham, A.; Albericio, F. *Tetrahedron Lett.* **1994**, *35*, 2279-2282.

(201) Castro, B.; Dormoy, J. R.; Dourtoglou, B.; Evin, G.; Selve, C.; Ziegler, J. C. *Synthesis-Stuttgart.* **1976**, 751-752.

(202) Coste, J.; Le-Nguyen, D.; Castro, B. *Tetrahedron Lett.* **1990**, *31*, 205-208.

(203) Albericio, F.; Cases, M.; Alsina, J.; Triolo, S. A.; Carpino, L. A.; Kates, S. A. *Tetrahedron Lett.* **1997**, *38*, 4853-4856.

(204) Carpino, L. A.; Imazumi, H.; El-Faham, A.; Ferrer, F. J.; Zhang, C.; Lee, Y.; Foxman, B. M.; Henklein, P.; Hanay, C.; Mügge, C. *Angew. Chem. Int. Ed.* **2002**, *41*, 441-445.

(205) Marder, O.; Shvo, Y.; Albiricio, F. *Chim. Oggi.* **2002**, *20*, 37-41.

(206) Sabatino, G.; Mulinacci, B.; Alcaro, M. C.; Chelli, M.; Rovero, P.; Papini, A. M. *Lett. Pept. Sci.* **2002**, *9*, 119-123.

(207) King, D. S.; Fields, C. G.; Fields, G. B. *Int. J. Pept. Protein Res.* **1990**, *36*, 255-266.

(208) Biemann, K. *Annu. Rev. Biochem.* **1992**, *61*, 977-1010.

(209) Sakurai, T.; Fujita, Y.; Matsuo, T.; Matsuda, H.; Katakuse, I.; Miseki, K. *Int. J. Mass Spectrom. Ion Processes.* **1985**, *66*, 283-290.

(210) Fenn, J.; Mann, M.; Meng, C.; Wong, S.; Whitehouse, C. *Science.* **1989**, *246*, 64-71.

(211) Bruins, A. P. *J. Chromatogr. A.* **1998**, *794*, 345-357.

(212) Karas, M.; Bahr, U.; Gießmann, U. *Mass Spectrom. Rev.* **1991**, *10*, 335-357.

(213) Tanaka, K.; Waki, H.; Ido, Y.; Akita, S.; Yoshida, Y.; Yoshida, T.; Matsuo, T. *Rapid Commun. Mass Spectrom.* **1988**, *2*, 151-153.

(214) Karas, M.; Bachmann, D.; Hillenkamp, F. *Anal. Chem.* **1985**, *57*, 2935-2939.

(215) Knochenmuss, R. *Analyst.* **2006**, *131*, 966-986.

(216) Karas, M.; Glückmann, M.; Schäfer, J. *J. Mass Spectrom.* **2000**, *35*, 1-12.

(217) Conlon, J. M. *Nat. Protoc.* **2007**, *2*, 191-197.

(218) Hancock, W.; Bishop, C.; Prestidge, R.; Harding, D.; Hearn, M. *Science.* **1978**, *200*, 1168-1170.

(219) Moreno, S.; Scheyer, T.; Romano, C. S.; Vojnov, A. A. *Free Radical Res.* **2006**, *40*, 223-231.

(220) Orlova, E. V.; Saibil, H. R. *Chem. Rev.* **2011**, *111*, 7710-7748.

(221) Kammlott, G. W. *Surf. Sci.* **1971**, *25*, 120-146.

(222) Vernon-Parry, K. D. *III-Vs Review.* **2000**, *13*, 40-44.

(223) Corrêa, D. H.; Ramos, C. H. *Afr. J. Biochem. Res.* **2009**, *3*, 164-173.

(224) Kelly, S. M.; Jess, T. J.; Price, N. C. *Biochim. Biophys. Acta, Proteins Proteomics.* **2005**, *1751*, 119-139.

(225) Johnson Jr, W. C.; Tinoco Jr, I. *J. Am. Chem. Soc.* **1972**, *94*, 4389-4390.

(226) Brahms, S.; Brahms, J. *J. Mol. Biol.* **1980**, *138*, 149-178.

(227) Wüthrich, K., *NMR of proteins and nucleic acids*. Wiley New York, **1986**.

(228) Cavanagh, J.; Fairbrother, W. J.; Palmer III, A. G.; Skelton, N. J., *Protein NMR spectroscopy: principles and practice*. Academic Press, **1995**.

(229) Wishart, D. S.; Sykes, B. D.; Richards, F. M. *J. Mol. Biol.* **1991**, *222*, 311-333.

(230) Dyson, H. J.; Wright, P. E. *Annu. Rev. Biophys. Biophys. Chem.* **1991**, *20*, 519-538.

(231) Karplus, M. *J. Am. Chem. Soc.* **1963**, *85*, 2870-2871.

(232) Pardi, A.; Billeter, M.; Wüthrich, K. *J. Mol. Biol.* **1984**, *180*, 741-751.

(233) Baxter, N. J.; Williamson, M. P. *J. Biomol. NMR.* **1997**, *9*, 359-369.

(234) Hruby, V. J. *Chem. Biochem. Amino Acids, Pept., Proteins.* **1974**, *3*, 1-188.

(235) Hinds, M. G.; Norton, R. S. *Mol. Biotechnol.* **1997**, *7*, 315-331.

(236) Braunschweiler, L.; Ernst, R. *J. Magn. Reson.* **1983**, *53*, 521-528.

(237) Bax, A. *Annu. Rev. Biochem.* **1989**, *58*, 223-256.

(238) Good, R. J. *J. Adhes. Sci. Technol.* **1992**, *6*, 1269-1302.

(239) Bernardin, J. D.; Mudawar, I.; Walsh, C. B.; Franses, E. I. *Int. J. Heat Mass Transfer.* **1997**, *40*, 1017-1033.

(240) Collins, R. W.; Kim, Y.-T. *Anal. Chem.* **1990**, *62*, 887A-900A.

(241) McCrackin, F. L.; Passaglia, E.; Stromberg, R. R.; Steinberg, H. L. *J. Res. Nat. Bur. Sect. A.* **1963**, *67*.

(242) Moulder, J. F.; Stickle, W. F.; Sobol, P. E.; Bomben, K. D., *Handbook of X-ray Photoelectron Spectroscopy*. Perkin-Elmer Corporation: Minnesota, United States of America, **1992**.

(243) Hollander, J. M.; Jolly, W. L. *Acc. Chem. Res.* **1970**, *3*, 193-200.

(244) Watts, J. F. *Vacuum.* **1994**, *45*, 653-671.

(245) Vogler, K.; Studer, R. *Experientia.* **1966**, *22*, 345-354.

(246) Vogler, K.; Studer, R.; Lanz, P.; Lergier, W.; Böhni, E. *Experientia.* **1964**, *20*, 365-366.

(247) Sharma, S.; Wu, A.; Chandramouli, N.; Fotsch, C.; Kardash, G.; Bair, K. *J. Pept. Res*. **1999**, *53*, 501-506.

(248) Tsubery, H.; Ofek, I.; Cohen, S.; Fridkin, M. *J. Med. Chem.* **2000**, *43*, 3085-3092.

(249) Sakura, N.; Itoh, T.; Uchida, Y.; Ohki, K.; Okimura, K.; Chiba, K.; Sato, Y.; Sawanishi, H. *Bull. Chem. Soc. Jpn.* **2004**, *77*, 1915-1924.

(250) de Visser, P.; Kriek, N.; Hooft, P.; Van Schepdael, A.; Filippov, D.; Marel, G.; Overkleeft, H.; Boom, J.; Noort, D. *J. Pept. Res.* **2003**, *61*, 298-306.

(251) Aletras, A.; Barlos, K.; Gatos, D.; Koutsogianni, S.; Mamos, P. *Int. J. Pept. Protein Res.* **1995**, *45*, 488-496.

(252) Murai, A.; Amino, Y.; Ando, T. *J. Antibiot.* **1985**, *38*, 1610-1613.

(253) Li, D.; Elbert, D. *J. Pept. Res.* **2002**, *60*, 300-303.

(254) Davies, J. S. *J. Pept. Sci.* **2003**, *9*, 471-501.

(255) Zimmer, S.; Hoffmann, E.; Jung, G.; Kessler, H. *Liebigs Ann. Chem.* **1993**, *1993*, 497-501.

(256) Tsubery, H.; Ofek, I.; Cohen, S.; Eisenstein, M.; Fridkin, M. *Mol. Pharmacol.* **2002**, *62*, 1036-1042.

(257) Okimura, K.; Ohki, K.; Sato, Y.; Ohnishi, K.; Uchida, Y.; Sakura, N. *Bull. Chem. Soc. Jpn.* **2007**, *80*, 543-552.

(258) O'Dowd, H.; Kim, B.; Margolis, P.; Wang, W.; Wu, C.; Lopez, S. L.; Blais, J. *Tetrahedron Lett.* **2007**, *48*, 2003-2005.

(259) Chihara, S.; Ito, A.; Yahata, M.; Tobita, T.; Koyama, Y. *Agric. Biol. Chem.* **1974**, *38*, 521-529.

(260) Tsubery, H.; Ofek, I.; Cohen, S.; Fridkin, M. *Peptides.* **2001**, *22*, 1675-1681.

(261) Scortichini, M.; Rossi, M. P. *J. Appl. Bacteriol.* **1991**, *71*, 113-118.

(262) Ferrante, P.; Scortichini, M. *Plant Path.* **2010**, *59*, 954-962.

(263) Tsubery, H.; Ofek, I.; Cohen, S.; Fridkin, M. Structure activity relationship study of polymyxin B nonapeptide. In *The Biology and Pathology of Innate Immunity Mechanisms*, Springer, USA, **2002**; pp 219-222.

(264) Vaara, M. *Drugs Exp. Clin. Res.* **1990**, *17*, 437-443.

(265) Kurihara, T.; Takeda, H.; Ito, H. *J. Pharm. Soc. Jpn.* **1972**, *92*, 129-134.

(266) Teuber, M. *Z. Naturforsch., B: J. Chem. Sci.* **1970**, *25*, 117-117.

(267) Srinivasa, B.; Ramachandran, L. *Indian J. Biochem. Biophys.* **1978**, *15*, 54-58.

(268) Porro, M., Synthetic peptides for detoxification of bacterial endotoxins and for the prevention and treatment of septic shock. Google Patents: 1994.

(269) Aletras, A.; Barlos, K.; Gatos, D.; Koutsogianni, S.; Mamos, P. *Int. J. Pept. Protein Res.* **1995**, *45*, 488-496.

(270) Barlos, K.; Gatos, D.; Kapolos, S.; Papaphotiu, G.; Schafer, W.; Yao, W. Q. *Tetrahedron Lett.* **1989**, *30*, 3947-3950.

(271) Barlos, K.; Chatzi, O.; Gatos, D.; Stavropoulos, G. *Int. J. Pept. Protein. Res.* **1991**, *37*, 513-20.

(272) Zimmer, S.; Hoffmann, E.; Jung, G.; Kessler, H. *Liebigs Ann. Chem.* **1993**, 497-501.

(273) Hardalo, C.; Edberg, S. C. *Crit. Rev. Microbiol.* **1997**, *23*, 47-75.

(274) Rossolini, G. M.; Mantengoli, E. *Clin. Microbiol. Infect.* **2005**, *11*, 17-32.

(275) Bodey, G. P.; Bolivar, R.; Fainstein, V.; Jadeja, L. *Rev. Infect. Dis.* **1983**, *5*, 279-313.

(276) Driscoll, J. A.; Brody, S. L.; Kollef, M. H. *Drugs.* **2007**, *67*, 351-368.

(277) Koch, C.; Hoiby, N. *The Lancet.* **1993**, *341*, 1065-1069.

(278) Govan, J. R.; Deretic, V. *Microbiol. Rev.* **1996**, *60*, 539-574.

(279) D'Agata, E. *Infect. Control.* **2004**, *25*, 842-846.

(280) Li, X.-Z.; Nikaido, H.; Poole, K. *Antimicrob. Agents Chemother.* **1995**, *39*, 1948-1953.

(281) Livermore, D. M. *Clin. Microbiol. Rev.* **1995**, *8*, 557-584.

(282) Poole, K. *Antimicrob. Agents Chemother.* **2005**, *49*, 479-487.

(283) Emori, T. G.; Gaynes, R. P. *Clin. Microbiol. Rev.* **1993**, *6*, 428-442.

(284) Archer, G. L. *Clin. Infect. Dis.* **1998**, *26*, 1179-1181.

(285) Barrett, F. F.; McGehee Jr, R. F.; Finland, M. *N. Engl. J. Med.* **1968**, *279*, 441-448.

(286) Udo, E.; Pearman, J.; Grubb, W. *J. Hosp. Infect.* **1993**, *25*, 97-108.

(287) Karmali, M.; Petric, M.; Steele, B.; Lim, C. *The Lancet.* **1983**, *321*, 619-620.

(288) Pennington, H. *The Lancet.* **2010**, *376*, 1428-1435.

(289) Rasko, D. A.; Webster, D. R.; Sahl, J. W.; Bashir, A.; Boisen, N.; Scheutz, F.; Paxinos, E. E.; Sebra, R.; Chin, C.-S.; Iliopoulos, D.; Klammer, A.; Peluso, P.; Lee, L.; Kislyuk, A. O.; Bullard, J.; Kasarskis, A.; Wang, S.; Eid, J.; Rank, D.; Redman, J. C.; Steyert, S. R.; Frimodt-Møller, J.; Struve, C.; Petersen, A. M.; Krogfelt, K. A.; Nataro, J. P.; Schadt, E. E.; Waldor, M. K. *N. Engl. J. Med.* **2011**, *365*, 709-717.

(290) Johnson, K. B.; Stockwell, V. O., *Biological control of fire blight. In Fire blight the disease and its causative agent, Erwinia amylovora*. CABI publishing, **2000**.

(291) Vanneste, J. L. *Fire blight: the disease and its causative agent, Erwinia amylovora.* **2000**, 1-6.

(292) Everett, K.; Taylor, R.; Romberg, M.; Rees-George, J.; Fullerton, R.; Vanneste, J.; Manning, M. *Australasian Plant Dis. Notes.* **2011**, *6*, 67-71.

(293) Greer, G.; Saunders, C., *The costs of Psa-V to the New Zealand kiwifruit industry and the wider community*. Lincoln University. Agricultural Economics Research Unit, **2012**.

(294) Goto, M.; Hikota, T.; Nakajima, M.; Takikawa, Y.; Tsuyumu, S. *Jpn. J. Phytopathol.* **1994**, *60*, 147-153.

(295) Nakajima, M.; Masao, G.; Tadaaki, H. *J. Gen. Plant Pathol.* **2002**, *68*, 68-74.

(296) Cameron, A.; Zoysa, G. H. D.; Sarojini, V. *Biopolymers.* **2014**, *102*, 88-96.

(297) Ferre, R.; Badosa, E.; Feliu, L.; Planas, M.; Montesinos, E.; Bardají, E. *Appl. Environ. Microbiol.* **2006**, *72*, 3302-3308.

(298) Storm, D. R.; Rosenthal, K. S.; Swanson, P. E. *Annu. Rev. Biochem.* **1977**, *46*, 723-763.

(299) Cochrane, S. A.; Lohans, C. T.; Brandelli, J. R.; Mulvey, G.; Armstrong, G. D.; Vederas, J. C. *J. Med. Chem.* **2014**, *57*, 1127-31.

(300) Moore, R. A.; Bates, N. C.; Hancock, R. *Antimicrob. Agents Chemother.* **1986**, *29*, 496-500.

(301) Ray, T.; Smith, A.; Carter, K.; Hignett, R. *J. Gen. Microbiol.* **1986**, *132*, 3159-3167.

(302) Katsuma, N.; Sato, Y.; Ohki, K.; Okimura, K.; Ohnishi, K.; Sakura, N. *Chem. Pharm. Bull.* **2009**, *57*, 332-336.

(303) Stead, D. E.; Sellwood, J. E.; Wilson, J.; Viney, I. *J. Appl. Bacteriol.* **1992**, *72*, 315-321.

(304) Nikaido, H. *Biochim. Biophys. Acta, Biomembr.* **1976**, *433*, 118-132.

(305) Oren, Z.; Shai, Y. *Biochemistry.* **2000**, *39*, 6103-6114.

(306) Pankuch, G. A.; Jacobs, M. R.; Appelbaum, P. C. *Antimicrob. Agents Chemother.* **1994**, *38*, 2065-2072.

(307) Tam, V. H.; Schilling, A. N.; Vo, G.; Kabbara, S.; Kwa, A. L.; Wiederhold, N. P.; Lewis, R. E. *Antimicrob. Agents Chemother.* **2005**, *49*, 3624-3630.

(308) Scortichini, M.; Marcelletti, S.; Ferrante, P.; Petriccione, M.; Firrao, G. *Mol. Plant Pathol.* **2012**, *13*, 631-640.

(309) Balestra, G.; Mazzaglia, A.; Quattrucci, A.; Renzi, M.; Rossetti, A. *Australasian Plant Dis. Notes.* **2009**, *4*, 34-36.

(310) Webb, R. *J. Bacteriol.* **1954**, *67*, 252-253.

(311) Kjærgaard, K.; Schembri, M. A.; Hasman, H.; Klemm, P. *J. Bacteriol.* **2000**, *182*, 4789-4796.

(312) Molecular Probes Live/Dead BacLight bacteria viability kit technical sheet. Inc, M. P., Ed. 1995.

(313) Flemming, H.-C.; Wingender, J. *Nat. Rev. Microbiol.* **2010**, *8*, 623-633.

(314) Gacesa, P. *Microbiology.* **1998**, *144*, 1133-1143.

(315) Chan, C.; Burrows, L. L.; Deber, C. M. *J. Pept. Res.* **2005**, *65*, 343-351.

(316) Cramton, S. E.; Gerke, C.; Schnell, N. F.; Nichols, W. W.; Götz, F. *Infect. Immun.* **1999**, *67*, 5427-5433.

(317) Vuong, C.; Voyich, J. M.; Fischer, E. R.; Braughton, K. R.; Whitney, A. R.; DeLeo, F. R.; Otto, M. *Cell. Microbiol.* **2004**, *6*, 269-275.

(318) Morrison, K. L.; Weiss, G. A. *Curr. Opin. Chem. Biol.* **2001**, *5*, 302-307.

(319) Kanazawa, K.; Sato, Y.; Ohki, K.; Okimura, K.; Uchida, Y.; Shindo, M.; Sakura, N. *Chem. Pharm. Bull.* **2009**, *57*, 240-244.

(320) Rasoul, F.; Ercole, F.; Pham, Y.; Bui, C. T.; Wu, Z.; James, S. N.; Trainor, R. W.; Wickham, G.; Maeji, N. J. *Pept. Sci.* **2000**, *55*, 207-216.

(321) Ede, N. J. *J. Immunol. Methods.* **2002**, *267*, 3-11.

(322) Feliu, L.; Subra, G.; Martinez, J.; Amblard, M. *J. Comb. Chem.* **2003**, *5*, 356-361.

(323) Basso, A.; Ernst, B. *Tetrahedron Lett.* **2001**, *42*, 6687-6690.

(324) Takahashi, T.; Nagamiya, H.; Doi, T.; Griffiths, P. G.; Bray, A. M. *J. Comb. Chem.* **2003**, *5*, 414-428.

(325) Matsuzaki, K. *Biochim. Biophys. Acta, Biomembr.* **2009**, *1788*, 1687-1692.

(326) Kolusheva, S.; Boyer, L.; Jelinek, R. *Nat. Biotechnol.* **2000**, *18*, 225-227.

(327) Cheng, Q.; Stevens, R. C. *Langmuir.* **1998**, *14*, 1974-1976.

(328) Kolusheva, S.; Shahal, T.; Jelinek, R. *J. Am. Chem. Soc.* **2000**, *122*, 776-780.

(329) Okada, S. Y.; Jelinek, R.; Charych, D. *Angew. Chem. Int. Ed.* **1999**, *38*, 655-659.

(330) Ramamoorthy, A.; Thennarasu, S.; Lee, D.-K.; Tan, A.; Maloy, L. *Biophys. J.* **2006**, *91*, 206-216.

(331) Luzzatto, L.; Apirion, D.; Schlessinger, D. *Proc. Natl. Acad. Sci. U. S. A.* **1968**, *60*, 873.

(332) Rosenthal, K. S.; Swanson, P. E.; Storm, D. R. *Biochemistry.* **1976**, *15*, 5783-5792.

(333) Loh, B.; Grant, C.; Hancock, R. E. W. *Antimicrob. Agents Chemother.* **1984**, *26*, 546-551.

(334) Nicoletti, I.; Migliorati, G.; Pagliacci, M. C.; Grignani, F.; Riccardi, C. *J. Immunol. Methods.* **1991**, *139*, 271-279.

(335) Stover, C. K.; Pham, X. Q.; Erwin, A.; Mizoguchi, S.; Warrener, P.; Hickey, M.; Brinkman, F.; Hufnagle, W.; Kowalik, D.; Lagrou, M. *Nature.* **2000**, *406*, 959-964.

(336) Ito, T.; Okuma, K.; Ma, X. X.; Yuzawa, H.; Hiramatsu, K. *Drug Resist. Update.* **2003**, *6*, 41-52.

(337) Kandasamy, S. K.; Larson, R. G. *Biochim. Biophys. Acta, Biomembr.* **2006**, *1758*, 1274-1284.

(338) Goldman, M. J.; Anderson, G. M.; Stolzenberg, E. D.; Kari, U. P.; Zasloff, M.; Wilson, J. M. *Cell.* **1997**, *88*, 553-560.

(339) Park, I. Y.; Cho, J. H.; Kim, K. S.; Kim, Y.-B.; Kim, M. S.; Kim, S. C. *J. Biol. Chem.* **2004**, *279*, 13896-13901.

(340) Tam, J. P.; Lu, Y.-A.; Yang, J.-L. *J. Biol. Chem.* **2002**, *277*, 50450-50456.

(341) Lee, D. G.; Park, Y.; Jin, I.; Hahm, K. S.; Lee, H. H.; Moon, Y. H.; Woo, E. R. *J. Pept. Sci.* **2004**, *10*, 298-303.

(342) Chen, Y.-H.; Yang, J. T.; Chau, K. H. *Biochemistry.* **1974**, *13*, 3350-3359.

(343) Sonnichsen, F.; Van Eyk, J.; Hodges, R.; Sykes, B. *Biochemistry.* **1992**, *31*, 8790-8798.

(344) Cammers-Goodwin, A.; Allen, T. J.; Oslick, S. L.; McClure, K. F.; Lee, J. H.; Kemp, D. *J. Am. Chem. Soc.* **1996**, *118*, 3082-3090.

(345) Rajan, R.; Balaram, P. *Int. J. Pept. Protein Res.* **1996**, *48*, 328-336.

(346) Bruch, M. D.; Cajal, Y.; Koh, J. T.; Jain, M. K. *J. Am. Chem. Soc.* **1999**, *121*, 11993-12004.

(347) Cajal, Y.; Ghanta, J.; Easwaran, K.; Surolia, A.; Jain, M. K. *Biochemistry.* **1996**, *35*, 5684-5695.

(348) BIOVIA, D. S. *Discovery Studio Modeling Environment*, DassaultSystèmes: San Diego, 2015.

(349) Kjaergaard, K.; Schembri, M. A.; Hasman, H.; Klemm, P. *J. Bacteriol.* **2000**, *182*, 4789-96.

(350) Subra, G.; Soulere, L.; Hoffmann, P.; Enjalbal, C.; Aubagnac, J. L.; Martinez, J. *QSAR Comb. Sci.* **2003**, *22*, 646-651.

(351) Stark, M.; Liu, L.-P.; Deber, C. M. *Antimicrob. Agents Chemother.* **2002**, *46*, 3585-3590.

(352) Lim, K.; Chua, R. R.; Saravanan, R.; Basu, A.; Mishra, B.; Tambyah, P. A.; Ho, B.; Leong, S. S. *ACS Appl. Mater. Interfaces.* **2013**, *5*, 6412-6422.

(353) Mishra, B.; Basu, A.; Saravanan, R.; Xiang, L.; Yang, L. K.; Leong, S. S. J. *RSC Adv.* **2013**, *3*, 9534-9543.

(354) Karplus, M. *J. Comput. Chem.* **1983**, *4*, 187-217.

(355) Siedenbiedel, F.; Tiller, J. C. *Polymers.* **2012**, *4*, 46-71.

(356) Alves, D.; Olivia Pereira, M. *Biofouling.* **2014**, *30*, 483-99.

(357) Abu El-Asrar, A.; Shibl, A.; Tabbara, K.; Al-Kharashi, S. *Int. Ophthalmol.* **1997**, *21*, 71-74.

(358) Nucci, M. L.; Shorr, R.; Abuchowski, A. *Adv. Drug Delivery Rev.* **1991**, *6*, 133-151.

(359) Kamal, G. D.; Pfaller, M. A.; Rempe, L. E.; Jebson, P. R. *JAMA.* **1991**, *265*, 2364-2368.

(360) Bach, A.; Darby, D.; Böttiger, B.; Böhrer, H.; Motsch, J.; Martin, E. *Intensive Care Med.* **1996**, *22*, 1066-1069.

(361) Thornton, J.; Todd, N. J.; Webster, N. R. *Anaesthesia.* **1996**, *51*, 1018-1020.

(362) Chen, R. X.; Cole, N.; Willcox, M. D. P.; Park, J.; Rasul, R.; Carter, E.; Kumar, N. *Biofouling.* **2009**, *25*, 517-524.

(363) Maki, D. G.; Cobb, L.; Garman, J. K.; Shapiro, J. M.; Ringer, M.; Helgerson, R. B. *Am. J. Med.* **1988**, *85*, 307-314.

(364) Bryers, J. D.; Jarvis, R. A.; Lebo, J.; Prudencio, A.; Kyriakides, T. R.; Uhrich, K. *Biomaterials.* **2006**, *27*, 5039-5048.

(365) Ravikumar, T.; Murata, H.; Koepsel, R. R.; Russell, A. J. *Biomacromolecules.* **2006**, *7*, 2762-2769.

(366) Darouiche, R. O.; Raad, I. I.; Heard, S. O.; Thornby, J. I.; Wenker, O. C.; Gabrielli, A.; Berg, J.; Khardori, N.; Hanna, H.; Hachem, R.; Harris, R. L.; Mayhall, G. *N. Engl. J. Med.* **1999**, *340*, 1-8.

(367) Bong, J. J.; Kite, P.; Wilco, M. H.; McMahon, M. J. *J. Clin. Pathol.* **2003**, *56*, 731-735.

(368) Lam, P.; Chan, E.; Ho, W.; Liew, C. *Br. J. Biomed. Sci.* **2003**, *61*, 125-127.

(369) Salwiczek, M.; Qu, Y.; Gardiner, J.; Strugnell, R. A.; Lithgow, T.; McLean, K. M.; Thissen, H. *Trends Biotechnol.* **2014**, *32*, 82-90.

(370) Willcox, M. D.; Hume, E. B.; Aliwarga, Y.; Kumar, N.; Cole, N. *J. Appl. Microbiol.* **2008**, *105*, 1817-25.

(371) Gabriel, M.; Nazmi, K.; Veerman, E. C.; Amerongen, A. V. N.; Zentner, A. *Bioconjugate Chem.* **2006**, *17*, 548-550.

(372) Chen, G.; Zhou, M.; Chen, S.; Lv, G.; Yao, J. *Nanotechnology.* **2009**, *20*, 465706.

(373) Peyre, J.; Humblot, V.; Methivier, C.; Berjeaud, J. M.; Pradier, C. M. *J. Phys Chem. B.* **2012**, *116*, 13839-47.

(374) Blin, T.; Purohit, V.; Leprince, J.; Jouenne, T.; Glinel, K. *Biomacromolecules.* **2011**, *12*, 1259-1264.

(375) Glinel, K.; Jonas, A. M.; Jouenne, T.; Leprince, J.; Galas, L.; Huck, W. T. *Bioconjugate Chem.* **2009**, *20*, 71-77.

(376) Laloyaux, X.; Fautré, E.; Blin, T.; Purohit, V.; Leprince, J.; Jouenne, T.; Jonas, A. M.; Glinel, K. *Adv. Mater.* **2010**, *22*, 5024-5028.

(377) Kulagina, N. V.; Shaffer, K. M.; Anderson, G. P.; Ligler, F. S.; Taitt, C. R. *Anal. Chim. Acta.* **2006**, *575*, 9-15.

(378) Humblot, V.; Yala, J.-F.; Thebault, P.; Boukerma, K.; Héquet, A.; Berjeaud, J.-M.; Pradier, C.-M. *Biomaterials.* **2009**, *30*, 3503-3512.

(379) Haynie, S. L.; Crum, G. A.; Doele, B. A. *Antimicrob. Agents Chemother.* **1995**, *39*, 301-307.

(380) Cho, W.-M.; Joshi, B. P.; Cho, H.; Lee, K.-H. *Bioorg. Med. Chem. Lett.* **2007**, *17*, 5772-5776.

(381) Bagheri, M.; Beyermann, M.; Dathe, M. *Bioconjugate Chem.* **2011**, *23*, 66-74.

(382) Shukla, A.; Fleming, K. E.; Chuang, H. F.; Chau, T. M.; Loose, C. R.; Stephanopoulos, G. N.; Hammond, P. T. *Biomaterials.* **2010**, *31*, 2348-2357.

(383) Gao, G.; Lange, D.; Hilpert, K.; Kindrachuk, J.; Zou, Y.; Cheng, J. T. J.; Kazemzadeh-Narbat, M.; Yu, K.; Wang, R.; Straus, S. K.; Brooks, D. E.; Chew, B. H.; Hancock, R. E. W.; Kizhakkedathu, J. N. *Biomaterials.* **2011**, *32*, 3899-3909.

(384) Gao, G.; Yu, K.; Kindrachuk, J.; Brooks, D. E.; Hancock, R. E. W.; Kizhakkedathu, J. N. *Biomacromolecules.* **2011**, *12*, 3715-3727.

(385) Wang, Q.; Uzunoglu, E.; Wu, Y.; Libera, M. *ACS Appl. Mater. Interfaces.* **2012**, *4*, 2498-2506.

(386) Vreuls, C.; Zocchi, G.; Garitte, G.; Archambeau, C.; Martial, J.; Van de Weerdt, C. *Biofouling.* **2010**, *26*, 645-656.

(387) Mohorčič, M.; Jerman, I.; Zorko, M.; Butinar, L.; Orel, B.; Jerala, R.; Friedrich, J. *J Mater Sci: Mater Med.* **2010**, *21*, 2775-2782.

(388) Etienne, O.; Picart, C.; Taddei, C.; Haikel, Y.; Dimarcq, J.; Schaaf, P.; Voegel, J.; Ogier, J.; Egles, C. *Antimicrob. Agents Chemother.* **2004**, *48*, 3662-3669.

(389) Shalev, T.; Gopin, A.; Bauer, M.; Stark, R. W.; Rahimipour, S. *J. Mater. Chem.* **2012**, *22*, 2026-2032.

(390) Ivanov, I. E.; Morrison, A. E.; Cobb, J. E.; Fahey, C. A.; Camesano, T. A. *ACS Appl. Mater. Interfaces.* **2012**, *4*, 5891-5897.

(391) Appendini, P.; Hotchkiss, J. *J. Appl. Polym. Sci.* **2001**, *81*, 609-616.

(392) Onaizi, S. A.; Leong, S. S. *Biotechnol Adv.* **2011**, *29*, 67-74.

(393) Wong, L. S.; Khan, F.; Micklefield, J. *Chem. Rev.* **2009**, *109*, 4025-4053.

(394) Bagheri, M.; Beyermann, M.; Dathe, M. *Antimicrob. Agents Chemother.* **2009**, *53*, 1132-1141.

(395) Hilpert, K.; Elliott, M.; Jenssen, H.; Kindrachuk, J.; Fjell, C. D.; Körner, J.; Winkler, D. F.; Weaver, L. L.; Henklein, P.; Ulrich, A. S. *Chem. Biol.* **2009**, *16*, 58-69.

(396) Bernik, D. L. *Recent Pat. Nanotechnol.* **2007**, *1*, 186-92.

(397) De Zoysa, G. H.; Cameron, A. J.; Hegde, V. V.; Raghothama, S.; Sarojini, V. *J. Med. Chem.* **2015**, *58*, 625-639.

(398) Nanci, A.; Wuest, J. D.; Peru, L.; Brunet, P.; Sharma, V.; Zalzal, S.; McKee, M. D. *J. Biomed. Mater. Res.* **1998**, *40*, 324-335.

(399) Xiao, S.-J.; Textor, M.; Spencer, N. D.; Sigrist, H. *Langmuir.* **1998**, *14*, 5507-5516.

(400) Howarter, J. A.; Youngblood, J. P. *Langmuir.* **2006**, *22*, 11142-11147.

(401) White, L.; Tripp, C. *J. Colloid Interface Sci.* **2000**, *232*, 400-407.

(402) Kim, J.; Seidler, P.; Wan, L. S.; Fill, C. *J. Colloid Interface Sci.* **2009**, *329*, 114-119.

(403) Cuypers, P. A.; Corsel, J. W.; Janssen, M. P.; Kop, J.; Hermens, W. T.; Hemker, H. C. *J. Biol. Chem.* **1983**, *258*, 2426-2431.

(404) Hermanson, G. T., *Bioconjugate techniques*. Academic Press, San Diego, **1996**.

(405) Moulder, J. F.; Stickle, W. F.; Sobol, P. E.; Bomben, K. D., *Handbook of X-ray Photoelectron Spectroscopy*. Perkin Elmer Corp, Eden Prairie, **1992**.

(406) Martin, H. J.; Schulz, K. H.; Bumgardner, J. D.; Walters, K. B. *Langmuir.* **2007**, *23*, 6645-6651.

(407) Shamsi, F.; Coster, H.; Jolliffe, K. A.; Chilcott, T. *Mater. Chem. Phys.* **2011**, *126*, 955-961.

(408) Olivares, O.; Likhanova, N.; Gomez, B.; Navarrete, J.; Llanos-Serrano, M.; Arce, E.; Hallen, J. *Appl. Surf. Sci.* **2006**, *252*, 2894-2909.

(409) Metson, J.; Bancroft, G.; McIntyre, N.; Chauvin, W. *Surf. Interface Anal.* **1983**, *5*, 181-185.

(410) Fleutot, S.; Dupin, J.-C.; Renaudin, G.; Martinez, H. *Phys. Chem. Chem. Phys.* **2011**, *13*, 17564-17578.

(411) Branch, D. W.; Wheeler, B. C.; Brewer, G. J.; Leckband, D. E. *Biomaterials.* **2001**, *22*, 1035-1047.

(412) Gavet, O.; Pines, J. *Dev. Cell.* **2010**, *18*, 533-543.